Chiral Symmetry and the Extraction of Hadron Properties from Lattice QCD

by

Stewart V. Wright, B.Sc.(Hons)

Thesis submitted for the degree of

Doctor of Philosophy

at

The University of Adelaide

(Department of Physics and Mathematical Physics)

December 2001

Acknowledgments

The PhD is a significant investment of time and energy, not only on my part, but from so many people who have been involved along the way. The journey is long and rocky and I offer my thanks to those that walked it with me.

First and foremost to my Mother and Cassie and Jack. Patience when I was short-tempered, encouragement when I needed it and support every moment of the day. Appreciation is a word that barely describes my position.

Better than a thousand days of diligent study is
one day with a great teacher.
JAPANESE PROVERB

The words on these pages are a result of the diligence and support from the physicists that it has been my pleasure to work with. My supervisors deserve special note. Tony Thomas, my teacher, mentor and friend — thank you. To Derek Leinweber, your enthusiasm is contagious and alongside Tony you have made this Ph.D. a blast, and last but not least I wish to thank Kazuo Tsushima for his willingness to help me over the last few years.

Douglas Adams wrote "Very strange people, physicists. In my experience the ones who aren't actually dead are in some way very ill". Without doubt my mental (in)sanity was maintained and fostered by Patrick Bowman and Sundance Bilson-Thompson. If enjoying life was an illness, these two are plague carriers and

I was a lucky victim! I should also mention Will Detmold, Waseem Kamleh, Ross (Mini-Me) Young and James Zanotti for special thanks for making the office we shared an enjoyable work environment.

Everyone at the Special Research Centre for the Subatomic Structure of Matter (CSSM), including Sharon, Sara and Cheryl were fun to work with. I wish to specially acknowledge Tony Williams, Wally Melnitchouk, Alex Kalloniatis, Ayse Kizilersu and Jonivar Skullerud for their willingness to spend time both discussing physics and having friendly chats.

During my time I was fortunate to have the opportunity to attend the HUGS summer school and visit a number of departments. I appreciate the time and interest shown to me by Tom Cohen and Xiangdong Ji at Maryland. I also would like to thank Peter Tandy and Pieter Maris at Kent State, Tim Londergan and Adam Szczepaniak at Indiana and finally Gerry Brown and Edward Shuryak at Stony Brook. The discussions and questions that were raised have helped me immensely by not only increasing my understanding but also my ability to think about problems laterally.

Numerous visitors to the CSSM took the time to chat and discuss physics. Many names escape me as I write this, but I appreciate the discussions I have had with Chris Allton, Steve Sharpe, Gerald Dunne, Pierre Guichon, Kim Maltman, Craig Roberts, Torleif and Magda Ericson and Alexander Sibirtsev. I must also thank Dan Schroeder for his helpful TEX macros which allowed me to do the contractions in Chapter 5.

The understanding shown by my friends outside of physics is much appreciated. David Cooke, Sarah Smith and Simon Del Fabbro deserve special mention. Putting up with me over the last few years, the unusual work hours, the varying workload and the mutterings about quarks is enough to show that these are true friends. Other friends deserving a mention are Carolyn Lam, Damien Seidel, Tracy

Hendrickson, David Goodfellow, Hayley Bignall, Robert Goler and Daniel Badger.

I know one of the biggest thanks I can offer must be to Ian McCarthy. His willingness to sit and talk to me when I was in year 10 of school, not lecture to this school child, but actually talking with me, is the reason I found physics. I was unsure of the path of my life, but after speaking with him, I had a clear notion of what I wanted to pursue. His willingness to chat with me at other times has reinforced my decision. I offer my most profound thanks to him.

During the writing of this thesis I came upon this quotation attributed to Charles Darwin. I know just how he felt.

> "...I am just now beginning to discover the difficulty of expressing one's ideas on paper. As long as it consists solely of description it is pretty easy; but where reasoning comes into play, to make a proper connection, a clearness and a moderate fluency, is to me, as I have said, a difficulty of which I had no idea ..."

Finally thanks to Chris Michael, who allowed me to finish this whilst working at Liverpool.

This thesis and the time of my PhD has taught me not how much I know about the subject contained herein, but how much I want to know about everything else.

Finally a special message for anyone into whose hands this thesis falls: the author may or may not have incorporated into the text, as a stimulus and a challenge to your perspicacity, one or more deliberate errors.[1]

[1] Source: Unknown

This work contains no material which has been accepted for the award of any other degree or diploma in any university or other tertiary institution and, to the best of my knowledge and belief, contains no material published or written by another person, except where due reference has been made in the text.

I give consent to this copy of my thesis, when deposited in the University Library, being available for loan and photocopying.

STEWART V. WRIGHT

The University of Adelaide

December 2001

Chiral Symmetry and the Extraction of Hadron Properties from Lattice QCD

Stewart V. Wright, Ph.D.
The University of Adelaide, 2001

Supervisors: Prof. A. W. Thomas
Dr. D. B. Leinweber

The extraction of the physical properties of hadrons from lattice Quantum Chromodynamics (QCD) calculations is an important and urgent area of research. It is difficult to make calculations of hadronic properties because QCD is a highly non-linear field theory. Lattice gauge theory is the only known *ab initio* way of making nonperturbative calculations of QCD. The lattice has been highly successful but the computational cost of simulating light quark masses means that hadronic calculations at physical quark masses are some way off.

We present a method of extrapolating from the heavy quark regime, where lattice calculations now occur, to physical quark masses, which carefully incorporates key, model independent constraints — especially those imposed by chiral symmetry. This extrapolation method not only allows one to extract physical hadron masses with high accuracy, but also allows the extraction of other properties, including the pion–nucleon sigma term and the J parameter for the vector mesons.

Contents

Chapter 1

Introduction

We shall not cease from exploration
And the end of all our exploring
Will be to arrive where we started
And know the place for the first time.
T.S. ELIOT, "LITTLE GIDDING"

On the surface it seems remarkable that still the primary unresolved problem in the Standard Model of particle physics relates to the strong interaction and its description from first principles. Quantum Chromodynamics (QCD), originally proposed by Gell-Mann [1] and Zweig [2] in the 1960s and 1970s, came about as a result of the exploding number of new particles being created by high energy particle colliders. To get a grasp on this variety of new matter, building blocks called *quarks* were introduced as simply a book-keeping trick. When it was found that one of these new particles, the Δ^{++}, was predicted to have a totally symmetric wave function, but was known to obey Fermi–Dirac statistics a hurdle was encountered. Following the cavalier approach of the initial formulation, a colour quantum number was assigned to the quarks. The baryons were required to be anti-symmetric under

the colour indices and the problems vanished. Imposing local gauge invariance on the colour fields and having the quarks interact by vector gluons crystallised the theory into the QCD we know today.

QCD is an asymptotically free theory — the effective strong coupling constant decreases at short distances. Perturbative QCD may be applied to processes involving large momentum transfer, for instance hadronic jets in high energy particle collisions. In principle all the properties of strongly interacting particles could be extracted from the QCD Lagrangian. It has been said[1] that *"In theory there is no difference between theory and practice; In practice there is."* This is especially true in the case of QCD in the low energy sector. The difficulty lies in the fact that QCD is formulated in terms of quarks and gluons, yet at low energy the world appears to be constructed of hadrons. To this date, no analytic studies of QCD have been able to extract non-perturbative results from first principles.

There are many approaches that have been applied to QCD in attempts to extract results in the non-perturbative region. The difficulty is that fundamental issues such as confinement and chiral symmetry are still not well understood. QCD motivated models attempt to build in some of the known properties whilst allowing the exploration of, and extrapolation to, other regions. There is of course a method that allows ab initio calculations in QCD to be performed — Lattice QCD.

On the lattice the entire theory of QCD is discretised. Space-time itself is discretised into a finite lattice. The quark fields are averaged about the grid-points and the gluon fields are defined on the links between the grid-points. The act of discretising the theory introduces, at a first approximation, errors of $\mathcal{O}(a)$, where a is the lattice spacing. The strength of the lattice is that these discretisation errors scale, that is, as the lattice gets finer, the errors reduce, and in the continuum limit lattice QCD is identical to QCD. Recent breakthroughs now allow the elimination

[1] Chuck Reid

of $\mathcal{O}(a)$ errors, and the remaining $\mathcal{O}(a^2)$ errors are small.

The Standard Model parameters of full QCD, the quark masses and the strong coupling constant, are also the parameters of freedom in lattice calculations. Where experimentally these are fixed quantities, the lattice allows investigation of how the theory of QCD behaves under variation of these parameters. The insights gained from exploring non-physical parameter sets is not only of interest as an intellectual exercise, but also forced upon us by technical issues. Computational and algorithmic limitations prevent full QCD lattice calculations at light quark masses, and force the extraction of hadron properties to occur at very heavy, entirely unphysical, quark masses. Improvements in actions, algorithms and computing power are occurring continuously, but it is a widely held view that we are still many years away from QCD calculations near the physical region. Two approaches to this difficulty have evolved.

The first is quenching where the theory is modified in a way as to effectively remove sea–quark loops. This approximation, whilst mutilating the theory, allows orders of magnitude reduction in computing costs. The other approach, which is the basis of this thesis, and in a modified form still important for the quenched theory, is to extrapolate the hadron properties from the heavy quark masses to physical masses. We investigate, as a first instance, the extrapolation of dynamical fermion lattice QCD results. Currently there is research under way to extend this approach to quenched and partially quenched results, but discussion of such is left to a future work.

The lattice approach is in its prime as a non-perturbative tool to explore QCD and hadronic properties. It has been observed that massless QCD obeys chiral symmetry, and this motivated the derivation of an effective field theory, Chiral Perturbation Theory (χPT). χPT is an effective theory containing the important low energy symmetries of QCD, and a theory in which it was simple enough to make

calculations. In chapter 3 we investigate the basis behind χPT, and derive the leading and next-to-leading non-analytic (in quark mass) contributions to the mass of the nucleon. We show that χPT predicts this non-analytic behaviour, including the model independent values for the coefficients, and that it is induced by Goldstone boson (pion) loops that are naturally associated with hadrons. χPT is a systematic approach to QCD that predicts the presence of non-analytic behaviour, and offers a systematic way to calculate the coefficients.

Chapter 4 discusses a phenomenologically motivated model of baryons — the Cloudy Bag Model (CBM). The CBM builds on the successful MIT bag model to allow investigation of baryons over a wide region of parameter space. The MIT bag introduced phenomenological constraints to enforce confinement, and the CBM introduced pions coupling to the quarks confined inside the bags. In the chiral limit, the CBM gives the correct behaviour that χPT tells us QCD possesses. In addition to this, form factors appear naturally in the model allowing it to be applied over a much greater range in quark, or equivalently pion mass. The radius of convergence of χPT is unknown, but since it is a perturbation about massless quarks, instinctively one feels that it would be surprising if it applied in the region where lattice QCD calculations occur (somewhere above four times the physical pion mass). The CBM however, through the introduction of form factors, which are related to the size of the source of the pion field, is able to probe from the chiral limit, through a region well into the available lattice calculations. We stress that this model is not QCD, but it does give an insight into the behaviour of the physics in the intermediate region. The CBM gives an intuitive feel for why the hadron properties behave as they do.

The many methods used to study hadronic physics including models, effective theories, perturbation theory and heavy quark theory are only giving insights from a few isolated vantage points. The need remains to use non-perturbative meth-

ods, and as we have stated, the only successful approach at this time is the lattice. We have alluded to the fact that whilst there are difficulties in making calculations on the lattice with physical parameters, one may extrapolate results calculated in a region with heavier quark masses to the physical. The exploration of extrapolation forms has not been a particularly active area of research and at first sight this is not surprising. Until quite recently there was no obvious need to extrapolate with anything other than a linear Ansatz — the lattice results appeared to be linear in m_π^2 to a good approximation. This linear behaviour is entirely expected, it is predicted as a precursor to Heavy Quark Effective Theory (HQET). The critical point is that HQET *does not* have χPT as a limit, but we know that lattice QCD does. In particular we know the non-analytic behaviour near the chiral limit. In chapter 3 we will show that the mass of the nucleon behaves like

$$m_N \sim m_0 + \alpha m_\pi^2 + \beta m_\pi^3 + \gamma m_\pi^4 + \xi m_\pi^4 \ln m_\pi^2 + \ldots$$

However fitting a form similar to this to lattice data is not reasonable. We show in chapters 5 and 6 that by fixing the coefficients β and ξ to their values known from χPT, it is impossible to find a fit. The other extreme is equally unpalatable. Relaxing the constraints on β and ξ, letting them become fit parameters means the loss of the benefits gained by using χPT in the first place. Our approach uses insights from the phenomenological CBM as to the behaviour of the mass in the region between the chiral limit and lattice results.

In chapters 5, 6 and 7 this work presents the development of an extrapolation scheme, one easily extended to other hadronic properties, that allows the extrapolation of dynamical fermion lattice QCD calculations of hadron masses to the physical region. We also discuss how this method allows the extraction of other properties of the hadrons, including the pion–nucleon sigma term, σ_N, and the J parameter for the vector mesons. We also present the first Edinburgh plots to display the cor-

rect behaviour in the extrapolation to the chiral limit. This scheme builds in the known behaviour in the chiral limit, in particular the leading and next-to-leading non-analytic behaviour with the correct coefficients as may be found in χPT. The extrapolation form smoothly interpolates between this chiral limit and the heavy quark regime, where hadron properties show smooth mass dependence. Finally the form automatically includes, and corrects for, the finite size effects introduced by the discretisation process. The functional form contains only three parameters, and the fitting involves an analytic sum which may be evaluated on a desktop PC in a short time frame. An analysis extrapolating to the chiral limit performed with this functional form would require virtually indistinguishable computing resources to the current analyses, and yet would contain the correct, known, physics. Having confidence in extrapolated values will allow a direct juxtaposition with experiment — testing QCD like never before.

Chapter 2

Lattice QCD

The particle physics community sowed its wild oats in a torrid affair with a beautiful gauge theory called Quantum Chromodynamics. It is the task of nuclear physics to bring up the unruly non-perturbative offspring.

THOMAS COHEN

A quantum field theory is a complex beast. In a weak coupling theory, like QCD at high energy, it may be expanded as a perturbative series of its n-point functions. The success of such an approach is highlighted by Quantum Electrodynamics where the theoretical prediction for the electron magnetic moment anomaly is known to 4 parts in 10^{-12}. The difficulty lies in the strong coupling region where a perturbative series often fails even to converge. The naïve perturbation, in QCD, around free particles is not well defined as the quarks are confined. Calculations in this region are, not surprisingly, known as *non-perturbative*. The coupling of QCD in the world we see around us runs with the scale of the process. Where in QED

the coupling was small at long distances, it is exactly the opposite in QCD. There is asymptotic freedom for hard processes, but for low energy processes there is confinement and perturbation theory breaks down. Therefore we realise that QCD is genuinely non-perturbative, and therefore we need tools in this region.

In the introduction to path integrals in Ref. [3] the following quote was attributed to Feynman:[1] "every theoretical physicist who is any good knows six or seven different theoretical representations for exactly the same physics." It is remarkably apt in this case. Quantum field theories may be formulated in the method of a path, or functional, integral. Effectively the n-point Green function of the theory is formulated in terms of an integral over all possible values of the fields at all space-time points. One of the strengths of lattice gauge theory is that it provides a method for approximating this functional path integral. The application of finite numerical methods to an infinite problem introduces approximations, but the strength of the lattice approach is that these approximations are systematically removable. In the words of one practitioner [4] "It is this possibility of controlling the systematic errors that makes lattice gauge theory increasingly popular."

A brief introduction to the construction of lattice gauge theory will be presented in this chapter. Additional information as well as a more detailed introduction can be found in [5, 6, 7, 8, 9, 10, 11, 12].

2.1 Lattice Field Theory

2.1.1 General Foundation

One builds a Lagrangian density, $\mathcal{L}(\Phi, \partial^\mu \Phi)$, of a theory from the appropriate degrees of freedom, the set of fields, Φ. The fields themselves are functions of the

[1] *The Character of Physical Law* (MIT Press, 1965), p. 168.

space-time they are embedded in, for example in Minkowski space time $\Phi \equiv \Phi(x)$ where $x^\mu = (x^0, \vec{x}) \equiv (t, \vec{x})$. In the specific case of QCD these degrees of freedom are associated with the quark and gluon fields. The action of such a Lagrangian is then found to be

$$S[\Phi] = \int d^4x \, \mathcal{L}(\Phi(x), \partial^\mu \Phi(x)) \,. \tag{2.1}$$

The generating functional of the theory is constructed as

$$\mathcal{Z}[\eta(x_i)] = \frac{1}{Z} \int [d\Phi] e^{iS[\Phi] - \int d^4x \eta(x_i)\Phi(x_i)} \,, \tag{2.2}$$

with the source terms in the theory denoted η, and the normalisation, Z, given by

$$Z = \int [d\Phi] e^{iS[\Phi]} \,. \tag{2.3}$$

The n-point, or *Green functions*[2], of the theory, which are the vacuum expectation values of time ordered products of the fields, then completely determine the theory:

$$\mathcal{G}^{(n)}(x_1, \ldots, x_n) = \mathcal{N} \langle 0 | \mathcal{T}[\Phi(x_1) \ldots \Phi(x_n)] | 0 \rangle \,, \tag{2.4}$$

where $\mathcal{N}$ is a normalisation constant. The Green functions are constructed by taking the derivative of the generating functional, Eq. (2.2), with respect to the sources, and then setting them to zero:

$$\mathcal{G}^{(n)}(x_1, \ldots, x_n) = \frac{1}{Z} \int [d\Phi] \Phi(x_1) \ldots \Phi(x_n) e^{iS[\Phi]} \,. \tag{2.5}$$

It should now be obvious that the normalisation constant, $\mathcal{N}$, is identically Z^{-1}. The mass of a particle, and all other physical observables of the system described by S can be derived from the Green functions. Returning to Feynman's quote, solving the field theory and solving Eq. (2.5) — with the explicit functional integration — are different ways of expressing the same physics.

[2]There is some discrepancy in the literature as whether these functions are *Green functions* or *Green's functions*. We follow the convention of [13] and use the former.

2.1.2 Building the Lattice

The difficulties of numerical calculations in a Minkowski space-time theory are removed by shifting to Euclidean space-time. This is the prevalent practice in the lattice QCD community and is not an approximation, but a complete transformation between the geometries. The transformation is a simple shift from regular time to imaginary time:

$$t \to -it\,. \tag{2.6}$$

This approach is justified as the Hamiltonian of QCD is time independent — it is unchanged by this transformation, and therefore so is the physics it describes. This change results in the following clean transformation from the original action to the Euclidean space action:

$$S = iS_E\,. \tag{2.7}$$

The highly oscillatory behaviour of the Green functions becomes exponentially damped, $e^{iS[\Phi]} \to e^{-S_E[\Phi]}$, making them numerical soluble. This exponential damping is reminiscent of statistical mechanics, and we shall return to this point shortly. The lattice quantum field theory can then be represented in terms of well defined functional integrals taken over the Euclidean lattice hypercube of length L and lattice spacing a. In an ideal world, the continuum limit, $a \to 0$, would be taken. However this is not possible because of the finite computational resources available. As was mentioned previously, this source of error is systematically improvable. The difficulty of finding a compromise between larger lattices and smaller lattice spacing is the subject of much work. The difficulty is by reducing a, to represent the continuous space, the size of the lattice, aL, will also decrease. However the lattice must be large enough to hold not only the object being explored but also longer range effects introduced by intermediate states. It is believed that the physical lattice size should be between 2.5 and 3.0 fm to avoid finite-size effects

[14, 15, 16, 17, 18]. We shall show in subsequent chapters that any finite size lattice will exclude some important physics.

Placing the theory on the lattice introduces two additional properties that are important to consider when extracting quantities from a calculation. By discretising the coordinate space in terms of a finite a and L, we change the available momenta. Since there is a finite number of lattice sites, it can be shown that the available momenta, k, in the finite periodic volume are also discrete

$$k_\mu = \frac{2\pi n_\mu}{aL_\mu}, \tag{2.8}$$

where L_μ is the number of lattice sites in the μ direction, and the integer n_μ obeys

$$-\frac{L_\mu}{2} < n_\mu \leq \frac{L_\mu}{2}. \tag{2.9}$$

We see from Eq. (2.8) that the short distance (ultraviolet) physics, $k_{\max} = \frac{\pi}{a}$, is determined by the lattice spacing a. This UV regularisation is required in any renormalisable quantum field theory as it allows the elimination of infinities in calculated observables. Naturally as the observables will be dependent on a one must ensure that they scale correctly as $a \to 0$. The lattice size, L_μ, determines the spacing between the allowed momenta. Thus, on a small lattice there is a large minimum non-zero momentum. In the particular case of a p-wave decay, where one unit of momentum is required, the decay is prevented because of the large energies required.

The realisation of the similarity between the formulation of lattice gauge theory and statistical mechanics — that is, systems with a large number of degrees of freedom, but with bulk properties — has allowed some of the experience and machinery of the field to be utilised. In particular the e^{-S_E} is reminiscent of the Boltzmann factor. Using this insight allows the generation of fields using the Markoff chain process. This ensures that the fields created are of the typical weight distribution of QCD. Such a generation process reduces the number of fields required for a

calculation by generating a larger percentage of fields that have a higher probability of being physically important. We leave the precise details of putting QCD on the lattice to the review texts mentioned in the introduction.

2.1.3 Region of Applicability

Lattice gauge theory is well defined over all lattice sizes, spacing, and quark masses. It obeys scaling, so for arbitrarily large and fine lattices with light enough quarks the properties will approach those of continuum QCD. There are some constraints however on how close to the physical world a calculation may be pushed:

- Simulations are expensive — the cost of a calculation is proportional to the square of the lattice volume and inversely proportional to the sixth power of the lattice spacing [4].
- Light quarks are non-local — thus they are extremely sensitive to finite volume effects. Technical reasons, in particular critical slowing in the fermion matrix inversion algorithms, also force the use of unphysical heavy quarks.
- Dynamical quarks are expensive — they increase by at least two orders of magnitude the cost of the simulation.
- Large lattices are needed — to avoid the major finite-size effects the physical lattice size must be at least 2.5 – 3.0 fm. [14, 15, 16, 17, 18].

These constraints convey the need to extrapolate results of lattice calculations to the physical region. The subsequent chapters will present a method of extrapolating masses in a way that reproduces the low energy properties of QCD whilst allowing contact with the region where lattice calculations occur.

2.2 Nucleon Mass

The most basic quantity to extract from a lattice calculation is the nucleon mass. It may be deduced from the asymptotic behaviour of the single particle Green function in large Euclidean time. We present below the derivation for the positive parity particle, which easily generalises to the negative parity case.

Consider first the generalised case of the two point Green function in Minkowski space, where a three-quark state is created with momentum $\vec{q}$:

$$\mathcal{G}(\vec{q},t) = \int d^3x\, e^{-i\vec{q}\cdot\vec{x}}\langle 0|\mathrm{T}\{\chi(x)\bar{\chi}(0)\}|0\rangle \tag{2.10}$$

$$= \sum_{\vec{x}} e^{-i\vec{q}\cdot\vec{x}}\langle 0|\mathrm{T}\{\chi(x)\bar{\chi}(0)\}|0\rangle\,, \tag{2.11}$$

where χ is an interpolating field for the nucleon, and we have presented both the continuum space and lattice form of the Green function. The construction of an appropriate Green function for the nucleon requires an interpolating field representing a three-quark state, with the quantum numbers of a nucleon, *in terms of* the quark fields. There are many possible choices, and in practice only a reasonable overlap with the physical nucleon wave function is required. The standard choices for such a field are

$$\chi_1 = \epsilon_{abc}(u^{a\mathrm{T}}\mathrm{C}\gamma_5 d^b)u^c\,, \tag{2.12}$$

$$\chi_2 = \epsilon_{abc}(u^{a\mathrm{T}}\mathrm{C}d^b\gamma_5)u^c\,, \tag{2.13}$$

with it having been shown in [19] that any spin-$\frac{1}{2}$, isospin-$\frac{1}{2}$ nucleon interpolating field without derivatives may be simplified as a linear combination of Eqs. (2.12) and (2.13). We now insert a complete set of nucleon states, N_i with spin s and momentum $\vec{p}$, into Eq. (2.11)

$$\mathcal{G}(\vec{q},t) = \sum_{\vec{x},\vec{p},s,i} e^{-i\vec{q}\cdot\vec{x}}\langle 0|\chi(x)|N_i(\vec{p},s)\rangle\langle N_i(\vec{p},s)|\bar{\chi}(0)|0\rangle\,, \tag{2.14}$$

and only consider positive time. The annihilation of a nucleon to the vacuum is defined as

$$\langle 0|\chi(0)|N_i(\vec{p},s)\rangle = \lambda_i u(\vec{p},E_i,s)\,, \tag{2.15}$$

with λ_i being the ability of the interpolating field to annihilate the nucleon, $E_i = \vec{p}^{\,2}+M_i^2$, and u is a spinor satisfying the Dirac equation. Using translation (Eq. (A.4)) allows the following simplification:

$$\begin{aligned} \mathcal{G}(\vec{q},t) &= \sum_{\vec{x},\vec{p},s,i} e^{-i\vec{q}\cdot\vec{x}}\langle 0|\chi(0)|N_i\rangle\langle N_i|\bar{\chi}(0)|0\rangle e^{i(\vec{p}\cdot\vec{x}-E_i t)} &(2.16)\\ &= \sum_{\vec{x},\vec{p},s,i} e^{i[(\vec{p}-\vec{q})\cdot\vec{x}-E_i t]}|\lambda_i|^2 u(\vec{p},E_i,s)\bar{u}(\vec{p},E_i,s)\,. &(2.17)\end{aligned}$$

By using the definition of the Kronecker-delta, $\sum_{\vec{x}} e^{i(\vec{p}-\vec{q})\cdot\vec{x}} \equiv \delta_{\vec{p}\vec{q}}$ we simplify the above expression as

$$\mathcal{G}(\vec{q},t) = \sum_{s,i} e^{-iE_i t}|\lambda_i|^2 u(q,s)\bar{u}(q,s)\,. \tag{2.18}$$

The sum over the spins of the spinors is simply [13]:

$$\sum_s u(q,s)\bar{u}(q,s) = \frac{\not{q}+M_i}{2M_i}\,, \tag{2.19}$$

resulting in the Green function being given by

$$\mathcal{G}(\vec{q},t) = \sum_i e^{-iE_i t}|\lambda_i|^2 \frac{\not{q}+M_i}{2M_i}\,. \tag{2.20}$$

At the quark level one contracts time ordered pairs of quark wave functions, which gives the non-perturbative quark propagator. Using the Dirac representation (Sec. A.3.1) we can see the Dirac matrix of the above expression has the form

$$\not{q}+M_i = \begin{pmatrix} (E_i+M_i)I & \vec{q}\cdot\vec{\sigma} \\ -\vec{q}\cdot\vec{\sigma} & (-E_i+M_i)I \end{pmatrix}\,. \tag{2.21}$$

In the particular case of a particle at rest ($\vec{q} \equiv 0$), the only non-zero elements are the $(1,1)$ and $(2,2)$ components. Changing to Euclidean space, $t \to -it$, it becomes clear that in large Euclidean times the ground state dominates, because of the mass dependence of the exponential damping. Practically, this ground state mass, $M_i \equiv E_i(q=0)$, is extracted from lattice evaluations of the two-point Green function, Eq. (2.10), by looking at the local slope of the (natural) logarithm of the ratio of the Green functions at t and $t+1$:

$$\ln\left(\frac{\mathcal{G}(t+1)}{\mathcal{G}(t)}\right) = \ln\left(\mathcal{G}(t+1)\right) - \ln\left(\mathcal{G}(t)\right) \tag{2.22}$$

$$= -E_i\,. \tag{2.23}$$

2.3 Setting the Scale

An issue suppressed in the previous discussion is that all quantities determined on the lattice, including masses, are actually dimensionless quantities. Thus there is the need, if we wish to represent the mass in physical units, to determine the scale of the lattice a. In this work, results from two collaborations [20, 21] are utilised. Since both groups use methods relating to the static quark potential to determine a we shall only mention that approach. An alternative relies on surrendering one observable O, for instance a mass, and extracting the lattice spacing from the quantity calculated on the lattice, aO. As we shall show in subsequent chapters, the extrapolations to physical quark masses that have previously been used are flawed, and hence these values will be incorrect.

We follow the work of Sommer [22] by utilising the force between static quarks at intermediate distances to set the hadronic scale. The calculation of the static quark potential at a separation r is conceptually one of the simplest quantities

that can be calculated on the lattice [23, for example], can be calculated to a high precision and may be parameterised as [24, 25, 26]:

$$V(r) = -\frac{e}{r} + \sigma r + V_0. \tag{2.24}$$

The force between the quarks is then simply given by the change in the potential as a function of the separation

$$F(r_0) = \left.\frac{\partial V}{\partial r}\right|_{r=r_0} = \left.\frac{e}{r^2} + \sigma\right|_{r=r_0}, \tag{2.25}$$

where the parameters are often determined by the static quark potential near r_0.

It is known that both the $\bar{b}b$ and $\bar{c}c$ spectra may both be described by a single effective non-relativistic Schrödinger equation potential [27]. Model calculations indicate that the rms radii of $\bar{b}b$ states is 0.2–0.7 fm, and the $\bar{c}c$ states have rms radii of 0.4–1.0 fm. Thus these spectra may be used to determine the effective potential in the range $r \simeq 0.2$ fm to $r \simeq 1.0$ fm, however it is clear that the best information is at a radius of around $r \sim 0.5$ fm. This information is then used to set the scale of the lattice by looking at the quantity

$$r_0^2 F(r_0) = c \tag{2.26}$$

$$= \left(\frac{e}{r_0^2} + \sigma\right) r_0^2. \tag{2.27}$$

In principle we can set $r_0^2 F(r_0)$ to any value. However it is common practice to choose $c = 1.63$ following Sommer's initial estimate of 1.65 and motivated by the Cornell [28] and Richardson [29] heavy quark models. This choice of c corresponds to $r_0 = 0.49$ fm. Thus we have a relationship between the string tension, σ, that is used by the CP-PACS collaboration, and r_0 favoured by UKQCD

$$r_0^2 = \frac{1.63 - e}{\sigma}, \tag{2.28}$$

with the constant e equal to 0.43 in agreement with [25]. Equation (2.26) is the preferred method for determining the scale on the lattice for a number of reasons. One

compelling argument is this approach only requires the evaluation of the force at moderate separations of the static quark-antiquark pair. This removes the difficulty associated with the extraction of the string tension, as beyond a certain separation it is expected that string breaking — $\bar{q}q$ creation — will occur. Virtual $\bar{q}q$ creation will act to screen the potential, rendering a precise definition of a string tension impossible. The above method is well defined in both quenched and dynamical calculations.

2.4 Results

There is a considerable difficulty and cost associated with calculating dynamical fermion results on the lattice. Until quite recently there were only two sets [20, 21] of results that were at sufficiently light quark mass for us to begin our investigations. In the following work we use dynamical, two-flavour fermion results from the CP-PACS [20] and UKQCD [21] collaborations. We note that in both data sets the continuum extrapolation has not been taken, resulting in a residual $\mathcal{O}(a^n)$ (for some n) error in the published results. The effects of the continuum extrapolation are beyond the scope of this work and are not considered in this thesis. We have, however, established a new formalism in this work, based on the excellent data mentioned, and anticipate the approach established here will become standard practice in future lattice publications.

CP-PACS

The CP-PACS [20] calculations, presented in Table 2.1, were made on either a $12^3 \times 32$ or $16^3 \times 32$ lattice. The calculations were performed using an Iwasaki [30] — plaquette plus rectangle gluon and clover fermion — action, with the Sheik-

holeslami and Wohlert [31] clover coefficient, $c_{\rm SW}$, determined via mean-field improvement. Since the publication of the work the value of $c_{\rm SW}$ has been determined non-perturbatively and is somewhat different from value used in [20]. Throughout this work we have used the results found with the perturbative $c_{\rm SW}$ to avoid introducing any systematic errors part-way through the analysis. As we have previously discussed, there is a relationship between σ and r_0, found from the static quark potential $V(r)$. However this approach neglects the quark-antiquark separation, r, dependence of e and σ in Eq. (2.26), meaning the result is not exact. As different methods for setting the scale were used by the CP-PACS and UKQCD collaborations (as discussed below) there is some uncertainty in setting the physical scale. However, for a particular choice of σ at the physical quark mass, for example CP-PACS sets $\sqrt{\sigma} = 440$ MeV, we may extract a value of r_0 from Eq. (2.28). We then use this value of r_0 in the UKQCD formalism for setting the scale, avoiding possible string breaking effects. We shall use this ambiguity later to improve the

β	K	$m_{\rm PS}a$	$m_{\rm V}a$	$m_{\rm N}a$	$m_{\Delta}a$	σa^2
1.9^a	0.1420	0.6992(19)	1.0134(60)	1.494 (12)	1.662(17)	0.2375(60)
1.9^a	0.1430	0.5414(18)	0.8861(71)	1.283 (13)	1.501(17)	0.2094(51)
1.9^a	0.1440	0.2906(41)	0.706 (15)	0.972 (25)	1.171(32)	0.1755(57)
1.9^b	0.1370	1.1918(12)	1.4091(28)	2.2172(91)	2.358(20)	0.3243(87)
1.9^b	0.1400	0.9334(17)	1.2033(39)	1.8573(95)	2.009(12)	0.2750(75)
1.9^b	0.1420	0.6983(18)	1.0149(45)	1.5195(78)	1.712(11)	0.2465(46)

Table 2.1: Results from the CP-PACS collaboration [20]. The lattice size for the rows indicated by the a is $16^3 \times 32$, whilst the rows indicated by b are on a $12^3 \times 32$ lattice.

agreement between the data sets we are investigating.

We feel some encouragement for our present work because of a statement in the article regarding the quark mass dependence of the hadron masses:

"The existence of curvature [at small quark masses] *is observed,*

necessitating a cubic ansatz for extrapolation to the chiral limit." [20]

The first section of this statement is related to the motivation of this work. This curvature is expected to be seen as the chiral limit is approached. It is a model independent result, that may be implicitly included in extrapolations, as we shall discuss in subsequent chapters. The second part of this statement is motivated by chiral perturbation theory. It is known from χPT that the leading non-analytic term in the mass of, for example, the ρ-meson is a term in m_π^3, thus a fit of the type

$$m_\rho a = A_\rho + B_\rho (m_\pi a)^2 + C_\rho (m_\pi a)^3 \tag{2.29}$$

has some theoretical motivation. Unfortunately such a simplistic approach is only correct in a small region around the chiral limit, not at the quark masses where lattice calculations occur, as we investigate in sections 5.4.1 and 6.6.2. The final issue we wish to raise is with regards to the CP-PACS result at $m_\pi/m_\rho \sim 0.4$. Although CP-PACS finds no evidence of residual finite size errors at this mass point, they caution that it is premature to draw firm conclusions based on the present low statistics of approximately 1000 trajectories.

UKQCD

The second source of results we have utilised is Ref. [21] from the UKQCD collaboration (Table 2.2). These dynamical fermion results were calculated on a $12^3 \times 24$ lattice at $\beta = 5.2$. They used the standard plaquette action for the gauge fields, and an $\mathcal{O}(a)$ improved Wilson fermion action. The lattice size was chosen so that the volume of the lattice was greater than (1 fm)^3 in the spatial dimensions. The physical scale was set by comparing the force, calculated from the interquark potential, to quarkonia models as was the justification for Eq. (2.26). Phenomenologically it is found that $r_0 \simeq 0.49$ fm, and this value is used to extract the physical lattice spacing, a.

κ	$m_{PS}r_0$	$m_V r_0$	$m_N r_0$	$m_\Delta r_0$	r_0/a
0.1370	$2.541\ ^{+23}_{-26}$	$2.973\ ^{+29}_{-31}$	$4.710\ ^{+\ 85}_{-\ 69}$	$4.907\ ^{+\ 79}_{-\ 49}$	$2.294\ ^{+20\ +\ 7}_{-23\ -\ 2}$
0.1380	$2.404\ ^{+33}_{-29}$	$2.915\ ^{+43}_{-36}$	$4.528\ ^{+\ 85}_{-\ 58}$	$4.763\ ^{+\ 99}_{-\ 56}$	$2.568\ ^{+34\ +34}_{-30\ -88}$
0.1390	$2.155\ ^{+44}_{-38}$	$2.746\ ^{+61}_{-48}$	$4.263\ ^{+106}_{-\ 80}$	$4.707\ ^{+123}_{-\ 83}$	$3.046\ ^{+58\ +42}_{-52\ -\ 7}$
0.1395	$1.916\ ^{+38}_{-35}$	$2.700\ ^{+49}_{-44}$	$4.045\ ^{+\ 95}_{-\ 65}$	$4.565\ ^{+\ 99}_{-\ 93}$	$3.435\ ^{+48\ +42}_{-47\ -\ 0}$
0.1398	$1.738\ ^{+17}_{-61}$	$2.578\ ^{+47}_{-61}$	$3.765\ ^{+101}_{-\ 78}$	$4.349\ ^{+113}_{-105}$	$3.652\ ^{+29\ +\ 7}_{-25\ -13}$

Table 2.2: Results from the UKQCD collaboration [21]. All results were calculated on a $12^3 \times 24$ lattice. The lattice spacing is determined from r_0/a where r_0 has the value 0.49 fm.

We present plots showing the data sets which we use in Fig. 2.1. The left hand plot shows the results using the central values for setting the physical scale. It is clear that the two data sets are not consistent, so we use the uncertainty in setting the physical scale to rescale both data sets by 5% to improve the agreement. This improved data is presented in the second plot. We also show linear ($m_H = a + b m_\pi^2$) fits to the data. This Ansatz reproduces the lattice results well between $m_\pi^2 \sim 0.2$ GeV^2 and $m_\pi^2 \sim 0.8$ GeV^2, but fails at both ends. The divergence at light pion mass (or equivalently quark mass, Sec. 3.1.3) is expected from chiral perturbation theory, and is the motivation of this work. The curvature at high pion mass, is an indication of higher order (in m_π^2) terms coming from the Gell-Mann–Oakes–Renner relation, or perhaps an indication that it does not apply. The details of the divergence are not of interest in this work, and so we restrict our investigation to data that lies below $m_\pi^2 \sim 0.8$ GeV^2.

2.5 Conclusion

Lattice gauge theory is the only known way to explore the properties of Quantum Chromodynamics from first principles. Whilst there are current limitations imposed by finite computing resources, they are systematically improvable, and the lattice is

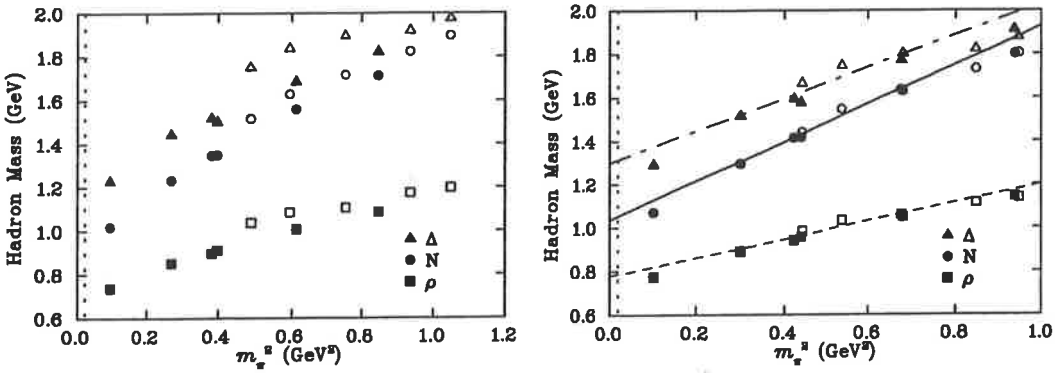

Figure 2.1: We present, in the left-hand plot, the results for the ρ, N and Δ masses from the CP-PACS [20] (filled symbols) and UKQCD [21] (open symbols) data sets presented in Tables 2.1 and 2.2. The right-hand plot uses the uncertainty in setting the physical scale to shift both masses by 5% to improve agreement. The vertical short-dashed line indicates the physical pion mass.

the only ab initio approach available. It is this property that has made the lattice an attractive field of research.

We discuss other approaches to investigating the predictions of QCD in the following chapters. In chapter 3 we briefly discuss the approaches of chiral symmetry and chiral perturbation theory, an effective theory in the low energy regime. Chapter 4 presents a model approach to the phenomenology of QCD, whilst preserving the symmetries of QCD. Each of these methods has their own strengths and weaknesses, and it is through utilising all of them we gain a greater insight. Truly the whole is greater than the sum of the parts.

Chapter 3

Chiral Perturbation Theory

Although this may seem a paradox, all exact science is dominated by the idea of approximation.

BERTRAND RUSSELL

Chiral perturbation theory (χPT) is a complete field in and of itself. A chapter in this thesis would not, and could not, do justice to the richness and diversity of the field. We do not attempt to present χPT in anything but generality, developing some of the concepts that will be important in the following chapters. There are many reviews [32] that allow the interested reader insights into the development of the field and the basic methodology used.

3.1 Chiral Symmetry

Chiral perturbation theory is built on the basis of chiral symmetry. We give a brief overview of chiral symmetry as an introduction to χPT. The starting point is the Dirac equation. For a vector wave functions, Ψ, the Dirac equation satisfies the

following requirements [13]:

1. The components of Ψ must satisfy the Klein-Gordon equation, so that a plane wave with $E^2 = \mathbf{p}^2 + m^2$ is a solution.

2. There exists a conserved four-vector current density, with positive density.

3. The components of Ψ are independent functions of x.

A free relativistic fermion is completely characterised by its energy, E, momentum, $\vec{p}$, and helicity $\hat{h} = \vec{\sigma} \cdot \vec{p}/|p|$. Thus for a massless, spin-$1/2$, free particle the Dirac equation may be written as

$$\mathcal{L} = i\overline{\Psi}\partial\!\!\!/\Psi \,. \tag{3.1}$$

For the particular case of massless fermions, helicity and chirality are identical concepts, thus we may decompose the spinor into left- and right-handed components, using the chirality operator γ_5:

$$\begin{aligned} \Psi &= \frac{1}{2}(1-\gamma_5)\Psi + \frac{1}{2}(1+\gamma_5)\Psi \\ &= P_L\Psi + P_R\Psi \\ &= \Psi_L + \Psi_R \,. \end{aligned}$$

Here $P_{L,R}$ are projection operators which obey the expected properties that the projection of a chirality eigenstate does not change its chirality, and that the group is closed under chirality projection. Mathematically these may be written as [33]:

$$P_L^2 = P_L, \quad P_R^2 = P_R, \quad P_L \cdot P_R = 0, \quad P_L + P_R = 1.$$

We also have the property that

$$\hat{h}\Psi_{L,R} = \pm\Psi_{L,R} \,,$$

however this is only exact in the case of massless fermions. This can be seen when one introduces mass into the Dirac equation, as one would find mixing between the left- and right-handed states:

$$\overline{\Psi} m \Psi = \overline{\Psi}_L m \Psi_R + \overline{\Psi}_R m \Psi_L \,. \tag{3.2}$$

In this case the $P_{L,R}$ are still projectors, but not of exact helicity. The helicity of massive particles is a frame dependent concept, a right-handed particle moving in the positive x-direction in one frame is left-handed and moving in the negative x-direction in a suitably boosted frame.

Returning to the massless state, it is clear we can separate the Lagrangian of Eq. (3.1) into a sum of the two helicity eigenstates

$$\mathcal{L} = i\overline{\Psi}_L \partial\!\!\!/ \Psi_L + i\overline{\Psi}_R \partial\!\!\!/ \Psi_R \,, \tag{3.3}$$

where there is no interaction between the left- and right-handed fermions. Thus the Lagrangian remains invariant under an arbitrary transformation of either the left- or right-handed fields by a generator of SU(3), ϵ:

$$\Psi_L \to \Psi'_L = e^{i\epsilon_L} \Psi_L, \quad \Psi_R \to \Psi'_R = e^{i\epsilon_R} \Psi_R \,. \tag{3.4}$$

In particular the group of these transformations is $\mathrm{SU}(3)_L \times \mathrm{SU}(3)_R$, where there are 3 light quarks, and the symmetry is referred to as the chiral symmetry. There are sixteen conserved currents, found from the application of Noether's theorem. It is common practice when describing the system to use the vector and axial currents (rather than the left- and right-handed currents)

$$V_a^\mu = \overline{\Psi} \gamma^\mu \frac{\lambda_a}{2} \Psi \,, \tag{3.5}$$

$$A_a^\mu = \overline{\Psi} \gamma^\mu \gamma_5 \frac{\lambda_a}{2} \Psi \,, \tag{3.6}$$

with the corresponding conserved charges

$$Q_a^V = \int d^3x\, V_a^0(x)\,, \tag{3.7}$$

$$Q_a^A = \int d^3x\, A_a^0(x)\,. \tag{3.8}$$

3.1.1 Dynamical Symmetry Breaking

If the ground state (vacuum) of QCD was chirally symmetric then, the **Wigner-Weyl** representation of chiral symmetry with a "trivial" vacuum would be realised and both vector and axial charge operators would annihilate the vacuum:

$$Q_a^V|0\rangle = Q_a^A|0\rangle = 0\,. \tag{3.9}$$

There is however, evidence from both low-energy hadron phenomenology and from lattice QCD calculations that chiral symmetry is *dynamically* broken. These results indicate the ground state of QCD does not share the chiral symmetry of the Lagrangian. If Wigner-Weyl was realised, the spectra of positive and negative parity states would have a close correspondence, as indicated by Eq. (3.9). There are many examples of where this correspondence breaks down. Two of the most striking include the lack of agreement in the masses of the vector and axial vector mesons and the mass gap of pseudoscalar meson parity partners.

Assuming Eq. (3.9) was correct would imply that the correlation functions of vector and axial vector currents would be identical: $\langle 0|V_a^\mu V_b^\nu|0\rangle = \langle 0|A_a^\mu A_b^\nu|0\rangle$. As a direct consequence, one would expect that the spectra of vector ($J^\pi = 1^-$) and axial vector ($J^\pi = 1^+$) mesons would also be identical. This is patently not true, the ρ meson has a mass ($m_\rho \simeq 0.77$ GeV) much smaller than that of the axial a_1 meson ($m_{a_1} \simeq 1.23$ GeV). Another indication that chiral symmetry does not hold is seen in the light pseudoscalar ($J^\pi = 0^-$) mesons, (π, K, ...), which have masses much lower that the lightest scalar ($J^\pi = 0^+$) mesons.

An alternate realisation of chiral symmetry is the **Nambu-Goldstone** representation. Here the observed, approximate validity of SU(3) flavour symmetry is found to be compatible with the assumption that

$$Q_a^V|0\rangle = 0\,. \tag{3.10}$$

One must therefore conclude

$$Q_a^A|0\rangle \neq 0. \tag{3.11}$$

Thus we see that the larger $\mathrm{SU}(3)_L \times \mathrm{SU}(3)_R$ symmetry must be broken down to the flavour group $\mathrm{SU}(3)_V$, which is consistent with observation.

3.1.2 Goldstone's Theorem

Goldstone's theorem states that for every broken continuous symmetry, the theory must contain a massless particle, the Goldstone boson [34, 35, 36]. We saw above that QCD has such a broken symmetry, and so we may apply Goldstone's theorem. Since the axial charge does not leave the vacuum invariant (Eq. (3.11)), there must be a physical state created from the vacuum

$$|\phi_a\rangle = Q_a^A|0\rangle\,. \tag{3.12}$$

As the axial charge commutes with the Hamiltonian, we can apply the Hamiltonian to the above expression with the result

$$\mathcal{H}|\phi_a\rangle = Q_a^A\mathcal{H}|0\rangle\,. \tag{3.13}$$

That is, the energy of the state ϕ_a is that of the vacuum. Thus, since there are eight generators of the axial charge, we have an equivalent number of *massless* pseudoscalar mesons.

This prediction is indeed reflected in nature as the lightest hadrons observed are eight in number and are pseudoscalar ($\pi^{\pm}$, π^0, $K^{\pm}$, K^0, $\bar{K}^0$, η). The reason

that these mesons are not massless is that the exact $\mathrm{SU}(3)_L \times \mathrm{SU}(3)_R$ symmetry of chiral symmetry is explicitly broken by massive quarks. As the quark masses are so small (a few MeV for the u and d quarks and around 150 MeV for the s quark) the predictions of $\mathrm{SU}(3)$ chiral symmetry are quite reasonable. In the $\mathrm{SU}(2)$ case (just the u and d quarks are assumed to be massless) we find just three Goldstone bosons, and a much better realisation of the approximate symmetry.

3.1.3 The Gell-Mann–Oakes–Renner Relation

Goldstone's theorem implies the existence of pseudoscalar bosons. We may define their state to be $|\pi_a(p)\rangle$, normalised as $\langle \pi_a(p)|\pi_b(p')\rangle = 2E_p\delta_{ab}(2\pi)^3\delta^3(\vec{p}-\vec{p}')$, where the four-momentum is defined as $p^\mu = (E_p, \vec{p})$. Additionally the divergence in the axial current (this is the Partially Conserved Axial Current (PCAC) of Gell-Mann, and Lévy and Nambu [37, 36]) is given by

$$\partial_\mu A_a^\mu = i\overline{\psi}\left\{\mathcal{M}, \frac{\lambda_a}{2}\right\}\gamma_5\psi\,, \tag{3.14}$$

$$\partial_\mu A_1^\mu = (m_u + m_d)\overline{\psi} i\gamma_5 \frac{\lambda_1}{2}\psi\,, \tag{3.15}$$

with the matrix $\mathcal{M}$ defined to be diagonal with the ith light quark mass at $\mathcal{M}_{ii}$. Goldstone's theorem also implies that the transition matrix element of the axial current is

$$\langle 0|A_a^\mu(x)|\pi_b(p)\rangle = ip^\mu f_0\delta_{ab}e^{-ip\cdot x}\,, \tag{3.16}$$

and hence the axial current is

$$\langle 0|Q_a^A(t=0)|\pi_b(p)\rangle = i\delta_{ab}f_0E_p(2\pi)^3\delta^3(\vec{p})\,. \tag{3.17}$$

Evaluating the vacuum expectation of the commutator of the axial current with the divergence of the axial current:

$$\left\langle 0\left|\left[Q_1^A, \partial_\mu A_1^\mu\right]\right|0\right\rangle = -\frac{i}{2}\left(m_u + m_d\right)\left\langle \overline{u}u + \overline{d}d\right\rangle. \tag{3.18}$$

Inserting a complete set of states, normalised such that

$$\int \frac{d^3p}{2E_p(2\pi)^3}|\pi_a(p)\rangle\langle\pi_a(p)| = 1\,, \tag{3.19}$$

it is simple to derive the Gell-Mann–Oakes–Renner (GMOR) relation [38]

$$m_\pi^2 = -\frac{1}{2f_0^2}(m_u + m_d)\langle\bar{u}u + \bar{d}d\rangle + \mathcal{O}(m_{u,d}^2)\,. \tag{3.20}$$

The pion decay constant in the vacuum is given by f_0, which is related to the physical decay constant by $f_\pi = f_0(1 + \mathcal{O}(m_q))$. Thus the difference from the physical value (92.4 ± 0.3 MeV [39]) is of $\mathcal{O}(m_{u,d}^2)$.

We now have a way of relating the observable world of hadrons, where we may measure the pion mass and decay constant, to the properties of QCD, expressed in terms of the fundamental quark degrees of freedom.

3.2 Chiral Perturbation Theory

The theory of elemental particle interactions that is presently accepted for the strong interaction, Quantum Chromodynamics, has proved to be a successful theory. It is elegant, and simple to write[1]

$$\mathcal{L}_{\text{QCD}} = \bar{q}(i\not{D} - m)q - \frac{1}{2}\text{tr}\, G_{\mu\nu}G^{\mu\nu}\,, \tag{3.21}$$

it is asymptotically free and more importantly for calculation purposes it is renormalisable. However, for the most important criteria, that it represents the physical world, there are some difficulties making comparisons in the low energy region. Some fundamental difficulties include

1. The theory is highly non-linear because of the gluon self interactions.

[1] *"If you are out to describe the truth, leave elegance to the tailor."* — ALBERT EINSTEIN, *"What a strange illusion it is to suppose that beauty is goodness."* — LEO TOLSTOY.

2. Usual perturbation theory is difficult to apply as the coupling, $g^2/4\pi$, is of order 1.

A way of dealing with these problems is via an effective theory, in which the predictions of QCD in the low energy regime are reproduced, with hadronic degrees of freedom. The low energy effective Lagrangian, $\mathcal{L}$, must also have the same symmetries as the QCD Lagrangian, $\mathcal{L}_{\rm QCD}$. Weinberg suggested a method [40] in which all terms allowed by the symmetries, to a particular order, of the fundamental theory are explicitly included, ensuring that any calculation to such an order will be consistent.

If we rewrite the QCD Lagrangian as a sum of a chirally symmetric piece and one that breaks chiral symmetry

$$\mathcal{L}_{\rm QCD} = \mathcal{L}^{\rm S}_{\rm QCD} + \mathcal{L}^{\rm SB}_{\rm QCD}\,, \tag{3.22}$$

our effective theory could, in an analogous manner, be separated into two parts, one where chiral chiral symmetry held, and one where is was broken

$$\mathcal{L}_{\rm Eff} = \mathcal{L}_0 + \mathcal{L}_{\rm SB}\,.$$

In this approach the symmetries of $\mathcal{L}_0$ would be those of $\mathcal{L}^{\rm S}_{\rm QCD}$, and the symmetry breaking term, $\mathcal{L}_{\rm SB}$ is small and may be treated perturbatively. Finally, by construction, the Goldstone bosons are the only massless, strongly interacting particles in the theory. Applying these constraints an effective theory of the strong interaction may be derived.

Numerous authors, for example [41, 42, 33], have investigated the derivation of the effective chiral Lagrangian for the meson, baryon and heavy baryon sectors. We leave the details to these authors, and will limit the further discussion to general comments on χPT. We derive the leading and next-to-leading non-analytic contri-

butions for the nucleon as a guide how to proceed. In the following sections we follow closely the works [43] and [44].

3.2.1 Leading Non-Analytic Contribution to the N mass

The derivation of the leading non-analytic contribution to the N mass is presented in Refs. [45, 33, 43]. The nucleon propagator extracted from the lowest order effective Lagrangian for QCD has the form

$$S_N(\omega) = \frac{i}{\omega + i\eta}\,, \quad \omega = v\cdot l\,, \quad \eta > 0\,, \tag{3.23}$$

where the nucleon four-velocity is given by v_μ and l_μ is the momenta of the pions in the theory. In this effective theory the Feynman insertion for the emission of a pion with momentum l from a nucleon is

$$\frac{g_A}{F_\pi}\tau^a S\cdot l\,, \tag{3.24}$$

where S is the covariant spin operator, with the anti-commutation relation

$$\{S_\mu, S_\nu\} = \frac{1}{2}(v_\mu v_\nu - g_{\mu\nu})\,. \tag{3.25}$$

Consider the case of a nucleon that emits a pion of momentum l, which is re-absorbed some time later. The mass shift δm is

$$\delta m = i\frac{3g_A^2}{F_\pi^2}\int \frac{d^dl}{(2\pi)^d}\frac{i}{l^2 - M_\pi^2 + i\eta}\frac{i}{-v\cdot l + i\eta} S\cdot(-l)\, S\cdot l\,, \tag{3.26}$$

where we have used the identity $\tau^a\tau^a = 3$. We use the property of the spin operator, Eq. (3.25), to simplify as

$$S_\mu S_\nu l_\mu l_\nu = \frac{1}{4}\left(v\cdot l\, v\cdot l + M_\pi^2 - l^2 - M_\pi^2\right)\,. \tag{3.27}$$

Thus we may rewrite Eq. (3.26) as

$$\begin{aligned}\delta m \;=\; & i\frac{3g_A^2}{4F_\pi^2}\int \frac{d^dl}{(2\pi)^d}\left[\frac{1}{v\cdot l - i\eta} + \frac{v\cdot l}{M_\pi^2 - l^2 - i\eta}\right. \\ & \left. - \frac{M_\pi^2}{(M_\pi^2 - l^2 - i\eta)(v\cdot l - i\eta)}\right]\,.\end{aligned} \tag{3.28}$$

Under dimensional regularisation it can be shown that the first term in the integral vanishes [46], and the second term also does not contribute as it is odd under $l \to -l$. Thus the integral may be simplified to

$$\delta m = \frac{3g_A^2}{4F_\pi^2} J(0) M_\pi^2 , \tag{3.29}$$

where the following definition has been made

$$J(0) = \frac{1}{i} \int \frac{d^d l}{(2\pi)^d} \frac{1}{(M_\pi^2 - l^2 - i\eta)(v \cdot l - i\eta)} . \tag{3.30}$$

Reference [43] discusses how to simplify this expression. The details do not add to discussion presented here and we just take the solution as

$$J(0) = -\frac{M_\pi}{8\pi} . \tag{3.31}$$

Substituting into Eq. (3.29) we see that the leading non-analytic contribution to the mass of the nucleon from the pion loop (to one loop order) is given by

$$\delta m = -\frac{3g_A^2}{32\pi} \frac{M_\pi^3}{F_\pi^2} . \tag{3.32}$$

3.2.2 Next-To-Leading Non-Analytic Contribution to the N mass

The work of Lebed [44] follows an alternative approach to deriving an effective chiral Lagrangian. This common method relies on creating an SU(3) matrix, $U = e^{i\Pi/f}$, from some field Π, and defining the effective Lagrangian as a series of terms with an increasing number of derivatives of U:

$$\mathcal{L}_{\text{eff}} = \mathcal{L}_{\text{eff}}^{(2)} + \mathcal{L}_{\text{eff}}^{(4)} + \dots , \tag{3.33}$$

where $\mathcal{L}_{\text{eff}}^{(n)}$ contains terms with n derivatives. Lorentz invariance requires the Lagrangian contain only terms with an even number of derivatives. Each of the terms

in the series contains both a chirally symmetric part and a symmetry breaking piece. For example the first term in Eq. (3.33) would have the form

$$\mathcal{L}_{\text{eff}}^{(2)} = \frac{f^2}{4}\text{Tr}\left[\partial_\mu U \partial^\mu U^\dagger\right] + \frac{\kappa}{2} f^2 \text{Tr}\left[\mathcal{M}(U + U^\dagger)\right] , \tag{3.34}$$

where $\mathcal{M}$ is the quark mass matrix.

As discussed above it is the octet that generates the leading non-analytic contribution to the self-energy of the nucleon. The next-to-leading non-analytic contribution is introduced by extending the formalism to include the baryon decuplet with non-degenerate masses. The correction to the baryon mass [44] is of the form

$$\delta m_B \sim \frac{m_\Pi^4}{16\pi^2 f_\pi^2 \Lambda_\chi} \ln m_\Pi^2 = \mathcal{O}(\mathcal{M}_q^2 \ln \mathcal{M}_q) . \tag{3.35}$$

We note that this term is at the same order as one-loop diagrams in χPT, and thus must be included in any discussion to one-loop order. The proof that this mass correction appears in the Lagrangian at the same order as one-loop diagrams is presented in Lebed [44].

We now have the leading two non-analytic (in quark mass) contributions to the mass of the baryon: Eqs. (3.32) and (3.35). The quark mass, $\mathcal{M}$, expansion of the baryon masses is thus

$$m_N \sim m_0 + \alpha\mathcal{M} + \beta\mathcal{M}^{3/2} + \gamma\mathcal{M}^2 + \xi\mathcal{M}^2 \ln \mathcal{M} + \ldots \tag{3.36}$$

In SU(2) flavour, a more accurate representation of reality, Eq. (3.36) becomes

$$m_N \sim m_0 + \alpha m_\pi^2 + \beta m_\pi^3 + \gamma m_\pi^4 + \xi m_\pi^4 \ln m_\pi^2 + \ldots \tag{3.37}$$

with, as discussed above, the coefficients β and ξ of the non-analytic contributions known explicitly.

3.3 Summary

The theory of the strong interaction, QCD, whilst being elegant in construction is none-the-less constructed in terms of degrees of freedom that make simple comparison with experiment impossible. An effective field theory, will be representative of QCD in some region, by constructing it about the symmetries of the larger theory. If quarks were massless, chiral symmetry would be exact in QCD. As the masses of the u and d quarks are so small this approximate symmetry is good to a few percent observationally. Whilst for the heavier strange quark the approximation is not so good. This approximate symmetry allows the construction of χPT, an effective theory which is equivalent to QCD at low energy, but fashioned from mesons and baryons.

The effective field theory, χPT, at low energy and small quark mass reveals the behaviour of the strong interaction in a more accessible way than QCD. Properties of the baryons, and in particular the quark mass dependence of these properties, are able to be extracted. Of particular interest for this work is the prediction of the leading and next-to-leading non-analytic (in quark mass) contributions to the self-energy of the nucleon, and the model independent results for the coefficients of these terms. Whilst we do not present the details here, there are analogous results for the Δ and ρ meson. In the subsequent work we shall be using this known non-analytic behaviour as well as the known coefficients to constrain the extrapolation of lattice QCD results rear the chiral limit.

The caveat that accompanies the χPT results is simple. Chiral symmetry is *only* a viable concept for massive fermions whilst the energy scale of the system is much larger than the eigenvalues of the quark mass matrix, but much less than the mass of the resonances, like the ρ meson.

Chapter 4

The Cloudy Bag Model

The opposite of a correct statement is a false statement. But the opposite of a profound truth may well be another profound truth.

NIELS BOHR

One of the observed properties of nature is quark confinement. Any model or theory describing hadrons needs to include this property. The MIT bag model evolved from a model developed by Bogolubov [47] in the late 1960's. This model was created in an attempt to phenomenologically describe confined, relativistic quarks in a finite region of space. Bogolubov considered the simplest case: a massless Dirac particle, moving freely within a spherical volume of radius R, surrounded by an attractive scalar potential. Bogolubov enforced confinement in the model by setting the potential equal to the quark mass and taking the limit of infinitely massive quarks. The phenomenological restrictions on Bogolubov's model resulted in the non-conservation of energy-momentum. This catastrophic failure of the model resulted in an improved model, which would obey energy-momentum

conservation.

4.1 The MIT Bag Model

The MIT bag model, developed in the mid 1970's, had composite hadrons constructed from light quarks moving freely inside a restricted volume, the bag. Confinement was achieved by constraining the bag to have a positive energy per unit volume, B. This Lorentz invariant restriction not only confines the quarks, but allows the internal structure to reproduce the general properties of Bjorken scaling. The simplest case has massless quarks confined in a bag of volume V, with surface S. The Lagrangian density is then

$$\mathcal{L}_{\text{MIT}} = \left(i\overline{\psi}\gamma^{\mu}\partial_{\mu}\psi - B\right)\theta_{\text{V}} - \frac{1}{2}\overline{\psi}\psi\delta_{\text{S}}\,, \tag{4.1}$$

where θ_{V} is defined to be one inside the volume and zero outside, and δ_{S} is a surface delta function. For practical reasons this model is most commonly simplified to the case of a static spherical bag of radius R. The wave function of the confined quarks is [48]:

$$\psi_{n,-1} = \frac{N_{n,-1}}{\sqrt{4\pi}} \begin{bmatrix} j_0\left(\frac{r}{R}\omega_{n,-1}\right) \\ i\vec{\sigma}\cdot\hat{r}j_1\left(\frac{r}{R}\omega_{n,-1}\right) \end{bmatrix} \chi_{-1}\,, \quad r < R\,, \tag{4.2}$$

where χ_{-1} is a Pauli spinor, n is the principal quantum number. The quark eigen frequency, $\omega_{n,\kappa}$, are solutions of

$$j_0(\omega_{n,\kappa}) = j_1(\omega_{n,\kappa})\,, \tag{4.3}$$

where $j_{0,1}$ are Bessel functions, and this is a product of confinement in the Bogolubov model. For example the $1s$ state has $\omega_{1-1} = 2.04$. The normalisation of the wave-function is

$$N^2_{n,-1} = \frac{\omega^3_{n,-1}}{2R^3(\omega_{n,-1}-1)\sin^2(\omega_{n,1})}. \tag{4.4}$$

The action of this model

$$S_{\rm MIT} = \int d^4x\, \mathcal{L}_{\rm MIT}(x) \tag{4.5}$$

is demanded to be stationary under variations of the field ($\psi \to \psi + \delta\psi$) and the bag surface S ($R \to R + \varepsilon$). This gives three constraints on the fields, the Euler-Lagrange equations of motion. The first relationship is the free Dirac equation for massless quarks, inside the bag

$$i\gamma^\mu \partial_\mu \psi = 0. \tag{4.6}$$

The next gives confinement in the bag

$$i\gamma^\mu n_\mu \psi(x) = \psi(x), \quad x \in \mathrm{S}, \tag{4.7}$$

where n_μ is a normal to the surface of the bag and has $n^2 = -1$. Equation 4.7 is known as the linear boundary condition (l.b.c.). We can show that this results in confinement by looking at the hermitian conjugate of Eq. (4.7) (multiplied by an appropriate factor of γ^0)

$$\overline{\psi}(x) = -i\overline{\psi}(x)\gamma^\mu n_\mu. \tag{4.8}$$

At the bag surface the current, $j^\mu = \overline{\psi}\gamma^\mu\psi$, normal to the surface is (up to a factor of $-i$)

$$\begin{aligned} i n_\mu j^\mu &= i n_\mu \overline{\psi}\gamma^\mu\psi \\ &= \left(\overline{\psi} i\gamma^\mu n_\mu\right)\psi = -\overline{\psi}\psi \\ &= \overline{\psi}\left(i\gamma^\mu n_\mu \psi\right) = +\overline{\psi}\psi \\ &= 0. \end{aligned} \tag{4.9}$$

Since there is no component of the quark current normal to the surface, they are confined in the bag. The final relationship is the non-linear boundary condition

(n.l.b.c.)

$$B = -\frac{1}{2} n_\mu \partial^\mu \left(\overline{\psi}(x) \psi(x) \right) = P_D, \quad x \in \mathrm{S}, \tag{4.10}$$

which equates the Dirac pressure of the quarks, P_D, with the vacuum pressure B thereby providing stability.

The model of Bogolubov [47], which forms the basis of the MIT bag model, did not conserve energy-momentum. However the inclusion of the energy density term, B, solves this problem. The energy-momentum tensor can be written as

$$\begin{aligned} T^{\mu\nu}_{\mathrm{MIT}} &= \left(T^{\mu\nu}_D + B g^{\mu\nu} \right) \theta_{\mathrm{V}} & (4.11) \\ &= \left(\frac{i}{2} \overline{\psi} \overleftrightarrow{\not\partial} \psi + B g^{\mu\nu} \right) \theta_{\mathrm{V}}, & (4.12) \end{aligned}$$

where $T^{\mu\nu}_D$ is the energy-momentum tensor for a free Dirac field. The n.l.b.c., Eq. (4.10), ensures that

$$\partial_\mu T^{\mu\nu}_{\mathrm{MIT}} = 0. \tag{4.13}$$

The energy of the lowest level, that is the $1s$-state, is found to be

$$\begin{aligned} E(R) &= \int d^3x \, T^{00} \\ &= \frac{3\omega_{1-1}}{R} + \frac{4\pi}{3} R^3 B. & (4.14) \end{aligned}$$

The first term is the same as it would be found in Bogolubov's model and represents the kinetic energy of the quarks in the bag. The second term is a remnant of the introduction of the bag constant, and is a volume ($\frac{4\pi}{3}R^3$) dependent term. That is, it suggests that an energy BV is required to make the bubble, or bag, in the vacuum.

It is assumed that, in the MIT bag model, the value for B is constant for all hadrons. The implications of this phenomenological addition, mocking up confinement, have been investigated by a number of authors. A different approach is suggested by Jin and Jennings [49], in which a discussion of a density dependent bag constant is undertaken. An alternative comes from Hasenfratz and Kuti [50]

who show that a surface tension term, or a linear combination of the surface tension and the bag constant, can produce results similar to those found for the MIT model. However by making this assumption we may investigate excited states directly.

4.1.1 Excited States and Radius Determination

The above calculation is only for quarks in the ground state. A theory allowing only non-excited quarks would be both naïve, and not much use in real calculations. Fortunately generalising Eq. (4.14) to include excited states is straight forward:

$$E(R) = \sum_i \frac{\omega_i}{R} + \frac{4\pi}{3} R^3 B. \tag{4.15}$$

Applying the n.l.b.c., Eq. (4.10) to the above equation leads to the following relationship

$$\frac{\partial E(R)}{\partial R} = 0 \tag{4.16}$$

$$= -\sum_i \frac{\omega_i}{R^2} + 4\pi R^2 B. \tag{4.17}$$

Initially a fit to some data is needed to determine B, but from that point the internal energy of the quarks determine the radius R of the bag uniquely. Solving for R we find it is given by

$$R^4 = \sum_i \frac{\omega_i}{4\pi B}.$$

Using this definition of R, Eq. (4.15) can be simplified as

$$E(R) \equiv E = \frac{4}{3}(4\pi B)^{1/4} \left(\sum_i \omega_i \right)^{3/4} \tag{4.18}$$

Further refinements were undertaken by the MIT team, including looking at the *hyperfine structure* leading to a spin-dependent one gluon exchange term. They also investigated how the *zero point* energy of the fields, and how *centre of mass*

corrections effected the mass. The details are beyond this work and we refer the reader to Ref. [48] for a full review of these refinements. A final improvement the MIT team included was non-zero quark mass, which we discuss below.

4.1.2 Massive Quarks

The discussion to this point has been purely for massless quarks. However, if the model is to be compared to the experimental observations, massless quarks are a problem. Under $SU(3)$ flavour symmetry the members of the octet containing the nucleon would all have degenerate mass. This is obviously not so. A natural solution to this discrepancy is to assign a non-zero mass to the strange quark, as discussed below.

Introducing a strange quark mass to the Dirac equation for the MIT bag model as simple as

$$\left(-i\gamma^{\mu}\nabla_{\mu} + \gamma^{0}E + m\right)\psi(r) = 0.$$

Solving this for the wave function in the $1s$ state results in the solution

$$\psi(\vec{r}) = \frac{N}{\sqrt{4\pi}} \begin{bmatrix} \alpha_{+}\, j_0\left(\frac{xr}{R}\right) \\ \alpha_{-}\, i\vec{\sigma}\cdot\hat{r}\, j_1\left(\frac{xr}{R}\right) \end{bmatrix} \chi_{-1}\,. \tag{4.19}$$

with the quark energy, E, and normalisation constant, N, related to the spatial eigen frequency, x, by

$$E = \frac{\Omega}{R} \quad \Omega = \sqrt{x^2 + (mR)^2}\,, \tag{4.20}$$

and

$$N^2 = \frac{\Omega(\Omega - mR)}{R^3 j_0^2(x)\left[2\Omega(\Omega-1) + mR\right]}\,.$$

Applying the l.b.c. to Eq. (4.10) it can be seen that the eigen frequency, x, satisfies:

$$\tan(x) = \frac{x}{1 - mR - \Omega},$$

and the coefficients $\alpha_{\pm}$ are given by $\sqrt{(E \pm m)/E}$.

Introducing all the above elements into a mass formula for the MIT bag model results in the following equation

$$M(R) = \sum_i \frac{\omega_i}{R} + \frac{4\pi}{3} B R^3 + \nabla E_g^M - \frac{Z}{R} . \tag{4.21}$$

The final two terms in the above expression are respectively the spin-dependent one gluon exchange interaction, and a consolidation of the zero point energy and centre of mass energies. There are four parameters in this formula to be determined: the mass of the strange quark m_s, the bag constant B, and the parameters describing the one gluon exchange and centre of mass corrections, α_c and Z respectively. The last two parameters relate to the last 2 terms in the above formula. For a further description of the last two terms the reader is directed to Refs. [48, 51].

4.1.3 Charge Current Conservation

Conserved currents are readily calculated from the Lagrangian density given in Eq. (4.1). This is achieved using Noether's theorem which states simply that for each symmetry of the Lagrangian there exists a conserved quantity. It is entirely analogous to the procedure used in chapter 3. We return to the massless case for this discussion to simplify the calculations.

Consider the following gauge transformation to give the simplest possible example of a conserved current:

$$\begin{aligned} \psi(x) &\rightarrow \psi(x) + i\varepsilon\psi(x), \\ \overline{\psi}(x) &\rightarrow \overline{\psi}(x) - i\varepsilon\overline{\psi}(x) . \end{aligned} \tag{4.22}$$

It is a trivial exercise to see that Eq. (4.1) is invariant under this transformation. There are only terms of the form $\overline{\psi}\psi$ in $\mathcal{L}$ which transform as

$$\overline{\psi}\psi \rightarrow \overline{\psi}\psi - i\varepsilon\overline{\psi}\psi + i\varepsilon\overline{\psi}\psi + \mathcal{O}(\varepsilon^2) = \overline{\psi}\psi . \tag{4.23}$$

Therefore, from Noether's theorem, there exists a conserved current

$$j^{\mu} = \frac{i}{2}\overline{\psi}(x)\gamma^{\mu}\left[i\psi(x)\right]\theta_{\mathrm{V}} - \frac{i}{2}\left[-i\overline{\psi}(x)\right]\gamma^{\mu}\psi(x)\theta_{\mathrm{V}}\,, \tag{4.24}$$

which, up to a relative minus sign, is

$$j^{\mu} = \overline{\psi}(x)\gamma^{\mu}\psi(x)\theta_{\mathrm{V}}, \tag{4.25}$$

the exact result used to show confinement in the MIT bag model. The charge distribution, j^0, and magnetic moment, $\vec{j}$, are simply evaluated from the above expression.

4.1.4 Isospin Conservation

Another symmetry may be obtained by making an arbitrary, infinitesimal rotation, with $\vec{\varepsilon}$ constant, in isospin:

$$\begin{aligned} \psi &\rightarrow \psi + i\left(\vec{\tau}\cdot\vec{\varepsilon}/2\right)\psi\,, \\ \overline{\psi} &\rightarrow \overline{\psi} - i\overline{\psi}\left(\vec{\tau}\cdot\vec{\varepsilon}/2\right)\,. \end{aligned} \tag{4.26}$$

Once again since $\mathcal{L}$ is invariant there is a conserved current, this time isospin $\vec{I}^{\mu}$:

$$\vec{I}^{\mu}(x) = \overline{\psi}\gamma^{\mu}\left(\vec{\tau}/2\right)\psi\,. \tag{4.27}$$

It must also be noted that since isospin is a conserved quantity, $\partial_{\mu}\vec{I}^{\mu} = 0$, the total isospin of the bag, $\vec{t}$, given by the integral of the isospin density

$$\vec{t} = \int d^3x\,\vec{I}^{0}(x)\,, \tag{4.28}$$

is also a constant of the motion.

4.1.5 Axial Current Non-conservation

One can extend the symmetry of Eq. (4.26) by introducing explicit dependence on the quarks helicity. This is simply achieved by introducing the chirality operator γ_5 as such:

$$\begin{aligned} \psi &\rightarrow \psi - i\,(\vec{\tau}\cdot\vec{\varepsilon}/2)\,\gamma_5\psi\,, \\ \overline{\psi} &\rightarrow \overline{\psi} - i\overline{\psi}\gamma_5\,(\vec{\tau}\cdot\vec{\varepsilon}/2)\,, \end{aligned} \tag{4.29}$$

resulting in the Lagrangian density transforming like

$$\begin{aligned} \mathcal{L} \rightarrow\ & \mathcal{L} + \frac{1}{2}\overline{\psi}\,(\gamma_5\gamma^\mu + \gamma^\mu\gamma_5)\overset{\leftrightarrow}{\partial}_\mu\,(\vec{\tau}\cdot\vec{\varepsilon}/2)\;\psi\,\theta_{\mathrm{V}} \\ & + \frac{i}{2}\overline{\psi}\vec{\tau}\cdot\vec{\varepsilon}\psi\delta_{\mathrm{S}}\,. \end{aligned} \tag{4.30}$$

The application of Eq. (A.11) makes it clear that the second term in this expression vanishes, but equally as obvious is the fact that the last term does not. A conserved current as defined by Noether's theorem requires that the Lagrangian density be invariant under a transformation. For the transformation given in Eq. (4.29) the Lagrangian is not invariant, and so Noether's theorem does not apply. The axial current associated with the transformations in Eq. (4.29) is

$$\vec{A}^\mu(x) = \overline{\psi}\gamma^\mu\gamma_5\,(\vec{\tau}/2)\,\psi\theta_{\mathrm{V}}, \tag{4.31}$$

and an alternative method of showing that this is not a conserved current is through the divergence

$$\partial_\mu\vec{A}^\mu = -\frac{i}{2}\overline{\psi}\gamma_5\vec{\tau}\psi\delta_{\mathrm{S}} \neq 0\,. \tag{4.32}$$

The last term in Eq. (4.30) is a surface term, is known as "*chirally odd*", and implies a violation of chiral symmetry. Physically one may visualise confinement as resulting in a reflection of the quark at the bag boundary. However there is no resultant spin-flip of the quark, thus there is a effective change in the chirality, as

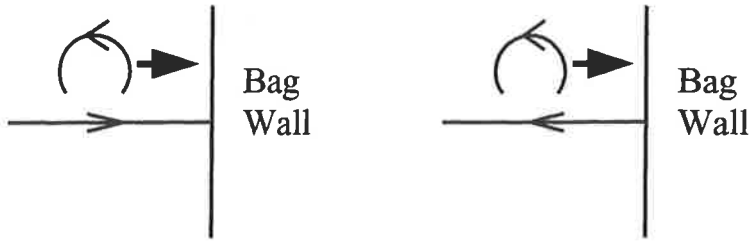

Figure 4.1: Violation of chiral symmetry at the bag surface [48].

illustrated in Fig. 4.1. This is in violation of the PCAC (Partially Conserved Axial Current) hypothesis of Gell-Mann and Lévy and Nambu [37, 36]. Chiral symmetry may be restored by the introduction of a Goldstone boson, as we shall explore in the Cloudy Bag Model next.

4.2 Description of the CBM

It is apparent that the MIT bag describes reasonably well the valence structure of the nucleon. There is however the problem of chiral symmetry violation. Chiral perturbation theory was discussed in chapter 3, and it is clear the objects of χPT — the pions — are missing from the formulation of the MIT bag model. The introduction of pions which may move freely through the bag, couple to the quarks at the surface, and only modify the bag perturbatively, are fundamental to an understanding of nuclear structure. This concept of a "*pion cloud*" surrounding and permeating the hadrons crystallised into the Cloudy Bag Model (CBM) of Théberge, Thomas and Miller [48, 52, 53]. The inclusion of pions to the MIT model to form the CBM is as simple as

$$\mathcal{L}_{\rm CBM} \cong \mathcal{L}_{\rm MIT} + \mathcal{L}_{\pi} + \mathcal{L}_{\rm int}\,, \tag{4.33}$$

where $\mathcal{L}_\pi$ is the Lagrangian density for free pions, and all the interactions between the bag and pions is contained in the term $\mathcal{L}_{\text{int}}$. The act of truncating this expression results in a reduction of chiral symmetry in the model to an approximate symmetry, however at the order we discuss we retain the leading and next-to-leading non-analytic terms from χPT, which as we shall show later are the two most important contributions in an extrapolation form. Retaining only terms to the second order in pion field, the linearised CBM is

$$\begin{aligned}\mathcal{L}_{\text{CBM}} \cong & \left(i\overline{\psi}\gamma_\mu\partial^\mu\psi - m\overline{\psi}\psi - B\right)\theta_{\text{V}} - \frac{1}{2}\overline{\psi}\psi\delta_{\text{S}} \\ & + \frac{1}{2}\left(\partial_\mu\pi\right)^2 - \frac{1}{2}m_\pi^2\pi^2 - \frac{i}{2f_\pi}\overline{\psi}\gamma_5\frac{\vec{\tau}}{2}\psi\cdot\vec{\pi}\delta_{\text{S}}\,. \end{aligned} \tag{4.34}$$

This linearised version of the CBM is required as the general, non-linear, case contains sets of highly non-linear equations [54] which are extremely difficult or possibly impossible to solve directly. Linearising the model has introduced two constraints into the system. Firstly there is the constraint that there are not "*too many*" pions in the air at one time. Mathematically this may be stated that the first order expansion of the (non-linear) Lagrangian density is adequate to describe the system. Secondly that the quark wave-functions are not perturbed by the pion field. This at first seems an unusual statement. The pions are themselves hadrons, and so constructed of quarks. In the CBM the pion is considered elementary, and in the low energy (long wavelength) region in which this model is applied, the internal structure of the pion may indeed be neglected. If we apply the treatment of Sec. 4.1.5 now to Eq. 4.34 we find that the axial current becomes

$$\vec{A}^\mu = \frac{1}{2}\overline{\psi}\gamma^\mu\gamma_5\vec{\tau}\psi\theta_{\text{V}} + f_\pi\partial^\mu\vec{\pi}\,, \tag{4.35}$$

and the divergence is exactly what is predicted by PCAC

$$\partial_\mu\vec{A}^\mu = -f_\pi m_\pi^2\vec{\pi} + \mathcal{O}\left(\vec{\pi}^2\right)\,. \tag{4.36}$$

4.2.1 Coupling Constants

The form of the Hamiltonian for the CBM is simple to write down from Eq. (4.33). Since there is a clean separation of MIT model, free pion, and pion–bag interaction, it is not surprising that the Hamiltonian has a similar break-down. If a bag model state is created by the operator $B^\dagger$ (an SU(6) spin-isospin bag state B is created, $|B\rangle = B^\dagger|0\rangle$, where $B^\dagger$ can be written in terms of products of three quark creation operators) we may write the Hamiltonian of the CBM as [51]:

$$\begin{aligned} H &= H_{\rm MIT} + H_\pi + H_{\rm int} && (4.37)\\ &= \sum_B \varepsilon_B B^\dagger B + \sum_k w_k a_k^\dagger a_k + \sum_{B,\tilde{B},k} \left[\tilde{B}^\dagger B a_k v_k^{\tilde{B}B} + \text{h.c.}\right], && (4.38)\end{aligned}$$

where the creation operator $a_k^\dagger$ creates a pion with momentum $\vec{k}$ and isospin i (we follow the convention of [51] and define $k = \{\vec{k}, i\}$ for simplicity), and w_k is the energy of the pion $\sqrt{k^2 + m_\pi^2}$. The matrix element for the pions coupling to baryon states is given by [51, 48]:

$$v_{\vec{k},j}^{\tilde{B}B} = \frac{i}{2f_\pi}\frac{1}{\sqrt{2w_k}} \int d^3r\, e^{-i\vec{k}\cdot\vec{r}}\delta(r-R)\langle\tilde{B}|\overline{\psi}(\vec{r})\gamma_5\tau_j\psi(\vec{r})|B\rangle\,. \qquad (4.39)$$

This expression allows the calculation of all the $\tilde{B}B\pi$ vertices within the CBM.

The $NN\pi$ Vertex

The simplest vertex we consider calculating in the model is the $NN\pi$ vertex. In this case all the quarks in the initial and final states are in the $1s_{1/2}$ orbital excitation and thus we may use the result of Eq. (4.2):

$$\begin{aligned} \overline{\psi}_{1,-1}(\vec{r})\gamma_5\psi_{1,-1}(\vec{r})\big|_{r=R} &= \frac{N_{1,-1}^2}{4\pi} 2ij_0(\omega)j_1(\omega)\vec{\sigma}\cdot\hat{r} && (4.40)\\ &= \frac{\Omega}{\Omega-1}\frac{i}{4\pi R^3}\vec{\sigma}\cdot\hat{r}\,, && (4.41)\end{aligned}$$

where we have assumed, for simplicity, massless quarks. Substituting this result into Eq. (4.39) we see

$$v_{\vec{k},i}^{N'N} = \frac{i}{2f_\pi}\frac{1}{\sqrt{2w_k}}\frac{\Omega}{\Omega-1}\frac{j_1(kR)}{kR} \times \left\langle N' \left| \sum_{q=1}^{3} \tau_{qi}\vec{\sigma}_q \cdot \vec{k} \right| N \right\rangle , \tag{4.42}$$

and we have evaluated the angular integral using the result [54]:

$$\int d\Omega\, \vec{\sigma}\cdot\hat{r}\, e^{-i\vec{k}\cdot\vec{r}} = -\frac{4\pi i\vec{\sigma}\cdot\vec{k}\, r}{3}\left[j_0(kR) + j_2(kR)\right] . \tag{4.43}$$

We define the form factor for the CBM to be

$$\begin{aligned} u(k) &= j_0(kR) + j_2(kR) \\ &\equiv 3j_1(kR)/kR . \end{aligned} \tag{4.44}$$

Note that this form factor appears naturally in the model, as the outcome of including the baryon internal structure. Finally, it may be shown that the axial coupling to the bag is given by [48]:

$$g_A^{\text{Bag}} = \frac{5}{9}\frac{\Omega}{\Omega-1} . \tag{4.45}$$

Comparison of the result of Eq. (4.42) with the usual $NN\pi$ coupling gives the relationship

$$\frac{g_{\pi NN}}{2M_N} = \frac{g_A}{2f_\pi} . \tag{4.46}$$

This is the Goldberger–Treiman relation and thus means one may evaluate the $NN\pi$ coupling consistently within the CBM.

Additional Vertices

In an analogous way to that presented above, the pion coupling between any bag model states, $\tilde{B}$ and B, may be calculated. The details of specific calculations are available in [48, 51, 54], and so we just present Table 4.1 from [54] giving the

	$f_0^{\tilde{B}B}/f_Q$	B N	Δ	Λ	Σ	Σ^*	Ξ	Ξ^*
	N	5	$4\sqrt{2}$	0	0	0	0	0
	Δ	$2\sqrt{2}$	5	0	0	0	0	0
	Λ	0	0	0	$2\sqrt{3}$	$2\sqrt{6}$	0	0
$\tilde{B}$	Σ	0	0	-2	$4\sqrt{6}/3$	$-4\sqrt{3}/3$	0	0
	Σ^*	0	0	2	$2\sqrt{6}/3$	$2\sqrt{30}/3$	0	0
	Ξ	0	0	0	0	0	-1	$-2\sqrt{2}$
	Ξ^*	0	0	0	0	0	2	$\sqrt{5}/3$

Table 4.1: The $\tilde{B}B\pi$ bare coupling constants $f_0^{\tilde{B}B}/f_Q$. The value of $f_0^{\tilde{B}B}$ is calculated in an analogous manner to Eq. (4.42). The bare coupling f_Q has a value of approximately 0.49, however it is unimportant in the context of this work as we shall always be taking the ratio of coupling constants. The results are from [54].

$\tilde{B}B\pi$ bare coupling constants for the SU(3) flavour, baryon octet and decuplet. An extension to $\mathrm{SU}(3)_L \times \mathrm{SU}(3)_R$ would allow the evaluation of kaon couplings in an equivalent manner.

4.2.2 The Physical Nucleon

It is clear in Eq. (4.38) that a physical hadron in this definition consists of a valence quark core "*dressed*" by a cloud of pions. In particular the CBM Hamiltonian has an eigenstate, the physical nucleon, with eigenvalue M_N:

$$H|\tilde{N}\rangle = M_N|\tilde{N}\rangle\,. \tag{4.47}$$

In first order perturbation theory the nucleon is given by the following states

$$|\tilde{N}\rangle = \sqrt{Z}\left\{|N\rangle + \sum_{B,k}\frac{\langle B\pi_k|H_{\mathrm{int}}|N\rangle}{M_N - w_k - M_B}|B\pi_k\rangle\right\} \tag{4.48}$$

$$\cong \sqrt{Z}|N\rangle + c|N\pi\rangle + c'|\Delta\pi\rangle\,. \tag{4.49}$$

4.2.3 Hadron Masses

The shift in the mass of the nucleon, to lowest non-trivial order is given by the two processes shown in Fig. 4.2(a,b). This corresponds to the second order of $H_{\rm int}$:

$$\begin{aligned} M_N &= M_N^{(0)} - \frac{3}{16\pi^2 f_\pi^2} g_A^2 \int_0^\infty dk \frac{k^4 u_{NN}^2(k)}{w^2(k)} \\ &\quad - \frac{3}{16\pi^2 f_\pi^2} \frac{32}{25} g_A^2 \int_0^\infty dk \frac{k^4 u_{N\Delta}^2(k)}{w(k)(\Delta M + w(k))} , \end{aligned} \tag{4.50}$$

where $\Delta M = M_\Delta^{(0)} - M_N^{(0)}$ and we have related the $N \to \Delta\pi$ coupling to g_A through the use of the SU(6) relation. To simplify this, and following calculations

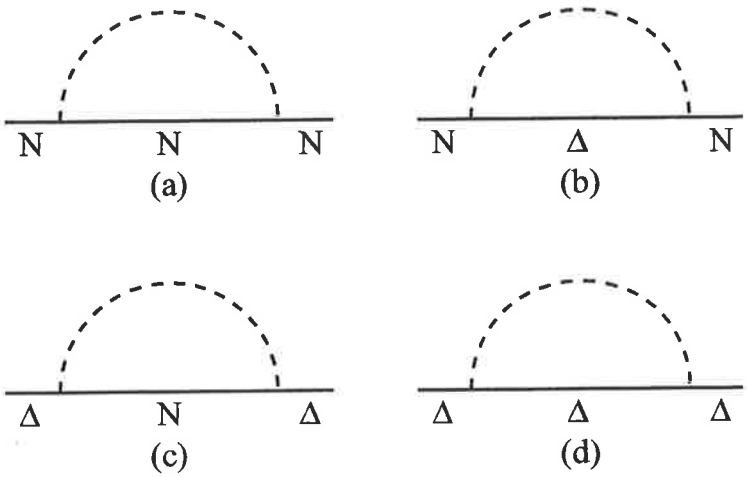

Figure 4.2: The processes that contribute in the lowest, non-trivial, order to the shift in the mass of the nucleon and Δ.

in this work, we have made a static approximation for the propagator of the heavy baryon. The correct chiral behaviour as $m_\pi \to 0$ is nevertheless preserved in this approximation. The leading non-analytic behaviour in the quark mass ($m_\pi \sim \sqrt{m_q}$) arising from Fig. 4.2(a) is:

$$\delta M_N^{\rm LNA} = -\frac{3}{32\pi f_\pi^2} g_A^2 m_\pi^3 , \tag{4.51}$$

as indicated by χPT. Equivalently the mass of the Δ, with self-energy corrections corresponding to Fig. 4.2(c,d), may be calculated:

$$\begin{aligned} M_\Delta &= M_\Delta^{(0)} - \frac{3}{16\pi^2 f_\pi^2} g_A^2 \int_0^\infty dk \frac{k^4 u_{\Delta\Delta}^2(k)}{w^2(k)} \\ &\quad + \frac{3}{16\pi^2 f_\pi^2} \frac{8}{25} g_A^2 \int_0^\infty dk \frac{k^4 u_{N\Delta}^2(k)}{w(k)(\Delta M - w(k))} \,. \end{aligned} \tag{4.52}$$

The factors of $32/25$ and $8/25$ in Eqs. (4.50) and (4.52) are a result of SU(6) symmetry and may be understood from the discussion in Sec. 4.2.1, and particular the results presented in Table 4.1. The coupling of a $N \to \Delta\pi$ is given by

$$\begin{aligned} f_{N\Delta\pi}^2 &= \left(\frac{f_{N\Delta\pi}^2}{f_{NN\pi}^2} \right) f_{NN\pi}^2 \\ &= \frac{32}{25} f_{NN\pi}^2 \,, \end{aligned} \tag{4.53}$$

and equivalently for the case of $\Delta \to N\pi$:

$$\begin{aligned} f_{\Delta N\pi}^2 &= \left(\frac{f_{\Delta N\pi}^2}{f_{NN\pi}^2} \right) f_{NN\pi}^2 \\ &= \frac{8}{25} f_{NN\pi}^2 \,. \end{aligned} \tag{4.54}$$

Thus we are able to rewrite couplings of the form $\tilde{B}B\pi$ as a constant times the bare $NN\pi$ coupling, which is known from the Goldberger–Treiman relation.

We have plotted the masses of the nucleon (circles) and Δ (triangles), Eqs. (4.50) and (4.52) respectively, in Fig. 4.3 as a function of pion mass. Rather than using the Bessel function form factor, Eq. (4.44), we have chosen a phenomenological dipole form:

$$u(k) = \left(\frac{\Lambda^2 - \mu_\pi^2}{\Lambda^2 + k^2} \right) \,, \tag{4.55}$$

where $\Lambda = 1.0$ GeV and μ_π is the physical pion mass, as the form factor for the calculation. The justification for such a choice will be explored in subsequent chapters. It is clear that the non-analytic behaviour introduced by the pions coupling to

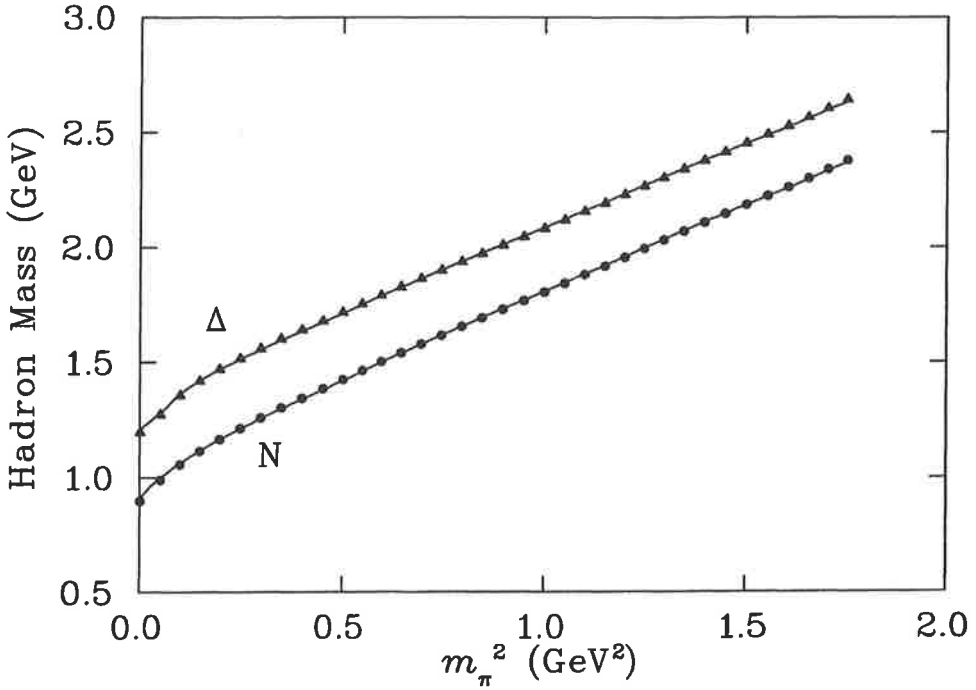

Figure 4.3: The pion mass dependence of the N (circles) and Δ (triangles) baryons generated in the CBM using a dipole form factor with $\Lambda = 1.0$ GeV. Fits of Eqs. (4.56) and (4.57) using a θ-function cut-off to the CBM results are illustrated by the curves.

other states than the bare bag is quickly suppressed, resulting in, an almost linear increase in both the N and Δ masses. We have attempted a fit to this data with the forms

$$M_N = c_0 + c_2 m_\pi^2 + \sigma_N(\Lambda, m_\pi)\,, \tag{4.56}$$

$$M_\Delta = \tilde{c}_0 + \tilde{c}_2 m_\pi^2 + \sigma_\Delta(\tilde{\Lambda}, m_\pi)\,, \tag{4.57}$$

where the σ_i represent the self-energy terms presented in Eqs. (4.50) and (4.52), with the particular choice of a θ-function cut-off. The motivation and derivation of such a form is discussed in the following chapters. It is not surprising that our simple three parameter phenomenological fitting functions, shown as the solid lines in Fig. 4.3 (evaluated with a θ-function cut-off), can reproduce N and Δ masses

calculated within the CBM (evaluated with a dipole form factor). It is not entirely unexpected that this agreement extends even to the non-analytic curvature at small pion masses. However, as the correct chiral behaviour of the baryons is being respected by the additional self-energy terms, it suggests that this method should also provide a reliable form for extrapolating lattice data into the region of small pion mass.

4.3 Summary

The Cloudy Bag Model is a natural extension of χPT. In the chiral limit it reproduces the results of χPT, whilst allowing a smooth transition to heavier quark masses. A form factor appears naturally in the formalism, mocking up the higher order terms introduced by the internal structure of the hadron. As the CBM may be applied across a wide range of m_π it is used to give insight as to the behaviour of hadron masses between the limits of χPT ($m_\pi \sim 139$ MeV) and lattice QCD calculations ($m_\pi \gg 139$ MeV). We use this direction in the subsequent chapters.

Chapter 5

The Rho Meson

A little learning is a dangerous thing;
Drink deep, or taste not the Pierian Spring:
There shallow draughts intoxicate the brain,
And drinking largely sobers us again.
ALEXANDER POPE, "ESSAY ON CRITICISM"

As the lightest vector meson, the ρ is of fundamental importance in the task of deriving hadron properties from QCD. As was mentioned in chapter 2, within lattice QCD the ratio of π to ρ masses is often used as a measure of the approach to the chiral limit. Until quite recently lattice calculations have been restricted to values of m_π/m_ρ above 0.8. As was mentioned in chapter 2 because of the remarkable improvements in actions, algorithms and computing power, there are now lattice QCD results with dynamical fermions available for hadron masses with current quark masses such that m_π/m_ρ is entering the chiral regime. Nevertheless, in order to compare with the properties of physical hadrons it is still necessary to extrapolate the results to realistic quark masses [55].

We show in this, and following chapters, that a formal expansion of hadron

properties in terms of m_π fails to converge up to the region where lattice data exists. The crucial physics insight which renders an accurate chiral extrapolation possible is that the source of the pion field is a complex system of quarks and gluons, with a finite size characterised by a scale Λ. When the pion mass is greater than Λ, so that the Compton wavelength of the pion is smaller than the extended source, pion loops are suppressed as powers of m_π/Λ and hadron properties are smooth, slowly varying functions of the quark mass. However, for pion Compton wavelengths bigger than the source ($m_\pi < \Lambda$) one sees rapid, non-linear variations. Phenomenologically this transition occurs at $m_\pi \sim 500$ MeV, or m_π/m_ρ around 0.5 – the region now being addressed by lattice simulations with dynamical fermions.

Another difficulty associated with the extrapolation of lattice results that is investigated, in part, is the discretisation of momenta inherent in all lattice calculations. In this regard we mention not only the finite lattice spacing but the fact that there is a minimum possible non-zero momentum available because of the finite volume of the lattice. This issue is absolutely critical to the interpretation of the recent CP-PACS data for dynamical fermions [20], in which a first result[1] is reported at $m_\pi/m_\rho \sim 0.4$. As we explain in detail, the only reason that it is possible to measure the ρ mass there is that the calculation is done in a finite volume. We show that taking the finite lattice size and finite lattice spacing into account is a necessary requirement when extrapolating to the physical region. These effects become especially significant for the case of the ρ meson which has a p-wave, two-pion decay mode.

In the next section we summarise the key physical ideas and the necessary formulas for extrapolating the mass of the ρ meson to the physical pion mass. This includes a discussion of the limiting behaviour at small and large quark mass. We

[1] Although CP-PACS finds no evidence of residual errors for the lowest mass point, they caution that it is premature to draw firm conclusions based on the present low statistics.

then show the result of our fitting procedure and analyse the uncertainty in extracting the ρ mass at the physical point. We show that a factor of 10 increase in the number of gauge field configurations at the lowest quark mass presently accessible would be sufficient to determine the physical ρ mass to within 5%. We also discuss the consequences of this analysis for the J-parameter and the $\rho\pi\pi$ phase shift. The successes of the work presented in this chapter are used as additional motivation for investigations into the baryon sector presented in the next chapter.

5.1 Extrapolation Formula

The successful extrapolation of the Cloudy Bag Model (CBM) model results discussed in chapter 4 are used to motivate a functional form. The CBM calculations indicate that an extrapolation based upon the inclusion of the self-energy contributions that vary the most rapidly with the quark mass near the chiral limit is required to accurately model the data.

The formal solution to the Dyson-Schwinger equation for the ρ propagator places the self-energy contributions in the denominator of the propagator and thereby modifies the ρ mass as [56] :

$$\begin{aligned} m_\rho &= \sqrt{m_0^2 + \Sigma^\rho} \\ &\approx m_0 + \frac{\Sigma^\rho}{2m_0}, \end{aligned} \tag{5.1}$$

where m_0 is the bare mass and Σ^ρ is the self-energy of the ρ-meson.

As has been discussed previously, lattice data at large m_π (that is, up to around 1 GeV) behaves linearly in m_π^2. Figure 5.1 shows this linear fit to the ρ-meson lattice results for $m_\pi^2 > 0.2$ GeV^2. Guided by the lattice data, we take m_0 to be analytic in the quark mass:

$$m_0 = c_0 + c_2 m_\pi^2 . \tag{5.2}$$

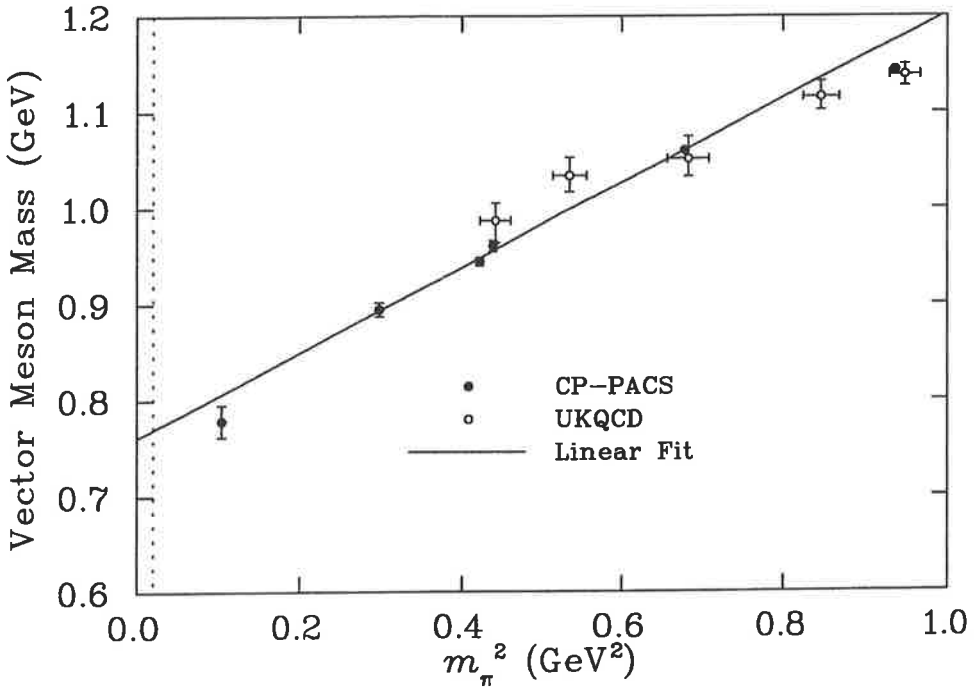

Figure 5.1: Vector (ρ) meson mass from CP-PACS [20] (filled circles) and UKQCD [21] (open circles) as a function of m_π^2. The linear (in m_π^2) fit is to the CP-PACS results for data having $0.2\,\mathrm{GeV}^2 \leq m_\pi^2 \leq 0.8\,\mathrm{GeV}^2$.

5.1.1 Self-Energy Contributions

For the case of the ρ meson the self-energy contributions that vary the most rapidly in the quark mass near the chiral limit are given by the $\rho \to \pi\omega$ and $\rho \to \pi\pi$ processes shown in Fig. 5.2. We will show below that these two terms yield the leading non-analytic (LNA) and next-to-leading non-analytic (NLNA) behaviour in the mass of the ρ meson, as predicted by χPT. Thus we define Σ^ρ in Eq. (5.1) to be

$$\Sigma^\rho = \Sigma^\rho_{\pi\pi} + \Sigma^\rho_{\pi\omega}\,.$$

Naturally there are other meson intermediate states that contribute to the self-energy, however these are suppressed by large mass terms in the denominators of the propagators, and also by smaller couplings. Most importantly, as these processes will

not vary rapidly near the chiral limit, they are mocked up in the definition of m_0.

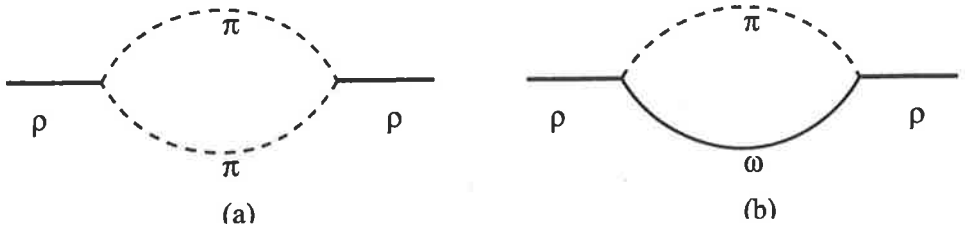

Figure 5.2: The most significant self-energy contributions to the ρ meson mass.

In order to evaluate the self-energy terms that contribute, we take the usual interactions [57, 58]:

$$\mathcal{L}_{\rho\pi\pi} = \frac{1}{2} f_{\rho\pi\pi}\, \vec{\rho}^{\,\mu} \cdot \left(\vec{\pi} \times (\partial_\mu \vec{\pi}) - (\partial_\mu \vec{\pi}) \times \vec{\pi}\right) , \tag{5.3}$$

and

$$\mathcal{L}_{\omega\rho\pi} = g_{\omega\rho\pi}\, \varepsilon_{\mu\nu\alpha\beta} \left(\partial^\mu \omega^\nu\right) \left(\partial^\alpha \vec{\rho}^{\,\beta}\right) \cdot \vec{\pi} \, . \tag{5.4}$$

Using Eq. (A.2) we can rewrite Eq. (5.3) as

$$\mathcal{L}_{\rho\pi\pi} = f_{\rho\pi\pi}\, \varepsilon_{abc} \rho_a^\mu \pi_b \left(\partial_\mu \pi_c\right) \, . \tag{5.5}$$

The Feynman diagram for the $\rho \rightarrow \pi\pi$ self-energy process is shown in Fig. 5.3. We

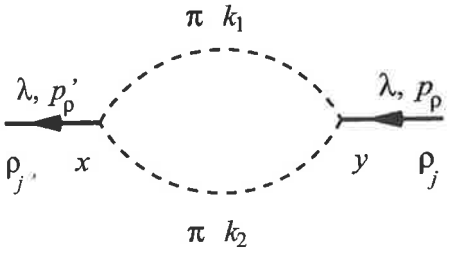

Figure 5.3: Feynman diagram for the $\rho \rightarrow \pi\pi$ self-energy.

follow the conventions of Pichowsky *et al.* [59], where the self-energy contribution

to the mass of the ρ is given by

$$\Pi_{jj'} = \langle \rho_{j'}; p'_\rho, \lambda | \mathrm{T} \left\{ \frac{i^2}{2} \int d^4x\, d^4y \; (f_{\rho\pi\pi}\, \varepsilon_{abc} \rho^\mu_a(x) \pi_b(x)\, (\partial_\mu \pi_c(x))) \right.$$
$$\left. (f_{\rho\pi\pi}\, \varepsilon_{a'b'c'} \rho^\nu_{a'}(y) \pi_{b'}(y)\, (\partial_\nu \pi_{c'}(y))) \right\} | \rho_j; p_\rho, \lambda \rangle \,, \qquad (5.6)$$

which can be simplified to

$$\Pi_{jj'} = -\frac{1}{2} f^2_{\rho\pi\pi} \varepsilon_{abc} \varepsilon_{a'b'c'} \int d^4x\, d^4y \, \langle \rho_{j'}; p'_\rho, \lambda | \mathrm{T} \{ \rho^\mu_a(x) \pi_b(x)\, (\partial_\mu \pi_c(x))$$
$$\rho^\nu_{a'}(y) \pi_{b'}(y)\, (\partial_\nu \pi_{c'}(y)) \} | \rho_j; p_\rho, \lambda \rangle \,. \qquad (5.7)$$

There are four possible Wick contractions for this expression:

$$\langle \rho_{j'}; p'_\rho, \lambda | \rho^\mu_a(x) \pi_b(x) (\partial_\mu \pi_c(x)) \rho^\nu_{a'}(y) \pi_{b'}(y) (\partial_\nu \pi_{c'}(y)) | \rho_j; p_\rho, \lambda \rangle \qquad (5.8)$$

$$\langle \rho_{j'}; p'_\rho, \lambda | \rho^\mu_a(x) \pi_b(x) (\partial_\mu \pi_c(x)) \rho^\nu_{a'}(y) \pi_{b'}(y) (\partial_\nu \pi_{c'}(y)) | \rho_j; p_\rho, \lambda \rangle \qquad (5.9)$$

$$\langle \rho_{j'}; p'_\rho, \lambda | \rho^\mu_a(x) \pi_b(x) (\partial_\mu \pi_c(x)) \rho^\nu_{a'}(y) \pi_{b'}(y) (\partial_\nu \pi_{c'}(y)) | \rho_j; p_\rho, \lambda \rangle \qquad (5.10)$$

$$\langle \rho_{j'}; p'_\rho, \lambda | \rho^\mu_a(x) \pi_b(x) (\partial_\mu \pi_c(x)) \rho^\nu_{a'}(y) \pi_{b'}(y) (\partial_\nu \pi_{c'}(y)) | \rho_j; p_\rho, \lambda \rangle \qquad (5.11)$$

We note that under the interchange of the space-time variables x and y, and the dummy indices (a, b, c) and (a', b', c') the expressions for Eq. (5.8) and Eq. (5.10) are equal, as are Eqs. (5.9) and (5.11). Thus we can replace the sum of these four expression as twice the sum of Eq. (5.8) and Eq. (5.9):

$$\Pi_{jj'} = -f^2_{\rho\pi\pi} \varepsilon_{abc} \varepsilon_{a'b'c'} \int d^4x\, d^4y \times$$
$$\left\{ \langle \rho_{j'}; p'_\rho, \lambda | \rho^\mu_a(x) \pi_b(x) (\partial_\mu \pi_c(x)) \rho^\nu_{a'}(y) \pi_{b'}(y) (\partial_\nu \pi_{c'}(y)) | \rho_j; p_\rho, \lambda \rangle \right.$$
$$\left. + \langle \rho_{j'}; p'_\rho, \lambda | \rho^\mu_a(x) \pi_b(x) (\partial_\mu \pi_c(x)) \rho^\nu_{a'}(y) \pi_{b'}(y) (\partial_\nu \pi_{c'}(y)) | \rho_j; p_\rho, \lambda \rangle \right\} \qquad (5.12)$$

We know from field theory, that the notion of the contraction of two fields is defined to be a Feynman propagator. The contraction of a field with an external leg is defined to give an exponential of the external momenta and position of the interaction, and a polarisation factor for the external leg (as discussed in Appendix A.2). We can therefore write

$$\begin{aligned}\Pi_{jj'} = -f^2_{\rho\pi\pi}\varepsilon_{abc}\varepsilon_{a'b'c'}\int d^4x\, d^4y\, \varepsilon^{\mu *}_{j'}(\lambda)\delta_{aj'}\varepsilon^{\nu}_{j}(\lambda)\delta_{a'j}e^{ip_\rho\cdot x}e^{-ip'_\rho\cdot y} \\ \times\left\{\delta_{bb'}\delta_{cc'}D_F(x-y)\partial^x_\mu\partial^y_\nu D_F(x-y)\right. \\ \left.+\delta_{bc'}\delta_{cb'}\left(\partial^y_\nu D_F(x-y)\right)\left(\partial^x_\mu D_F(x-y)\right)\right\}. \qquad (5.13)\end{aligned}$$

Using these insights we can substitute the Feynman propagators and simplify:

$$\begin{aligned}\Pi_{jj'} &= -f^2_{\rho\pi\pi}\varepsilon_{abc}\varepsilon_{a'b'c'}\int d^4x\, d^4y\, \varepsilon^{\mu *}_{j'}(\lambda)\delta_{aj'}\varepsilon^{\nu}_{j}(\lambda)\delta_{a'j}e^{ip'_\rho\cdot x - ip_\rho\cdot y} \\ &\times(-1)\left\{\delta_{bb'}\delta_{cc'}\int\frac{d^4k_1d^4k_2}{(2\pi)^8}\,\frac{k_{2\mu}k_{2\nu}e^{-i(k_1+k_2)\cdot(x-y)}}{(k_1^2-m_\pi^2+i\epsilon)\,(k_2^2-m_\pi^2+i\epsilon)}\right. \\ &\left.+\delta_{bc'}\delta_{cb'}\int\frac{d^4k_1d^4k_2}{(2\pi)^8}\,\frac{k_{1\nu}k_{2\mu}e^{-i(k_1+k_2)\cdot(x-y)}}{(k_1^2-m_\pi^2+i\epsilon)\,(k_2^2-m_\pi^2+i\epsilon)}\right\}. \qquad (5.14)\end{aligned}$$

Naturally, since the process is elastic, the sum of the intermediate pion momenta, k_1 and k_2, are equal to the momenta of the incoming rho meson, p_ρ, i.e.

$$k_1 + k_2 = p_\rho\,.$$

We use the degree of freedom in defining the polarisation vector to set $\varepsilon_j(\lambda)\cdot p_\rho = 0$. This is easily seen for the case of a ρ at rest, and we apply Lorentz covariance to generalise the result for a ρ-meson with arbitrary 4-momentum, p_ρ. We use these results to express the dot products of the polarisation with momentum k_2 as dot products with k_1:

$$\varepsilon^*_j\cdot k_2 = -\varepsilon^*_j\cdot k_1\,, \qquad (5.15)$$

$$\varepsilon_j\cdot k_2 = -\varepsilon_j\cdot k_1\,. \qquad (5.16)$$

A simplification may also be made by collecting the exponentials together in the following manner:

$$e^{i(p'_\rho\cdot x)-i(p_\rho\cdot y)}e^{-i(k_1+k_2)\cdot(x-y)} = e^{i(p'_\rho-k_1-k_2)\cdot x}e^{-i(p_\rho-k_1-k_2)\cdot y}\,. \tag{5.17}$$

If we now look at the integral over x, it is exactly of the form of the identity for the Dirac Delta function, Eq. (A.3):

$$\int d^4x\, e^{i(p'_\rho-k_1-k_2)\cdot x} = (2\pi)^4\delta^4(p'_\rho-k_1-k_2)\,. \tag{5.18}$$

Taking the result of Eq. (5.18) means the integrations over k_2 simplify as:

$$\begin{aligned}\int \frac{d^4k_2\,d^4x}{(2\pi)^4}e^{i(p'_\rho-k_1-k_2)\cdot x}\mathcal{F}(k_2) &= \int d^4k_2\,\delta^4(p'_\rho-k_1-k_2)\mathcal{F}(k_2)\\ &= \mathcal{F}(p'_\rho-k_1)\,, &(5.19)\\ \therefore\quad k_2 &\to p'_\rho-k_1\,. &(5.20)\end{aligned}$$

Finally, the integration over y is, once again, the identity for the Dirac delta function:

$$\begin{aligned}\int d^4y\, e^{-i(p_\rho-k_1-k_2)\cdot y} &= (2\pi)^4\delta^4(k_1+k_2-p_\rho) &(5.21)\\ &= (2\pi)^4\delta^4(p'_\rho-p_\rho)\,. &(5.22)\end{aligned}$$

After making these simplifications we now just have a single integration over the variable k_1. For simplicity, we rename the variable such that $k_1 \to k$, and apply the delta functions relating a, a' and j, j':

$$\begin{aligned}\Pi_{jj'} &= -f^2_{\rho\pi\pi}\varepsilon_{j'bc}\varepsilon_{jb'c'}(2\pi)^4\delta^4(p'_\rho-p_\rho)(-1)\left(\delta_{bb'}\delta_{cc'}-\delta_{bc'}\delta_{cb'}\right)\\ &\quad\times\int\frac{d^4k}{(2\pi)^4}\frac{\left(\varepsilon^*_{j'}\cdot k\right)\left(\varepsilon_j\cdot k\right)}{\left(k^2-m_\pi^2+i\epsilon\right)\left((p'_\rho-k)^2-m_\pi^2+i\epsilon\right)}\,,\end{aligned} \tag{5.23}$$

where $\varepsilon_j \equiv \varepsilon_j(\lambda)$. We now simplify this expression by

$$\begin{aligned}
\varepsilon_{j'bc}\varepsilon_{jb'c'}\left(\delta_{bb'}\delta_{cc'} - \delta_{bc'}\delta_{cb'}\right) &= \varepsilon_{j'bc}\varepsilon_{jbc} - \varepsilon_{j'bc}\varepsilon_{jcb} \\
&= 2\varepsilon_{j'bc}\varepsilon_{jbc} \\
&= 2\left(\delta_{j'j}\delta_{bb} - \delta_{j'b}\delta_{bj}\right) \\
&= 2\left(3\delta_{j'j} - \delta_{j'j}\right) \\
&= 4\delta_{j'j}\,.
\end{aligned}$$

Thus we come to the following expression for the $\rho \to \pi\pi$ process shown in Fig. 5.3:

$$\begin{aligned}
\Pi_{jj'} &= (2\pi)^4\delta^4(p'_\rho - p_\rho)\delta_{j'j} \times \\
&\quad 4f^2_{\rho\pi\pi}\int \frac{d^4k}{(2\pi)^4}\frac{\left(\varepsilon^*_{j'}\cdot k\right)\left(\varepsilon_j\cdot k\right)}{\left(k^2 - m_\pi^2 + i\epsilon\right)\left((p'_\rho - k)^2 - m_\pi^2 + i\epsilon\right)}\,. \qquad (5.24)
\end{aligned}$$

The normalisation factor in the above expression, $(2\pi)^4\delta^4(p'_\rho - p_\rho)\delta_{jj'}$, is related to contribution from a bare ρ propagator. Thus the self-energy contribution to the ρ-meson mass from the $\pi\pi$ intermediate state is related to the above expression by

$$\Sigma^\rho_{\pi\pi} = i(2\pi)^4\delta(p'_\rho - p_\rho)\Pi_{jj}\,. \qquad (5.25)$$

Non-Relativistic Reduction

We now make the non-relativistic reduction, assuming the ρ is at rest

$$p_\rho = (m_\rho, \vec{0})\,,$$

and sum over the polarisation vectors $\varepsilon_j(\lambda)$:

$$\begin{aligned}\sum_\lambda \left(\varepsilon_j^*(\lambda)\cdot k\right)\left(\varepsilon_j(\lambda)\cdot k\right) &= k^\mu k^\nu\left(-g_{\mu\nu}+\frac{p_{\rho\mu}p_{\rho\nu}}{m_\rho^2}\right)\\ &= -k^2+\frac{(p_\rho\cdot k)^2}{m_\rho^2}\\ &= -(k_0^2-\vec{k}^2)+\frac{(m_\rho k_0)^2}{m_\rho^2}\\ &= \vec{k}^2\,. \end{aligned} \tag{5.26}$$

In the denominator of Eq. (5.24) we have the following term, involving the difference of the 4-momentum of the ρ and of the pion in the loop. This can be rewritten as

$$\begin{aligned}(p_\rho-k)^2 &= m_\rho^2-2p_\rho\cdot k+k^2\\ &= m_\rho^2-2m_\rho k_0+k_0^2-\vec{k}^2\\ &= k_0^2-2m_\rho k_0+m_\rho^2-\vec{k}^2\,. \end{aligned} \tag{5.27}$$

After making these simple substitutions, the self-energy is of a simpler form

$$\begin{aligned}-i\Sigma_{\pi\pi}^\rho &= 4f_{\rho\pi\pi}^2\int\frac{d^4k}{(2\pi)^4}\vec{k}^2\frac{1}{k_0^2-m_\pi^2-\vec{k}^2+i\epsilon}\\ &\qquad\frac{1}{k_0^2-2m_\rho k_0+m_\rho^2-m_\pi^2-\vec{k}^2+i\epsilon}\,. \end{aligned} \tag{5.28}$$

We can now integrate out another degree of freedom, that is, the k_0 contribution. We use the Residue Theorem, Eq. (A.5), to integrate the function in a counter clockwise direction in the complex k_0 plane:

$$\int_{-\infty}^{\infty}\frac{dk_0}{2\pi}f(k_0)=i\sum_{k_{0i}}\mathrm{Res}\,f(k_{0i})\,, \tag{5.29}$$

where k_{0i} are the poles of the function f. There are two terms in the denominator of the integrand of $\sigma_{\pi\pi}^\rho$ that could contribute poles. The first is

$$k_0^2-m_\pi^2-\vec{k}^2+i\epsilon=0\,. \tag{5.30}$$

This expression may be factorised as:

$$(k_0 - w_\pi + i\epsilon)\,(k_0 + w_\pi - i\epsilon) = 0\,, \tag{5.31}$$

where we define $w_\pi(k)$ to be the energy of the pion in the loop. We take the usual contour for the integral, as discussed in [13]. The pole that then contributes to the residue is

$$\begin{aligned} k_0 &= -\sqrt{m_\pi^2 + \vec{k}^2} + i\epsilon \\ &\equiv -w_\pi(|\vec{k}|) + i\epsilon\,. \end{aligned} \tag{5.32}$$

The other pole in this integral is of the form

$$k_0^2 - 2m_\rho k_0 + m_\rho^2 - m_\pi^2 - \vec{k}^2 + i\epsilon = 0\,, \tag{5.33}$$

with k_0 found by completing the squares

$$(k_0 - m_\rho - w_\pi + i\epsilon)\,(k_0 - m_\rho + w_\pi - i\epsilon) = 0\,. \tag{5.34}$$

Once again, if we take the usual contour for we find that the contributing residue is

$$\begin{aligned} k_0 &= m_\rho - \sqrt{m_\pi^2 + \vec{k}^2} + i\epsilon \\ &\equiv m_\rho - w_\pi(|\vec{k}|) + i\epsilon\,. \end{aligned} \tag{5.35}$$

The application of the Residue Theorem means we can replace the numerator of the integral in Eq. (5.28) by the sum over the residues. We also have made the definition that the magnitude of the pion momenta, $|k|$, is to be k. The integrand, I, of Eq. (5.24) is now simplified as

$$\begin{aligned} I &= \frac{1}{-2w_\pi(k)(-m_\rho)(-m_\rho - 2w_\pi(k))} + \frac{1}{m_\rho(m_\rho - 2w_\pi(k))(-2w_\pi(k))} \\ &= -\frac{1}{2m_\rho w_\pi(k)(m_\rho + 2w_\pi(k))} - \frac{1}{2m_\rho w_\pi(k)(m_\rho - 2w_\pi(k))} \\ &= \frac{-2m_\rho}{2m_\rho w_\pi(k)\left(m_\rho^2 - 4w_\pi^2(k)\right)} \\ &= \frac{1}{4}\,\frac{1}{w_\pi(k)\left(w_\pi^2(k) - m_\rho^2/4\right)}\,. \end{aligned} \tag{5.36}$$

Averaging over the spins of the incoming ρ introduces a further factor of $1/3$, and leads to the final expression:

$$\begin{aligned} -i\Sigma^{\rho}_{\pi\pi} &= \frac{if^2_{\rho\pi\pi}}{3}\int \frac{d^3k}{(2\pi)^3}\frac{\vec{k}^2}{w_\pi(k)\left(w^2_\pi(k)-m^2_\rho/4\right)} \\ &= \frac{if^2_{\rho\pi\pi}}{6\pi^2}\int dk \frac{k^4}{w_\pi(k)\left(w^2_\pi(k)-m^2_\rho/4\right)}. \end{aligned} \tag{5.37}$$

where $\Sigma^{\rho}_{\pi\pi}$ is the self-energy.

The Self Energies

The evaluation of the $\rho \to \pi\omega$ self-energy is a similar process to that outlined above and therefore we do not present the intermediate working here. The expressions for the self energies for the $\pi\pi$ and $\omega\pi$ processes that we use here are:

$$\begin{aligned} \Sigma^{\rho}_{\pi\pi} &= \frac{-f^2_{\rho\pi\pi}}{6\mu_\rho\pi^2}\int_0^\infty dk \frac{k^4 u^2_{\pi\pi}(k)}{w_\pi(k)} \\ &\quad \left\{\frac{1}{(w_\pi(k)+\mu_\rho/2-i\epsilon)} - \frac{1}{(w_\pi(k)-\mu_\rho/2-i\epsilon)}\right\} \qquad (5.38) \\ &= \frac{-f^2_{\rho\pi\pi}}{6\pi^2}\int_0^\infty dk \frac{k^4 u^2_{\pi\pi}(k)}{w_\pi(k)\left(w^2_\pi(k)-\mu^2_\rho/4\right)}, \qquad (5.39) \end{aligned}$$

and

$$\begin{aligned} \Sigma^{\rho}_{\pi\omega} &= \frac{-(\mu_\rho g_{\omega\rho\pi})^2}{6\pi^2}\int_0^\infty \frac{dk\, k^4 u^2_{\pi\omega}(k)}{w_\pi(k)-w_\omega(k)+\mu_\rho} \\ &\quad \left\{\frac{1}{(w_\pi(k)-i\epsilon)(w_\pi(k)+w_\omega(k)+\mu_\rho-i\epsilon)}\right. \\ &\quad \left. -\frac{1}{(w_\pi(k)-i\epsilon)(w_\pi(k)+w_\omega(k)-\mu_\rho-i\epsilon)}\right\} \qquad (5.40) \\ &= \frac{-g^2_{\omega\rho\pi}\mu_\rho}{12\pi^2}\int_0^\infty \frac{dk\, k^4 u_{\pi\omega}(k)}{w^2_\pi(k)}. \qquad (5.41) \end{aligned}$$

where we have set the mass of the on-shell ρ-meson to the physical value, denoted μ_ρ. In obtaining Equations (5.39) and (5.41) we have taken the limit where the mass

of the vector mesons (ρ and ω, taken to be degenerate) is much bigger than the mass of the pion. Also, in analogy with the heavy baryon limit, we have neglected the kinetic energy of the heavy vector mesons. The pion (omega) energy is given by $w_{\pi(\omega)}(k) = \sqrt{k^2 + m^2_{\pi(\omega)}}$.

We have introduced form factors $u_{\pi\pi}$ and $u_{\pi\omega}$ to model the finite size of the pion source. We have done this because a formal expansion of hadron properties in terms of m_π fails to converge up to the region where lattice data exists. The crucial physics insight which renders an accurate chiral extrapolation possible is that the source of the pion field is a complex system of quarks and gluons, with a finite size characterised by a scale Λ. When the pion mass is greater than Λ, so that the Compton wavelength of the pion is smaller than the extended source, pion loops are suppressed as powers of Λ/m_π and hadron properties are smooth, slowly varying functions of the quark mass. However, for pion Compton wavelengths bigger than the source ($m_\pi < \Lambda$) one sees rapid, non-linear variations. Phenomenologically this transition occurs at $m_\pi \sim 500$ MeV, or m_π/m_ρ around 0.5 — the region now being addressed by lattice simulations with dynamical fermions.

The form factors are chosen to be dipoles defined as

$$u_{\pi\pi}(k) = \left(\frac{\Lambda^2_{\pi\pi} + \mu^2_\rho}{\Lambda^2_{\pi\pi} + 4w^2_\pi(k)}\right)^2, \tag{5.42}$$

$$u_{\pi\omega}(k) = \left(\frac{\Lambda^2_{\pi\omega} - \mu^2_\pi}{\Lambda^2_{\pi\omega} + k^2}\right)^2, \tag{5.43}$$

where μ_ρ and μ_π are the physical masses of the ρ and π mesons. The normalisation of $u_{\pi\pi}$ is chosen to be unity at the ρ pole and the coupling constant, $f_{\rho\pi\pi} = 6.028$, is chosen to reproduce the width of the ρ (as discussed in section 5.3). In the $\rho \to \pi\omega$ case we take $g_{\omega\rho\pi} = 16$ GeV^{-1} [60].

5.1.2 Extrapolation formula

Collecting these results together, we define the expression for the mass of the ρ-meson as a function of m_π^2 as:

$$m_\rho = c_0 + c_2 m_\pi^2 + \frac{\Sigma^\rho_{\pi\pi}(\Lambda_{\pi\pi}, m_\pi) + \Sigma^\rho_{\pi\omega}(\Lambda_{\pi\omega}, m_\pi)}{2(c_0 + c_2 m_\pi^2)}, \tag{5.44}$$

with $\Sigma^\rho_{\pi\pi}$ and $\Sigma^\rho_{\pi\omega}$ defined by Eqs. (5.39) and (5.41) respectively.

We find in our research that the lattice data alone cannot separately determine $\Lambda_{\pi\pi}$ and $\Lambda_{\pi\omega}$. In order to constrain them we make the reasonable physical assumption that the size of the source of the pion field should be the same regardless of whether the intermediate state involves an ω or a π. This is achieved by requiring that $\Lambda_{\pi\pi}$ is chosen so as to reproduce the same mean-square radius of the source as would be generated by the choice of $\Lambda_{\pi\omega}$.

The size of the source is determined by the choice of form factor, and can be found by comparing the Taylor series expansion of the form factor, Eq. (5.45), with Eq. (5.46):

$$u(k) = u(0) + k^2 u'(0) + \frac{k^4}{2!}u''(0) + \ldots \tag{5.45}$$

$$= u(0)\left[1 - \frac{k^2}{6}\langle r^2\rangle + \ldots\right], \tag{5.46}$$

where $u' = du/dk^2$. For the dipoles chosen here, Eqs. (5.42) and (5.43) we find

$$\langle r^2\rangle_{\pi\pi} = \frac{48}{(\Lambda^2_{\pi\pi} + 4\mu_\pi^2)}, \tag{5.47}$$

$$\langle r^2\rangle_{\pi w} = \frac{12}{\Lambda^2_{\pi\omega}}. \tag{5.48}$$

Equating the mean-square radii results in the following relationship:

$$\Lambda_{\pi\pi} = 2\sqrt{\Lambda^2_{\pi\omega} - \mu_\pi^2}. \tag{5.49}$$

An alternative procedure, which could be imposed in future analyses, would be to constrain the difference in the meson self-energy terms to reproduce the observed $\rho - \omega$ mass difference [59, 61, 62, 63].

5.2 Limiting Behaviour

It is important to know both the large and small m_π limit behaviour of Eq. (5.44). As has been discussed previously, chiral symmetry is a useful tool for exploring the properties of QCD near the chiral limit. Chiral symmetry has been used in obtaining results in Chiral Perturbation Theory (χPT). The behaviour of hadron properties for large quark masses is not quite so well known, but we do have insights from Heavy Quark Effective Theory (HQET), Dyson Schwinger equation investigations and the static quark limit.

5.2.1 The Chiral Limit

It was mentioned in section 3.2 that some important, but limited, information is calculable in χPT. Of particular use here is the behaviour and coefficients of the non-analytic (in quark mass) term in the self-energy expression for the ρ meson. In the particular case of the ρ-meson, the leading non-analytic term is $\mathcal{O}(m_\pi^3)$, with a known coefficient.

From the form of Eq. (5.44) it is easy to see that all non-analytic behaviour must come from the $\Sigma^\rho_{\pi\pi}$ and $\Sigma^\rho_{\pi\omega}$ terms. We find that in the chiral limit ($m_\pi \to 0$) these expressions for the ρ-meson self-energy can be evaluated analytically. Using a sharp cutoff ($\theta(\Lambda - k)$) for the form factor, the $\rho \to \omega\pi$ self-energy is easily evaluated:

$$\Sigma^\rho_{\pi\omega} = -\frac{g_{\omega\rho\pi}\mu_\rho}{12\pi^2}\left(m_\pi^3 \arctan\left(\frac{\Lambda}{m_\pi}\right) + \frac{\Lambda^3}{3} - \Lambda m_\pi^2\right). \tag{5.50}$$

The coefficients of the m_π terms of various powers can be obtained by expanding in m_π about the chiral limit:

$$\Sigma^\rho_{\pi\omega} = -\frac{g_{\omega\rho\pi}\mu_\rho}{12\pi^2}\left(\frac{\Lambda^3}{3} - \Lambda m_\pi^2 + \frac{\pi}{2}m_\pi^3 - \frac{1}{\Lambda}m_\pi^4 + \mathcal{O}(m_\pi^6)\right),$$

with the leading non-analytic term being of order m_π^3:

$$\Sigma^\rho_{\pi\omega}|_{\rm LNA} = -\frac{\mu_\rho g^2_{\omega\rho\pi}}{24\pi} m_\pi^3 \,. \tag{5.51}$$

The $\rho \to \pi\pi$ self-energy contribution is slightly more complicated. If we again choose a θ-function for the form factor we can analytically integrate Eq. (5.39) giving

$$\begin{aligned}
\Sigma^\rho_{\pi\pi} \;=\; & -\frac{f^2_{\rho\pi\pi}}{6\pi^2}\frac{1}{2(\mu_\rho/2)}\left(2\sqrt{m_\pi^2-(\mu_\rho/2)^2}(m_\pi^2-(\mu_\rho/2)^2)\times\right. \\
& \left\{\arctan\left(\frac{\Lambda-(\mu_\rho/2)+\sqrt{\Lambda^2+m_\pi^2}}{\sqrt{m_\pi^2-(\mu_\rho/2)^2}}\right)\right. \\
& -\arctan\left(\frac{\Lambda+(\mu_\rho/2)+\sqrt{\Lambda^2+m_\pi^2}}{\sqrt{m_\pi^2-(\mu_\rho/2)^2}}\right) \\
& \left.-\arctan\left(\frac{m-(\mu_\rho/2)}{\sqrt{m_\pi^2-(\mu_\rho/2)^2}}\right)+\arctan\left(\frac{m+(\mu_\rho/2)}{\sqrt{m_\pi^2-(\mu_\rho/2)^2}}\right)\right\} \\
& -\Lambda(\mu_\rho/2)\sqrt{\Lambda^2+m_\pi^2} \\
& \left.-(3m_\pi^2-2(\mu_\rho/2)^2)(\mu_\rho/2)\ln\left(\frac{\sqrt{\Lambda^2+m_\pi^2}+\Lambda}{m_\pi}\right)\right)\,,
\end{aligned} \tag{5.52}$$

where Λ once again regulates the cutoff of the integral.

The region in which we are interested has $m_\pi < (\mu_\rho/2)$. We replace all the terms of the form $\sqrt{m_\pi^2-(\mu_\rho/2)^2}$ by $i\sqrt{(\mu_\rho/2)^2-m_\pi^2}$, making the complex nature of these terms explicit. We then rewrite the arctans (which have complex arguments) as logarithms of real arguments by using [64]

$$\arctan(z) = \frac{i}{2}\ln\left(\frac{1-iz}{1+iz}\right)\,. \tag{5.53}$$

Simplifying the expression by collecting logarithms together we now have

$$\begin{aligned}\Sigma^{\rho}_{\pi\pi} &= -\frac{f^2_{\rho\pi\pi}}{6\pi^2}\frac{1}{2(\mu_\rho/2)}\Big[-\left((\mu_\rho/2)^2-m_\pi^2\right)^{3/2}\ln\Big\{m_\pi^2(m_\pi^2-(\mu_\rho/2)^2)\\ &\quad \Lambda^2(m_\pi^2-2(\mu_\rho/2)^2)-2\Lambda(\mu_\rho/2)\sqrt{(\Lambda^2+m_\pi^2)((\mu_\rho/2)^2-m_\pi^2)}\Big\}\\ &\quad -\ln\left(m_\pi^2(\Lambda^2+m_\pi^2-(\mu_\rho/2)^2)\right)-\left(3m_\pi^2-2(\mu_\rho/2)^2\right)\\ &\quad \times(\mu_\rho/2)\ln\left(\frac{\sqrt{\Lambda^2+m_\pi^2}+\Lambda}{m_\pi}\right)-\Lambda(\mu_\rho/2)\sqrt{\Lambda^2+m_\pi^2}\Big]\,. \end{aligned} \tag{5.54}$$

Looking at just the lowest order, non-analytic terms in the expansion about $m_\pi^2=0$ we have

$$\begin{aligned}\Sigma^{\rho}_{\pi\pi}|_{\rm NLNA} &= -\frac{f^2_{\rho\pi\pi}}{6\pi^2}\frac{1}{2(\mu_\rho/2)}\left(\left(2(\mu_\rho/2)^3-3(\mu_\rho/2)m_\pi^2+\frac{3}{4}\frac{m_\pi^4}{(\mu_\rho/2)}\right)\right.\\ &\quad \left.\left(3m_\pi^2-2(\mu_\rho/2)^2\right)(\mu_\rho/2)\right)\ln(m_\pi)\\ &= -\frac{f^2_{\rho\pi\pi}}{8\pi^2\mu_\rho^2}m_\pi^4\ln(m_\pi)\,. \end{aligned} \tag{5.55}$$

Whilst these expressions were found for the particular choice of a sharp cutoff for the form factor, the results are more general than that. In fact, these results are independent of the form chosen for the ultra-violet regulators, $u_{\pi\pi}$ and $u_{\pi\omega}$.

To compare these results to χPT we use the result of Eq. (5.1) that

$$\sigma^\rho = \frac{\Sigma^\rho}{2m_0}\,. \tag{5.56}$$

In principal these expressions should be evaluated at the chiral limit. However the variations of the masses (e.g. the ρ mass, μ_ρ) and coupling constants from the physical values are typically of the order 10%, and we therefore use the physical values. We find that both the LNA and NLNA behaviour predicted by χPT are reproduced. For example, in Ref. [65] the m_π dependence of the LNA term to the ρ mass is given by

$$\sigma^\rho|_{\rm LNA} = -\frac{1}{12\pi f^2}\left(\frac{2}{3}g_2^2+g_1^2\right)m_\pi^3\,. \tag{5.57}$$

This results in a value of the m_π^3 coefficient of -1.71 GeV^2, in excellent agreement with the value ($g^2_{\omega\rho\pi}/48\pi = -1.70$ GeV^2) found here.

5.2.2 The Static Quark Limit

It is expected from the naïve quark model and from heavy quark effective theory (HQET) that the mass of the hadrons should become proportional to the masses of their constituent quarks as the quark mass increases. Whilst the data sets investigated here do not truly enter the HQET region, Dyson Schwinger equation studies suggest that in the mass range investigated the constituent quark mass in fact does vary linearly with the (current) quark mass. In addition, other lattice calculations suggest an approximate proportionality between m_π^2 and the quark mass, and thus there is the expectation that the mass of the hadron should become proportional to the square of the pion mass. This behaviour is indeed seen in lattice results.

The expression we use for the bare ρ-meson is of the required form, it only remains to investigate the properties of the self energies in this limit. We have found that for the choice of a dipole for the form factors, the self energies are suppressed as inverse powers of m_π, once m_π is comparable with the dipole mass (this behaviour may be seen in Fig. 5.4). Naturally for other choices of form factor we have a similar suppression.

5.2.3 The Mass in the Chiral Limit

It must be noted that the bare mass, m_0 is not the mass of the ρ in the chiral limit. The self-energy terms $\Sigma^\rho_{\pi\pi}$ and $\Sigma^\rho_{\pi\omega}$ are non-vanishing at $m_\pi = 0$, as indicated by Eqs. (5.50) and (5.54). The mass of the ρ in the chiral limit is in fact given by the

evaluation of Eq. (5.44) at the point where $m_\pi = 0$.

$$m_\rho^{(0)} = c_0 + \frac{\Sigma^\rho_{\pi\pi}(\Lambda_{\pi\pi}, m_\pi = 0) + \Sigma^\rho_{\pi\omega}(\Lambda_{\pi\omega}, m_\pi = 0)}{2c_0}. \tag{5.58}$$

5.3 The Width of The ρ-Meson

It is well know that the ρ-meson has a decay channel to two pions. It is possible to calculate the width for this process with the Feynman rules we are using here. It is also an experimentally known result [39]. We extract a theoretical estimate for the width by taking the imaginary part of the $\rho \to \pi\pi$ self-energy. By equating this result with the experimental value, we have a way of determining the $\rho\pi\pi$ coupling, $f_{\rho\pi\pi}$, consistently. If we simplify Eq. (5.38)

$$\begin{aligned}\Sigma^\rho_{\pi\pi} &= \frac{f^2_{\rho\pi\pi}}{6\mu_\rho\pi^2}\int_0^\infty \frac{dk\,k^4\,u^2_{\pi\pi}(k)}{w_\pi(k)}\frac{-\mu_\rho}{(w_\pi(k)-i\epsilon)^2-\mu_\rho^2/4} \\ &= -\frac{f^2_{\rho\pi\pi}}{6\pi^2}\int_0^\infty \frac{dk\,k^4\,u^2_{\pi\pi}(k)}{w_\pi(k)}\frac{1}{w_\pi^2(k)-\mu_\rho^2/4-i\epsilon}.\end{aligned}$$

We use the definition of the energy of the pion in the loop, $w_\pi(k) = \sqrt{k^2+m_\pi^2}$, to re-write the denominator as

$$\begin{aligned}w_\pi^2(k) - \mu_\rho^2/4 - i\epsilon &= m_\pi^2 + k^2 - \mu_\rho^2/4 - i\epsilon \\ &= k^2 - (\mu_\rho^2/4 - m_\pi^2) - i\epsilon\,,\end{aligned} \tag{5.59}$$

and by using Dirac's expression

$$\frac{1}{x-i\epsilon} = \frac{\mathcal{P}}{x} + i\pi\delta(x)\,,$$

we can now write

$$\begin{aligned}\Sigma^\rho_{\pi\pi} = &-\frac{f^2_{\rho\pi\pi}}{6\pi^2}\int_0^\infty \frac{dk\,k^4\,u^2_{\pi\pi}(k)}{w_\pi(k)}\times \\ &\left\{\frac{\mathcal{P}}{k^2-((\mu_\rho^2/4)-m_\pi^2)} + i\pi\delta\left(k^2-((\mu_\rho^2/4)-m_\pi^2)\right)\right\}.\end{aligned} \tag{5.60}$$

The δ-function can be split into two terms, one of which corresponds to a positive k and one to a negative loop momentum k (Eq. (A.1)). However a value of k which is negative is unphysical, therefore we retain only the positive k contribution to the imaginary part of the $\rho \to \pi\pi$ self-energy:

$$\begin{aligned}
\mathrm{Im}\Sigma^{\rho}_{\pi\pi} &= -\frac{f^2_{\rho\pi\pi}}{6\pi^2}\int_0^\infty \frac{dk\, k^4\, u^2_{\pi\pi}(k)}{w_\pi(k)} \times \\
&\quad \frac{\pi}{2\sqrt{(\mu_\rho^2/4)-m_\pi^2}}\,\delta\left(k-\sqrt{(\mu_\rho^2/4)-m_\pi^2}\right) && (5.61)\\
&= -\frac{f^2_{\rho\pi\pi}}{6\pi}\frac{u^2_{\pi\pi}(k)}{2\sqrt{(\mu_\rho^2/4)-m_\pi^2}}\frac{k^4}{w_\pi(k)}\bigg|_{k=\sqrt{(\mu_\rho^2/4)-m_\pi^2}} && (5.62)\\
&= -\frac{f^2_{\rho\pi\pi}}{48\pi}\mu_\rho^2\left(1-\frac{4m_\pi^2}{\mu_\rho^2}\right)^{3/2} && (5.63)\\
&= -\mu_\rho\Gamma_\rho\,. && (5.64)
\end{aligned}$$

Thus we find that the width of the ρ, Γ_ρ, is given by the following simple expression:

$$\Gamma_\rho = \frac{f^2_{\rho\pi\pi}}{48\pi}\mu_\rho\left(1-\frac{4m_\pi^2}{\mu_\rho^2}\right)^{3/2}\,. \qquad (5.65)$$

The experimental value for the width of the ρ is 149 MeV, and this naturally is measured at the physical pion mass. We can replace m_π in Eq. (5.65) and extract the value of the $\rho\pi\pi$ coupling to be 6.028.

5.4 Fitting to Lattice Results

At first sight the fact that CP-PACS [20] is able to extract a measurement of the ρ mass, in full QCD, at $m_\pi/m_\rho < 0.5$ is extremely surprising. Once the ρ is able to decay one would expect to measure not the ρ mass but the two-pion threshold. The origin of this result is in the quantisation of the pion momentum on the lattice and, in particular, the fact that the lowest (non-zero) pion momentum available is

$2\pi/aL$, where is L is the spatial dimension of the lattice. This result was discussed in some detail in Sec. 2.1.2. For the relatively small lattice used by CP-PACS at the lowest pion mass this corresponds to more than 400 MeV/c momentum. This is why the ρ remains stable.

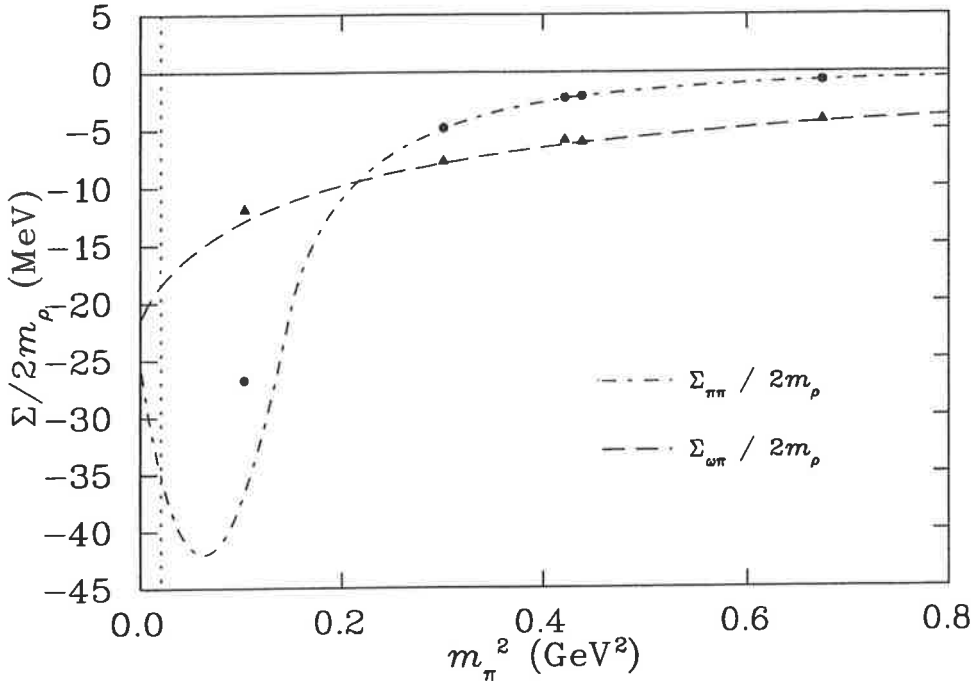

Figure 5.4: Variation with pion mass of the self-energy contributions to the ρ meson, Eqs. (5.41) and (5.39), for a dipole form factor with $\Lambda_{\pi\omega} = 630$ MeV. The solid points indicate the value of this self-energy when calculated at the discrete momenta allowed on the lattices considered in this investigation. The difference between the curves and points is an indication of the physics missing because of finite lattice size and spacing.

We use the results discussed in Sec. 2.1.2 to evaluate the self-energy integrals of Eq. (5.44) by summing the integrands at the allowed values of the lattice 3-momenta

$$4\pi \int_0^\infty k^2 dk = \int d^3k \approx \frac{1}{V}\left(\frac{2\pi}{a}\right)^3 \sum_{k_x,k_y,k_z}, \tag{5.66}$$

where the k_μ are defined by Eq. (2.8). The results for the self-energy contributions

are presented in Fig. 5.4. The self-energy calculated on the lattice (the solid circles and triangles) differs little from the full self-energy calculation in the high quark mass (m_π^2) region. Furthermore, the effect in the $\rho \to \omega\pi$ self-energy contribution is also small at low pion mass. The biggest change is in the $\rho \to \pi\pi$ self-energy calculation at lower quark mass. This is the region in which one might expect the biggest corrections because one is approximating a principal value integral on a finite mesh. This change in behaviour, particularly at the lowest data point ($m_\pi^2 \approx 0.1$ GeV^2), indicates that the $\pi\pi$ self-energy contribution is significantly understated in the lattice simulations. Upon calculating the full self-energy contribution via the continuous integrals, the magnitude of the self-energy is increased by about 10 MeV, which is 30% of the self-energy contribution at this point. These results for $\Sigma^\rho_{\pi\pi}$ and $\Sigma^\rho_{\pi\omega}$ are used in Eq. (5.44) to fit the lattice data.

That the self-energy is understated is a function of the lattice size, spacing and choice of m_π. Figure 5.5 shows the same $\rho \to \pi\pi$ continuous integral, but also the behaviour of the self-energy evaluated as a discrete sum over a variety of quark masses. We choose the lattice size and spacing to be that of the lowest CP-PACS data point ($L = 16$, $a = 0.18$ fm). As can be clearly seen, the dashed curve reproduces the full results well at large quark mass, but severely breaks down at lower quark mass (m_π^2). If the CP-PACS data point was at $m_\pi = 250$ MeV the self-energy contribution would have been overestimated, unlike the underestimation we find here.

5.4.1 Naïve Chiral Fits

The recent dynamical fermion lattice QCD results of the CP-PACS and UKQCD collaborations (listed in Tables 2.1 and 2.2) are presented in Fig. 5.6. The scale parameters relating the lattice QCD results to physical quantities have been adjusted

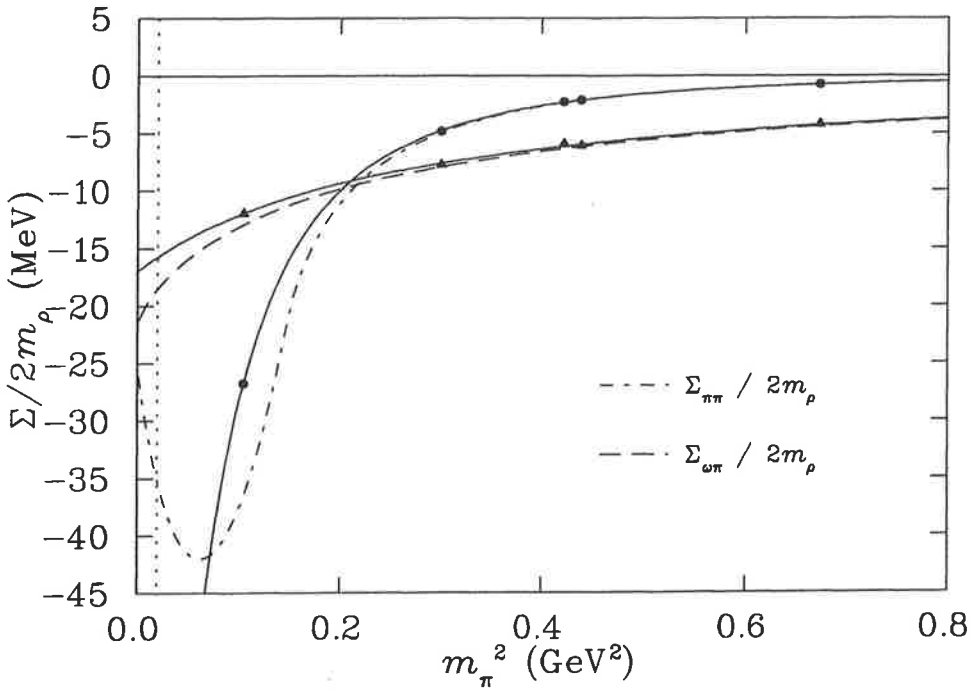

Figure 5.5: Variation with pion mass of the self-energy contributions to the ρ meson, for a dipole form factor with $\Lambda_{\pi\omega} = 630$ MeV. The solid curves are the respective self-energy contributions calculated over the discrete momenta permitted on the lattice.

[66] by 5% for the CP-PACS and UKQCD results. The effect is to increase the ρ mass from CP-PACS and decrease the mass from UKQCD, providing better agreement between the two independent simulations. This discrepancy is an interesting observation which may be related to the different choices of fermion and gluon actions used by the groups. As the χ^2 of the following fits is dominated by the CP-PACS data, we focus on this data set.

In Fig. 5.1 we presented a linear fit to the lattice results. Another popular method within the lattice community is to fit using the following three parameter form:

$$m_\rho = c_0 + c_2 m_\pi^2 + c_3 m_\pi^3 \,. \tag{5.67}$$

The inclusion of a term of order m_π^3 is motivated by chiral perturbation theory.

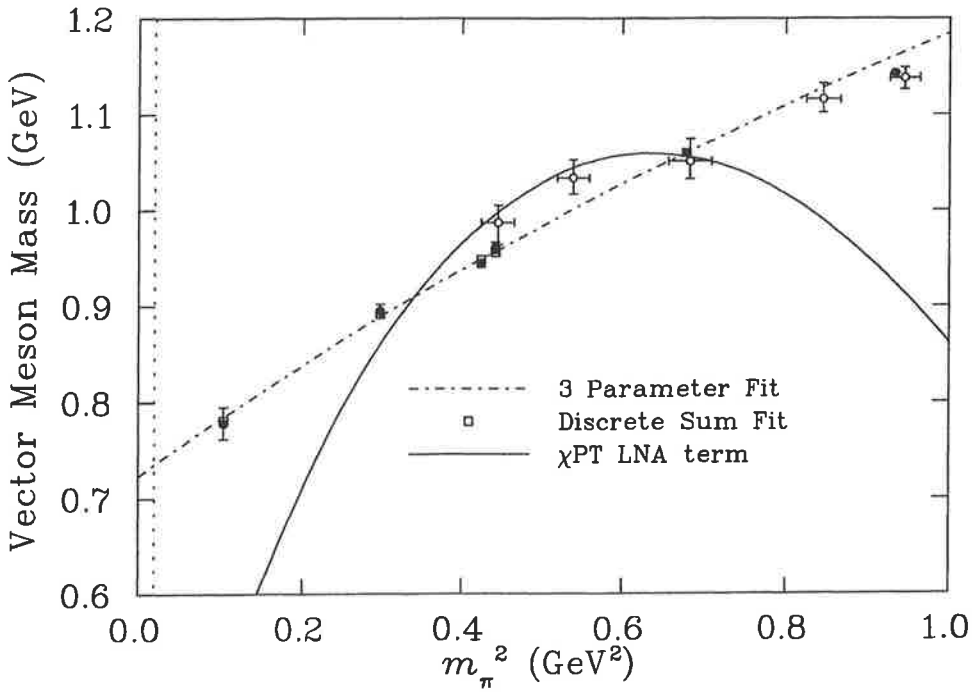

Figure 5.6: Vector meson (ρ) mass from CP-PACS [20] (filled circles) and UKQCD [21] (open circles) as a function of m_π^2. The dash-dot curve is the naïve three parameter fit, Eq. (5.67). The open squares (which are barely distinguishable from the data) represent the fit of Eq. (5.44) to the data with the self-energy contributions calculated as a discrete sum of allowed lattice momenta. We have used a dipole form factor, with $\Lambda_{\pi\omega} = 630$ MeV. The solid curve is Eq. (5.67) with the parameter c_3 fixed to the value given by chiral perturbation theory.

In Fig. 5.6, the dash-dot curve represents a fit of this form to the data, with the parameters of the fit listed in Table 5.1. Since the value of c_3 in Eq. (5.67) is treated as a fitting parameter, we are not guaranteed that it has the correct value required by Chiral Perturbation Theory (χPT). The value for the best fit is found to be -0.21 GeV^{-2}. As outlined above, our expressions for the ρ self-energies have the correct LNA and NLNA coefficients by construction. Indeed, if the coefficient c_3 is constrained to the correct value[2] ($-g_{\omega\rho\pi}^2/48\pi = -1.70$ GeV^{-2}), the best fit

[2]In Ref. [65] the m_π dependence of the LNA term to the ρ mass is given by $-\frac{1}{12\pi f^2}(\frac{2}{3}g_2^2 + g_1^2)\, m_\pi^3$. This would result in a value of the m_π^3 coefficient of -1.71 GeV^{-2}, in excellent agreement

possible by varying c_1 and c_2 is shown as the solid line in Fig. 5.6. As was also found in the case of the nucleon [66], the lack of convergence of the formal expansion is such that it is not sufficient to fix the coefficient of the LNA term in a cubic fit to that predicted by χPT, as the resulting form will not fit the data.

5.4.2 Improved Chiral Fits

Our fits to the data use Eq. (5.44) with the integrals evaluated at the discrete values of the allowed momentum on the lattice. The fits are based on the lowest five lattice masses given by CP-PACS. We selected the lowest lying masses because to move further away from the chiral limit would necessitate additional terms beyond the first two analytic terms of Eq. (5.44). The results of the fit are shown as the open squares in Figs. 5.6, 5.7, and 5.8. The parameters of the fit c_0, c_2, and $\Lambda_{\pi\omega}$, are then used in an exact evaluation of Eq. (5.44) using the full integrals in Eqs. (5.39) and (5.41). This result is illustrated by the solid lines in Figs. 5.7 and 5.8.

The best fit value of $\Lambda_{\pi\omega} = 630$ MeV results in the ρ meson having a radius of about 0.6 fm from Eq. (5.48). We do not consider the fact that the form factor is softer than found in some earlier work to be of concern because, as we discuss below, the current lattice results at low m_π are not yet sufficiently precise to constrain the chiral behaviour.

It is interesting to note the similarity of the predictions for the value of the physical ρ mass from the cubic and dipole calculations with that of other authors. An analogous result was found in Ref. [56]. There it was found that fitting quenched lattice data with a linear extrapolation, and improving the extrapolation by adding on the $\rho \to \pi\pi$ effects, predicted essentially the same physical mass, but that the chiral behaviour was significantly different. This is exactly the behaviour we see

with the value used here.

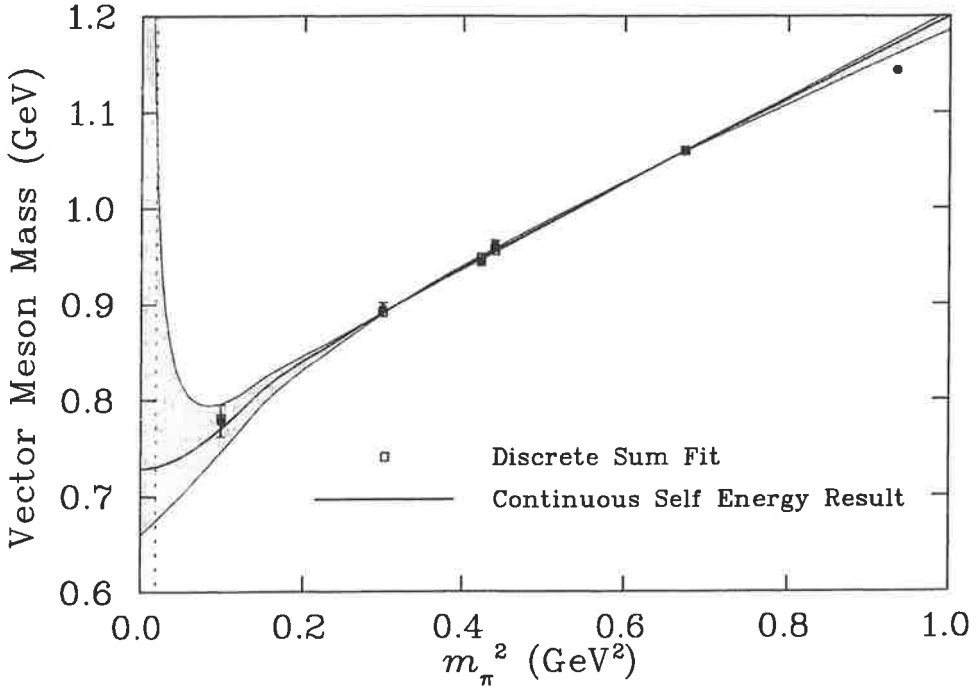

Figure 5.7: Analysis of the lattice data for the vector meson (ρ) mass calculated by CP-PACS as a function of m_π^2. The squares represent the fit of Eq. (5.44) to the data with the self-energy contributions calculated as a discrete sum of allowed lattice momenta. The solid curve is for continuous (integral) self-energy contributions to Eq. (5.44). We have used a dipole form factor, with optimal $\Lambda_{\pi\omega} = 630$ MeV. The shaded area is bounded below by a 1σ error bar. The upper bound is limited by the constraint $\Lambda_{\pi\omega} > \mu_\pi$ as discussed in the text.

here.

The importance of the accuracy of the lowest mass point cannot be overstated. We stress that CP-PACS emphasised the preliminary nature of the lowest data point, because of the relatively low statistics. Nevertheless, in order to prepare for future more accurate data, we have carried out a standard error analysis including this point and the results are presented in Fig. 5.7. The lower bound on the shaded area was found by increasing the minimum χ^2 per degree of freedom of the fit by 1. We were unable to do this with the upper bound. The result is actually limited by the physics of the process. In the case of a dipole form factor this means

$\Lambda_{\pi\omega} > \mu_\pi$ (from Eq. (5.49)), and that is the upper limit we have shown here.

Improved Statistics

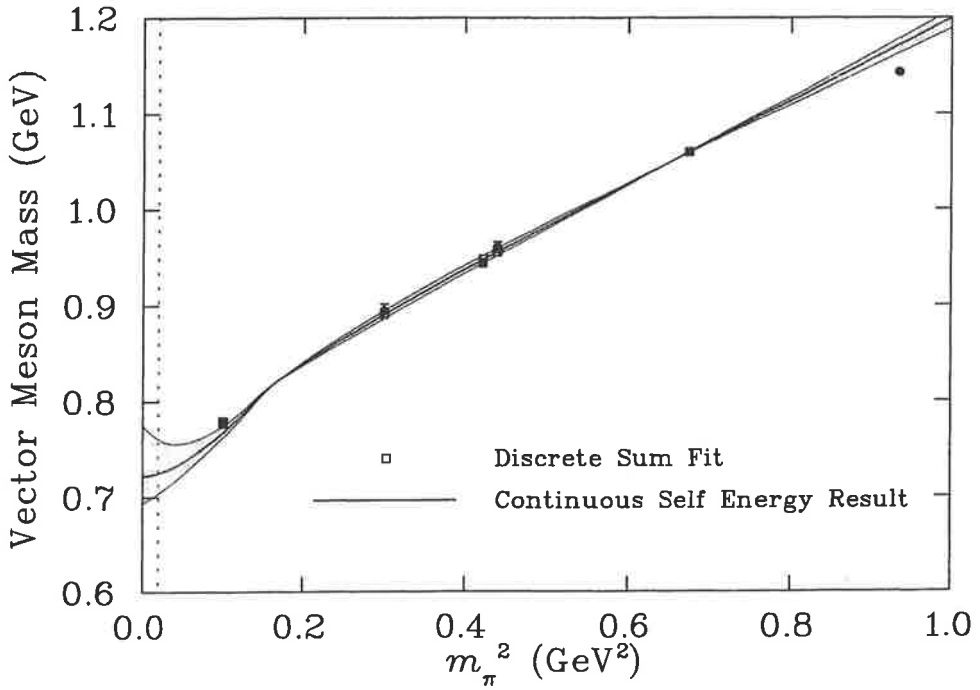

Figure 5.8: The graph is as described in Fig. 5.7 except that the error bar on the lowest data point ($m_\pi^2 \approx 0.1$ GeV^2) has been reduced by a factor of $\sqrt{10}$. This equates to an improvement of 10 times in the statistics, which we do not consider an unreasonable goal for the future. The dipole mass of the best fit is then $\Lambda_{\pi\omega} = 660$ MeV. The shaded area is bounded above and below by a 1σ error bar.

It is not unreasonable to expect an improvement in the accuracy of the calculated lattice mass values, and as a Gedanken experiment we have explored the possibility of a ten-fold increase in the number of gauge configurations at the lowest pion mass. For the purposes of the simulation we did not change the value of the data point, but simply reduced the size of the error bar by $\sqrt{10}$. As can be seen in Fig. 5.8 the improvement in the predictive power is dramatic. The uncertainty in the physical mass has been reduced to the 2% level. Additional improvement in the

accuracy of the extrapolation would result from the availability of additional data in the low pion mass region. However, it must be noted that the provision of data around 0.2 GeV^2 and higher would probably not assist greatly in the determination of the dipole mass (Λ); it is primarily determined by points nearer the physical region. We present the parameters of these fits in Table 5.1.

Fit Form	c_0	c_2	c_3	$\Lambda_{\pi\omega}$	M_ρ	J	m_π^2
Cubic	0.723	0.668	−0.207	—	0.735	0.44 (8)	0.223 (7)
Dipole	0.776	0.427	—	0.630	0.731	0.45 (7)	0.225 (4)
(Imp)	0.779	0.425	—	0.660	0.725	0.45 (3)	0.225 (2)

Table 5.1: Table of fit parameters c_0, c_2, c_3, $\Lambda_{\pi\omega}$, the ρ-meson mass at μ_π, the value of the J-parameter, and the pion mass at which the J parameter is calculated. All values are in appropriate powers of GeV. The **Cubic** fit refers to Eq. (5.67) while the **Dipole** refers to Eq. (5.44) with a dipole form factor, **Imp** is a dipole fit with the increased statistics. We find that the error in the J-parameter is halved if the statistics on the lowest point are increased by a factor of 10.

Form Factor Dependence

We have examined the model dependence of our work by repeating the above fits with a monopole form factor. As can be seen in Fig. 5.9 the model dependence is at the level of 15 MeV at the physical pion mass with current data, and at the few MeV level had the error bar been reduced by a factor of $\sqrt{10}$. This reinforces the claim in Ref. [66] that this extrapolation method is not very sensitive to the form chosen for the ultra-violet cut-off. In Sec. 6.6 we investigate the extrapolation form factor dependence in greater detail for the specific cases of the N and Δ masses.

5.5 The J-Parameter

A commonly perceived failure with quenched lattice QCD calculations of meson masses is the inability to correctly determine the J-parameter. This dimensionless

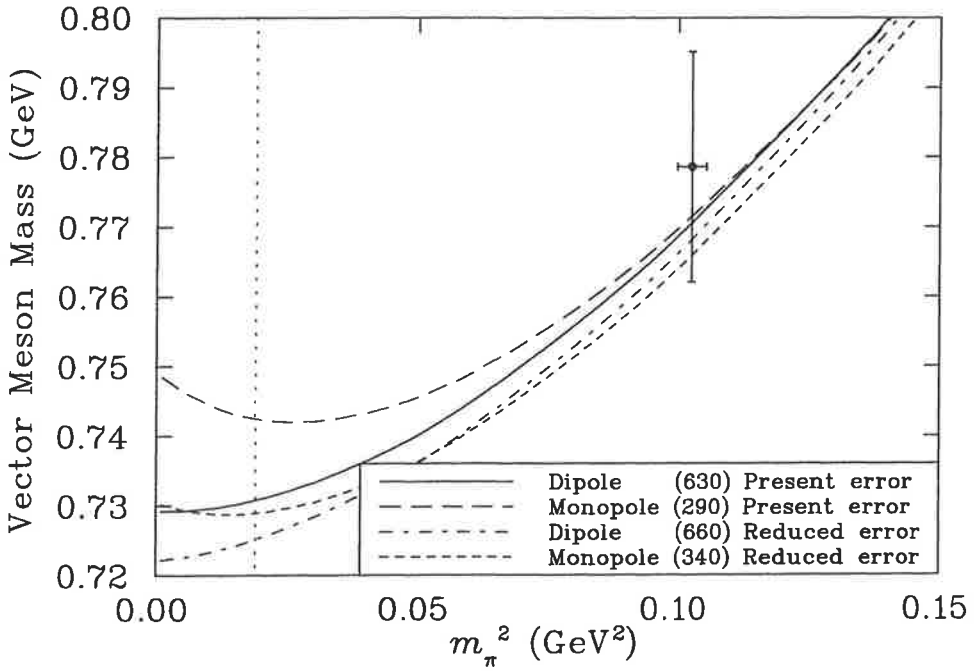

Figure 5.9: A magnification of the physical pion mass region of our extrapolation results. The solid and long dashed lines represent the best fit dipole and monopole results for a fit with the present accuracy of the lattice QCD results. The dash-dot and short dashed lines are the dipole and monopole results for a reduction in the error bar of the lowest lattice data by a factor of $\sqrt{10}$. The model dependence of the choice of form factor is $\mathcal{O}(2\%)$.

parameter was proposed as a quantitative measure, independent of chiral extrapolations, thus making it an ideal lattice observable [67]. The form of the J-parameter is:

$$J = m_\rho \left.\frac{dm_\rho}{dm_\pi^2}\right|_{m_\rho/m_\pi=1.8} \tag{5.68}$$

$$\simeq m_{K^*} \frac{m_{K^*} - m_\rho}{m_K^2 - m_\pi^2} . \tag{5.69}$$

By using Eq. (5.69) and the experimentally measured masses of the K (495.7 MeV), K^* (892.1 MeV), π (138.0 MeV) and ρ (770.0 MeV) Lacock and Michael [67]

determined

$$J = 0.48(2)\,.$$

However previous attempts by the lattice community to reproduce this value have been around 20% too small. In the case of quenched calculations this has been cited as evidence of a quenching error (see, for example the review in [68]). It was noted by Lee and Leinweber [69] that the inclusion of the self-energy of the ρ-meson generated by two-pion intermediate states (excluded in the quenched calculations) acts to increase the J-parameter. This fact has not been addressed in many analyses by the lattice community.

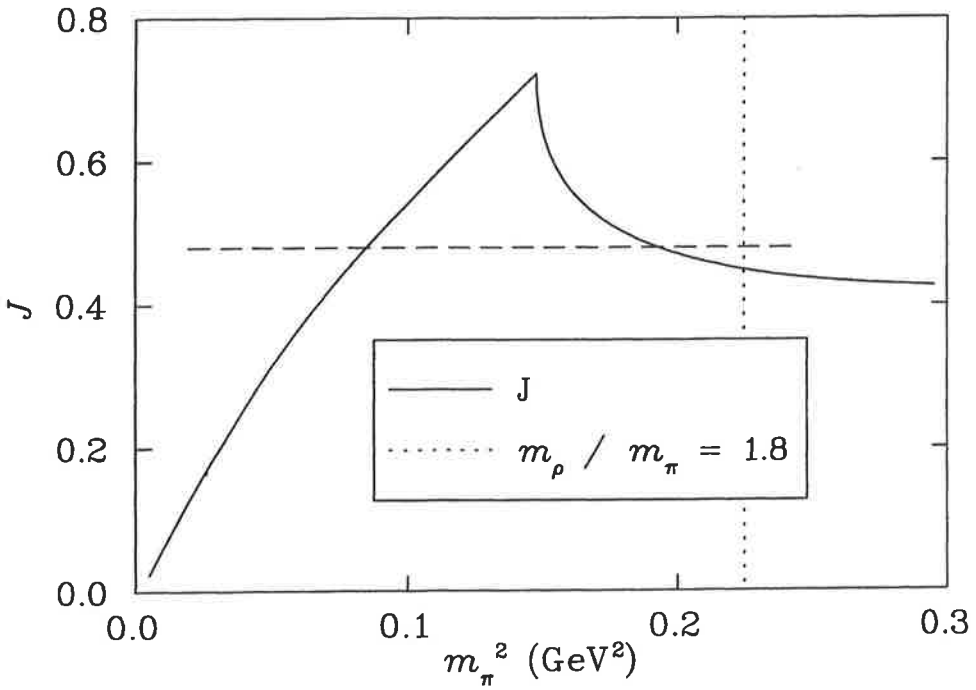

Figure 5.10: The solid curve is a plot of the value of the J-parameter as a function of m_π^2 obtained from Eq. (5.68) and the best fit to the lattice results given by Eq. (5.44). The vertical dotted line shows the point at which the J-parameter is evaluated ($m_\rho/m_\pi = 1.8$). The horizontal line displays the experimental value (0.48) plotted between the physical values of m_π^2 and m_K^2.

In Fig. 5.10 we present the value of the J parameter obtained from Eq. (5.68)

and our best fit to the lattice results using Eq. (5.44). The vertical dotted line indicates the value of m_π^2 where the J parameter is to be evaluated, i.e. $m_\rho/m_\pi = 1.8$. The horizontal dashed line, plotted between the values of the squares of the physical pion and kaon masses, shows the experimental estimate of the J parameter from (5.69). This equation suggests that the evaluation of J may be approximated by the slope of the vector meson mass extrapolation between these points. The cusp shown in Fig. 5.10, associated with the cut in $\Sigma^\rho_{\pi\pi}$, suggests otherwise. We stress that while the detailed slope of the curve is parameter dependent, the presence of the cusp is a model independent consequence of the two pion cut in the ρ spectral function.

As a point of comparison we have also calculated J using the naïve cubic chiral extrapolation, Eq. (5.67), described above. The results of our investigations are summarised in Table 5.1. The value of the J parameter is similar for both fits as it is evaluated at $m_\pi^2 \sim 0.22$ GeV^2. The effects introduced into the extrapolations by chiral physics do not begin playing a large role until m_π^2 falls below 0.2 GeV^2. Had the J parameter been evaluated at $m_\pi^2 = 0.19$ GeV^2 or 0.09 GeV^2 one would find perfect agreement with the linear Ansatz of Eq. (5.69).

5.6 The $\rho\pi\pi$ Phase Shift

The $\rho\pi\pi$ phase shift is related to the transition matrix for the ρ. The transition matrix is proportional to δ

$$T(E) \propto e^{i\delta} \sin\delta \,, \tag{5.70}$$

and the value of δ may be measured experimentally. The form of the transition matrix is

$$T(E) = \frac{1}{E^2 - m_\rho^2 - \Sigma(E)} \,, \tag{5.71}$$

where

$$\begin{aligned}\Sigma(E) &\sim \int dk \frac{k^4 u^2(k)}{w(k)(E^2 - i\epsilon - 4w^2(k))} \\ &\sim \Sigma^{\rho}_{\pi\pi} .\end{aligned}$$

We can evaluate the scattering phase shift using

$$\frac{\mathrm{Im}T}{\mathrm{Re}T} = \tan\delta .$$

We know that $E = \mu_\rho$ at the ρ pole, and that $\delta = 90^o$. This implies that the real part of T vanishes, and so we have a constraint on m_ρ. The imaginary part of T is just the inverse of Eq. (5.63) with the ρ mass, μ_ρ, replaced by the energy of the system, E.

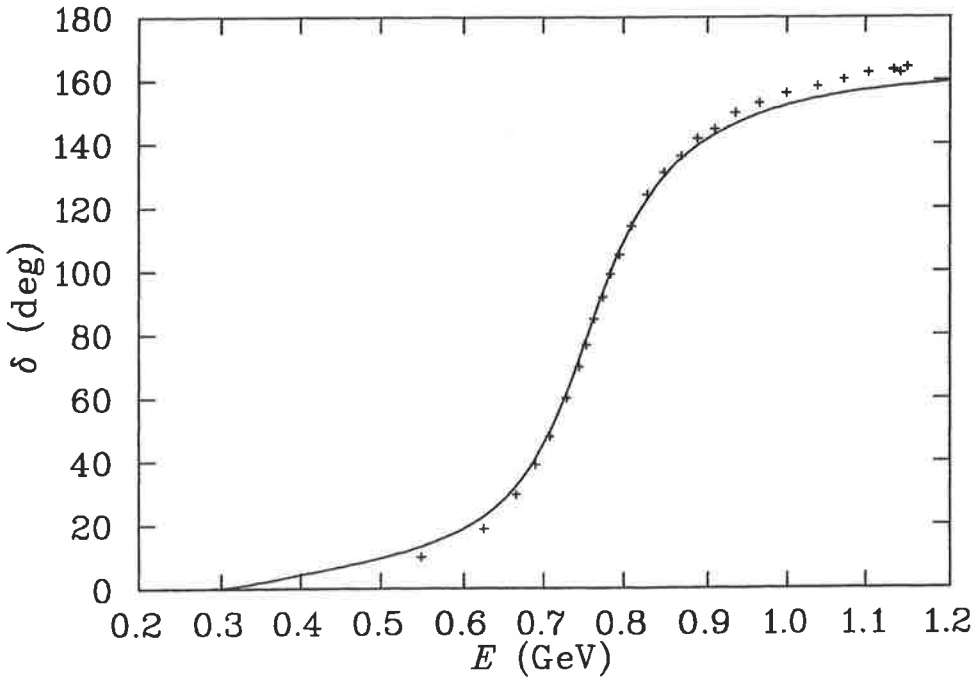

Figure 5.11: The $\rho\pi\pi$ phase shift as a function of energy. The experimental points are from [70].

Figure 5.11 shows the phase shift for $\pi\pi$ scattering in the ρ channel, as calculated with our best fit $\Lambda_{\pi\omega} = 630$ MeV. We reproduce the experimental results

of [70] in the resonance region, however the fit is not perfect in the higher and lower energy regions. Additional resonances, that have been ignored in our analysis, are expected to play a role in the high energy region, while there can be other small, background contributions in the low energy regime.

5.7 Summary

We have found our method for extrapolating lattice QCD results for the lightest vector meson at large quark masses to lighter masses successful. For the best fit parameters, not only have we reproduced a realistic physical mass for the ρ meson, whilst implicitly building in the correct chiral behaviour, but in addition the ρ of our calculations has the correct decay width to two pions. The extrapolation method reproduces the experimentally extracted value of the J-parameter (with some caveats), and it reproduces the $\rho\pi\pi$ phase shift in the 2π resonance region. These results are tempered by the error analysis, which shows that with data of the accuracy currently available the true predictive power of an extrapolation is negligible. The redeeming feature is that a ten-fold increase in the statistics of the lowest data point will result in a tool with predictive power at the 5% level. In the next section we apply a similar analysis to investigate the lightest two baryons: the N and Δ.

Chapter 6

Baryon Masses

. That man is best who reasons for himself,
Considering the future. Also good
Is he who takes another's good advice.
But he who neither thinks himself nor learns
From others, is a failure as a man.
HESIOD, "WORKS AND DAYS"

The two most studied particles on both the lattice and in chiral perturbation theory are the lightest spin-$\frac{1}{2}$ (N) and spin-$\frac{3}{2}$ (Δ) baryons. The lowest mass full QCD lattice data available is indeed for these baryons. We present a study of these two baryons as a general example of the issues involved with any baryon extrapolation. As in the previous chapter we show that an expansion in m_π of hadron properties fails to converge, and in particular has the wrong functional form in the large quark mass region (Sec. 6.6.4). The sigma commutator, investigated in Sec. 6.7, is a direct source of information on chiral symmetry breaking within QCD. We will show that provided the correct chiral behaviour of QCD is respected

in the extrapolation, one can indeed obtain a fairly reliable determination.

6.1 The Nucleon

The successes of the previous chapter concerning the extrapolation of the ρ-meson mass leads us to consider a similar approach to the latest two-flavour, dynamical QCD data on the nucleon. Once again our guiding principle is to retain those self-energy contributions which yield the most rapid variation with m_π near the chiral limit — i.e. those terms which yield the leading non-analytic (LNA) behaviour and the next-to-leading non-analytic (NLNA) behaviour. In the limit where the baryons are heavy, the pion induced self-energies of the N and Δ, to one loop, are given by the processes shown in Fig. 6.1. Note that we have restricted the intermediate baryon states to those most strongly coupled, namely the N and Δ states. The discussion of the Δ baryon calculations are deferred to section 6.3.

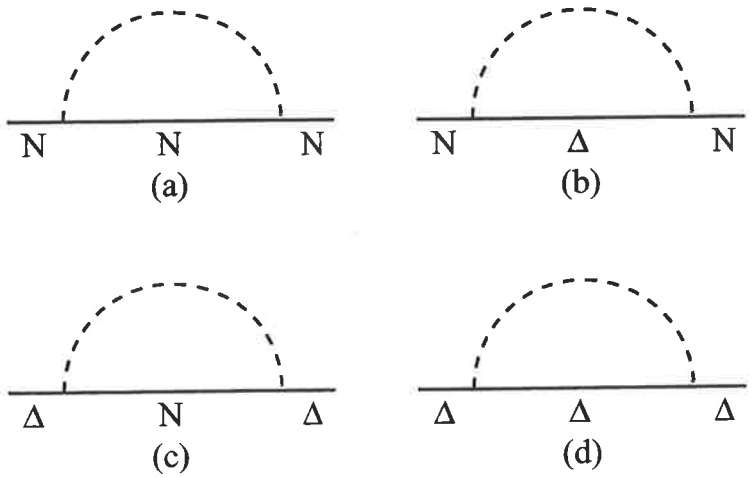

Figure 6.1: The one-loop pion induced self-energy of the N and Δ.

As the nucleon propagator is linear in the baryon mass, it is natural to intro-

duce the self-energy correction as:

$$m_N = m_0 + \sigma^N \,. \tag{6.1}$$

In the case of the ρ-meson we motivated the definition of m_0 by observations of lattice results. Here we use both the insights gained from the linear behaviour of the results of lattice QCD, as shown in Fig. 2.1, and the CBM results Fig. 6.3. We again take the bare mass, m_0, to be analytic in the quark mass:

$$m_0 = c_0 + c_2 m_\pi^2 \,. \tag{6.2}$$

6.1.1 Self-Energy Contributions

Once again we only include in the expression for the baryon masses the self-energy contributions that vary the most rapidly in quark mass near the chiral limit. In the case of the nucleon the two processes that contribute the most significantly are $N \to N\pi$ and $N \to \Delta\pi$. In chapter 5 we saw that the two contributing self-energy terms yielded the leading non-analytic and next-to-leading non-analytic behaviour of the ρ meson mass. It is not surprising that the self-energy contributions we investigate for the nucleon (and the Delta discussed below) also contribute the same LNA and NLNA chiral behaviour to the nucleon.

As was discussed in Ref. [66], the formal analytic expression for the pion cloud correction to the masses of the N are of the form [71]:

$$\sigma^N_{N\pi} = -\frac{3}{16\pi^2 f_\pi^2} g_A^2 \int_0^\infty dk \frac{k^4 u^2_{NN}(k)}{w^2_\pi(k)} \,, \tag{6.3}$$

$$\sigma^N_{\Delta\pi} = -\frac{3}{16\pi^2 f_\pi^2} \frac{32}{25} g_A^2 \int_0^\infty dk \frac{k^4 u^2_{N\Delta}(k)}{w_\pi(k)(\Delta M + w_\pi(k))} \,, \tag{6.4}$$

where g_A is the axial charge of the nucleon and has the value 1.26. The mass difference between the Δ and N is given by ΔM, and once again the energy of the

pion with momentum k is given by $w_\pi(k)$. The coupling constants have been related to the $NN\pi$ coupling through SU(6) symmetry, which itself has been related, by chiral symmetry, to $g_A/2f_\pi$. These relationship are discussed in some detail in Sec. 4.2.1. We again use the insight that the size of the source of the pions is finite in extent, to motivate the introduction of the form factors u_{NN}, and $u_{N\Delta}$. This simple physical insight will regulate the integrals so that they do not become divergent.

As for the case of the ρ we choose a dipole for the form factors, which is a common phenomenological choice. We have investigated the model dependence of this choice in Sec. 6.6. We take our preferred dipole for the form factors:

$$u_{NN}(k) = u_{N\Delta}(k) = \left(\frac{\Lambda_N^2 - \mu_\pi^2}{\Lambda_N^2 + k^2}\right)^2 , \tag{6.5}$$

where we follow the convention of this thesis by defining μ_π to be the physical pion mass, and k being the magnitude of the loop (3-)momentum. We define the dipole mass, for the case of the nucleon, to be Λ_N. This definition will allow us to distinguish the result from that of the Δ, Λ_Δ, discussed later in this chapter.

6.1.2 Extrapolation Formula

If we collect together the definition of the nucleon mass, Eq. (6.1), with the definition of the bare mass, Eq. (6.2), and the results of Eqs. (6.3) and (6.4) we have the following expression of the nucleon mass, as a function of m_π:

$$m_N = c_0 + c_2 m_\pi^2 + \sigma_{N\pi}^N(\Lambda_N, m_\pi) + \sigma_{\Delta\pi}^N(\Lambda_N, m_\pi) . \tag{6.6}$$

6.2 Limiting Conditions For m_N

Chiral symmetry for the nucleon is well defined for both the leading and next-to-leading non-analytic behaviour in the quark mass. The case of the $\rho \to \pi\pi$ had the

inherent difficulty that both intermediate state particles were light. This is not the case here, both the N and Δ are considered heavy in χPT. As was discussed in the case of the ρ-meson, by construction, all the non-analytic behaviour of Eq. (6.6) is restricted to the self-energy terms $\sigma^N_{N\pi}$ and $\sigma^N_{\Delta\pi}$. Thus we need only to investigate the self-energy terms to see how they behave in the limits.

6.2.1 The Chiral Limit

The LNA and NLNA behaviour of Eqs. (6.3) and (6.4) is associated with the infrared behaviour of the integrals, i.e. the behaviour as $k \to 0$. As a consequence, the leading non-analytic behaviour should not depend on the details of the high momentum cut-off, or the form factors. In particular, it should be sufficient for studying the LNA contributions to evaluate the self-energy integrals using a simple sharp cut-off, $u(k) = \theta(\Lambda - k)$. Another perspective on this is to say the leading non-analytic (LNA) terms are those which correspond to the lowest order non-analytic functions of m_q – i.e. odd powers or logarithms of m_π.

Using a θ-function for the form factors, the $NN\pi$ integral (c.f. Fig. 6.1(a)) is easily evaluated in the heavy baryon approximation used here:

$$\begin{aligned}\sigma^N_{N\pi} &= -\frac{3}{16\pi^2 f_\pi^2} g_A^2 \int_0^\Lambda dk \frac{k^4}{w_\pi^2(k)} \\ &= -\frac{3g_A^2}{16\pi^2 f_\pi^2}\left(m_\pi^3 \arctan\left(\frac{\Lambda}{m_\pi}\right) + \frac{\Lambda^3}{3} - \Lambda m_\pi^2\right) . \end{aligned} \tag{6.7}$$

Looking at the behaviour of Eq. (6.7) in the limit $m_\pi \to 0$, allows the extraction of the non-analytic behaviour. It should be noted that the integrand is of exactly the same form as Eq. (5.41), and therefore it should come as no surprise that the leading non-analytic term is $\mathcal{O}(m_\pi^3)$, in agreement with [72]:

$$\sigma^N_{N\pi}\big|_{\text{LNA}} = -\frac{3}{32\pi f_\pi^2} g_A^2 m_\pi^3 . \tag{6.8}$$

The integral corresponding to the process shown in Fig. 6.1(b), the $N \to \Delta\pi$ self-energy, with a θ-function form factor, may be analytically evaluated. For $m_\pi > \Delta M$

$$\begin{aligned}\sigma^N_{\Delta\pi} &= -\frac{g_A^2}{25\pi^2 f_\pi^2}(12(m_\pi^2-\Delta M^2)^{3/2}\left\{\arctan\left(\frac{\sqrt{m_\pi^2+\Lambda^2}+\Delta M+\Lambda}{\sqrt{m_\pi^2-\Delta M^2}}\right)\right.\\ &\left.-\arctan\left(\frac{\Delta M+m_\pi}{\sqrt{m_\pi^2-\Delta M^2}}\right)\right\}\\ &+3\Delta M(3m_\pi^2-2\Delta M^2)\ln\left(\frac{\sqrt{m_\pi^2+\Lambda^2}+\Lambda}{m_\pi}\right)\\ &-3\sqrt{m_\pi^2+\Lambda^2}\Delta M\Lambda+6\Delta M^2\Lambda-6m_\pi^2\Lambda+2\Lambda^3)\,, \end{aligned} \tag{6.9}$$

while for $m_\pi < \Delta M$ we find

$$\begin{aligned}\sigma^N_{\Delta\pi} &= -\frac{g_A^2}{25\pi^2 f_\pi^2}\left(-6(\Delta M^2-m_\pi^2)^{3/2}\times\right.\\ &\left[\ln\left(\frac{\sqrt{\Delta M^2-m_\pi^2}+\sqrt{m_\pi^2+\Lambda^2}+\Delta M+\Lambda}{\sqrt{\Delta M^2-m_\pi^2}-\sqrt{m_\pi^2+\Lambda^2}-\Delta M-\Lambda}\right)\right.\\ &\left.\left.-\ln\left(\frac{\sqrt{\Delta M^2-m_\pi^2}+\Delta M+m_\pi}{\sqrt{\Delta M^2-m_\pi^2}-\Delta M-m_\pi}\right)\right]\right.\\ &+3\Delta M(3m_\pi^2-2\Delta M^2)\ln\left(\frac{\sqrt{m_\pi^2+\Lambda^2}+\Lambda}{m_\pi}\right)\\ &\left.-3\sqrt{m_\pi^2+\Lambda^2}\Delta M\Lambda+6\Delta M^2\Lambda-6m_\pi^2\Lambda+2\Lambda^3\right)\,. \end{aligned} \tag{6.10}$$

This result is reminiscent of the result for $\Sigma^\rho_{\pi\pi}$. Both self-energies involve transitions, $\rho \to \pi$ and $N \to \Delta$, which are characterised by branch points at $m_\pi = \mu_\rho/2$ and $m_\pi = \Delta M$ respectively. The effect of this branch point is reduced by a cancellation in the logarithmic terms at $m_\pi = \Delta M$, unlike the result for the $\Delta \to N\pi$ self-energy which is explored in section 6.4.1.

An expansion of Eq. (6.10) leads to the result for the NLNA term in the

nucleon self-energy:

$$\sigma^N_{\Delta\pi}\big|_{\rm NLNA} = \frac{3g_A^2}{16\pi^2 f_\pi^2}\frac{32}{25}\frac{3}{8\Delta M} m_\pi^4 \ln(m_\pi)\,, \tag{6.11}$$

which is again as expected from χPT [44].

Of course, our concern with respect to lattice QCD is not so much the behaviour as $m_\pi \to 0$, but the extrapolation from high pion masses to the physical pion mass. In this context the branch point at $m_\pi^2 = \Delta M^2$ is at least as important as the LNA near $m_\pi = 0$. We shall return to this point later. We note that Banerjee and Milana [73] found the same non-analytic behaviour as $m_\pi \to \Delta M$ that we find. However they were not concerned with finding a form that could be used at large pion masses — i.e. one that is consistent with heavy quark effective theory.

6.2.2 The Static Quark Limit

Heavy quark effective theory suggests that as $m_\pi \to \infty$ the quarks become static and hadron masses become proportional to the quark mass. This has been rather well explored in the context of successful non-relativistic quark models of charmonium and bottomium [74]. However, as discussed previously, we are not in the heavy quark limit (where $m_\pi \propto m_q$), but in the region where the baryon masses are indeed becoming proportional to the quark mass and yet $m_\pi^2 \propto m_q$ still. In this spirit, corrections are expected to be of order $1/m_q$ where m_q is the heavy quark mass. Thus we would expect the pion induced self-energy to vanish at least as fast as $1/m_q$ as the pion mass increases. The presence of a fixed cut-off Λ acts to suppress the pion induced self-energy for increasing pion masses, as evidenced by the m_π^2 in the denominators of Eqs. (6.3) and (6.4). While some m_π^2 dependence in Λ is expected, this is a second-order effect and does not alter the qualitative features.

By expanding the arctan (Λ/m_π) term in Eq. (6.7) for small Λ/m_π, we find

$$\sigma_{N\pi}^{N} = -\frac{3g_A^2}{16\pi^2 f_\pi^2} m_\pi^3 \sum_{i=0}^{\infty} \frac{(-1)^i}{(2i+5)} \left(\frac{\Lambda}{m_\pi}\right)^{2i+5} \tag{6.12}$$

$$= -\frac{3g_A^2}{16\pi^2 f_\pi^2} \frac{\Lambda^5}{5m_\pi^2} + \mathcal{O}\left(\frac{\Lambda^7}{m_\pi^4}\right), \tag{6.13}$$

which vanishes for $m_\pi \to \infty$. Indeed, in the large m_π (heavy quark) limit, Eq. (6.10) also tends to zero as $1/m_\pi^2$.

6.2.3 The Mass in the Chiral Limit

It was mentioned in section 5.2.3 that the bare mass m_0 that is discussed here is not actually the mass of the hadron in the chiral limit. We emphasise the point again here. The fact that the bare mass is only part of the chiral mass, is a direct consequence of the concepts argued for here in requiring the self-energy terms in the extrapolation. The non-analytic structure of the chiral mass is predicted by chiral perturbation theory. We have shown above that we do in fact reproduce the leading and next-to-leading non-analytic behaviour of this chiral mass, but that this non-analytic structure comes only from the self-energy contributions. Without such terms an extrapolation formula has little grounding in physics, missing well known behaviour. As can be seen in Fig. 6.4 the contributions from the self-energy terms $\sigma_{N\pi}^{N}$, Eq. (6.3), and $\sigma_{\Delta\pi}^{N}$, Eq. (6.4) are non-vanishing at the chiral limit, and so our mass for the nucleon in the chiral limit is

$$m_N^{(0)} = c_0 + \sigma_{N\pi}^{N}(\Lambda_N, m_\pi = 0) + \sigma_{\Delta\pi}^{N}(\Lambda_N, m_\pi = 0)\,. \tag{6.14}$$

6.3 The Δ Baryon

The functional form for the mass of the Δ is motivated in exactly the same way as were the nucleon and ρ-meson masses discussed previously. We follow our golden

rule of retaining the self-energy contributions which yield the most rapid variation with m_π near the chiral limit. The point has been made previously that these terms in fact yield the leading, and next-to-leading, non-analytic behaviour. We presented in Fig. 6.1 the pion induced self-energies to Δ. Once again we have restricted the intermediate baryon states to those most strongly coupled, namely the N and Δ states. As was the case for the nucleon, we have the Δ mass modified as

$$m_\Delta = m_0 + \sigma^\Delta \,. \tag{6.15}$$

Observation of lattice results motivates the definition of the bare mass, m_0, to be analytic in the quark mass:

$$m_0 = c_0 + c_2 m_\pi^2 \,. \tag{6.16}$$

This is the exactly the same form as was used in Eq. (6.2) for the nucleon and Eq. (5.2) for the ρ-meson. This behaviour is indicated by the lattice, and not entirely unexpected. The concept of a bare object that is dressed in some manner is common in both nuclear and particle physics. The Dyson-Schwinger equation is a perfect example. Here we see that, to one pion loop, that lattice is indicating that hadrons are a *bare core* with corrections that are quark mass dependent.

6.3.1 Self-Energy Contributions

The greatest contributions to the self-energy of the Δ are from the two processes shown in Fig. 6.1, that is $\Delta \to \Delta\pi$ and $\Delta \to N\pi$. These are retained as they satisfy our requirement of providing the most rapid variation with quark mass near the chiral limit. We show below that as was the case for the nucleon and the ρ-meson these two terms contain both the LNA and NLNA chiral behaviour. We define the self-energy contribution to the mass, σ^Δ, by

$$\sigma^\Delta = \sigma^\Delta_{\Delta\pi} + \sigma^\Delta_{N\pi} \,.$$

References [66, 71] present the formal analytic expressions for these pion cloud correction to the mass of the Δ. We reproduce those results here:

$$\begin{aligned}\sigma^{\Delta}_{\Delta\pi}(\Lambda_\Delta, m_\pi) &= \sigma^{N}_{N\pi} \\ &= -\frac{3}{16\pi^2 f_\pi^2} g_A^2 \int_0^\infty dk \frac{k^4 u^2_{\Delta\Delta}(k)}{w^2_\pi(k)}, \qquad (6.17)\\ \sigma^{\Delta}_{N\pi}(\Lambda_\Delta, m_\pi) &= \frac{3}{16\pi^2 f_\pi^2}\frac{8}{25} g_A^2 \int_0^\infty dk \frac{k^4 u^2_{\Delta N}(k)}{w_\pi(k)(\Delta M - w_\pi(k))}, \qquad (6.18)\end{aligned}$$

where we use the notation and definitions described below Eq. (6.4). We take the phenomenologically motivated dipole for our form factors

$$u_{\Delta\Delta}(k) = u_{N\Delta}(k) = \left(\frac{\Lambda_\Delta^2 - \mu_\pi^2}{\Lambda_\Delta^2 + k^2}\right)^2, \qquad (6.19)$$

with the dipole mass given by Λ_Δ, and the usual definitions for the magnitude of the loop (3-)momentum, k, and the physical pion mass μ_π.

6.3.2 Extrapolation Formula

We showed in Eq. (6.15) how the mass of the Δ would be modified by pion induced self-energy contributions. By substituting the appropriate definitions for the bare mass, Eq. (6.16), and the pion induced self energies, Eqs. (6.17) and (6.18), we come to the following expression for the Δ mass, as a function of m_π:

$$m_\Delta = c_0 + c_2 m_\pi^2 + \sigma^{\Delta}_{\Delta\pi}(\Lambda_\Delta, m_\pi) + \sigma^{\Delta}_{N\pi}(\Lambda_\Delta, m_\pi). \qquad (6.20)$$

6.4 Limiting Conditions For m_Δ

As was discussed in section 6.2 the non-analytic behaviour of the nucleon mass is well defined in chiral symmetry. The same is true for the Δ, which is also considered heavy in the χPT framework. Once again, by construction, all the non-analytic

(in quark mass) behaviour of Eq. (6.20) is limited to the pion induced self-energy contributions, $\sigma^{\Delta}_{\Delta\pi}$ and σ^{Δ}_{π}. Thus when we investigate the behaviour near the chiral limit we need only to look at the behaviour of the self-energy terms.

6.4.1 The Chiral Limit

We have previously motivated the use of a sharp cut-off, $u(k) = \theta(\Lambda - k)$, for the form factors when investigating the infrared behaviour of the self-energy contributions to the baryon masses. The behaviour as the loop momentum $k \to 0$ allows the extraction of the lowest order non-analytic behaviour of these expressions as functions of m_π. We then compare this behaviour to the model independent predictions of χPT, showing that we reproduce the LNA and NLNA behaviour that is expected to be present in the functional form for the mass.

Since the form of $\sigma^{\Delta}_{\Delta\pi}$ is exactly that of the $\sigma^{N}_{N\pi}$ we may use the result of Eq. (6.7) to write down directly the analytic form for this integral:

$$\begin{aligned}
\sigma^{\Delta}_{\Delta\pi} &\equiv \sigma^{N}_{N\pi} \\
&= -\frac{3}{16\pi^2 f_\pi^2} g_A^2 \int_0^\Lambda dk \frac{k^4}{w_\pi^2(k)} \\
&= -\frac{3g_A^2}{16\pi^2 f_\pi^2} \left(m_\pi^3 \arctan\left(\frac{\Lambda}{m_\pi}\right) + \frac{\Lambda^3}{3} - \Lambda m_\pi^2 \right) . \qquad (6.21)
\end{aligned}$$

Naturally we have exactly the same result for the chiral limit, that is $m_\pi \to 0$, as we had in the $\sigma^{N}_{N\pi}$ case. The leading non-analytic term is once again $\mathcal{O}(m_\pi^3)$:

$$\sigma^{\Delta}_{\Delta\pi}|_{\rm LNA} = -\frac{3}{32\pi f_\pi^2} g_A^2 m_\pi^3 . \qquad (6.22)$$

The other self-energy contribution to the Δ mass is from that shown in Fig. 6.1(c), the $\Delta \to N\pi$ self-energy. When we evaluate the integral, with a θ-function form factor, the result is similar to that of Eq. (6.9). Again, as there is a branch point

at $m_\pi = \Delta M$ we present the two limits independently. For $m_\pi > \Delta M$ we have

$$\begin{aligned}\sigma^{\Delta}_{N\pi} &= \frac{g_A^2}{100\pi^2 f_\pi^2}(-12(m_\pi^2-\Delta M^2)^{3/2}\left\{\arctan\left(\frac{\sqrt{m_\pi^2+\Lambda^2}-\Delta M+\Lambda}{\sqrt{m_\pi^2-\Delta M^2}}\right)\right.\\ &\left.+\arctan\left(\frac{\Delta M-m_\pi}{\sqrt{m_\pi^2-\Delta M^2}}\right)\right\}\\ &+3\Delta M(3m_\pi^2-2\Delta M^2)\ln\left(\frac{\sqrt{m_\pi^2+\Lambda^2}+\Lambda}{m_\pi}\right)\\ &-3\sqrt{m_\pi^2+\Lambda^2}\Delta M\Lambda-6\Delta M^2\Lambda+6m_\pi^2\Lambda-2\Lambda^3)\,, \end{aligned} \tag{6.23}$$

whilst the form for $m_\pi < \Delta M$ is

$$\begin{aligned}\sigma^{\Delta}_{N\pi} &= \frac{g_A^2}{100\pi^2 f_\pi^2}\left(6(\Delta M^2-m_\pi^2)^{3/2}\times\right.\\ &\left[\ln\left(\frac{\sqrt{\Delta M^2-m_\pi^2}+\sqrt{m_\pi^2+\Lambda^2}-\Delta M+\Lambda}{\sqrt{\Delta M^2-m_\pi^2}-\sqrt{m_\pi^2+\Lambda^2}+\Delta M-\Lambda}\right)\right.\\ &\left.\left.+\ln\left(\frac{\sqrt{\Delta M^2-m_\pi^2}+\Delta M-m_\pi}{\sqrt{\Delta M^2-m_\pi^2}-\Delta M+m_\pi}\right)\right]\right.\\ &+3\Delta M(3m_\pi^2-2\Delta M^2)\ln\left(\frac{\sqrt{m_\pi^2+\Lambda^2}+\Lambda}{m_\pi}\right)\\ &\left.-3\sqrt{m_\pi^2+\Lambda^2}\Delta M\Lambda-6\Delta M^2\Lambda+6m_\pi^2\Lambda-2\Lambda^3\right)\,. \end{aligned} \tag{6.24}$$

It should be noted that the branch point at $m_\pi = \Delta M$ is important in this situation. In the case of the nucleon, there was a cancellation between the first two terms at the opening of the cut, resulting in a zero weighting there. However, in the case of the Δ, there is a reinforcement between these terms.

The effect of this branch point at $m_\pi = \Delta M$ is seen as a point of inflection at $m_\pi^2 \sim 0.1$ GeV^2 in, for example, Fig. 6.4. It occurs exactly at the point where the decay of the Δ to $N\pi$ is energetically allowed. The correct description of this curvature is clearly very important if one wishes to obtain the Δ–N mass difference at the physical pion mass. It must be noted that the previous attempts at extrapolation formulae, as discussed in section 5.4.1, and also below, do not include this

behaviour. We showed that in the case of the ρ-meson the opening of a decay channel is important, and we show below that this is even more important in the case of the extrapolation of the Δ mass.

Though there is the important distinction between the behaviour of $\sigma^N_{\Delta\pi}$ and $\sigma^\Delta_{N\pi}$ around the cut, the non-analytic behaviour is quite similar. The leading non-analytic term contributed by $\sigma^\Delta_{N\pi}$ is $\mathcal{O}\left(m_\pi^4 \ln(m_\pi)\right)$, and so in Eq. (6.20) it will contribute the NLNA term (the LNA term is $\mathcal{O}(m_\pi^3)$ from $\sigma^N_{\Delta\pi}$):

$$\sigma^\Delta_{N\pi}|_{\text{NLNA}} = -\frac{3g_A^2}{16\pi^2 f_\pi^2}\frac{8}{25}\frac{3}{8\Delta M} m_\pi^4 \ln(m_\pi)\,. \tag{6.25}$$

As has been the case in the previous cases presented in this thesis we have evaluated these self-energy contributions in the heavy baryon approximation.

6.4.2 The Static Quark Limit

Observationally it is clear that the functional differences between the expressions for $\sigma^N_{\Delta\pi}$ and $\sigma^\Delta_{N\pi}$ become less important as the quarks become heavier. Equivalently since the expressions for $\sigma^N_{N\pi}$ and $\sigma^\Delta_{\Delta\pi}$ are identical, we therefore can use the results presented in section 6.2.2 to explore the behaviour of the extrapolation formula in this limit.

We explored the large m_π behaviour of Eq. (6.21) (which is analogous to Eq. (6.12)) and found

$$\sigma^\Delta_{\Delta\pi} = -\frac{3g_A^2}{16\pi^2 f_\pi^2}\frac{\Lambda^5}{5m_\pi^2} + \mathcal{O}\left(\frac{\Lambda^7}{m_\pi^4}\right)\,, \tag{6.26}$$

which, as expected, vanishes for $m_\pi \to \infty$. We also state (without further explanation) that in the large m_π limit, Eq. (6.24) also tends to zero as $1/m_\pi^2$.

As has been previously mentioned these expressions are only a first order approximation, and the corrections to the baryon mass are expected to be of order

of the inverse of the heavy quark mass. This is exactly the behaviour we already see, suggesting such effects will not change the general detail of the results presented. It is also expected that this characteristic feature would not be altered by second-order effects, including possible m_π^2 dependence in Λ. We reiterate that Λ is related

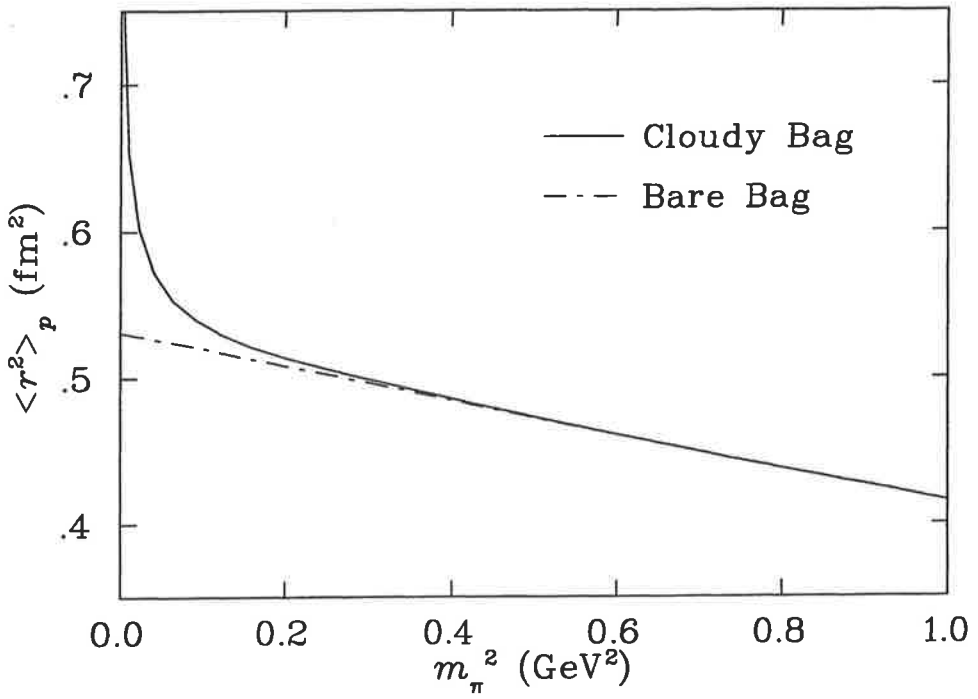

Figure 6.2: The mean charge square radius of the proton calculated in the Cloudy Bag Model (CBM). The solid line is the value calculated within the CBM including the pion cloud effects. The dot–dashed line is the contribution from the bare bag. The change in the size of the bag over the range is at the 10% level.

to size of the baryon *core*. The size of the core, or bare baryon, is not expected to vary significantly over the range of pion masses we are investigating. Indeed a simple CBM calculation of the mean square radius of the proton, Fig. 6.2, suggests that the change in the size of the core is only at the 10% level over the range we discuss.

6.4.3 The Δ Mass in the Chiral Limit

The inclusion of the self-energy terms in the mass formula for the Δ provides the correct leading non-analytic and next-to-leading non-analytic structure that is required by χPT. Notionally we have dressed the bare Δ with a pion cloud, in a similar way to the Cloudy Bag Model dressing a bare bag, with a pion cloud. This means however that the chiral mass is not simply that of the bare Δ. We have seen in the cases of the nucleon and ρ that the physical mass is only slightly more complicated though, and that is also the case here:

$$m_{\Delta}^{(0)} = c_0 + \sigma_{\Delta\pi}^{\Delta}(\Lambda_{\Delta}, m_{\pi} = 0) + \sigma_{N\pi}^{\Delta}(\Lambda_{\Delta}, m_{\pi} = 0)\,. \tag{6.27}$$

The self-energy contributions to the Δ (and also nucleon) mass for a 1 GeV dipole are shown in Fig. (6.4). It is clear that they are non-vanishing at the chiral limit, reinforcing the need to retain these terms when taking the chiral limit.

6.5 Cloudy Bag Model Results

The Cloudy Bag Model (CBM) was discussed in chapter 4, and so there is little need to go into the reasoning behind why we undertook investigations in the model. The benefits that were gained by having a model that incorporated both chiral symmetry and the heavy quark limit, whilst allowing us to access the region between these two limits was extremely useful. We needed some insight into how the hadron masses might behave between these limits, and the CBM did this admirably.

In Sec. 4.2.3 Fig. 4.3, reproduced here as Fig. 6.3, was presented showing how both the CBM results, and our extrapolation formulae depend on m_{π}^2. At the time the derivation of, and reasoning behind, the formula was not presented. The previous sections of this chapter will hopefully have made some of this clearer.

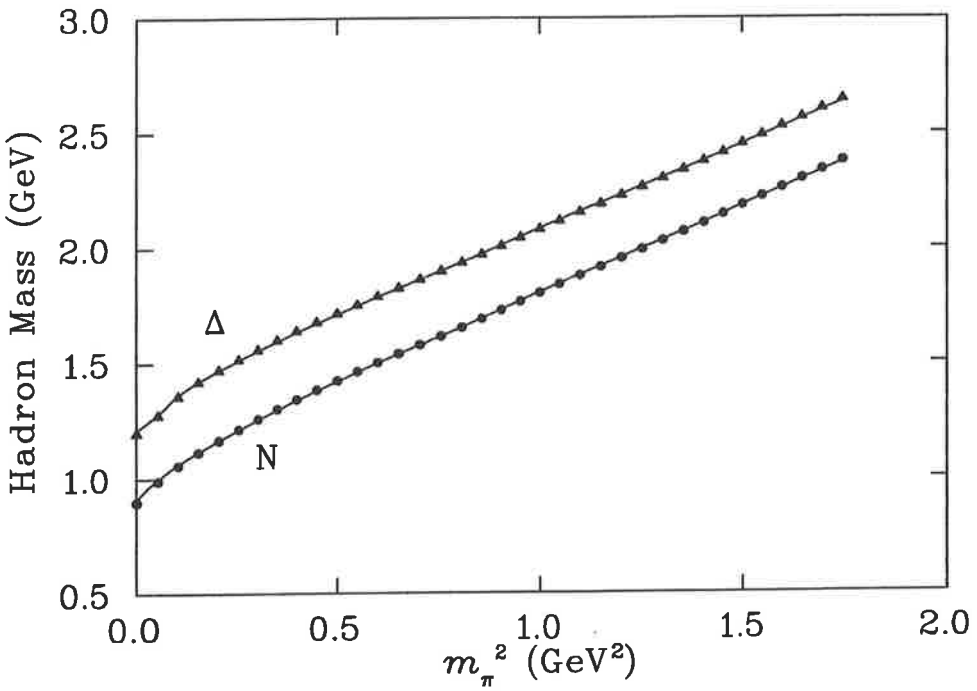

Figure 6.3: The pion mass dependence of the N and Δ baryons generated in the CBM using a dipole form factor with $\Lambda = 1.0$ GeV. This is a reproduction of Fig. 4.3.

Figure 6.3 shows the behaviour of the N and Δ masses in the CBM as a function of m_π^2 for the particular choice of a 1 GeV dipole. The solid lines show the fits using Eqs. (6.6) and (6.20) — with a sharp (θ-function) cut-off. We choose a sharp cut-off as we wish to explore what model dependence there is in the extrapolation of the CBM data. This different perspective on model dependence from strictly lattice results removes some inherent bias.

Baryon	c_0 (GeV)	c_2 (GeV^{-1})	Λ (GeV)	m_B (GeV)	Error
N	1.09	0.739	0.455	0.948	0.8%
Δ	1.37	0.725	0.419	1.236	0.3%

Table 6.1: Parameter sets for the fit to the CBM data. The form factor used in Eqs. (6.6) and (6.20) is a sharp cut-off, the CBM data was calculated with a 1.0 GeV dipole form factor.

It can be seen that our extrapolation to the physical pion mass is in good agreement with the CBM calculations. At the physical pion mass the extrapolated N mass is within 0.8% of the experimental value to which the CBM was fitted, while the Δ is within 0.3% of the experimental value. We present the parameters of our fit in Table 6.1. The value for the sharp cut-off $(\Lambda_N, \Lambda_\Delta)$ is $(0.455, 0.419)$ GeV, compared to $\Lambda = 1.0$ GeV for the dipole form factor used to generate the CBM results.

It was noted in sections 6.2.3 and 6.4.3 that the constant c_0 in our functional form is not the mass of the baryon in the chiral limit, but rather this is given by $m_N^{(0)} = c_0 + \sigma_{N\pi}^N(\Lambda, 0) + \sigma_{\Delta\pi}^N(\Lambda, 0)$ — with an analogous expression for the Δ. We find that the extrapolated N and Δ masses in the chiral (SU(2)-flavour) limit are $(M_N^{(0)}, M_\Delta^{(0)}) = (905, 1210)$ MeV, compared with the CBM values $(898, 1197)$ MeV.

The mass dependence of the pion induced self-energies, $\sigma_{j\pi}^i$, for the 1 GeV dipole form factor, is displayed in Fig. 6.4. The choice of a 1.0 GeV dipole corresponds to the observed axial form factor of the nucleon [75], which is probably our best phenomenological guide to the pion-nucleon form factor [76]. We note that $\sigma_{N\pi}^N$ tends to zero smoothly as m_π grows and it is only below $m_\pi^2 \sim 0.2$ GeV^2 that there is any rapid variation. That this behaviour cannot be well described by a polynomial expansion is illustrated by the dotted curve in Fig. 6.4. There we expanded $\sigma_{N\pi}^N$ about $m_\pi = 0$ as a simple polynomial, $c_0 + c_2 m_\pi^2 + c_3 m_\pi^3$, with c_3 fixed at the value required by chiral symmetry, in analogy with section 5.4.1. Clearly the expansion fails badly for m_π beyond 300–400 MeV.

The behaviour of the $N\pi$ contribution to the self-energy of the Δ is especially interesting. In particular, the effect of the branch point at $m_\pi = \Delta M$ is seen in the curvature at $m_\pi^2 \sim 0.1$ GeV^2. For comparison, we note that while there is also a branch point in the nucleon self-energy at the same point — see Eq. (6.9) –

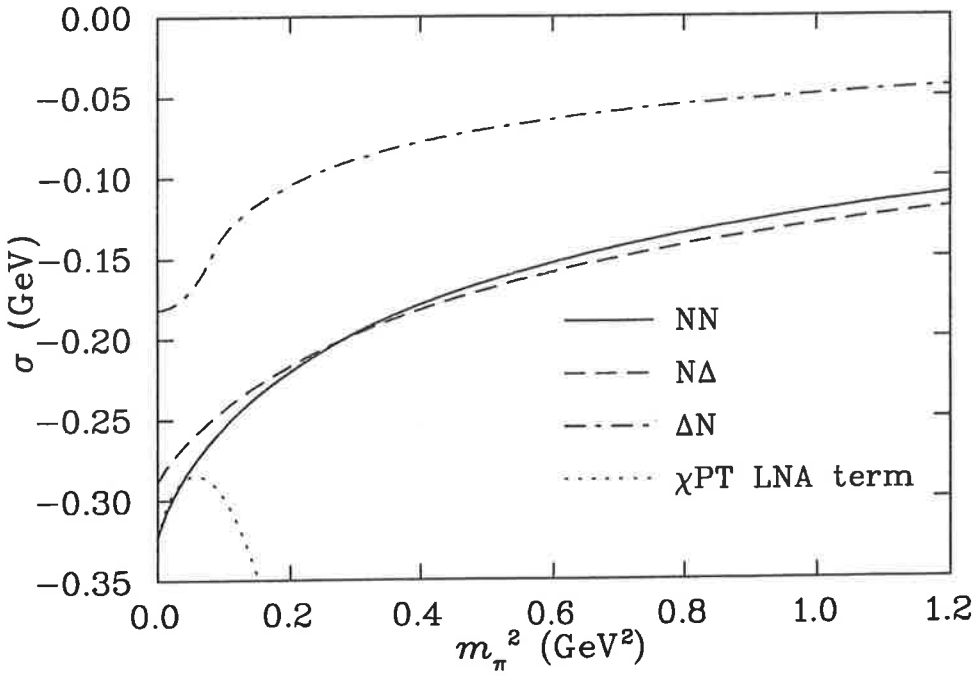

Figure 6.4: Variation with pion mass of the self-energy contributions to the nucleon and Δ, Eqs. (6.3), (6.4), and (6.18), for a dipole form factor with $\Lambda = 1.0$ GeV. We note that $\sigma^{\Delta}_{\Delta\pi} \equiv \sigma^{N}_{N\pi}$ in this case. The LNA term of χPT tracks the $NN\pi$ contribution up to $m_\pi \sim 0.2$ GeV, beyond which the internal structure of the nucleon becomes important.

the coefficient of $(m_\pi^2 - \Delta M^2)^{3/2}$ vanishes at this point. As a consequence there is little or no curvature visible in the latter quantity at the same point.

Figure 6.5 illustrates the degree of residual model dependence in our use of Eqs. (6.6) and (6.20). There the variation of the nucleon self-energy, $\sigma^N_{N\pi}$, calculated with a 1.0 GeV dipole form factor (solid curve) is fit using the form $\alpha + \beta m_\pi^2 + \sigma^N_{N\pi}(\Lambda, m_\pi)$ (dash curve, with $\alpha = -0.12$ GeV, $\beta = 0.39$ GeV^{-1} and $\Lambda = 0.57$ GeV). Note that the deviations are at the level of a few MeV. For the Δ the self-energy, $\sigma^{\Delta}_{N\pi}$, is again calculated using a 1.0 GeV dipole form factor and fit with our standard fitting function, $\alpha + \beta m_\pi^2 + \sigma^{\Delta}_{N\pi}(\Lambda, m_\pi)$. The quality of the fit (with $\alpha = -0.062$GeV, $\beta = 0.024$ GeV^{-1} and $\Lambda = 0.53$ GeV) is not as good as for

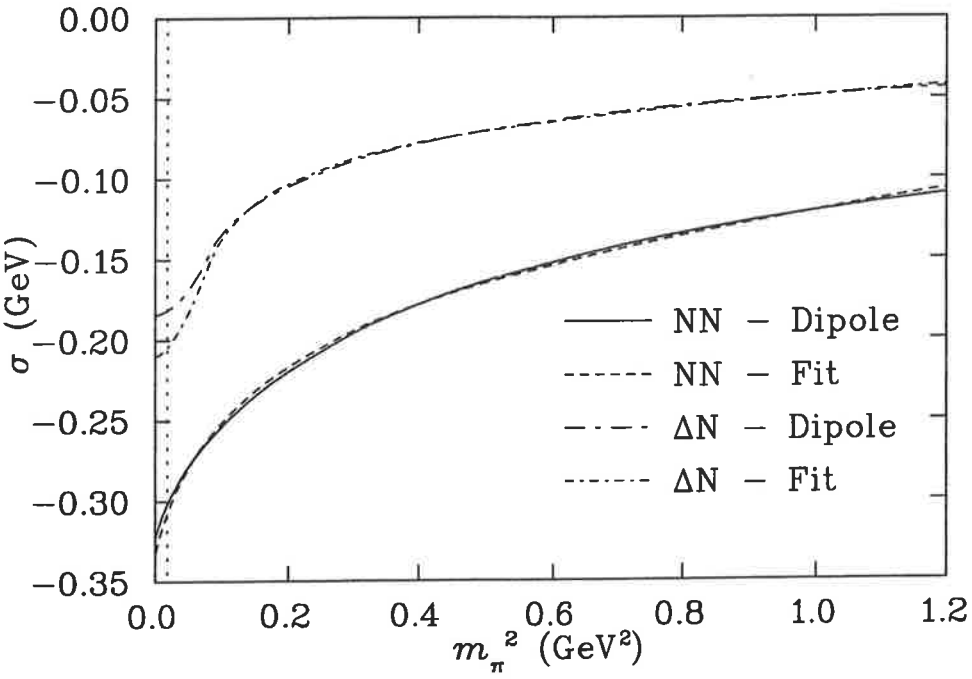

Figure 6.5: Comparison between the nucleon and Δ self-energies, $\sigma^N_{N\pi}$ and $\sigma^\Delta_{N\pi}$, calculated using a dipole form factor (solid and long-dash dot curves, respectively) and fits using the form $\alpha + \beta m_\pi^2 + \sigma_{ij}(\Lambda, m_\pi)$, based on a sharp cut-off in the momentum of the virtual pion (dash and short-dash dotted curves respectively).

the nucleon case. Nevertheless, the difference between the two curves at the physical pion mass (vertical dotted line) is only about 20 MeV. At the present stage of lattice calculations this seems to be an acceptable level of form factor dependence for such a subtle extrapolation. However, in the following sections we will show that the choice of the sharp cut-off is not a reasonable choice for the form factor, and the model dependence for a reasonable choice of form factor (the meaning of reasonable will become obvious shortly) is quite small.

6.6 Fitting to Lattice Results

In chapter 5 we showed that taking in to account the discretisation of available momenta on the lattice was important. We also discussed that the model dependence of the results, based on the choice of form factor, was small. Here we will expand the discussion by presenting more results for three choices of form factor, and also by looking further at the dependence of the results on the discretisation of momenta.

In particular we will be investigating our preferred form factor, the dipole

$$u^D(k) = \left(\frac{\Lambda^2 - \mu_\pi^2}{\Lambda^2 + k^2}\right)^2 , \tag{6.28}$$

as discussed below Eq. (6.5), with μ_π being the physical pion mass. It is a simple extension from the dipole to the choice of a monopole. However we will show, that the monopole

$$u^M(k) = \left(\frac{\Lambda^2 - \mu_\pi^2}{\Lambda^2 + k^2}\right) , \tag{6.29}$$

does not give as good a fit to the lattice data as a dipole. The goodness of fit (we use the χ^2 per degree of freedom as this measure) for the monopole is sufficient however for it to be considered a reasonable choice of form factor, reinforcing our claims that this work is only weakly model dependent. The final form factor that we investigate is the θ-function, or sharp cut-off:

$$u^S(k) = \theta(\Lambda - k) . \tag{6.30}$$

We know that the behaviour of the self-energies in the chiral, or infrared, limit is independent of the choice of form factor, and we used the sharp cutoff to derive the leading, and next-to-leading behaviour in this limit. The appropriateness of such a form factor at higher masses however was not as well known before the investigations outlined below. In Fig. 6.6 we present the shapes of these form factors as a function of loop momentum, k. The solid and dashed lines are for the values

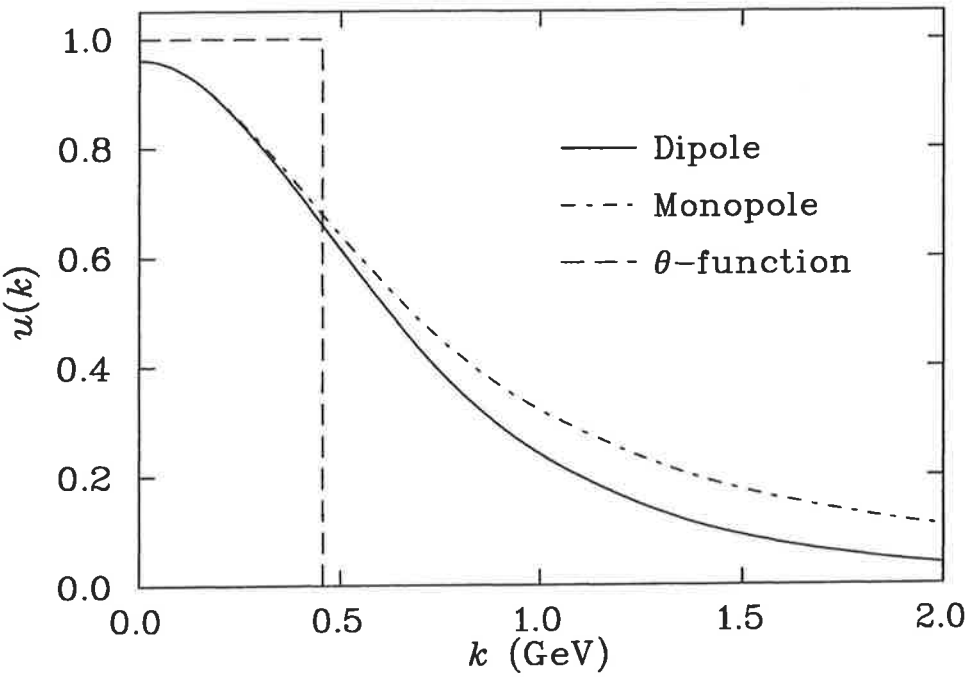

Figure 6.6: Loop momentum, k, dependence of three choices of form factor. The solid curve, a dipole given in Eq. (6.28) has $\Lambda_D = 1.0$ GeV. The monopole, Eq. (6.29), has the same mean-squared radius as the dipole, this results in $\Lambda_M = \Lambda_D/\sqrt{2}$ GeV. The dashed curve is a sharp cut-off with Λ chosen to give the best fit to the CBM results ($\Lambda = 0.455$ GeV).

of Λ discussed in section 6.5 for the best fits to the Cloudy Bag Model. It is clear that whilst the majority of the chiral behaviour of the self-energies comes from the infrared, or equivalently low-k, region the significant difference between the non-vanishing dipole and the identically zero sharp cut-off θ-function in the region up to 2.0 GeV undoubtedly makes a difference in the contributions from the self-energies.

6.6.1 Sharp Cut-Off Form Factor

We begin by considering the functional forms suggested in section 6.1.2 and 6.3.2 with the form factor chosen to be a θ-function with Λ fixed to the value determined by fitting the CBM calculations. As has been mentioned previously the data sets

from the UKQCD [21], and CP-PACS [20] collaborations are not consistent at their quoted values (Fig. 2.1). It has been our practice to shift the results within the quoted errors, as discussed in section 2.4, to improve the consistency.

The resulting fits to the baryon masses were investigated in our previous work [66]. There we explored the dependence of the parameters on the scaling of the data. Since there is 10% uncertainty in setting the scale for both the UKQCD and CP-PACS results we calculated fits for no scaling of the data, a 5% scaling on both data sets, and also adjusting just one data set to match the other. We found that even though the scaling adjusts the parameters of the extrapolation, the variance at the physical pion mass is of the order of 10%.

The evaluation of the self-energy contributions as a sum over discrete momenta was not undertaken in this case. However, we realise that a sharp cut off in the momenta of the pions emitted from a hadron is not at all realistic. The sharp cut off is an acceptable choice in the low momentum region. It permits analytic evaluation of the self-energy integrals which then allow the physical structure to be observed. Away from this region however the approximation breaks down.

Another reason for not investigating the sharp cut off is related to the discretisation of momenta itself. In our CBM investigations we found that the cut off was at a momenta about 450 MeV. The lowest available momenta on the lattices investigated are greater than this value! To have any contribution from the self-energy terms the cutoff must be pushed above the minimum non-zero lattice momenta, which would then decrease the goodness-of-fit. These two opposing pressures play off against each other resulting in an unacceptable goodness-of-fit.

6.6.2 Naïve Chiral Fits

In section 5.4.1 we commented that a popular approach to fitting lattice data involves a functional form motivated by chiral symmetry. The idea is to add to a linear (in m_π^2) formula a term that is of the same order as the leading non-analytic term predicted by chiral symmetry. In Sec 6.4.1 we saw that the LNA term for the nucleon is $\mathcal{O}(m_\pi^3)$. This is also the same order as the LNA term for the Δ and ρ-meson. Thus Eq. (5.67) is identically the result that the community uses as a

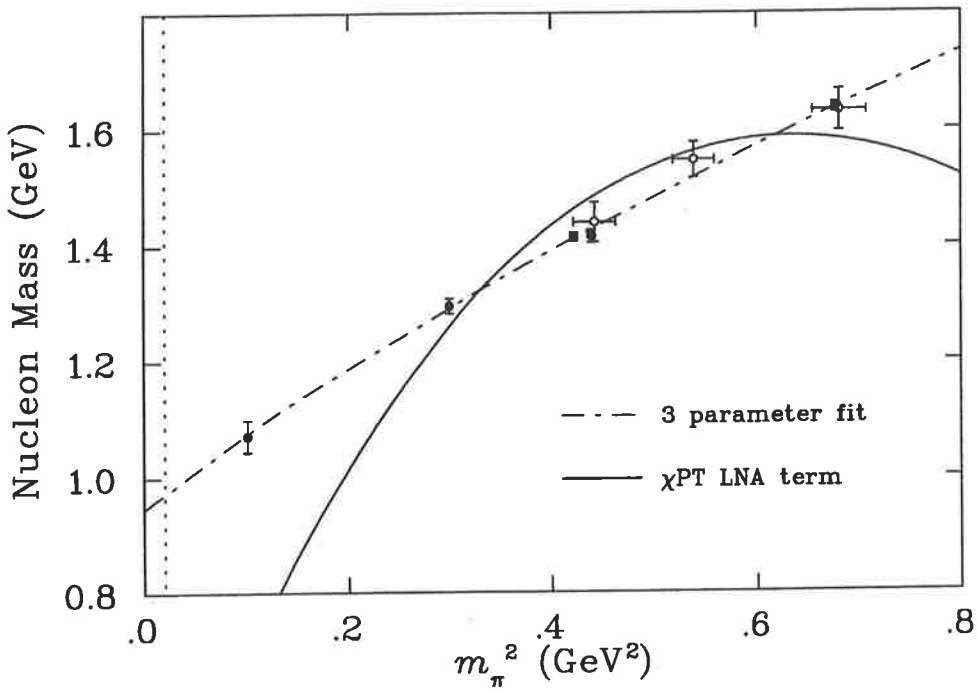

Figure 6.7: A comparison between phenomenological fitting functions for the mass of the nucleon. The solid curve corresponds to using Eq. 6.31 with c_3 set equal to the value known from χPT. The three parameter fit corresponds to letting c_3 vary as an unconstrained fit parameter.

chirally motivated extrapolation formula:

$$m_H = c_0 + c_2 m_\pi^2 + c_3 m_\pi^3 \,. \tag{6.31}$$

The results of such a fit for the nucleon are shown as the dashed-dot curve in Fig. 6.7. There is an analogous result for the Δ. We present the results of the fits for the N and Δ in Table 6.2. In section 5.4.1 we mentioned that the value of c_3 is known in

Fit		c_0 (GeV)	c_2 (GeV^{-1})	c_3 (GeV^{-2})	m_B (GeV)
N	(a)	0.18	6.68	-5.60	0.293
	(b)	0.95	1.42	-0.48	0.973
Δ	(a)	0.44	6.50	-5.60	0.556
	(b)	1.19	1.31	-0.55	1.22

Table 6.2: Parameter sets for the fits to the nucleon (shown in Fig. 6.7) and Δ. Set (a) is for the 2 parameter fit of (6.31) with c_3 from the known χPT result, and (b) for the 3 parameter fit of (6.31).

χPT for the ρ-meson. The same claim applies here. In section 6.4.1 we showed that our extrapolation formula has the correct coefficient for the leading non-analytic term in the self-energy for the nucleon. When we fix the value of c_3 in Eq. (6.31) to that of χPT and repeat the fit we find a similar result as that of section 5.4.1. The fit (shown as the solid line in Fig. 6.7) is reminiscent of the result we found with the ρ meson. This expression fails to converge in the region in which the lattice results exist. Chiral perturbation theory is applied outside the region in which it is expected to be valid. If we do not force the coefficient of the cubic term to be that of χPT we expect, and indeed find it to be small. The cubic term will attempt to mock-up the slight curvature in the masses at heavy quark masses. The act of allowing it to be a fit parameter has resulted in the loss of the advantages introduced by including a term motivated by χPT.

6.6.3 Improved Chiral Fits

We again base out fits on lattice results restricted to the region below 0.8 GeV^2. The rational as previously stated is that to move further away from the chiral limit

would dictate higher order analytic terms beyond the first two in our extrapolation formulae, Eqs. (6.6) and (6.20). We have used a dipole as our preferred fitting form, and evaluated the self-energy contributions using the discrete sum, Eq. (5.66), discussed in Secs. 2.1.2 and 5.4. The results of this fit, following the convention set in chapter 5, are shown as the open squares in the following graphs of the hadron mass. The parameters of the fit c_0, c_2, and Λ_N are then used in an exact evaluation of Eq. (6.6) using the integrals Eqs. (6.3), (6.4) for the nucleon. A similar prescription applies to the Δ where we evaluate the self-energy integrals (6.17) and (6.18) for the appropriate parameters. We do not consider that there is enough information currently provided in the data to independently constrain both Λ_N and Λ_Δ, and so we constrain out fits to have the same form factor dependence ($\Lambda_N \equiv \Lambda_\Delta$). Thus we have 5 independent parameters for our fits: c_{0N}, c_{2N}, $c_{0\Delta}$, $c_{2\Delta}$ and Λ.

Figure 6.8 shows the behaviour of the self-energy contributions to the nucleon and Δ as a function of pion mass. The effect of the $\Delta \to N\pi$ decay channel opening is clearly visible in the $\sigma^{\Delta}_{N\pi}$ plot. As has been previously mentioned, this behaviour is neglected in other extrapolation methods, but is important in obtaining the correct behaviour of the Δ in this region. We also indicate the fall off of the self-energy terms as m_π^2 increases as we expected.

The fits to the nucleon and Δ data is presented in Fig. 6.9 with the parameters in Table 6.3. We find predictions for the physical masses of the nucleon and the Δ to be 940 MeV and 1173 MeV respectively.[1] As was in the case of the ρ meson, it is the lowest data point that influences the curvature of the fit. We shall investigate the effect of decreasing the errors on this lowest point shortly.

We also investigate the effects of requiring the fit to reproduce the physical mass of the baryons. The large uncertainty in setting the scale of the CP-PACS and

[1] The excellent agreement with the experimantal mass of the nucleon is coincidental, but encouraging.

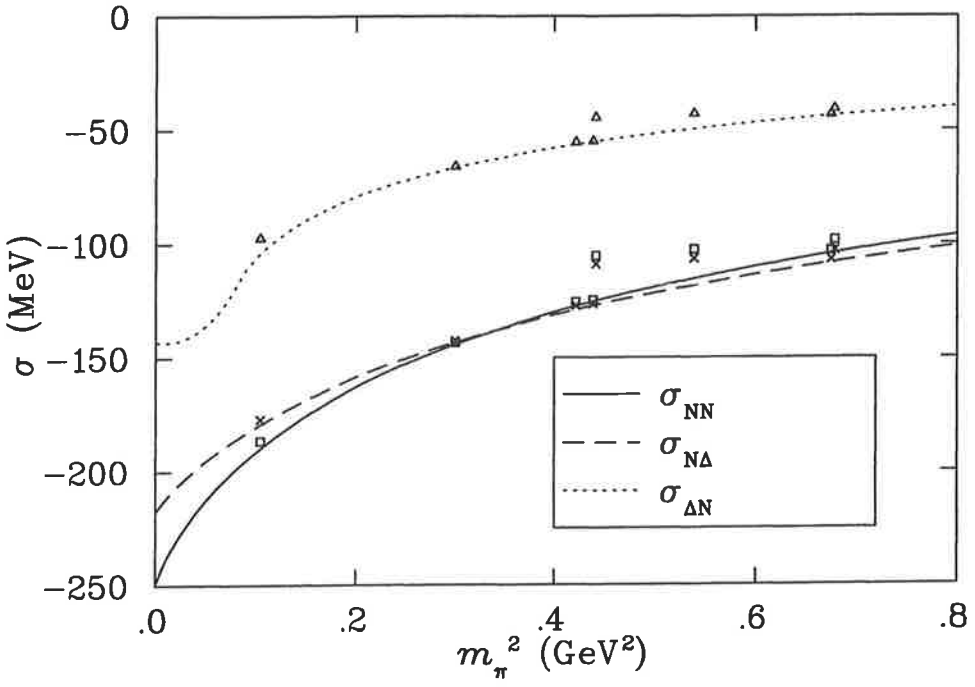

Figure 6.8: Variation with pion mass of the nucleon and Δ self-energy contributions to their respective masses. The form factor is chosen to be a dipole with $\Lambda_N = \Lambda_\Delta$ and set the best fit values of 921 MeV. The solid points indicated the value of the self-energy when calculated at the discrete momenta allowed on the lattices considered in this investigation. The difference between the curves and points is an indication of the missing physics because of finite lattice size and spacing.

UKQCD results realistically suggests a mass within 10% is acceptable. However, we introduce *pseudo*-data points at the physical pion mass with the mass of the nucleon and Δ. We repeat the fit, with the proviso that the self energies are calculated as integrals at this physical point. At the other points we evaluate the sum over the discrete momenta. Effectively we are mocking up an infinite volume lattice with infinitesimal lattice spacing at the physical point. A surprisingly acceptable value for the goodness-of-fit is found with this artificial data. We present the value of the fit in Table 6.3. As can be seen, even with the restriction introduced by the pseudo-data points the χ^2 per degree of freedom are still of order unity. We shall use these

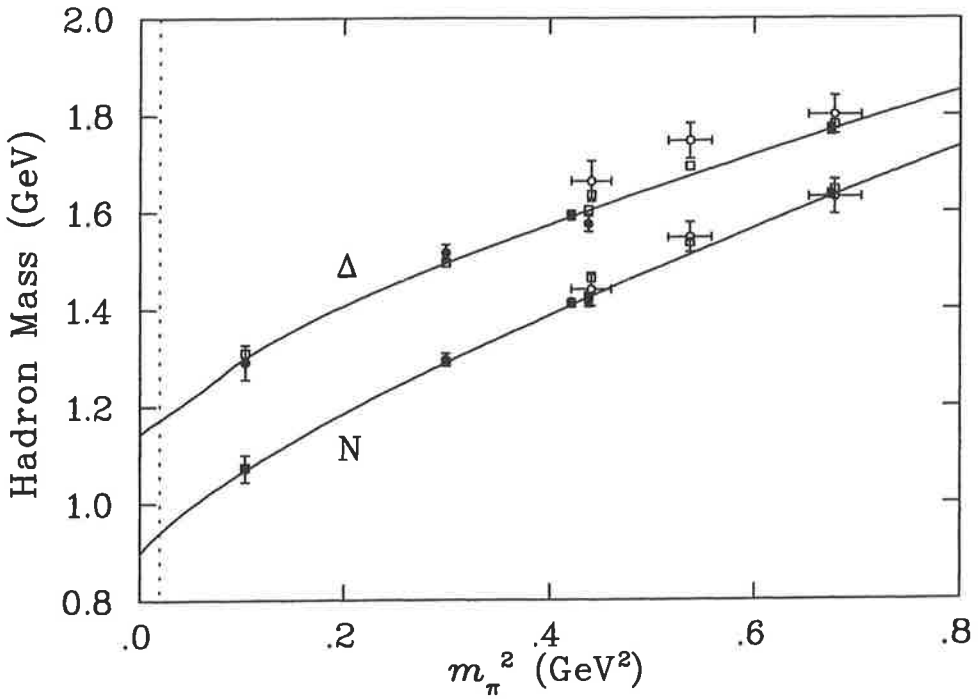

Figure 6.9: Analysis of the lattice data for the N and Δ baryon masses calculated by the CP-PACS (filled symbols) and UKQCD (open symbols) collaborations as a function of m_π^2. The squares represent the fit of Eqs. (6.6) and (6.20) respectively to the data with the self-energy contributions calculated as a discrete sum of allowed lattice momenta. The solid curves are for continuous (integral) self-energy contributions to the same equations. We have used a dipole form factor, with optimal $\Lambda_N = \Lambda_\Delta = 921$ MeV. The vertical line is at the physical pion mass.

fits in chapter 7.

6.6.4 Series Expansion

Section 6.6.2 contains a discussion regarding the use of a chirally motivated formula for fitting lattice hadron masses. We explore the properties of a series expansion further in this section. The series of Eq. (6.31) is motivated by taking the first three terms that are known to contribute to the self-energy of the hadron from χPT. These terms were calculated by taking the series expansion of the chiral Lagrangian

	c_0 [GeV]	c_2 [GeV^{-1}]	Λ [GeV]	χ^2/DoF ($\Lambda_N \equiv \Lambda_\Delta$)	χ^2/DoF (Forced)	m^{P} [GeV]	
N	1.36	0.710	0.921	3.12		0.940	Dipole
	1.36	0.715	0.917		0.282	0.940	
	1.18	0.830	0.394	5.21		0.958	Monopole
	1.22	0.811	0.417		0.578	0.940	
Δ	1.54	0.565	0.921	3.12		1.173	Dipole
	1.38	0.647	0.715		1.55	1.232	
	1.39	0.669	0.394	5.21		1.220	Monopole
	1.37	0.681	0.374		2.03	1.232	

Table 6.3: Parameters of the fits to the N and Δ data for dipole (Eq. (6.28)) and monopole (Eq. (6.29)) form factors with the requirement that $\Lambda_N \equiv \Lambda_\Delta$. The calculation is repeated with the Λ_N and Λ_Δ unconstrained, however requiring the physical mass of the N or Δ is reproduced. This fit is indicated by the *"(Forced)"* label.

around massless quarks, or more accurately $m_\pi \to 0$.

For the investigation we wish to undertake, we simplify our extrapolation formula to

$$m_N = c_0 + c_2 m_\pi^2 + \sigma_{N\pi}^N , \tag{6.32}$$

dropping the $N \to \Delta\pi$ contribution. To allow a simple analytic investigation we take a sharp cut-off for the form factor and analytically integrate the self-energy contribution (Eq. (6.7)). We then fit this analytic expression, rather than the sum over the discrete momenta. This process is to simplify the mechanics of our model fit, allowing a clarification of the significant issues. In short, the functional form we fit with is:

$$m_N = c_0 + c_2 m_\pi^2 - \frac{3g_A^2}{16\pi^2 f_\pi^2}\left(m_\pi^3 \arctan\left(\frac{\Lambda}{m_\pi}\right) + \frac{\Lambda^3}{3} - \Lambda m_\pi^2\right) . \tag{6.33}$$

The parameters of the fit are $(c_0, c_2, \Lambda) = (1.18, 0.78, 0.62)$ and it is presented as the solid curve in Fig. 6.10. This expression is exact for all values of m_π, and so we are able to expand it in both the small- and large-m_π limits. The coefficients of all terms in both expansions are explicitly determined, thus we can calculate a series

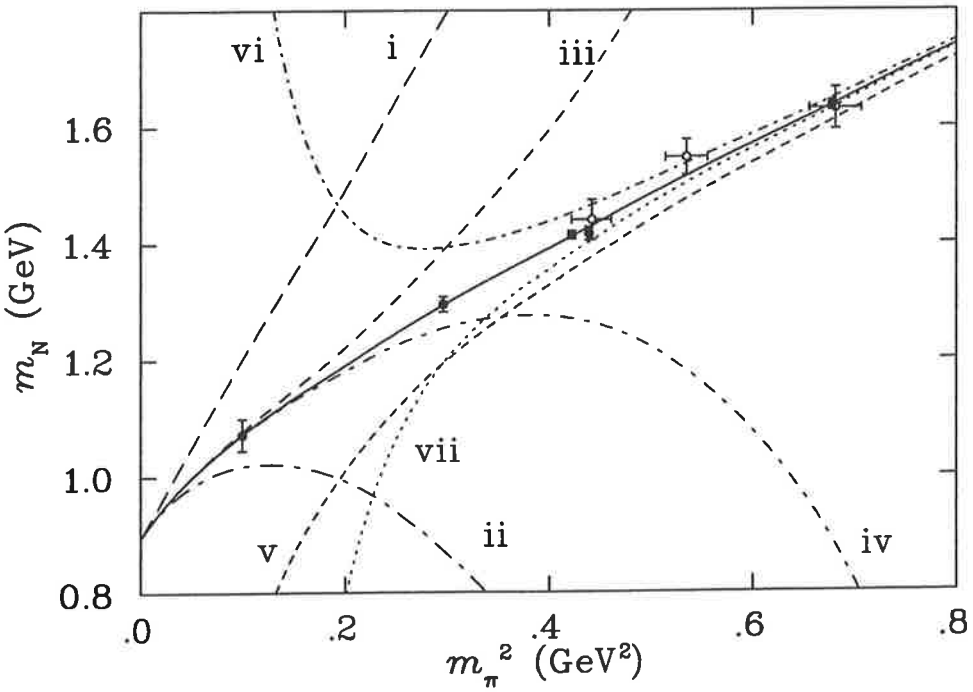

Figure 6.10: Fit of Eq. (6.33), and the analytic series expansion in both the heavy and light m_π limit, to various powers. The analytic forms of (i) – (vii) are presented in the text.

expansion in both limits with full knowledge of all the terms. We have done this for both limits. In the small mass limit we have plotted the following series expansions truncated at different orders (where we make the substitution $\kappa \equiv -\frac{3g_A^2}{16\pi^2 f_\pi^2}$):

i. $m_N = \left(c_0 + \frac{\kappa\Lambda^3}{3}\right) + (c_2 - \kappa\Lambda)\, m_\pi^2$

ii. $m_N = \left(c_0 + \frac{\kappa\Lambda^3}{3}\right) + (c_2 - \kappa\Lambda)\, m_\pi^2 + \left(\frac{\kappa\pi}{2}\right) m_\pi^3$

iii. $m_N = \left(c_0 + \frac{\kappa\Lambda^3}{3}\right) + (c_2 - \kappa\Lambda)\, m_\pi^2 + \left(\frac{\kappa\pi}{2}\right) m_\pi^3 - \left(\frac{\kappa}{\Lambda}\right) m_\pi^4$

iv. $m_N = \left(c_0 + \frac{\kappa\Lambda^3}{3}\right) + (c_2 - \kappa\Lambda)\, m_\pi^2 + \left(\frac{\kappa\pi}{2}\right) m_\pi^3 - \left(\frac{\kappa}{\Lambda}\right) m_\pi^4 + \left(\frac{\kappa}{3\Lambda^3}\right) m_\pi^6$

Note the coefficient of the m_π^3 term is, as we have previously stated, exactly as predicted by χPT. The series expansions in the heavy quark limit are given by:

v. $m_N = c_0 + c_2 m_\pi^2 + \frac{\kappa\Lambda^5}{5m_\pi^2}$

vi. $m_N = c_0 + c_2 m_\pi^2 + \frac{\kappa\Lambda^5}{5m_\pi^2} - \frac{\kappa\Lambda^7}{7m_\pi^4}$

vii. $m_N = c_0 + c_2 m_\pi^2 + \frac{\kappa\Lambda^5}{5m_\pi^2} - \frac{\kappa\Lambda^7}{7m_\pi^4} + \frac{\kappa\Lambda^9}{9m_\pi^6}$

It can be seen in Fig. 6.10 that none of the curves (i) – (vii) reproduce the solid curve over 6 the region where the lattice data lies. It is clear that the series in the small mass region, given by

$$\begin{aligned} m_N &= \left(c_0 + \frac{\kappa\Lambda^3}{3}\right) + (c_2 - \kappa\Lambda)\, m_\pi^2 + \left(\frac{\kappa\pi}{2}\right) m_\pi^3 \\ &\quad + \kappa m_\pi^3 \sum_{i=0}^{\infty} \frac{(-1)^{i+1}}{(2i+1)} \left(\frac{m_\pi}{\Lambda}\right)^{2i+1}, \end{aligned} \tag{6.34}$$

will never converge to the series in the large mass region:

$$m_N = c_0 + c_2 m_\pi^2 + \kappa m_\pi^3 \sum_{i=0}^{\infty} \frac{(-1)^i}{(2i+5)} \left(\frac{\Lambda}{m_\pi}\right)^{2i+5}. \tag{6.35}$$

This result may be extended to show that no series expansion of chiral perturbation theory, to any order, will reproduce the correct m_π^2 behaviour of a mass in the heavy quark region. The only way to reproduce both regions is by having an interpolating function, like Eq. (6.33), that reproduces both limits.

This failure of a series expansion to reproduce a known function has been explored in the case of effective field theory in [77]. Here the exact solution of the Euler-Heisenberg QED effective action is known, and the series expansion in the large and small electron mass, m, limits can to be evaluated. In the small mass (strong external field B) limit logarithmic terms and odd powers of m^2/eB appear. However the large mass (weak external field) expansion has no logarithmic terms and only even powers of eB/m^2. Thus it can be seen that the exact integral expression for the one-loop Euler-Heisenberg effective action has two very different expansions in the limits, similar to the result we have presented above.

6.7 Sigma Commutator

In the quest to understand hadron structure within QCD, small violations of fundamental symmetries play a vital role. The sigma commutator, σ_N:

$$\sigma_N = \frac{1}{3} \langle N | \left[Q_{i5}, \left[Q_{i5}, \mathcal{H} \right] \right] | N \rangle \ , \tag{6.36}$$

(with Q_{i5} being the two-flavour ($i = 1, 2, 3$) axial charge) is an extremely important example. Because Q_{i5} commutes with the QCD Hamiltonian in the chiral SU(2) limit, the effect of the double commutator is to pick out the light quark mass term from $\mathcal{H}$:

$$\sigma_N = \langle N | \left(m_u \bar{u} u + m_d \bar{d} d \right) | N \rangle \ . \tag{6.37}$$

Neglecting the very small effect of the $u-d$ mass difference we can write Eq. (6.37) in the form

$$\sigma_N = \langle N | \bar{m} \left(\bar{u} u + \bar{d} d \right) | N \rangle \tag{6.38}$$

$$= \bar{m} \frac{\partial m_N}{\partial \bar{m}} , \tag{6.39}$$

with $\bar{m} = (m_u + m_d)/2$. Equation (6.39) follows from the Feynman-Hellman theorem [78].

While there is no direct experimental measurement of σ_N, the value inferred from world data has been 45 ± 8 MeV [79] for some time. Recently there has been considerable interest in this value because of progress in the determination of the pion-nucleon scattering lengths [80, 81] and new phase shift analyses [82, 83]. For an excellent summary of the sources of the proposed variations and the disagreements between various investigators we refer to the excellent review of Kneckt [84]. For our purposes the experimental value is of limited interest as the full lattice QCD calculations upon which our work is based involve only two active flavours.

Numerous calculations of σ_N have been made within QCD motivated models [85] and there has been considerable work within the framework of chiral perturbation theory [86]. However, direct calculations of σ_N within QCD itself have proven to be difficult. Early attempts [87] to extract σ_N from the quark mass dependence of the nucleon mass in quenched QCD (using Eq. (6.39)) produced values in the range 15 to 25 MeV. Attention subsequently turned to determining σ_N by calculating the scalar matrix element of the nucleon $\langle N|\bar{u}u + \bar{d}d|N\rangle$. There it was discovered that the sea quark loops make a dominant contribution to σ_N [88, 89]. These works, based on quenched QCD simulation, found values in the 40 to 60 MeV range, which are more compatible with the experimental values quoted above.

On the other hand, the most recent estimate of σ_N, and the only one based on a two-flavour, dynamical-fermion lattice QCD calculation, comes from the SESAM collaboration. They obtain a value of 18 ± 5 MeV [90], through a direct calculation of the scalar matrix element $\langle N|\bar{u}u + \bar{d}d|N\rangle$.

The discrepancy from the quenched results of Refs. [88, 89] is not so much an unquenching effect in the scalar matrix element but rather a significant suppression of the quark mass in going from quenched to full QCD. The difficulty in all approaches which evaluate $\langle N|\bar{u}u + \bar{d}d|N\rangle$ is that neither it nor $\bar{m}$ is renormalization group invariant. One must reconstruct the scale invariant result from the product of the scale dependent matrix element and the scale dependent quark masses. The latter are extremely difficult to determine precisely and are the chief source of uncertainty in this approach.

An additional difficulty in extracting σ_N from lattice studies is the need to extrapolate from quite large pion masses, typically above 500 or 600 MeV. An important innovation adopted by Dong *et al.*, but not by the SESAM collaboration, was to extrapolate the computed values of $\langle N|\bar{u}u + \bar{d}d|N\rangle$ using a form motivated by chiral symmetry, namely $a + b\bar{m}^{1/2}$. On the other hand, the value of b used was

not constrained by chiral symmetry and higher order terms of the chiral expansion were not considered. Furthermore, since the work was based on a quenched calculation, the chiral behaviour implicit in the lattice results involves incorrect chiral coefficients [91].

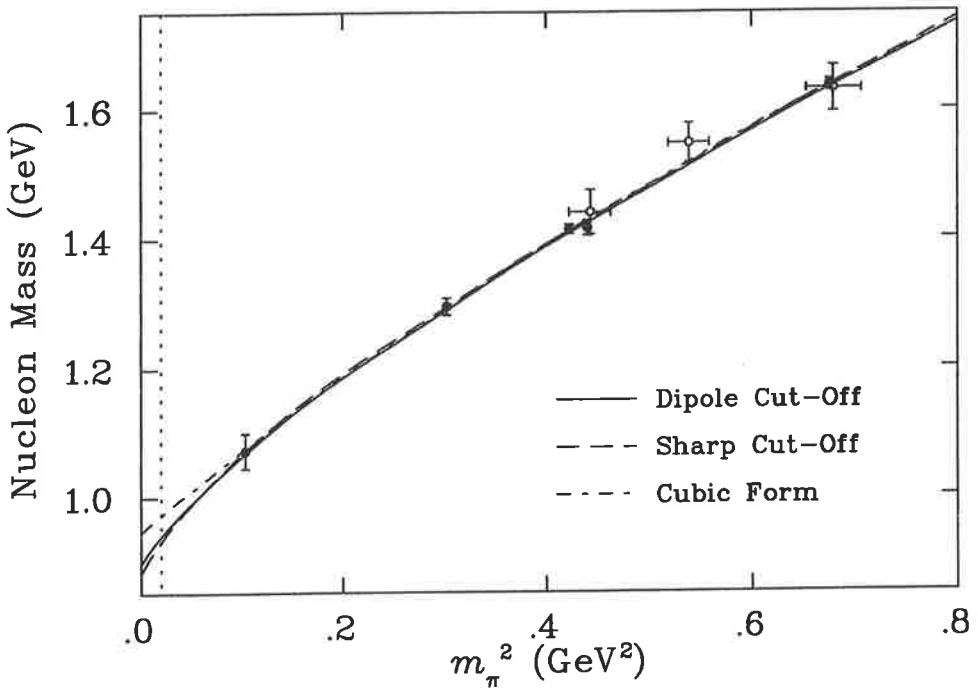

Figure 6.11: Nucleon mass calculated by CP-PACS (solid points) and UKQCD (open points), as a function of m_π^2, both are scaled by 5% to improve consistency. The solid curve is a fit to Eq. (6.6) with a 921 MeV dipole form factor, the dashed curve is a fit using a sharp (θ-function) cut-off, $\Lambda = 513$ MeV, with the self-energy contributions evaluated as integrals. The dash-dot curve is a fit to Eq. (6.31). The vertical line indicates the physical pion mass.

In section 6.6.2 we discussed the relative merits of extrapolating the baryon masses with a chirally motivated, cubic, form (Eq. (6.31)). The corresponding fit to the combined UKQCD and CP-PACS data set, is shown as the short-dashed curve in Fig. (6.11) and the parameters $(\tilde{c}_0, \tilde{c}_2, \tilde{c}_3) = (0.946, 1.42, -0.483)$ (the units are appropriate powers of GeV). This yields a value for the sigma commutator,

$\sigma_N^{(P)} = 25.7$ MeV, where the superscript stands for "phenomenological".

The difficulty with such a purely phenomenological analysis has been discussed above and also in Ref. [66]. The point we wish to emphasise is that the value of $\tilde{c}_3$ (-0.483) is almost an order of magnitude smaller than the model independent LNA term, $c_3^{\text{LNA}} = -5.60$ GeV^2. Clearly this discrepancy must present concern when evaluating σ_N, because of the requirement of taking the derivative of the mass formula. If one evaluates the LNA contribution to the value of σ_N with this phenomenological value of c_3 the contribution is about -2 MeV. With the model independent value of c_3 this contribution jumps to -23 MeV, about 50% of the absolute value of the sigma commutator. It should be noted that the contribution from the cubic term in both cases actually acts to decrease the value of σ_N. Undoubtedly the curvature associated with the chiral corrections at low quark mass is extremely important in the evaluation of σ_N. The extrapolation method we present not only includes the correct coefficient for the cubic term, but includes higher order terms which conspire to increase the value of the sigma commutator. The extracted value of σ_N is determined by the present data, the result being 37.3 MeV. The result is somewhat reduced from our previously published calculation [92] because of two factors. In this calculation we have constrained the form factor parameter Λ between the fits of the N and Δ, and secondly we have fit taking into account the discretisation of the momenta available to the pion on the lattice. These two improvements in the procedure whilst reducing the value of σ_N, still reproduce a value that is consistent, within errors, to the experimental prediction. It is this relative stability of the predictions that give confidence to our assertions.

Since the process of setting the physical mass scale via the string tension is thought to have a systematic error of 10%, one might naively expect this to apply to σ_N. However, *all* masses in the problem including the pion (or quark) mass, as well as that of the nucleon, scale with the lattice parameter a. It turns out that when one

uses Eq. (6.39) at the physical pion mass (which means a slightly different value of $\bar{m}a$ if a changes), the value of σ_N is extremely stable. If, for example, one raises the CP-PACS data by 15% and the UKQCD data by 5% (instead of 5% and -5%, respectively) the value of σ_N shifts from 37.3 to 36.7 MeV. We present calculations in Table 6.4 that show, for a variety of scalings of the lattice data, how stable our results are.

Scaling (%)		σ_N		
CP-PACS	UKQCD	Dipole	Sharp	Cubic
5	-5	37.3	43.2	29.7
10	0	37.0	43.2	28.6
0	-10	37.4	43.2	31.0

Table 6.4: Sigma Commutator Values. The **Dipole** and **Sharp** results were calculated with our preferred form of $c_0 + c_2 m_\pi^2 + \sigma_{N\pi}^N(\Lambda, m_\pi) + \sigma_{\Delta\pi}^N(\Lambda, m_\pi)$ with either a dipole or monopole form factor for the $N\pi$ vertex. The values of dipole parameter (Λ) were (921, 927, 910) MeV, and for the sharp (513, 520, 506) MeV. The **Cubic** results are for the $c_0 + c_2 m_\pi^2 + c_3 m_\pi^3$ extrapolation function, with c_3 *unconstrained* by chiral symmetry — as explained in the text this produces an unreliable value for σ_N.

The remaining issue, for the present data, is the model dependence associated with the choice of a dipole form factor. We believe that any model satisfying the essential chiral constraints and fitting the lattice data should give essentially the same answer. We checked this by numerically fitting the lattice data (long-dashed curve in Fig. 6.11) with the form of Eq. (6.6) but with $\sigma_{N\pi}^N$ and $\sigma_{\Delta\pi}^N$ calculated over a continuum of momenta with a sharp cut-off (θ-function) form factor at all pion-baryon vertices. This is the procedure discussed in Ref. [92]. We recognise that the sharp cut-off is not as physically sensible as the dipole form factor, however, even this approach gives an acceptable result for σ_N. Since the preferred phenomenological form of the $N\pi$ form factor is a dipole, we regard the dipole result shown in the first line of Table 6.4 as our best estimate, namely $\sigma_N = 37.3$ MeV with fit

parameters $(c_0, c_2, \Lambda_D) = (1.36, 0.710, 0.921)$. A remaining source of error is that, although the lattice results are calculated with an improved action, there still is an error associated with the extrapolation to the infinite volume, continuum limit.

6.8 Summary

The importance of the inclusion of the correct chiral behaviour has again been emphasised by the fact that it increases the value of the sigma commutator from less than 30 MeV of the unconstrained cubic fit to around 37 MeV for our functional form which explicitly includes this correct chiral behaviour. Clearly an enormous amount of work remains to be done before we will fully understand the structure of the baryons within QCD. It is vital that the rapid progress on improved actions and faster computers continue and that we have three flavour calculations within full QCD at masses as close as possible to the physical quark masses. Nevertheless, it is a remarkable result that the present lattice data for dynamical-fermion, two-flavour QCD, yields such a stable and accurate answer for the sigma commutator, an answer which is already within the range of the experimental values. In addition, we have also shown that functional forms that interpolate between the known behaviour in the chiral and heavy quark mass limits are able to give insight into the mass dependence of the lightest spin-$\frac{1}{2}$ and $\frac{3}{2}$ baryons. Finally an investigation of the applicability of a series expansion over such a range has shown that a chiral series expansion, to any finite order, will never reproduce the heavy quark behaviour of the baryons.

Chapter 7

Edinburgh Plots

What you can't do on your own, you don't understand.

RICHARD FEYNMAN

As discussed in Sec. 6.7, there are difficulties in calculating the sigma commutator, in some approaches, because of the need to set the scale at which the masses are calculated. The Edinburgh (m_π/m_ρ vs. m_N/m_ρ), and APE ($(m_\pi/m_\rho)^2$ vs. m_N/m_ρ), plots avoid this difficulty as the scale is removed in taking the ratio of the masses.

In the case of the Edinburgh plot we know the exact values of the ratios in the heavy quark and physical limits. The physical masses of the π, ρ and N are known, giving us the ratio at the physical point. In the heavy quark limit we expect the mass of the hadrons to become proportional to the mass of the constituent quarks. Assuming equal current quark masses, we have the ratio of the π to ρ masses being 1, and the ratio of the nucleon to the ρ being $3/2$.

The data from CP-PACS [20] (filled symbols) and UKQCD [21] (open sym-

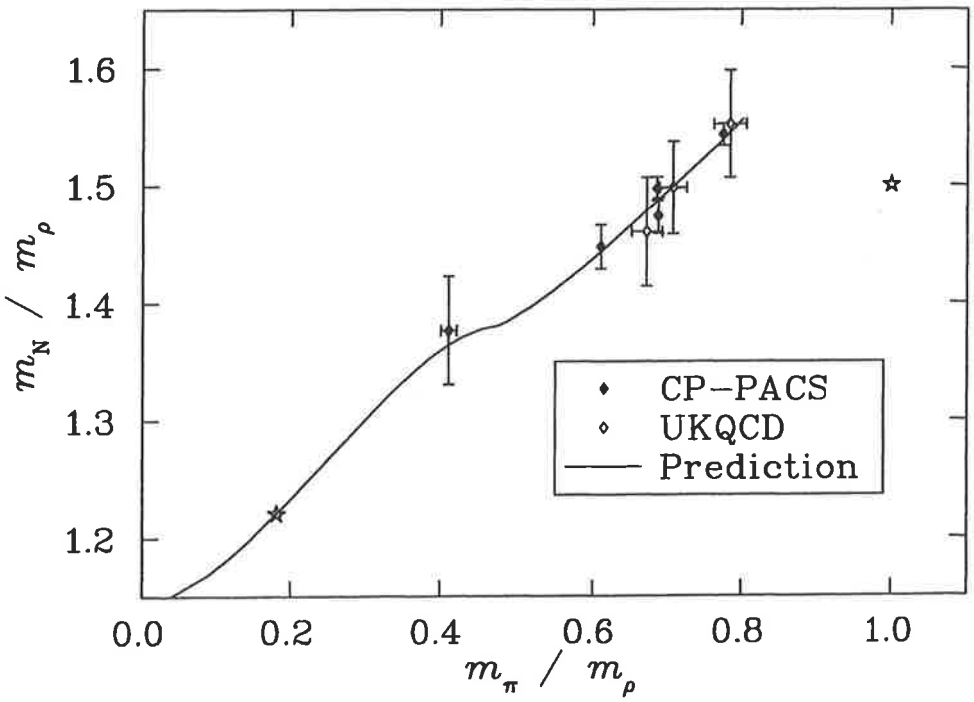

Figure 7.1: Edinburgh plot for CP-PACS and UKQCD results as used previously in this work. The stars represent the known limiting cases, at the physical and heavy quark limits respectively. The solid line is the infinite volume, continuum limit behaviour predicted by our functional forms for the extrapolation of the N and ρ masses.

bols), as previously used in this thesis, are presented in the subsequent figures. The stars at $m_\pi/m_\rho \sim 0.2$ and 1.0 are the known limits of the ratios. The first point to note is that some of the data lies above the heavy quark limit. This behaviour is not unexpected and is explained by forms that attempt to extrapolate from the heavy quark limit down to somewhat lighter masses [93]. There is a turn over in the extrapolation form allowing matching to not only heavy quark lattice data, but also the theoretical point at $m_\pi/m_\rho = 1.0$. These extrapolations, however, do not attempt to enter the chiral region in which we are working. The region in which these heavy quark extrapolation methods overlap our chiral extrapolation is not explored in this work.

As the value in the physical limit is known for the Edinburgh plot, we introduced a *pseudo*-data point, at the physical mass of the appropriate hadron, and repeated the fits of Eqs. (5.44), (6.6) and (6.20). The changes in the χ^2/DoF for

	χ^2/DoF		
	ρ	N	Δ
Unconstrained	1.34	0.332	1.53
Constrained	1.37	0.282	1.55

Table 7.1: The χ^2/DoF for the extrapolation formulae Eqs. (5.44), (6.6) and (6.20). Constrained refers to the inclusion of a data point at the physical mass of the hadron. The fits without this extra data point (Unconstrained) are the standard fits presented in previous chapters.

the various fits are shown in Table 7.1. It can be clearly seen that the extra, phenomenological, requirement does not significantly effect the ability of the extrapolation forms to reproduce the lattice data. We take this as an indication that the general structure of the prediction for the Edinburgh curve is stable.

The alternative method used for calculating the extrapolation for the Edinburgh (APE) curve to the physical point have involved using a form

$$m = c_0 + c_2 m_\pi^2 + c_3 m_\pi^3 \,, \tag{7.1}$$

for the extrapolation of the baryon/meson mass. Discussions in chapters 5 and 6 have presented evidence as to why such an extrapolation is flawed.

In Fig. 7.1 we present our prediction (solid curve) for the infinite volume, continuum limit behaviour of the ratio of the N/ρ masses. As mentioned above, we have constrained our fits to reproduce the physical masses, and hence the curve goes through the point at the physical ratio. The negligible difference between our continuum prediction and the data is expected. It is because of the fact that both the UKQCD and CP-PACS collaborations have used non-perturbative clover improvements in their actions. The expectation of such an improvement is that there

will be only a small $\mathcal{O}(a^2)$ dependence in the calculations at large quark masses. The pion-induced self-energy effects are suppressed at these masses, and we see effectively the ratio of a bare N and ρ. There is a point of inflexion in the curve around $m_\pi/m_\rho \sim 0.5$. This aspect is a result of the $\rho \to \pi\pi$ decay channel opening at this point. This behaviour is not reproduced in other extrapolations, as they do not include the physics of this decay channel. We see similar points of inflexion in the Δ Edinburgh plot, as there is an analogous decay channel, $\Delta \to N\pi$.

7.1 Predictions for the Finite Lattice

In previous sections we have discussed how the construction of the lattice restricts the available momenta of the intermediate particles. The momenta available in the finite periodic volume are (Eq. (2.8)):

$$k_\mu = \frac{2\pi n_\mu}{aL_\mu} \quad \text{where} \quad -\frac{L_\mu}{2} < n_\mu \leq \frac{L_\mu}{2}. \tag{7.2}$$

We have used this information to make predictions for the behaviour of the Edinburgh plots for the two data sets we have been analysing.

We have taken the lattice size, L, and spacing, a, of the lowest data point for the UKQCD and CP-PACS data sets and calculated the self-energy contributions to the mass extrapolation formulae Eqs. (5.44), (6.6) and (6.20), for a variety of quark masses. We present L, a, and the minimum available momentum in Table 7.2.

	a (fm)	L	k_{Min} (MeV)
UKQCD	0.13	12	795
CP-PACS	0.18	16	408

Table 7.2: The lattice spacing (a) and size (L) for the lightest mass points in the CP-PACS and UKQCD data sets used in this work. We also present the minimum momenta available on that lattice — as found from Eq. (2.8).

7.1.1 The N Edinburgh Plot

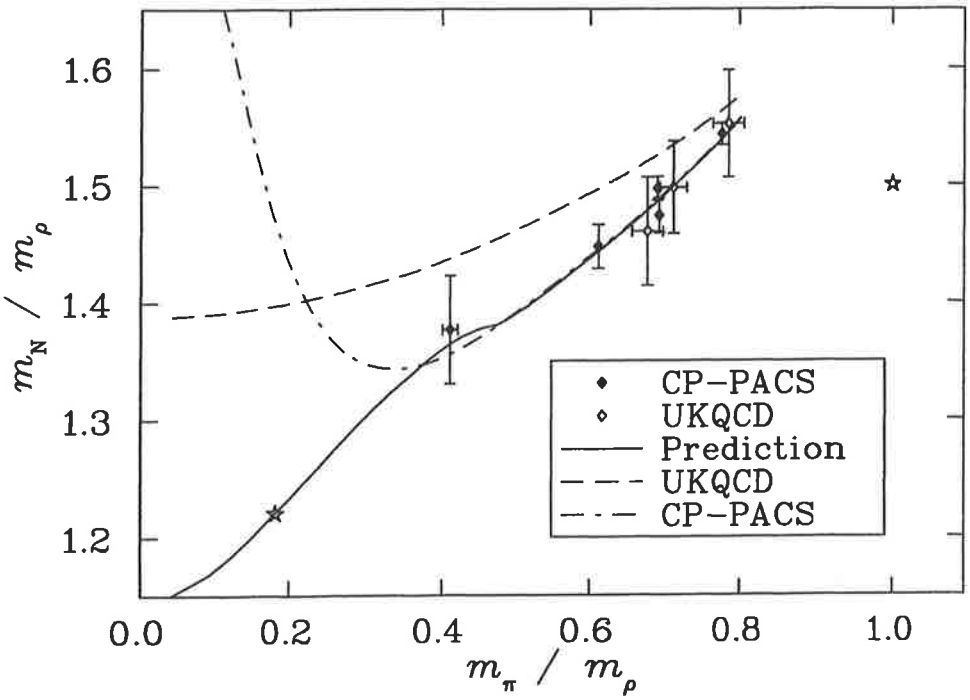

Figure 7.2: Edinburgh plot with data as described in Fig. 7.1. The solid line is the infinite volume, continuum limit behaviour predicted by our functional forms for the extrapolation of the N and ρ masses. The dashed and dashed-dot curves are the predicted behaviour of the UKQCD and CP-PACS lattices respectively.

We present the predicted Edinburgh plot for both UKQCD and CP-PACS in Fig. 7.2. The prediction for the CP-PACS lattice (dashed-dot curve) reproduces our continuum prediction for m_π/m_ρ above 0.5. We expect the larger volume lattices of CP-PACS to be less effected by volume effects for heavy quarks. This is because of the use of an $\mathcal{O}(a)$ improved fermion action which is known to have small $\mathcal{O}(a^2)$ artifacts. Thus the heavy quark masses should be an excellent approximation to the continuum limit. The discrepancy between the CP-PACS and continuum curves below $m_\pi/m_\rho \sim 0.5$ is caused by the inclusion of the opening of the $\rho \to \pi\pi$ decay channel, previously noticed in Fig. 5.7. Since the nucleon is stable on the

lattice we do not see another inflexion in the continuum limit curve. The predicted behaviour on the CP-PACS lattice diverges (but remains finite) below $m_\pi/m_\rho \sim 0.2$, a consequence of our approximation for the mass of the ρ-meson. Equation (5.1) does not apply here as the self-energies are of the order of the square of the bare ρ mass, $m_0^{(\rho)}$.

The prediction for the UKQCD lattice (dashed curve) lies high purely because the fits to the N and ρ masses are dominated by the smaller errors of the CP-PACS data. In Figs. (5.7) and (6.9) the squares representing the UKQCD data do not overlap the data points, as is the case for the CP-PACS results. This difference, in predictions of both the N and ρ masses is the cause of the discrepancy between the data and the predicted line here. As the minimum momentum accessible on the UKQCD lattice is much larger than the $\rho \to \pi\pi$ threshold in this case, thus the curve is smooth over the entire region. This is another example of our claim that whilst the precise details of the fits are not entirely determined at this time, the structure of the extrapolation is well defined. The conclusion that may be drawn from these plots is that we do not expect, on a finite lattice, that the Edinburgh plot will reproduce the physical N/ρ mass ratio even if a calculation could be performed at the physical pion mass. The exclusion of important, low momentum, contributions to the pion induced self-energy prevents an accurate mass calculation.

7.1.2 The Δ Edinburgh Plot

An analogous plot to that presented for the N above may be made for the Δ/ρ mass ratio. This calculation is interesting as it contains two open channels, $\Delta \to N\pi$ and $\rho \to \pi\pi$, at the physical quark mass. As has been previously stated, prior attempts at extrapolation formulae have ignored these decay channels, and will therefore miss the effects that are undoubtedly important near the chiral limit.

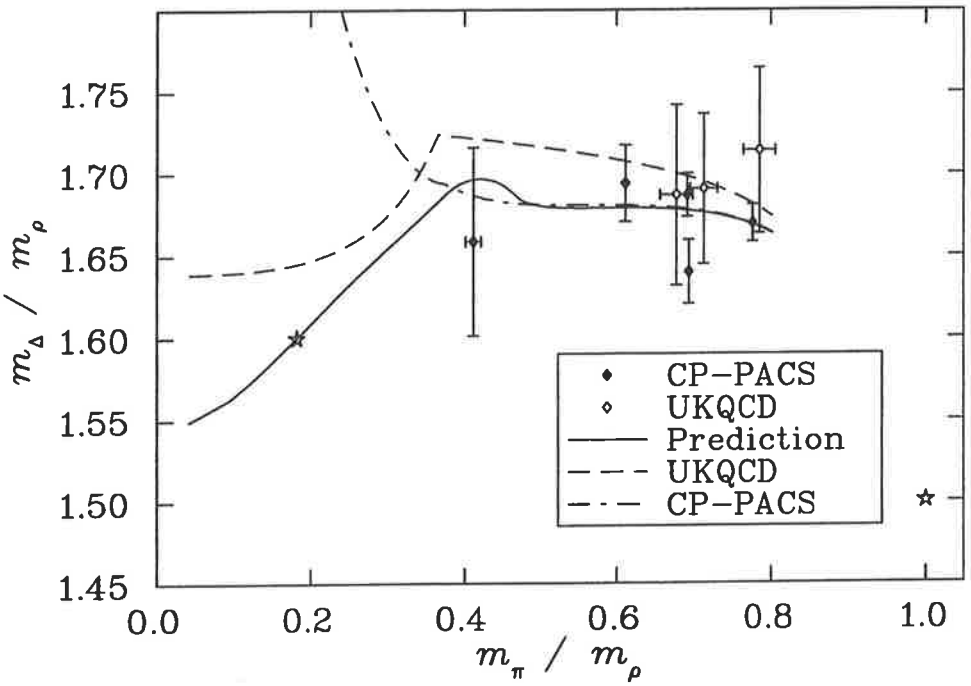

Figure 7.3: Edinburgh plot for the Δ, ρ and π with data as described in Fig. 7.1. The solid line is the infinite volume, continuum limit behaviour predicted by our functional forms for the extrapolation of the Δ and ρ masses. The dashed and dashed-dot curves are the predicted behaviour of the UKQCD and CP-PACS lattices respectively. The opening of the $\rho \to \pi\pi$ channel is missed by both lattices, but the inflexion at the opening of the $\Delta \to N\pi$ channel is visible around $m_\pi/m_\rho \sim 0.35$ GeV.

The solid curve in Fig. 7.3 again represents the infinite volume, continuum limit as predicted by our functional forms for the Δ and ρ masses. Again a point of inflexion may be seen at $m_\pi/m_\rho \sim 0.5$ which is, as previously explained, the 2π channel opening for the ρ-meson. There is also another point of inflexion at $m_\pi/m_\rho \sim 0.35$, the point where the $\Delta \to N\pi$ channel opens.

As was the case for the N Edinburgh plot, the dashed-dot curve showing the predicted behaviour for the CP-PACS lattice, reproduce the continuum curve above $m_\pi/m_\rho \sim 0.5$. Once again there is an obvious discrepancy, occurring at the opening of the $\rho \to \pi\pi$ channel. We note again the behaviour as the self-energy

grows, making our extrapolation unreliable below $m_\pi/m_\rho \sim 0.3$ for the CP-PACS lattice. We stress that the movement predicted is a robust effect, however the details require a more thorough treatment of the self-energy contributions.

The predicted UKQCD curve (dashed) shows no effect induced by the 2π channel opening, but does show effects because of the $\Delta \to N\pi$ decay channel. Therefore we again state that we do not expect to see lattice data reproducing the physical mass ratios because of the missing chiral physics.

7.2 Quenched vs. Dynamical Quarks

It is appropriate at this point to make a brief diversion into the quenched approximation. Quenching can be thought of as removing dynamical quark loops. Figure 7.4

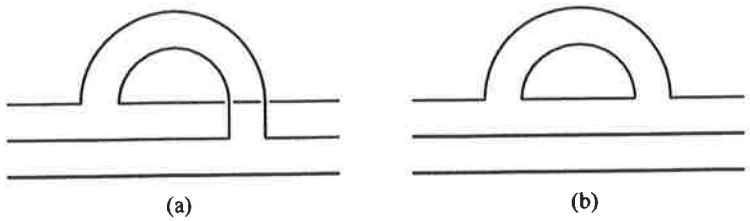

Figure 7.4: The quark flow lines corresponding to a pion loop dressing a baryon. Diagram (a) is included in both dynamical fermion and quenched lattice calculations, whilst diagram (b) is only present in dynamical fermion calculations because of the presence of the sea quark loop.

is an example of the two types of diagrams that contribute to the self-energy terms in full, dynamical fermion, QCD. Diagram (b), with the disconnected quark loop is not included in quenched calculations. There are other contributing diagrams in the quenched case, however we will not discuss them further. The effects of such a quenched chiral extrapolation are explored in [94]. A recent publication of Bernard *et al.* [95] investigated how dynamical quarks affected the light hadron spectrum, as

have several other groups [96, 97]. The comparison between quenched and dynamical fermions is interesting because of the use of an Edinburgh plot. The conclusion drawn was that there was *"no discernible change when dynamical quarks are introduced"*. The data set used in the calculation is at masses above $m_\pi/m_\rho = 0.5$, save a single quenched point. The effects of the pion induced self energies have been shown to be suppressed as $1/m_\pi^2$ in this region, resulting in a linear form for the extrapolation. This result is general statement for the quenched and unquenched cases, meaning that it is expected that the pion induced effects are negligible in both cases at such masses. The other difficulty in comparing quenched and unquenched results is the difficulty in setting the scale, but as has been mentioned earlier in this chapter, by taking the ratios, as in the Edinburgh plot, this scale is removed. Thus the results of Ref. [95] are entirely consistent with the results found here, as well as in Ref. [94]. A prediction of our work is that quenched and full QCD should agree well for $m_\pi^2 \gtrsim 0.2$ GeV^2. Differences between quenched and unquenched results will only be seen in lighter m_q calculations.

Chapter 8

Summary and Outlook

Nature will bear the closest inspection. She invites us to lay our eye level with her smallest leaf, and take an insect view of its plain.

HENRY DAVID THOREAU

The extraction, from theory, of the properties of the lightest octet (N) and decuplet (Δ) baryons and the vector (ρ) meson are of great practical interest. The comparison of the predictions of QCD to experiment is the most fundamental test of the theory. As has been discussed in this work, the only non-perturbative tool available at low energy is a lattice QCD calculation, but technical reasons restrict these lattice calculations to large quark masses.

This work provides a scheme for extrapolating hadronic properties to lighter quark masses, and in particular to *physical* quark masses. It has been shown that it is possible to obtain very good predictions for the physical masses of these low lying hadrons.

Chiral Perturbation Theory (χPT), a description of QCD at light quark mass,

will describe results from lattice calculations at sufficiently light quark mass. However, the radius of convergence is unknown. We have utilised the Cloudy Bag Model (CBM), a successful phenomenological chiral quark model to give direction as to the behaviour of the masses away from the chiral limit. The extrapolation form derived here, has been shown to reproduce to better than 1% the physical mass predicted by the CBM, and it also reproduces the general behaviour over an extended range of pion (or equivalently quark) mass.

The functional forms derived herein may be generalised to

$$m_H = c_0 + c_2 m_\pi^2 + \sigma(\Lambda, m_\pi)\,,$$

where σ contains the self-energy corrections to the hadron being extrapolated. We have applied this form to two-flavour, dynamical fermion, lattice QCD calculations performed by the CP-PACS [20] and UKQCD [21] collaborations. Among the various successes of this approach are predicting the physical masses of the N, Δ and ρ to within 0.1%, 4.7%, and 5.0% respectively. Work remains because the uncertainty in these results is significant, as we showed in the case of the ρ meson. Fortunately this uncertainty is entirely because of the statistical errors associated with the lattice results, and a reasonable $\sqrt{10}$ reduction in the statistical errors at the lightest mass point considered will bring the uncertainty to the 2% level. Additionally we have been able to calculate the sigma commutator, the J parameter and the $\rho \to \pi\pi$ phase shift. Finally we have presented the first Edinburgh plots showing the correct chiral behaviour in the extrapolation to the chiral limit.

The main features of our functional forms are as follows

- Includes the correct chiral and heavy quark physics — The extrapolation forms reproduce the known non-analytic behaviour, with the correct model independent coefficients, in the chiral limit. The form smoothly interpolates

between this chiral limit and the heavy quark regime where hadron properties show smooth quark mass dependence.

- Includes channel opening effects — The effects of decay channels are included. This is particularly important in reproducing the hyperfine splitting between the N and Δ, the latter having an open πN channel, and the behaviour of the ρ which has an open 2π channel at the physical quark mass. Such effects have been ignored in previous extrapolation methods. The branch points in the self energies because of the channels opening is important physics that has previously been ignored.

- Systematic way of extending corrections — Higher order effects may be incorporated by the straightforward inclusion of additional self-energy contributions.

- Includes, and corrects for, finite size effects — The discretisation of momenta on the finite volume lattice means some decay channels are not accessible on the lattice, but would be in the continuum. The extrapolation form takes these effects into account.

- Weak model dependence — We have investigated the model dependence of the form factor used to regulate the integrals and we find that it is at most a few MeV.

- Computationally cheap — The extrapolation procedure is not significantly more computationally expensive than current linear, or polynomial, extrapolations.

- Intuitive — The effects influencing the extrapolation are simple to understand, from a basic nuclear physics perspective.

In summary, this extrapolation method offers a new method of moving towards the goal of comparing lattice QCD with experimental results. Even with new, more powerful computers coming online regularly and improvements in actions, calculations near the physical region are some time off. The extrapolation of the new data remains an exciting challenge. Currently, the approach presented here is the only way known for connecting lattice QCD to experiment, incorporating the physics known to be essential.

Appendix A

Mathematical Conventions

Arithmetic is where the answer is right and everything is nice and you can look out of the window and see the blue sky — or the answer is wrong and you have to start all over and try again and see how it comes out this time.

CARL SANDBURG, "COMPLETE POEMS"

A.1 Useful Identities

The Dirac delta function of the difference between the squares of the variable and a constant may be simplified as

$$\delta\left(x^2 - a^2\right) = \frac{1}{2a}\left\{\delta(x-a) + \delta(x+a)\right\} . \tag{A.1}$$

The vector cross product may be written in terms of the elements of the vectors as

$$\vec{a} \times \vec{b} = \varepsilon_{ijk} a_i b_j . \tag{A.2}$$

The Dirac delta function is defined as

$$\int d^4x e^{ik\cdot x} = (2\pi)^4\delta^4(k)\,. \tag{A.3}$$

Translation in quantum mechanics is given as the property

$$\chi(x) = e^{-i(\vec{k}\cdot\vec{x}-Et)}\chi(0)e^{i(\vec{k}\cdot\vec{x}-Et)}\,, \tag{A.4}$$

where the state being described has energy E and associated 3-momentum $\vec{k}$.

A.1.1 Residue Theorem

Let $f(z)$ be a function that is analytic inside a simple closed path C and on C, except for finitely many singular points $z_1, z_2, \ldots, z_k$ inside C. Then

$$\oint_C f(z)dz = 2\pi i \sum_{j=1}^{k} \mathrm{Res}_{z=z_j} f(z)\,, \tag{A.5}$$

the integral being taken counterclockwise around the path C. [98]

A.2 Wick Contractions

The contraction of two scalar fields is defined as

$$\overbrace{\phi(x)\phi}(y) = D_F(x-y)\,, \tag{A.6}$$

where the Feynman propagator is defined as

$$D_F(x-y) = \int \frac{d^4p}{(2\pi)^4}\frac{i}{p^2-m^2+i\epsilon}e^{-ip\cdot(x-y)}\,. \tag{A.7}$$

Whilst the contraction of a field with external states is given by

$$\overbrace{\phi(x)|\mathbf{p}\rangle} = e^{-ip\cdot x}\,, \tag{A.8}$$

$$\langle\overbrace{\mathbf{p}|\phi}(x) = e^{+ip\cdot x}\,, \tag{A.9}$$

A.3 Dirac Matrices

The Dirac matrices satisfy

$$\{\gamma^\mu, \gamma^\nu\} = \gamma^\mu\gamma^\nu + \gamma^\nu\gamma^\mu = 2g^{\mu\nu} \tag{A.10}$$

$$\{\gamma_5, \gamma^\mu\} = 0 \tag{A.11}$$

A.3.1 Dirac Representation

$$\gamma^0 = \begin{pmatrix} I & 0 \\ 0 & -I \end{pmatrix} \tag{A.12}$$

$$\gamma^i = \begin{pmatrix} 0 & \sigma^i \\ -\sigma^i & 0 \end{pmatrix} \tag{A.13}$$

$$\begin{aligned} \gamma_5 &= \gamma^5 \\ &= i\gamma^0\gamma^1\gamma^2\gamma^3 \\ &= \begin{pmatrix} 0 & I \\ I & 0 \end{pmatrix} \end{aligned} \tag{A.14}$$

A.3.2 Chiral Representation

$$\gamma^0 = \begin{pmatrix} 0 & -I \\ -I & 0 \end{pmatrix} \tag{A.15}$$

$$\gamma^i = \begin{pmatrix} 0 & \sigma^i \\ -\sigma^i & 0 \end{pmatrix} \tag{A.16}$$

$$\begin{aligned} \gamma^5 &= i\gamma^0\gamma^1\gamma^2\gamma^3 \\ &= \begin{pmatrix} I & 0 \\ 0 & -I \end{pmatrix} \end{aligned} \tag{A.17}$$

Where the σ^i are the Pauli matrices

$$\sigma^1 = \begin{pmatrix} 0 & 1 \\ 1 & 0 \end{pmatrix} \quad \sigma^2 = \begin{pmatrix} 0 & -i \\ i & 0 \end{pmatrix} \quad \sigma^3 = \begin{pmatrix} 1 & 0 \\ 0 & -1 \end{pmatrix} \tag{A.18}$$

Bibliography

[1] M. Gell-Mann *Phys. Lett.* **8** (1964) 214–215.

[2] G. Zweig, "An SU(3) model for strong interaction symmetry and its breaking. 2." CERN-TH-412.

[3] M. E. Peskin and D. V. Schroeder, *An Introduction to Quantum Field Theory*. Addison–Wesley, Reading, Massachusetts, Second Ed., 1995.

[4] P. O. Bowman, *On Improvement in the Study of the Lattice Gluon Propagator*. Ph.D. thesis, University of Adelaide, Department of Physics and Mathematical Physics, Nov. 14, 2000.

[5] M. Creutz, *Quarks, Gluons and Lattices*. Cambridge Monographs On Mathematical Physics. Cambridge University Press, Cambridge, UK, 1983.

[6] I. Montvay and G. Munster, *Quantum fields on a lattice*. Cambridge Monographs On Mathematical Physics. Cambridge University Press, Cambridge, UK, 1994.

[7] H. J. Rothe, *Lattice Gauge Theories: An Introduction*, Vol. 43 of *World Scientific Lecture Notes in Physics*. World Scientific, Singapore, 1997.

[8] G. P. Lepage, "Redesigning lattice QCD," `hep-lat/9607076`.

[9] R. Gupta, "Introduction to lattice QCD," hep-lat/9807028.

[10] D. G. Richards, "Lattice gauge theory: QCD from quarks to hadrons," nucl-th/0006020.

[11] T. Muta, *Foundations of Quantum Chromodynamics: An Introduction to Perturbative Methods in Gauge Theories*, Vol. 57 of *World Scientific Lecture Notes in Physics*. World Scientific, Singapore, Second Ed., 1998.

[12] R. Haag, *Local quantum physics: Fields, particles, algebras*. Texts and monographs in physics. Springer, Berlin, Germany, 1992.

[13] C. Itzykson and J. Zuber, *Quantum Field Theory*. Physics Series. McGraw–Hill, International Ed., 1985.

[14] F. Butler, H. Chen, J. Sexton, A. Vaccarino, and D. Weingarten *Nucl. Phys.* **B430** (1994) 179–228, hep-lat/9405003.

[15] M. Fukugita, N. Ishizuka, H. Mino, M. Okawa, and A. Ukawa *Phys. Rev.* **D47** (1993) 4739–4769.

[16] S. Aoki *et al. Phys. Rev.* **D50** (1994) 486–494.

[17] S. Gottlieb *Nucl. Phys. Proc. Suppl.* **B53** (1997) 155.

[18] C. W. Bernard *et al. Phys. Rev.* **D48** (1993) 4419–4434, hep-lat/9305023.

[19] Y. Chung, H. G. Dosch, M. Kremer, and D. Schall *Nucl. Phys.* **B197** (1982) 55.

[20] **CP-PACS** Collaboration, S. Aoki *et al. Phys. Rev.* **D60** (1999) 114508, hep-lat/9902018.

[21] **UKQCD** Collaboration, C. R. Allton *et al. Phys. Rev.* **D60** (1999) 034507, hep-lat/9808016.

[22] R. Sommer *Nucl. Phys.* **B411** (1994) 839–854, hep-lat/9310022.

[23] G. S. Bali *Phys. Rept.* **343** (2001) 1–136, hep-ph/0001312.

[24] **UKQCD** Collaboration, S. P. Booth *et al. Phys. Lett.* **B294** (1992) 385–390, hep-lat/9209008.

[25] C. W. Bernard *et al. Phys. Rev.* **D62** (2000) 034503, hep-lat/0002028.

[26] C. W. Bernard *et al. Phys. Rev.* **D64** (2001) 054506, hep-lat/0104002.

[27] E. Eichten and F. Feinberg *Phys. Rev.* **D23** (1981) 2724.

[28] E. Eichten, K. Gottfried, T. Kinoshita, K. D. Lane, and T.-M. Yan *Phys. Rev.* **D21** (1980) 203.

[29] J. L. Richardson *Phys. Lett.* **B82** (1979) 272.

[30] Y. Iwasaki, K. Kanaya, T. Kaneko, and T. Yoshie *Phys. Rev.* **D56** (1997) 151–160, hep-lat/9610023.

[31] B. Sheikholeslami and R. Wohlert *Nucl. Phys.* **B259** (1985) 572.

[32] See for example [42]; [99]; [41]; [33]; [43]; [100].

[33] V. Bernard, N. Kaiser, and U.-G. Meissner *Int. J. Mod. Phys.* **E4** (1995) 193–346, hep-ph/9501384.

[34] J. Goldstone *Nuovo Cim.* **19** (1961) 154–164.

[35] J. Goldstone, A. Salam, and S. Weinberg *Phys. Rev.* **127** (1962) 965–970.

[36] Y. Nambu *Phys. Rev. Lett.* **4** (1960) 380–382.

[37] M. Gell-Mann and M. Lévy *Nuovo Cim.* **16** (1960) 705.

[38] M. Gell-Mann, R. J. Oakes, and B. Renner *Phys. Rev.* **175** (1968) 2195–2199.

[39] **Particle Data Group** Collaboration, D. E. Groom *et al. Eur. Phys. J.* **C15** (2000) 1–878.

[40] S. Weinberg *Physica* **A96** (1979) 327.

[41] B. R. Holstein, "Introduction to Chiral Perturbation Theory." Lectures given at HUGS, June, 1999.

[42] J. Gasser, M. E. Sainio, and A. Svarc *Nucl. Phys.* **B307** (1988) 779.

[43] U.-G. Meissner, "Chiral nucleon dynamics," `hep-ph/9711365`.

[44] R. F. Lebed *Nucl. Phys.* **B430** (1994) 295–318, `hep-ph/9311234`.

[45] V. Bernard, N. Kaiser, J. Kambor, and U. G. Meissner *Nucl. Phys.* **B388** (1992) 315–345.

[46] J. C. Collins, *Renormalization.* Cambridge Monographs On Mathematical Physics. Cambridge University Press, Cambridge, UK, 1984.

[47] P. N. Bogolubov *Annales Poincare Phys. Theor.* **8** (1968) 163–190.

[48] A. W. Thomas *Adv. Nucl. Phys.* **13** (1984) 1–137.

[49] X. Jin and B. K. Jennings *Phys. Lett.* **B374** (1996) 13–19, `nucl-th/9511021`.

[50] P. Hasenfratz and J. Kuti *Phys. Rept.* **40** (1978) 75–179.

[51] A. W. Thomas and W. Weise, *The Structure of the Nucleon.* WILEY–VCH, Verlag Berlin GmbH, Berlin, First Ed., 2001.

[52] S. Theberge, A. W. Thomas, and G. A. Miller *Phys. Rev.* **D22** (1980) 2838. **D23** (1981) 2106(E).

[53] A. W. Thomas, S. Theberge, and G. A. Miller *Phys. Rev.* **D24** (1981) 216.

[54] S. Théberge, *The Cloudy Bag Model.* Ph.D. dissertation, University of British Columbia, Department of Physics, Mar., 1982.

[55] D. B. Leinweber, A. W. Thomas, K. Tsushima, and S. V. Wright *Phys. Rev.* **D64** (2001) 094502, `hep-lat/0104013`.

[56] D. B. Leinweber and T. D. Cohen *Phys. Rev.* **D49** (1994) 3512–3518, `hep-ph/9307261`.

[57] P. A. Carruthers, *Introduction to Unitary Symmetry.* Interscience Publishers, New York, 1966.

[58] R. K. Bhaduri, *Models of the Nucleon: From Quarks to Soliton*, Vol. 22 of *Lecture Notes and Supplements in Physics.* Addison-Wesley, Redwood City, USA, 1988.

[59] M. A. Pichowsky, S. Walawalkar, and S. Capstick *Phys. Rev.* **D60** (1999) 054030, `nucl-th/9904079`.

[60] M. Lublinsky *Phys. Rev.* **D55** (1997) 249–254, `hep-ph/9608331`.

[61] K. L. Mitchell and P. C. Tandy *Phys. Rev.* **C55** (1997) 1477–1491, `nucl-th/9607025`.

[62] L. C. L. Hollenberg, C. D. Roberts, and B. H. J. McKellar *Phys. Rev.* **C46** (1992) 2057–2065.

[63] Refer to [101]; [102]; [103].

[64] M. Abramowitz and I. A. Stegun, *Handbook of Mathematical Functions.* Dover Publications, Inc., New York, Ninth Ed., 1972.

[65] E. Jenkins, A. V. Manohar, and M. B. Wise *Phys. Rev. Lett.* **75** (1995) 2272–2275, hep-ph/9506356.

[66] D. B. Leinweber, A. W. Thomas, K. Tsushima, and S. V. Wright *Phys. Rev.* **D61** (2000) 074502, hep-lat/9906027.

[67] **UKQCD** Collaboration, P. Lacock and C. Michael *Phys. Rev.* **D52** (1995) 5213–5219, hep-lat/9506009.

[68] T. Yoshie *Nucl. Phys. Proc. Suppl.* **63** (1998) 3, hep-lat/9711017.

[69] F. X. Lee and D. B. Leinweber *Phys. Rev.* **D59** (1999) 074504, hep-lat/9711044.

[70] C. D. Froggatt and J. L. Petersen *Nucl. Phys.* **B129** (1977) 89.

[71] A. W. Thomas and G. Krein *Phys. Lett.* **B456** (1999) 5, nucl-th/9902013.

[72] E. Jenkins *Nucl. Phys.* **B368** (1992) 190–203.

[73] M. K. Banerjee and J. Milana *Phys. Rev.* **D54** (1996) 5804–5811, hep-ph/9508340.

[74] Refer to [104]; [105]; [28].

[75] T. Kitagaki *et al. Phys. Rev.* **D28** (1983) 436–442.

[76] Refer to [106]; [107]; [108].

[77] G. V. Dunne, A. W. Thomas, and S. V. Wright, "Chiral extrapolation: An analogy with effective field theory," `hep-th/0110155`.

[78] Refer to [109];[110]; [111];[112].

[79] J. Gasser, H. Leutwyler, and M. E. Sainio *Phys. Lett.* **B253** (1991) 252–259.

[80] D. Sigg *et al. Nucl. Phys.* **A609** (1996) 269–309.

[81] T. E. O. Ericson, B. Loiseau, and A. W. Thomas *Nucl. Phys.* **A663** (2000) 541–544, `hep-ph/9907433`.

[82] M. M. Pavan, R. A. Arndt, I. I. Strakovsky, and R. L. Workman *PiN Newslett.* **15** (1999) 118–122, `nucl-th/9912034`.

[83] D. V. Bugg *PiN Newslett.* **15** (1999) 319–328.

[84] M. Knecht *PiN Newslett.* **15** (1999) 108–113, `hep-ph/9912443`.

[85] Refer to [113]; [114].

[86] Refer to [115]; [116].

[87] See for example: [117].

[88] S. J. Dong, J. F. Lagae, and K. F. Liu *Phys. Rev.* **D54** (1996) 5496–5500, `hep-ph/9602259`.

[89] M. Fukugita, Y. Kuramashi, M. Okawa, and A. Ukawa *Phys. Rev.* **D51** (1995) 5319–5322, `hep-lat/9408002`.

[90] **SESAM** Collaboration, S. Gusken *et al. Phys. Rev.* **D59** (1999) 054504, hep-lat/9809066.

[91] S. R. Sharpe *Phys. Rev.* **D56** (1997) 7052–7058, hep-lat/9707018.

[92] D. B. Leinweber, A. W. Thomas, and S. V. Wright *Phys. Lett.* **B482** (2000) 109–113, hep-lat/0001007.

[93] S. Ono *Phys. Rev.* **D17** (1978) 888.

[94] R. D. Young, D. B. Leinweber, A. W. Thomas, and S. V. Wright, "Systematic Correction of the Chiral Properties of Quenched QCD," hep-lat/0111041.

[95] **MILC** Collaboration, C. W. Bernard *et al. Nucl. Phys. Proc. Suppl.* **94** (2001) 237–241, hep-lat/0010065.

[96] **QCDSF** Collaboration, D. Pleiter *Nucl. Phys. Proc. Suppl.* **94** (2001) 265–268, hep-lat/0010063.

[97] **UKQCD** Collaboration, A. C. Irving *Nucl. Phys. Proc. Suppl.* **94** (2001) 242–245, hep-lat/0010012.

[98] E. Kreyszig, *Advanced Engineering Mathematics*. John Wiley & Sons, Inc., Seventh Ed., 1993.

[99] J. Gasser and H. Leutwyler *Nucl. Phys.* **B250** (1985) 465.

[100] U. G. Meissner *Rept. Prog. Phys.* **56** (1993) 903–996, hep-ph/9302247.

[101] P. Geiger and N. Isgur *Phys. Rev. Lett.* **67** (1991) 1066–1069.

[102] P. Geiger and N. Isgur *Phys. Rev.* **D41** (1990) 1595.

[103] P. Geiger and N. Isgur *Phys. Rev.* **D44** (1991) 799–808.

[104] D. B. Leinweber *Nucl. Phys.* **A470** (1987) 477–487.

[105] R. K. Bhaduri, L. E. Cohler, and Y. Nogami *Nuovo Cim.* **A65** (1981) 376–390.

[106] R. Bockmann, C. Hanhart, O. Krehl, S. Krewald, and J. Speth *Phys. Rev.* **C60** (1999) 055212, `nucl-th/9905043`.

[107] A. W. Thomas and K. Holinde *Phys. Rev. Lett.* **63** (1989) 2025–2027.

[108] P. A. M. Guichon, G. A. Miller, and A. W. Thomas *Phys. Lett.* **B124** (1983) 109.

[109] R. P. Feynman *Acta Phys. Polon.* **24** (1963) 697–722.

[110] R. P. Feynman *Phys. Rev.* **56** (1939) 340.

[111] H. Hellman, *Einführung in die Quantenchemie*. Deutick Verlag, Leipzig, 1937.

[112] S. T. Epstein *Amer. J. Phys.* **22** (1954) 614.

[113] I. Jameson, A. A. Rawlinson, and A. W. Thomas *Austral. J. Phys.* **47** (1994) 45–48.

[114] R. E. Stuckey and M. C. Birse *J. Phys.* **G23** (1997) 29–40, `hep-ph/9602312`.

[115] U.-G. Meissner, "Chiral dynamics: Status and perspectives," `hep-ph/9810276`.

[116] V. Bernard, N. Kaiser, and U. G. Meissner *Z. Phys.* **C60** (1993) 111–120, hep-ph/9303311.

[117] S. Cabasino *et al. Nucl. Phys. Proc. Suppl.* **20** (1991) 399–405.

Related Publications by the Author

1. *Hadron Mass Extraction from Lattice QCD*
   S. V. Wright, D. B. Leinweber, A. W. Thomas, and K. Tsushima
   [arXiv:hep-lat/0111053]

2. *Systematic Correction of the Chiral Properties of Quenched QCD*
   R. D. Young, D. B. Leinweber, A. W. Thomas, and S. V. Wright
   [arXiv:hep-lat/0111041]

3. *Chiral extrapolation: An analogy with effective field theory*
   G. V. Dunne, A. W. Thomas, and S. V. Wright
   [arXiv:hep-th/0110155]

4. *Chiral behaviour of the rho meson in lattice QCD*
   D. B. Leinweber, A. W. Thomas, K. Tsushima, and S. V. Wright
   Phys. Rev. **D64** (2001) 094502,
   [arXiv:hep-lat/0104013]

5. *A new slant on hadron structure*
   W. Detmold, D. B. Leinweber, W. Melnitchouk, A. W. Thomas, and
   S. V. Wright
   Pramana **57** (2001) 251–262,
   [arXiv:nucl-th/0104043]

6. *The sigma commutator from lattice QCD*
   S. V. Wright, D. B. Leinweber, and A. W. Thomas
   Nucl. Phys. **A680** (2000) 137–140,
   [arXiv:nucl-th/0005003]

7. *Lattice QCD calculations of the sigma commutator*
   D. B. Leinweber, A. W. Thomas, and S. V. Wright
   Phys. Lett. **B482** (2000) 109–113,
   [arXiv:hep-lat/0001007]

8. *Chiral corrections to baryon masses calculated within lattice QCD*
   A. W. Thomas, D. B. Leinweber, K. Tsushima, and S. V. Wright
   Nucl. Phys. **A663** (2000) 973–976,
   [arXiv:nucl-th/9909041]

9. *Baryon mass extrapolation*
   D. B. Leinweber, A. W. Thomas, K. Tsushima, and S. V. Wright
   Nucl. Phys. Proc. Suppl. **83** (2000) 179–181,
   [arXiv:hep-lat/9909109]

10. *Baryon masses from lattice QCD: Beyond the perturbative chiral regime*
    D. B. Leinweber, A. W. Thomas, K. Tsushima, and S. V. Wright
    Phys. Rev. **D61** (2000) 074502,
    [arXiv:hep-lat/9906027]

ADP–01 – 48/T480
LTH–526

Hadron Mass Extraction from Lattice QCD

S. V. Wright[a*], D. B. Leinweber[a], A. W. Thomas[a] and K. Tsushima[a†]

[a]Department of Physics and Mathematical Physics
and Special Research Centre for the Subatomic Structure of Matter,
University of Adelaide, Adelaide 5005, Australia

The extraction of quantities from lattice QCD calculations at realistic quark masses is of considerable importance. Whilst physical quark masses are some way off, the recent advances in the calculation of hadron masses within full QCD now invite improved extrapolation methods. We show that, provided the correct chiral behaviour of QCD is respected in the extrapolation to realistic quark masses, one can indeed obtain a fairly reliable determination of masses, the sigma commutator and the J parameter. We summarise these findings by presenting the nonanalytic behaviour of nucleon and rho masses in the standard Edinburgh plot.

1. INTRODUCTION

There are well-known difficulties associated with making dynamical fermion lattice QCD calculations at light quark masses. There is the need however, to relate quantities calculated on the lattice with physical observables, hence results are required at physical quark masses. These two mutually exclusive restrictions on the field have motivated the necessity for extrapolation from the region in which calculations are able to be performed — that is, the region of unphysically heavy quarks — to lighter masses, including the physical quark masses. In this paper we discuss the construction and application of an extrapolation method for masses [1,2] that respects the correct chiral behaviour of QCD and also allows the extraction of other quantities [2,3]. This approach is not limited to the case of masses in dynamical fermion lattice QCD calculations. Other successes of this approach may be found, for example, in the extrapolation of baryon charge radii [4], magnetic moments [5], structure functions [6,7] and quenched QCD data [8].

*Present address: Division of Theoretical Physics, Department of Mathematical Sciences, University of Liverpool, Liverpool L69 3BX, UK
†Present address: Department of Physics and Astronomy, University of Georgia, Athens, GA 30602, USA

1.1. Goldstone Boson Loops

It is accepted that Goldstone Boson loops play an important role in all hadronic properties — their role is in one sense the basis of Chiral Perturbation Theory (χPT). Lattice QCD calculations, as an ab initio approach to calculating quantities in QCD, implicitly includes these loop contributions. It has become clear recently, with calculations appearing at lighter quark masses [9,10], that the naïve linear extrapolation methods are not reproducing the data. In particular in [10] it was stated

> "The existence of curvature [at small quark masses] is observed, necessitating a cubic Ansatz for extrapolation to the chiral limit."

The following section reviews how the inclusion of chiral physics allows reliable extrapolations of lattice QCD calculations [1,2]. Section 3 reports new results for the Edinburgh plot.

2. EXTRAPOLATION METHODS

In QCD chiral symmetry is dynamically broken, and the pion is almost a Goldstone boson. It plays a significant role in the self-energy contributions to the N and Δ, because of the strong coupling to the baryons. Chiral symmetry requires that, in the region where perturbations around

light quarks makes sense, the mass of the nucleon has the form

$$m_N(m_\pi) = m_N^{(0)} + \alpha m_\pi^2 + \beta m_\pi^3 + \gamma m_\pi^4 \ln m_\pi + \ldots , \quad (1)$$

where $m_N^{(0)}$, α, β and γ are functions of the strong coupling constant. In particular the values of the coefficients of the non-analytic (in quark mass) terms — recall that $m_\pi^2 \propto m_q$ — are known exactly from χPT. However it is only recent results from the lattice that have indicated any need of higher order terms beyond that of a linear extrapolation in quark mass (or m_π^2).

2.1. Chirally Motivated Form

An attempt at having a chirally motivated form for extrapolating masses has been

$$m_N(m_\pi) = m_0 + \tilde{\alpha} m_\pi^2 + \tilde{\beta} m_\pi^3 , \quad (2)$$

where m_0, $\tilde{\alpha}$ and $\tilde{\beta}$ are fit parameters. Naïvely this is a good choice. It reflects the known non-analyticity from χPT and still reproduces the lattice results. The problem with this method is associated with the choice of $\tilde{\beta}$. The value of the coefficient of the cubic term is known explicitly in χPT. So a functional form, motivated by chiral symmetry, should preserve the known value of $\tilde{\beta}$. Optimising $\tilde{\beta}$ via a best fit to existing lattice data provides -0.55 GeV^{-2}. However, the result from χPT is -5.6 GeV^{-2}. That the coefficient is so small is not surprising. The functional form attempts to reproduce the lattice data over a large range of m_π^2, where the data is predominantly linear — as can be seen in Fig. 1. However χPT is an expansion about the massless quark limit and would not be expected to be applicable (or even convergent) at such large quark masses.

2.2. Current Calculation

It has been found [1,2] that by retaining the contributions to the self-energy of the hadron mass that vary the most rapidly with m_π near the chiral limit, a successful extrapolation method may be formed. This methodology includes the most important non-analytic structure in the hadron mass near the chiral limit with *exactly* the correct coefficients. The pion mass dependence of the masses of the N, Δ and ρ are:

$$m_N = a_0 + a_2 m_\pi^2 + \sigma_{NN\pi}(\Lambda_N, m_\pi) + \sigma_{N\Delta\pi}(\Lambda_N, m_\pi) \quad (3)$$

$$m_\Delta = b_0 + b_2 m_\pi^2 + \sigma_{\Delta\Delta\pi}(\Lambda_\Delta, m_\pi) + \sigma_{\Delta N\pi}(\Lambda_\Delta, m_\pi) \quad (4)$$

$$m_\rho = c_0 + c_2 m_\pi^2 + \sigma_{\rho\omega\pi}(\Lambda_\rho, m_\pi) + \sigma_{\rho\pi\pi}(\Lambda_\rho, m_\pi) \quad (5)$$

where σ_{ABC} indicates the contribution from the $A \to BC \to A$ self-energy process. The expressions for these self-energy contributions for the N and Δ may be found in [1]. The two significant processes for the ρ are the $\rho \to \omega\pi$ and $\rho \to \pi\pi$ self-energies and they are presented in [2].

An additional level of detail explicitly included in these extrapolation methods is the inclusion of the decay channels (in the case of the Δ the process $\Delta \to N\pi$). This process is not included in other methods, and yet is a vitally important and physically based consideration. However, because of the finite nature of the lattice, decays are not always possible. The finite periodic volume of the lattice restricts the available momenta to discrete values

$$k_\mu = \frac{2\pi n_\mu}{a L_\mu}, \quad \text{with} \quad -\frac{L_\mu}{2} < n_\mu \leq \frac{L_\mu}{2} \quad (6)$$

where L_μ and a are the lattice size and spacing in the μ direction, respectively.

Figure 1 indicates the expected behaviour of the masses of the N, Δ and ρ using Eqs. (3), (4) and (5), with the physical masses being 0.940, 1.173, 0.713 GeV respectively.[3] We also present an error analysis of the fitting for the particular case of the ρ meson in Fig. 2. The shaded region is bounded below by an increase of 1σ in the χ^2 per degree of freedom of the fit, and above by a physical constraint in our approach. It is clear that whilst the central value of the extrapolation gives an acceptable value for the physical mass, the uncertainties are large. A Gedanken experiment performed in [2] suggests that a ten-fold increase in the number of configurations at the lowest pion mass data point ($m_\pi^2 \sim 0.1$ GeV^2)

[3] The excellent agreement with the experimental mass of the nucleon is coincidental.

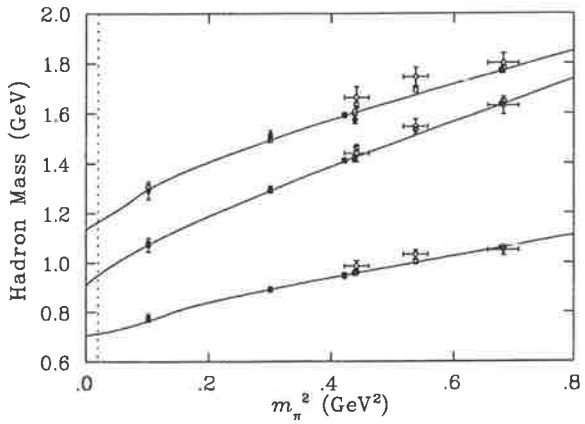

Figure 1. Two-flavour, dynamical fermion lattice QCD data for the Δ, N and vector meson (ρ) mass data from UKQCD [9] (open circles) and CP-PACS [10] (filled circles). The solid lines are the continuum limit, infinite volume predictions of Eqs. (4), (3) and (5). The squares (barely discernable from the data) are the predicted masses on a lattice of the same dimensions as the data at that pion mass.

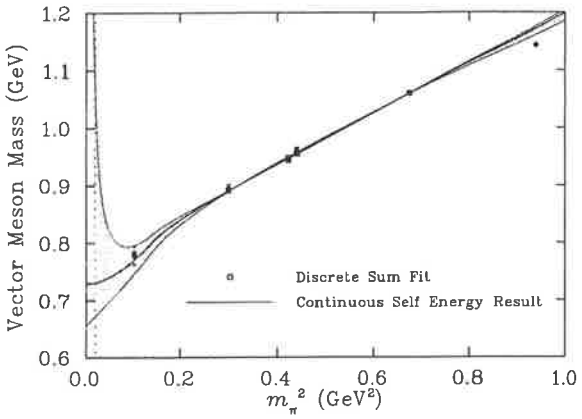

Figure 2. Analysis of the lattice data for the vector meson (ρ) mass calculated by CP-PACS [10] as a function of m_π^2. The shaded area is bounded below by a 1σ error bar. The upper bound is limited by a physical constraint discussed in [2].

would reduce the uncertainty in the extrapolated value to the 5% level.

3. OTHER QUANTITIES

The advantage of calculating the mass of the hadrons in the manner described above is that the form allows the direct extraction of other properties of the hadron that depend upon the quark mass dependence of the hadron mass.

3.1. The Sigma Commutator

The sigma commutator is a direct source of information about chiral symmetry breaking within QCD [11]. As such it is a quantity of considerable importance to extract from lattice QCD calculations. The form of the commutator is

$$\sigma_N = \bar{m}\langle N|\bar{u}u + \bar{d}d|N\rangle \quad (7)$$

$$= \bar{m}\frac{\partial m_N}{\partial \bar{m}}, \quad (8)$$

where $\bar{m}$ is the average mass of the *up* and *down* quarks.

σ_N is not directly accessible via experiment, however world data suggests a value of 45 ± 8 MeV [12]. Early attempts at evaluating Eq. (8) found results in the range 15 to 25 MeV, and the attention soon changed to evaluating the matrix element, Eq. (7), directly. In quenched calculations the results were in the 40–60 MeV range, but a two flavour dynamical fermion calculation by the SESAM collaboration [13] found a value of 18 ± 5 MeV. The difficulties associated with these approaches are two-fold. Firstly, the scale independent quantity of σ_N must be constructed from the renormalisation depended quantities $\bar{m}$ and $\langle N|\bar{u}u+\bar{d}d|N\rangle$. Additionally there still is the need to extrapolate the quantities to the physical pion mass.

Our recent work showed that provided the extrapolation method is under control the evaluation of σ_N at $m_\pi = 140$ MeV, is a straightforward calculation. The important advantage of this approach is that one need only work with renormalisation group invariant quantities.

We discussed previously how a chirally moti-

vated form, Eq. (2), will not reproduce the lattice data if the coefficient of the m_π^3 term is the value required by χPT. However we also showed that allowing this coefficient to be a fit parameter results in a value that is wrong by almost an order of magnitude. This becomes even more significant in the case of the sigma commutator. The required derivative promotes this coefficient to greater significance *and* the sign of the terms acts to reduce the value of σ_N. However this is not an issue with the extrapolation forms discussed above. The sign and magnitude of the cubic term is exactly that predicted by χPT, but the effects are countered by higher order terms — resulting in a prediction for the value of σ_N that included the correct chiral physics. We find [3] that the value of the sigma commutator is approximately 45 MeV.

3.2. The J Parameter

This dimensionless parameter was proposed as a quantitative measure, independent of the need for extrapolation — an ideal lattice observable [14]. It has the form

$$J = m_\rho \left.\frac{dm_\rho}{dm_\pi^2}\right|_{m_\rho/m_\pi=1.8} \quad (9)$$

$$\simeq m_{K^*}\frac{m_{K^*}-m_\rho}{m_K^2-m_\pi^2}\,, \quad (10)$$

which, by substituting the experimental mass values, yields the value [14]

$J = 0.48(2)\,,$

In Fig. 3 we present the value of the J parameter as obtained from Eqs. (5) and (9). The detailed slope of the curve is parameter dependent, however the presence of the cusp is model independent. The cusp is a result of the two pion cut in the rho spectral function and has been ignored in previous attempts at evaluating the J parameter. We find a value for the J parameter of 45(7) in good agreement with the experimental value. We note, however, that if the point of evaluation corresponded to $m_\pi^2 \sim 0.15$ GeV^2 the J parameter would have been around 50% larger.

3.3. Edinburgh Plot

The baryon and meson masses on the lattice are all determined modulo the lattice spacing – a scale that must be determined from some piece of data external to the lattice. One method of removing this scale is by plotting a ratio of masses — the Edinburgh plot. In Fig. 4 we present a prediction for the infinite volume, continuum limit extrapolation of the lattice data previously presented. The two points known explicitly are indicated by open stars on the plot. The first known point is ratio of the physical masses of the π, ρ and N. The second point is the heavy quark limit, when the masses of the hadrons become proportional to the constituent quarks. The effect of the opening of the decay channel of the rho is visible at $m_\pi/m_\rho = 0.5$. The effects induced, and the expected behaviour on the finite sized lattice will be presented in a future work [15].

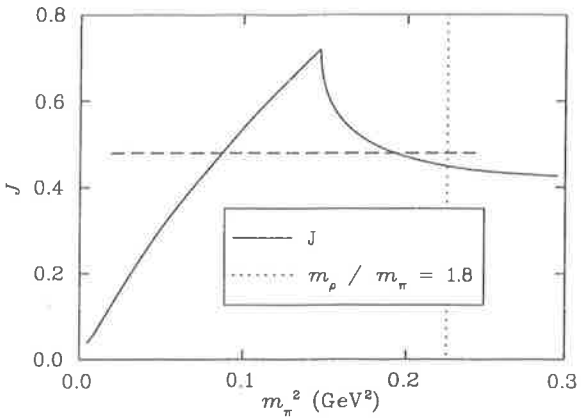

Figure 3. The solid curve is a plot of the value of the J-parameter as a function of m_π^2 obtained from Eq. (9) and the best fit to the lattice results. The vertical dotted line shows the point at which the J-parameter is evaluated ($m_\rho/m_\pi = 1.8$). The horizontal line displays the experimental value (0.48) plotted between the physical values of m_π^2 and m_K^2.

4. SUMMARY

The importance of including the correct chiral behaviour in extrapolation methods is becoming more important as dynamical lattice QCD re-

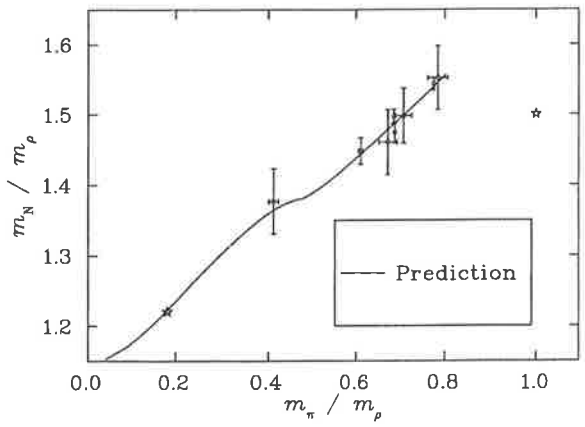

Figure 4. Edinburgh plot for CP-PACS (filled symbols) and UKQCD (open symbols) results. The stars represent the known limiting cases, at the physical and heavy quark limits respectively. The solid line is the infinite volume, continuum limit behaviour predicted by our functional forms for the extrapolation of the N and ρ masses.

sults appear at lighter quark masses. The successes of the approach outlined above include not only predictions for the physical masses of the hadrons investigated, but other quantities successfully reproduced. These other successes include the sigma commutator and the J parameter — both of which have been a thorn in the side of dynamical fermion calculations. It is through the inclusion of the dominant chiral physics, the recognition that decay channels are important, and the understanding of some of the finite size lattice artifacts that we have been able to successfully extrapolate the Edinburgh plot to the known physical limit.

Acknowledgements

This work was supported by the Australian Research Council and the University of Adelaide.

REFERENCES

1. D. B. Leinweber, A. W. Thomas, K. Tsushima and S. V. Wright, Phys. Rev. D **61**, 074502 (2000) [arXiv:hep-lat/9906027].
2. D. B. Leinweber, A. W. Thomas, K. Tsushima and S. V. Wright, Phys. Rev. D **64**, 094502 (2001) [arXiv:hep-lat/0104013].
3. D. B. Leinweber, A. W. Thomas and S. V. Wright, Phys. Lett. B **482**, 109 (2000) [arXiv:hep-lat/0001007].
4. E. J. Hackett-Jones, D. B. Leinweber and A. W. Thomas, Phys. Lett. B **494** (2000) 89 [arXiv:hep-lat/0008018].
5. E. J. Hackett-Jones, D. B. Leinweber and A. W. Thomas, Phys. Lett. B **489** (2000) 143 [arXiv:hep-lat/0004006].
6. W. Detmold, W. Melnitchouk, J. W. Negele, D. B. Renner and A. W. Thomas, Phys. Rev. Lett. **87** (2001) 172001 [arXiv:hep-lat/0103006].
7. W. Detmold, W. Melnitchouk and A. W. Thomas, Eur. Phys. J. directC **13** (2001) 1 [arXiv:hep-lat/0108002].
8. D.B. Leinweber, A.W. Thomas, S.V. Wright and R. Young, in preparation.
9. C. R. Allton *et al.* [UKQCD Collaboration], Phys. Rev. D **60**, 034507 (1999) [arXiv:hep-lat/9808016].
10. S. Aoki *et al.* [CP-PACS Collaboration], Phys. Rev. D **60**, 114508 (1999) [arXiv:hep-lat/9902018].
11. M. E. Sainio, "Pion-nucleon sigma-term - a review," arXiv:hep-ph/0110413.
12. J. Gasser, H. Leutwyler and M. E. Sainio, Phys. Lett. B **253**, 252 (1991).
13. S. Gusken *et al.* [SESAM Collaboration], Phys. Rev. D **59**, 054504 (1999) [arXiv:hep-lat/9809066].
14. P. Lacock and C. Michael [UKQCD Collaboration], Phys. Rev. D **52**, 5213 (1995) [arXiv:hep-lat/9506009].
15. D. B. Leinweber, A. W. Thomas and S. V. Wright, in preparation.

Systematic Correction of the Chiral Properties of Quenched QCD

R. D. Young[1], D. B. Leinweber[1], A. W. Thomas[1] and S. V. Wright[1,2].
[1] *Special Research Centre for the Subatomic Structure of Matter, and Department of Physics and Mathematical Physics, Adelaide University, Adelaide SA 5005, Australia*
[2] *Division of Theoretical Physics, Department of Mathematical Sciences, University of Liverpool, Liverpool L69 3BX, U.K.*
(November 23, 2001)

We extend a technique for the chiral extrapolation of lattice QCD data for hadron masses to quenched simulations. The method ensures the correct leading and next-to-leading non-analytic behaviour for either QCD or quenched QCD in the chiral limit, as well as the correct large quark mass behaviour. The results for the nucleon and delta suggest that within current errors the quenched and dynamical data are in agreement once one corrects for those pion loops which give rise to the different leading and next-to-leading non-analytic behaviour. Since the chiral corrections should be largest for the nucleon and delta, this result opens the possibility of systematically correcting quenched mass calculations and hence allowing a direct comparison with experimental data.

Modern computing facilities, combined with innovations in improved actions for lattice QCD, mean that it is now possible to perform accurate quenched QCD (QQCD) simulations at quite low quark masses [1–3]. For simulations with dynamical fermions (full QCD) the situation is much more difficult, but there are initial results at quark masses as low as 30 MeV [4]. The latter development has inspired studies of chiral extrapolation aimed at using the full QCD data over a range of masses to reliably extract the physical hadron mass.

In general, effective field theories, such as chiral perturbation theory, lead to divergent or asymptotic expansions [5,6]. While this raises doubts about the direct application of chiral perturbation theory to lattice data, studies of the mass dependence of hadron properties in QCD-inspired models [7–9], as well as the exactly soluble Euler-Heisenberg problem [10], suggest that one can develop surprisingly accurate extrapolation formulas, provided one builds in the correct behaviour in both the small *and* large mass limits. For the nucleon (N) and delta (Δ) masses (and by trivial extension all other baryons), Leinweber et al. [11] have suggested an extrapolation method which ensures both the exact low mass limit of chiral perturbation theory (technically its leading (LNA) and next-to-leading non-analytic (NLNA) behaviour) and the heavy quark limit of heavy quark effective theory (HQET). The transition between the chiral and heavy quark regimes is characterised by a mass scale Λ, related to the inverse of the size of the hadron "core" (i.e. the size of the pion cloud source). The rapid, non-analytic variation of hadron properties, characteristic of chiral perturbation theory, is rapidly suppressed once the pion Compton wavelength is smaller than this size (i.e. $m_\pi > \Lambda$).

It is straightforward to extend the method of Ref. [11] to QQCD. One simply includes all the Goldstone loops (including both π and η') which give rise to the LNA and NLNA behaviour of quenched chiral perturbation theory (QχPT) [12,13]. Phenomenological investigations [8,14] of the role of the pion cloud in hadronic charge radii indicate that results consistent with experiment can be obtained by adding full-QCD chiral corrections to the results of quenched simulations [15] at moderate to heavy quark masses. This suggests that the size of the pion-cloud source is not changed in going from the quenched approximation to full QCD. By taking the "core" to have the same size in QQCD and QCD (i.e. parameter Λ is unchanged), there are no unconstrained parameters and one can not only study the mass dependence of the QQCD data, but by replacing the QQCD chiral loops by those in full QCD one can make a direct comparison to dynamical fermion simulations. The results reported here, based on this approach, have profound implications for our understanding of hadron structure.

By replacing the chiral loops which give rise to the LNA and NLNA behaviour in QQCD by the corresponding chiral loops in full QCD we find that the quenched and dynamical lattice data sets are in excellent agreement for the entire quark mass dependence of M_N and M_Δ. Since the chiral corrections are expected to be larger for these two baryons than for others, this suggests that a similar technique may be applicable to *all* baryons. This would be a tremendous step forward for hadron spectroscopy within the framework of lattice QCD.

With regard to the properties of the N and Δ we find a spectacular difference in QQCD. Whereas the extrapolation of the N mass is essentially linear in the quark mass, the Δ exhibits some upward curvature in the chiral limit. As a result, the Δ mass in QQCD is expected to be of the order 400–500 MeV above its mass in full QCD. The success of the extrapolation scheme also lends confidence to the interpretation of the $\Delta - N$ mass splitting as receiving a contribution of order 100 MeV from pion loops in full QCD and up to 400 MeV in QQCD. The residual splitting in full QCD would then be naturally ascribed to some shorter range mechanism, such as the traditional one-gluon-exchange [16].

The method for extrapolating baryon masses proposed by Leinweber et al. [11] is to fit the lattice data with the form:

$$M_B = \alpha_B + \beta_B m_\pi^2 + \Sigma_B(m_\pi, \Lambda), \quad (1)$$

where Σ_B is the sum of those pion loop induced self-energies which give rise to the LNA and NLNA behaviour of the mass, M_B. In the case of the N this is the sum of the processes $N \to N\pi \to N$ and $N \to \Delta\pi \to N$, while for the Δ it involves $\Delta \to \Delta\pi \to \Delta$ and $\Delta \to N\pi \to \Delta$. In the heavy baryon limit, these four contributions ($B \to B'\pi \to B$) can be summarised as:

$$\sigma_{BB'}^{\pi} = \frac{3}{16\pi^2 f_\pi^2} G_{BB'} \int_0^\infty dk \frac{k^4 u_{BB'}^2(k)}{\omega(k)(\omega_{BB'} + \omega(k))}, \quad (2)$$

where $\omega(k) = \sqrt{k^2 + m_\pi^2}$ and $\omega_{BB'} = (M_{B'} - M_B)$, and the constants $G_{BB'}$ are standard SU(6) couplings [11].

The factor $u(k)$, which acts as an ultraviolet regulator, may be interpreted physically as the Fourier transform of the source of the pion field. Whatever choice is made, the form of these meson loop contributions guarantees the exact LNA and NLNA structure of chiral perturbation theory (χPT). Furthermore, such a form factor causes the self-energies to decrease as $1/m_\pi^2$ for $m_\pi >> \Lambda$. One commonly uses a dipole, $u(k) = (\Lambda^2 - \mu^2)^2/(\Lambda^2 + k^2)^2$ (with μ the physical pion mass). Unfortunately full QCD data is not sufficiently accurate at low mass to constrain Λ well, but a best fit to the N and Δ data, assuming a common value, yields a value around 0.92 GeV (with $[\alpha_N, \beta_N] = [1.36(4), 0.71(8)]$ and $[\alpha_\Delta, \beta_\Delta] = [1.54(5), 0.56(10)]$ and all masses in GeV). This agrees with quite general expectations that it should be somewhat smaller than that for the axial form factor [17–19].

Quenched χPT is a low energy effective theory for quenched QCD [12,13], analogous to χPT for full QCD [20]. Sea quark loops are formally removed from QCD by including a set of degenerate, bosonic quarks. These bosonic fields have the effect of cancelling the fermion determinant in the functional integration over the quark fields. This gives a Lagrangian field theory which is equivalent to the quenched approximation simulated on the lattice. The low energy effective theory is then constructed using the symmetry groups of this Lagrangian.

A study of the chiral structure of baryon masses within the quenched approximation has been carried out by Labrenz and Sharpe [13]. The essential differences from full QCD are: a) in the quenched theory the chiral coefficients differ from their standard values and b) new non-analytic structure is also introduced. The leading order form of the baryon mass expansion about $m_\pi = 0$ is

$$M_B = M_B^{(0)} + c_1^B m_\pi + c_2^B m_\pi^2 + c_3^B m_\pi^3 + c_4^B m_\pi^4 + c_{4L}^B m_\pi^4 \log m_\pi + \ldots \quad (3)$$

where the coefficients of terms non-analytic in the quark mass are model-independent [13] (throughout we use couplings as given in this reference). We note that, whereas in Ref. [13] the N and Δ are treated as degenerate states in the chiral limit, we have replaced this with a more accurate expression which takes into account the explicit octet–decuplet mass splitting [21]. As a consequence the corresponding m_π^3 terms become instead $m_\pi^4 \log m_\pi$. We also stress that the term in m_π is absent in full QCD — such a term being unique to the quenched case.

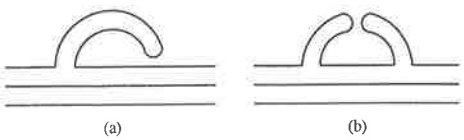

FIG. 1. Quark flow diagrams of chiral η' loop contributions appearing in QQCD: (a) single hairpin, (b) double hairpin.

In fitting quenched data we wish to replicate the analysis for full QCD while incorporating the known chiral structure of the quenched theory. The meson-loop, self-energy corrections to baryon masses can be modelled in the same form as for full QCD. The effect of quenching can be absorbed into a redefinition of the couplings in the loop diagrams in order that they yield exactly the same LNA and NLNA structure as given by QχPT. For example, the analytic expressions for the pion cloud corrections to the masses of the N and Δ have the same form as the full QCD integrals (Eq. 2) with redefined quenched couplings (again using SU(6) symmetry) — we refer to Ref. [21] for details.

In addition to the usual pion loop contributions, QQCD contains loop diagrams involving the flavour singlet η' which also give rise to important non-analytic structure. Within full QCD such loops do not play a role in the chiral expansion because the η' remains massive in the chiral limit. On the other hand, in the quenched approximation the η' is also a Goldstone boson [12,22] and the η' propagator is exactly the same as that of the pion. As a consequence there are two new chiral loop contributions unique to the quenched theory. The first of these, $\tilde{\sigma}_B^{\eta'(1)}$, corresponds to a single hairpin diagram such as that indicated in Fig. 1(a). This diagram is the source of the term proportional to m_π^3 (involving the couplings γ and γ' [13]) in the chiral expansion Eq. (3). The structure of this diagram is exactly the same as the pion loop contribution where the internal baryon is degenerate with the external state. The second of these new η' loop diagrams, $\tilde{\sigma}_B^{\eta'(2)}$, arises from the double hairpin vertex as pictured in Fig. 1(b). This contribution is particularly interesting because it involves two Goldstone boson propagators and is therefore the source of the non-analytic term linear in m_π.

The total meson loop contribution to the baryon self energy within the quenched approximation is given by the sum of these four diagrams:

$$\tilde{\Sigma}_B = \tilde{\sigma}_{BB}^{\pi} + \tilde{\sigma}_{BB'}^{\pi} + \tilde{\sigma}_B^{\eta'(1)} + \tilde{\sigma}_B^{\eta'(2)}. \quad (4)$$

As the pion couplings in QQCD are quite a bit smaller than the corresponding full QCD couplings, $\tilde{\Sigma}_B$ is smaller in magnitude than Σ_B. It is also notable that $\tilde{\sigma}^{\pi}_{\Delta N}, \tilde{\sigma}^{\eta(1)}_{\Delta}$ and $\tilde{\sigma}^{\eta(2)}_{\Delta}$ are all repulsive, so that the total quenched chiral loop contribution to the Δ mass is repulsive, whereas it is attractive in full QCD. (We leave a presentation of the details of the calculation to Ref. [21].)

It is now straightforward to fit the quenched lattice data with the form:

$$\tilde{M}_B = \tilde{\alpha}_B + \tilde{\beta}_B m_\pi^2 + \tilde{\Sigma}_B(m_\pi, \Lambda), \qquad (5)$$

which is directly analogous to that used for full QCD. Once again the linear part should be thought of as accounting for the baryon "core" (not dressed by its pion cloud). It includes the expected behaviour of HQET where the π and η' loop contributions are suppressed. Since, as discussed earlier, the meson–baryon vertices are characterised by the source distribution, which is expected to be similar in quenched and full QCD, we take all vertices to have the same momentum dependence — i.e. a common form factor mass, Λ, equal to the value found earlier in the full QCD fit. With this parameter fixed there are just two free parameters, $\tilde{\alpha}$ and $\tilde{\beta}$, to fit the quenched data for each baryon. We demonstrate the insensitivity of our results to the η' coupling by showing a comparison of the fit with the couplings half their preferred values.

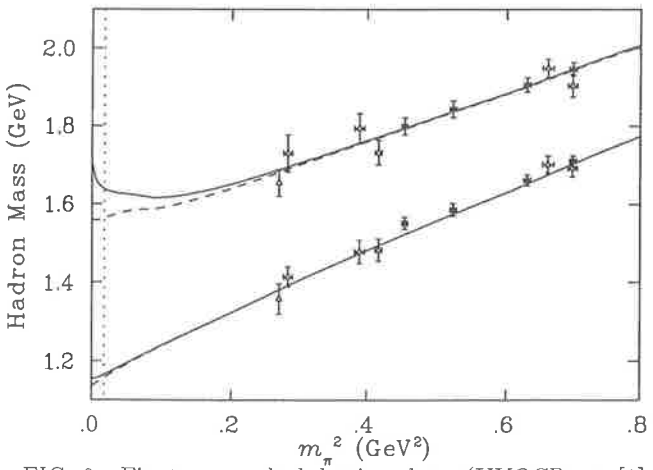

FIG. 2. Fit to quenched lattice data (UKQCD: △ [1], ▲ [24]) with form factor regulated meson-loop self-energies, for the N (lower curve) and Δ (upper curve). The dashed curves show fits with the η' couplings half their preferred value.

As described in Ref. [23] we replace the continuum integral over the intermediate pion momentum by a discrete sum over the pion momenta available on the lattice. The quenched lattice data which we use comes from two papers of the UKQCD Collaboration [1,24], in which both N and Δ masses are reported. Both sets of results are obtained using a non-perturbatively improved clover fermion action, which is known to have small $\mathcal{O}(a^2)$ scaling violations [25]. Unlike the standard Wilson fermion action, masses determined at finite lattice spacing are excellent estimates of the continuum limit results. A plot of the fit to quenched N and Δ masses is shown in Fig. 2, with $[\tilde{\alpha}_N, \tilde{\beta}_N] = [1.34(7), 0.66(12)]$ and $[\tilde{\alpha}_\Delta, \tilde{\beta}_\Delta] = [1.54(9), 0.62(15)]$. Note that, the physical scale has been set via the static quark potential where chiral corrections are negligible [21].

In fact, the fit parameters, α and β, obtained in both the quenched and full fits agree within errors — unlike the case of a purely linear extrapolation, where the self-energy terms are omitted. This suggests that the structure of the core baryon is quite similar in full and quenched QCD, meaning that the dominant errors associated with quenching can be attributed to the first order meson loop corrections. As a demonstration of the size of this effect we subtract the self-energy terms from the fit to quenched data, retain the fit parameters $\tilde{\alpha}$ and $\tilde{\beta}$ and restore the self-energy corrections as appropriate to full QCD. Because we only expect the form factor to be of similar size in the quenched theory we allow Λ to vary by ± 10%. This then gives a band indicative of the size of the error involved in predicting full QCD masses from QQCD data. Results of these adjustments are shown in Figs. 3 and 4 for the N and Δ, respectively.

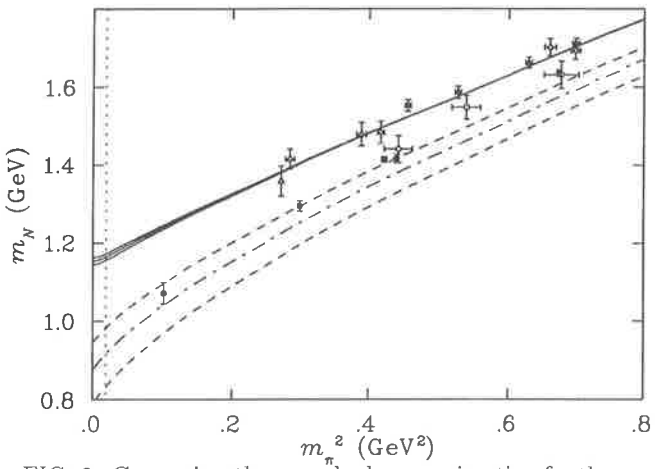

FIG. 3. Correcting the quenched approximation for the nucleon. Full QCD data [4,26] is shown by the circles. The central dash-dot line shows the correction for the preferred form factor mass, $\Lambda = 0.92$ GeV, while the upper and lower dashed lines are for $\Lambda = 0.85$ GeV and $\Lambda = 1.00$ GeV, respectively.

We have investigated the quark mass dependence of the N and Δ masses within the quenched approximation. The leading chiral behaviour of hadron masses in quenched QCD is known to differ from the full theory. This knowledge has been used to guide the construction of a functional form which both reproduces this correct chiral structure, and is consistent with current lattice

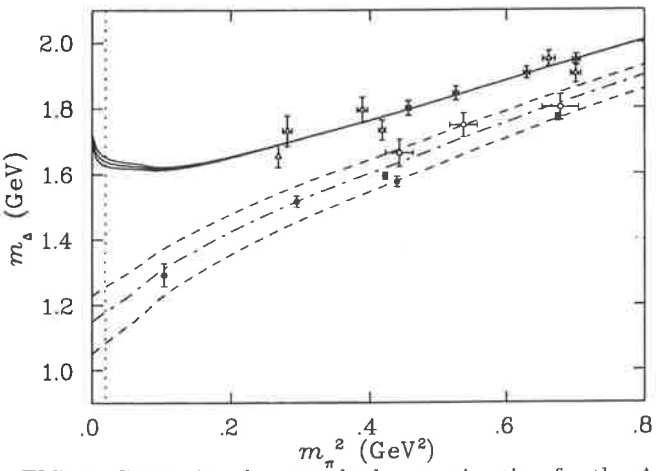

FIG. 4. Correcting the quenched approximation for the Δ – triangles are from QQCD simulations and circles from full QCD. The curves are as in Fig. 3.

simulations. The success of this method in the quenched case further verifies the importance of including meson loop diagrams when extrapolating lattice results.

We find that, although the quenched approximation gives rise to more singular behaviour in the chiral limit, this is not likely to be observed in lattice simulations as these contributions are quickly suppressed with increasing quark mass. In the nucleon, the effects of quenching reduce the amount of curvature expected as lighter quark masses are simulated. In contrast, for the Δ we find some upward curvature of the mass in QQCD as the quark mass approaches zero. In addition, the Δ–N mass splitting increases to 400–500 MeV at the physical point. As a consequence of this behaviour, the Δ mass in the quenched approximation is expected to differ from the physical mass by approximately 25%.

Our calculations suggest that the one loop meson graphs which generate the leading and next-to-leading non-analytic behaviour are the primary difference between baryon masses in quenched and full QCD. In particular, if the chiral loops appearing in the fits to quenched data are replaced by the corresponding loops in full QCD, we find a remarkable agreement with existing full QCD lattice data — as shown in Figs. 3 and 4. Thus, rather than quenched lattice QCD being regarded as an uncontrolled approximation, in combination with appropriate chiral corrections it may actually provide an efficient and accurate estimate of hadron properties. It is vital to test this result with data at lower quark masses and other baryons. Nevertheless, this discovery represents a remarkable step forward in relating lattice QCD to observed hadronic properties.

We would like to thank S. Sharpe for numerous enlightening discussions concerning QχPT as well as W. Detmold, M. Oettel, A. Williams and J. Zanotti for helpful conversations. We also thank C. Allton and the UKQCD Collaboration for sending data from Ref. [24] in advance of print. This work was supported by the Australian Research Council and the University of Adelaide.

[1] **UKQCD** Collaboration, K. C. Bowler *et al. Phys. Rev.* **D62** (2000) 054506.
[2] **CP-PACS** Collaboration, K. Kanaya *et al. Nucl. Phys. Proc. Suppl.* **73** (1999) 189–191.
[3] C. Bernard *et al. Phys. Rev.* **D64** (2001) 054506.
[4] **CP-PACS-Collaboration** Collaboration, S. Aoki *et al. Phys. Rev.* **D60** (1999) 114508.
[5] F. J. Dyson *Phys. Rev.* **85** (1952) 631–632.
[6] J. C. Le Guillou and J. Zinn-Justin, eds., *Large order behavior of perturbation theory.* Amsterdam, Netherlands: North-Holland (1990) 580 p.
[7] D. B. Leinweber, D. H. Lu, and A. W. Thomas *Phys. Rev.* **D60** (1999) 034014; E. J. Hackett-Jones, D. B. Leinweber, and A. W. Thomas *Phys. Lett.* **B489** (2000) 143.
[8] E. J. Hackett-Jones, D. B. Leinweber, and A. W. Thomas *Phys. Lett.* **B494** (2000) 89–99.
[9] W. Detmold *et al. Phys. Rev. Lett.* **87** (2001) 172001.
[10] G. V. Dunne, A. W. Thomas, and S. V. Wright, `arXiv:hep-th/0110155`.
[11] D. B. Leinweber, A. W. Thomas, K. Tsushima, and S. V. Wright *Phys. Rev.* **D61** (2000) 074502.
[12] C. W. Bernard and M. F. L. Golterman *Phys. Rev.* **D46** (1992) 853–857.
[13] J. N. Labrenz and S. R. Sharpe *Phys. Rev.* **D54** (1996) 4595–4608.
[14] D. B. Leinweber and T. D. Cohen *Phys. Rev.* **D47** (1993) 2147–2150.
[15] D. B. Leinweber, R. M. Woloshyn, and T. Draper *Phys. Rev.* **D43** (1991) 1659–1678.
[16] N. Isgur *Phys. Rev.* **D62** (2000) 054026.
[17] A. W. Thomas and W. Weise, *The Structure of the Nucleon.* Wiley-VCH, Berlin, 2001.
[18] P. A. M. Guichon, G. A. Miller, and A. W. Thomas *Phys. Lett.* **B124** (1983) 109.
[19] A. W. Thomas and K. Holinde *Phys. Rev. Lett.* **63** (1989) 2025–2027.
[20] V. Bernard, N. Kaiser, and U.-G. Meissner *Int. J. Mod. Phys.* **E4** (1995) 193–346.
[21] R. D. Young, D. B. Leinweber, A. W. Thomas, and S. V. Wright. In preparation.
[22] S. R. Sharpe *Phys. Rev.* **D46** (1992) 3146-3168.
[23] D. B. Leinweber, A. W. Thomas, K. Tsushima, and S. V. Wright *Phys. Rev.* **D64** (2001) 094502.
[24] **UKQCD** Collaboration, C. R. Allton *et al.* `arXiv:hep-lat/0107021`.
[25] R. G. Edwards, U. M. Heller, and T. R. Klassen *Phys. Rev. Lett.* **80** (1998) 3448–3451.
[26] **UKQCD** Collaboration, C. R. Allton *et al. Phys. Rev.* **D60** (1999) 034507.

Chiral Extrapolation: An Analogy with Effective Field Theory

Gerald V. Dunne
Department of Physics, University of Connecticut, Storrs CT 06269, USA

Anthony W. Thomas and Stewart V. Wright
Special Research Centre for the Subatomic Structure of Matter, and Department of Physics and Mathematical Physics, University of Adelaide, Adelaide SA 5005, Australia

We draw an analogy between the chiral extrapolation of lattice QCD calculations from large to small quark masses and the interpolation between the large mass (weak field) and small mass (strong field) limits of the Euler-Heisenberg QED effective action. In the latter case, where the exact answer is known, a simple extrapolation of a form analogous to those proposed for the QCD applications is shown to be surprisingly accurate over the entire parameter range.

I. INTRODUCTION

The challenge to find an accurate and reliable method of chiral extrapolation for hadronic properties calculated in lattice QCD at large quark mass is a matter of considerable current importance. While computer limitations mean that lattice simulations at physical quark masses are many years away, recent progress in chiral extrapolation suggests that it may well be possible to obtain accurate hadronic properties based on the calculations which will be possible with the next generation of supercomputers, available within just a few years, in the 10 Tera-flops range. Fundamental to this scheme is the development of extrapolation methods which incorporate the model independent constraints of chiral symmetry [1,2], notably the leading non-analytic (LNA) behaviour of chiral perturbation theory [3,4], as well as the heavy quark limit [5].

Although these extrapolations are designed to match the leading behaviour in the extreme limits of small and large quark mass, there has been little guidance as to their reliability in the intermediate mass region. It is very unclear what precision to expect from such a simple extrapolation into the intermediate mass region, because the large mass expansion is presumably asymptotic, and the small mass limit has a log divergence plus finite corrections with a small radius of convergence. Here we attack this question from a novel direction by considering a remarkably close analogy between this problem and a well-known, exactly soluble system in effective field theory — the Euler–Heisenberg effective action [6–8]. The Euler–Heisenberg system exhibits many of the features found in the QCD calculations: at small electron mass (equivalently, strong external field) there is a logarithmic branch point, while at large mass (equivalently, weak external field) one has an asymptotic series expansion in inverse powers of mass. In this Letter, we show that a simple two-parameter interpolation formula (of the form used in the context of chiral extrapolation), which builds in the correct leading behaviour in both the small and large mass limits, yields an excellent approximation to the exact Euler–Heisenberg answer over the entire range of mass. We discuss possible consequences of this observation for the chiral extrapolation of lattice data.

Effective field theory (EFT) plays an important role in modern theoretical physics [9–11]. In pioneering work in the 1930's, Heisenberg and Euler [6], and Weisskopf [7], studied the quantum corrections to classical electrodynamics associated with vacuum polarization effects. Renormalization properties and a more formal "proper-time" version were later studied by Schwinger [8]. In modern language, they computed the low energy effective action for the electromagnetic field, to leading order in the derivative expansion, by integrating out the electron degrees of freedom in the presence of a constant background electromagnetic field. This one-loop effective action can be expressed as [12]

$$S = -i \ln \det(i\not{D} - m), \tag{1}$$

where $\not{D} = \gamma^\nu \left(\partial_\nu + ieA_\nu\right)$, and A_ν is the fixed classical gauge potential with field strength tensor $F_{\mu\nu} = \partial_\mu A_\nu - \partial_\nu A_\mu$. As shown in [6–8], this effective action can be computed in a simple closed form when the background field strength $F_{\mu\nu}$ is constant. For simplicity, we consider the case when the background is a constant magnetic field of strength B (and we choose eB to be positive). Then the exact, renormalized, one-fermion-loop effective action has the following integral representation:

$$S = -\frac{e^2 B^2}{8\pi^2} \int_0^\infty \frac{ds}{s^2} \left(\coth s - \frac{1}{s} - \frac{s}{3} \right) e^{-m^2 s/(eB)}. \tag{2}$$

The $\frac{1}{s}$ term is a subtraction of the zero field ($B = 0$) effective action, while the $\frac{s}{3}$ subtraction corresponds to a logarithmically divergent charge renormalization [8].

We stress that Eq. (2) is an exact, non-perturbative result. However, it can of course be expanded in two obvious limits. In the large mass limit, $m^2 \gg eB$ (which is equivalently the weak field limit), it is straightforward to develop an (asymptotic) expansion of this integral:

$$\begin{aligned} S &= -\frac{2e^2B^2}{\pi^2}\left(\frac{eB}{m^2}\right)^2 \sum_{n=0}^{\infty} \frac{2^{2n}\mathcal{B}_{2n+4}}{(2n+4)(2n+3)(2n+2)}\left(\frac{eB}{m^2}\right)^{2n} \\ &= -\frac{e^2B^2}{8\pi^2}\left[-\frac{1}{45}\left(\frac{eB}{m^2}\right)^2 + \frac{4}{315}\left(\frac{eB}{m^2}\right)^4 - \frac{8}{315}\left(\frac{eB}{m^2}\right)^6 + \ldots\right] \end{aligned} \tag{3}$$

Here the $\mathcal{B}_{2n}$ are the Bernoulli numbers [13]. The large mass expansion, Eq. (3), of the effective action has the standard form, $S = m^4 \sum_n \frac{\mathcal{O}^{(n)}}{m^n}$, of a low energy effective action [9,10], where the higher-dimension operators $\mathcal{O}^{(n)}$ (of dimension n) are balanced by n powers of the mass scale m, below which the low energy effective action is meaningful. In this case, "low energy" means that the cyclotron energy scale $\frac{eB}{m}$ is much smaller than the energy scale set by the electron mass m. That is, $\frac{eB}{m^2} \ll 1$. An alternate perspective on the large mass expansion is as a perturbative expansion in powers of the coupling e, with the n^{th} power of e being associated with a one-fermion-loop diagram with n external photon lines (the divergent $\mathrm{O}(e^2B^2)$ self-energy term is not included, as it contributes to the bare action by charge renormalization [8]). We note that, as a consequence of charge conjugation (Furry's theorem), only even powers of $\frac{eB}{m^2}$ appear in the perturbative expansion of Eq. (3). It is interesting to note that the series expansion of Eq. (3) is divergent, because the Bernoulli numbers grow factorially as $\mathcal{B}_{2n} \sim 2(-1)^{n+1}\frac{(2n)!}{(2\pi)^{2n}}$ for large n, consistent with very general results for perturbation theory [14,15]. It is in fact an asymptotic series, and the proper-time integral representation in Eq. (2) is just the straightforward Borel sum [16] of this asymptotic series [17].

The large mass limit may equivalently be characterized by the relevant length scales: the electron Compton wavelength $\lambda_e = \frac{1}{m}$, and the cyclotron radius ("magnetic length") $\lambda_B = \frac{1}{\sqrt{eB}}$. In terms of these length scales, the large mass limit corresponds to the situation where the electron Compton wavelength is much smaller than the cyclotron radius: $\lambda_e \ll \lambda_B$.

Since the Euler–Heisenberg system is exactly soluble, we can also use the exact integral representation (2) to study the small mass, or strong field, limit where $m^2 \ll eB$. In terms of the length scales, in this limit the electron Compton wavelength is much greater than the cyclotron radius: $\lambda_e \gg \lambda_B$. Then, from Eq. (2), one finds (using results in Ref. [18]):

$$\begin{aligned} S = -\frac{e^2B^2}{8\pi^2}\Bigg\{&\left[\frac{1}{3} + \frac{m^2}{eB} + \frac{1}{2}\left(\frac{m^2}{eB}\right)^2\right]\log\frac{m^2}{eB} + \left[\frac{1}{3} - \frac{1}{3}\log 2 - 4\zeta'(-1)\right] + [\log\pi - 1]\frac{m^2}{eB} \\ &+ \left[-\frac{3}{4} + \frac{\gamma}{2} - \frac{1}{2}\log 2\right]\left(\frac{m^2}{eB}\right)^2 - 4\sum_{k=2}^{\infty}\frac{(-1)^k\zeta(k)}{k(k+1)}\left(\frac{m^2}{2eB}\right)^{k+1}\Bigg\} \\ = -\frac{e^2B^2}{8\pi^2}&\left\{\frac{1}{3}\log\frac{m^2}{eB} + 0.763969 + \mathrm{O}\left(\frac{m^2}{eB}, \frac{m^2}{eB}\log\frac{m^2}{eB}\right)\right\}. \end{aligned} \tag{4}$$

Note that the coefficient, $-\frac{e^2B^2}{24\pi^2}$, of the leading term, the $\log\frac{m^2}{eB}$ term, is fixed by the (one-loop) QED beta function [19]. In (4), γ is Euler's constant, and $\zeta(s)$ is the Riemann zeta function [13]. Note that $\zeta'(-1) \approx -0.165421$.

It is instructive to contrast this small mass expansion, Eq. (4), with the large mass expansion, Eq. (3). In the small mass limit, analogous to the chiral limit in QCD, we see the appearance of logarithmic terms, analogous to the "chiral logs" of QCD. In addition, note that both even and odd powers of $\frac{m^2}{eB}$ appear in the small mass expansion, Eq. (4). On the other hand, in the large mass expansion, Eq. (3), there are no non-analytic log terms, and only even powers of $\frac{eB}{m^2}$ appear. So, we see that the one-loop Euler–Heisenberg effective action, which is given by the exact integral representation (2), has two very different expansions in the two limits of large and small electron mass. The transition between these two extreme regions is governed by whether the electron Compton wavelength, λ_e, is larger or smaller than the cyclotron radius, λ_B. In Fig. 1 we plot the exact Euler–Heisenberg effective action, Eq. (2), with an overall factor of $-\frac{e^2B^2}{8\pi^2}$ removed, as a function of $\frac{m^2}{eB}$, and compare it to the leading large mass term $-\frac{1}{45}\left(\frac{eB}{m^2}\right)^2$ from Eq. (3), and to the leading small mass terms $\frac{1}{3}\log\frac{m^2}{eB} + 0.763969$ from Eq. (4). From this figure it is clear that these leading terms accurately capture the extreme behaviours of the exact result, but do not interpolate in the intermediate region where the scales are comparable.

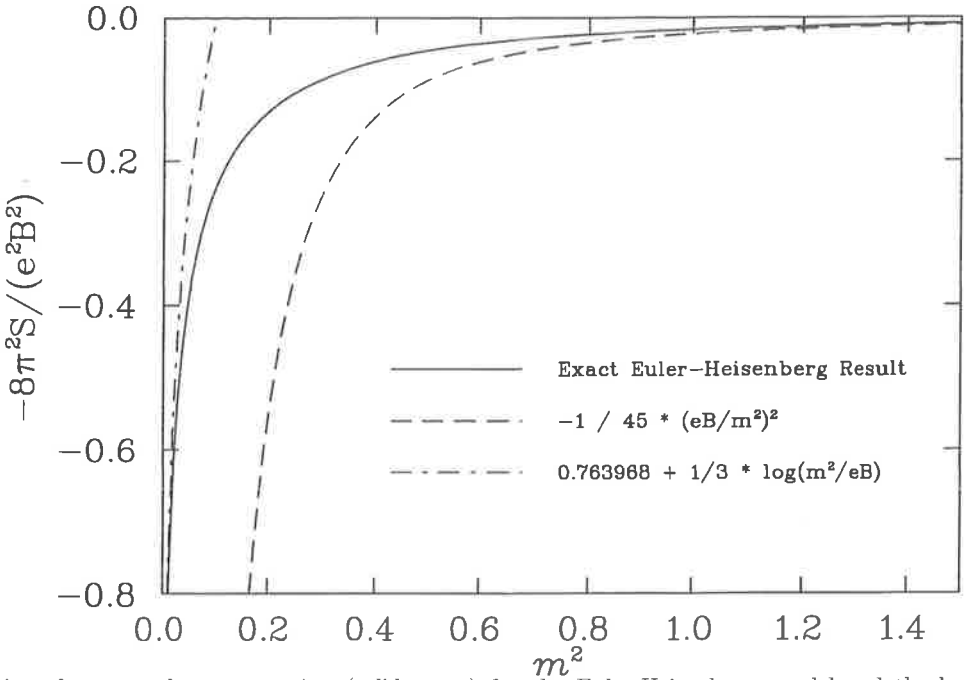

FIG. 1. Comparison between the exact action (solid curve) for the Euler-Heisenberg model and the leading terms in the expansions about the weak (dashed curve) and strong field (dash-dot curve) limits. Note that m^2 is measured in units of eB.

Having reviewed these pertinent aspects of the Euler–Heisenberg effective action, we now turn to what appears at first glance to be a completely different problem: the calculation of hadron properties as a function of quark mass, or through the Gell-Mann–Oakes–Renner relation ($m_\pi^2 \propto m_q$), pion mass. Chiral perturbation theory permits a rigorous expansion of hadron properties about the chiral limit, where $m_\pi \to 0$. For example, for the nucleon charge radius one finds [20]

$$\langle r^2 \rangle_E = c_1 \pm \chi_N \log \frac{m_\pi}{\mu} + c_2 m_\pi^2 + \ldots \tag{5}$$

where $\pm$ refers to the proton or neutron respectively. (Here μ just sets the scale against which the pion mass is measured. It is arbitrary in the sense that a change in μ is equivalent to a change in the constant term, c_1.) Note that the charge radius diverges logarithmically in the chiral limit, with a model independent coefficient

$$\chi_N = -\frac{(1+5g_A^2)}{(4\pi f_\pi)^2}. \tag{6}$$

On the other hand, in the large m_π limit, heavy quark effective theory suggests that the charge radius should decrease as

$$\langle r^2 \rangle_E = \frac{\bar{c}}{m_\pi^2} + \ldots \tag{7}$$

plus higher inverse powers of m_π^2.

As discussed at length in Ref. [3], current lattice data for charge radii are confined to pion masses greater than 600 MeV. The corresponding pion Compton wavelength, λ_π, is then smaller than the calculated charge radius, which we may take as an indication of the size, R, of the source of the pion field. The lattice data shows only a very slow variation of $\langle r^2 \rangle_E$ in the mass range where the lattice calculations have been made, with no indication of a chiral log. Yet, in order to compare with the physical charge radii one must extrapolate these lattice results to the chiral regime where $\lambda_\pi \gg R$ and the chiral log is important. This is the challenge of chiral extrapolation.

We wish to draw an analogy between the Euler–Heisenberg system discussed above and this system. In this analogy, the pion Compton wavelength, λ_π, plays the role of the electron Compton wavelength, λ_e, and the source size, R, plays the role of the magnetic cyclotron radius, λ_B, (equivalently, the mass scale μ^2 plays the role of the magnetic field strength eB). The chiral perturbation theory expansion of Eq. (5), where $\lambda_\pi \gg R$, is analogous to the leading terms in the small mass expansion of Eq. (4), where $\lambda_e \gg \lambda_B$. The heavy quark effective theory result presented in Eq. (7), where $\lambda_\pi \ll R$, is similarly analogous to the leading term in the large mass expansion in Eq. (3) where $\lambda_e \ll \lambda_B$.

In the QCD context, following earlier studies of magnetic moments [2], where it was found that a simple Padé approximant was able to describe the mass dependence arising in a particular chiral quark model, Hackett-Jones *et al.* [3] extrapolated the lattice data from $m_\pi^2 > 0.4\ GeV^2$ to $m_\pi^2 = 0.02\ \mathrm{GeV}^2$ (the physical point) using an interpolating formula which was chosen as the simplest two-parameter form consistent with the constraints imposed by the extreme behaviours in the large and small pion mass limits, Eq. (7) and Eq. (5) respectively. (Recall that χ_N is model independent, and note that the data could constrain no more than two parameters.) In the light of later experience [1], we choose to use a slightly modified argument in the chiral log:

$$\langle r^2 \rangle_E = \frac{c_1 \pm \frac{\chi_N}{2} \log \frac{m_\pi^2}{\mu^2 + m_\pi^2}}{1 + \bar{c}_2 m_\pi^2}. \tag{8}$$

Here, rather than being arbitrary, μ assumes physical significance as the scale above which the chiral log is suppressed - of course, Eq. (8) preserves the correct behaviour in the chiral limit. From experience with moments of structure functions, magnetic moments and hadron masses, this scale is expected to be $\mu \sim 500$ MeV. As the lattice data is not yet able to constrain μ, we simply fix it to 500 MeV and adjust only c_1 and $\bar{c}_2$. Figure 2 shows the resulting fit to the proton charge radius and the corresponding extrapolation to the physical pion mass. As discussed in [3], this chiral extrapolation fit is closer to the physical value than a naive linear fit through the lattice data. However, in the absence of lattice data at lower quark masses, it is difficult to be more precise about the quality of the fit.

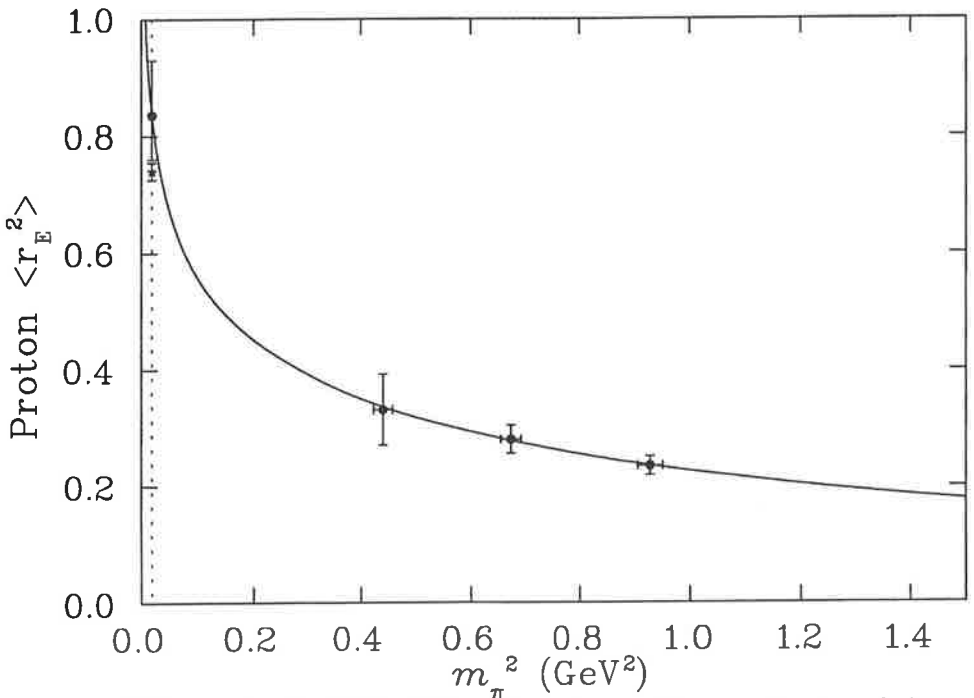

FIG. 2. Fit to the lattice QCD data for the square of the proton charge radius as a function of pion mass squared, using Eq. (8). The extrapolated value at the physical pion mass (indicated by the vertical dotted line) is shown by the solid dot with the large error bar, while the star indicates the experimentally observed value.

In view of the close parallel between this hadronic problem and the Euler–Heisenberg system in QED, we return to the Euler–Heisenberg system, where we can be much more quantitative concerning the accuracy of an interpolating fit. We ask the following question. Suppose that we did not know the exact integral representation answer (2) for the effective action, but that we did know the *leading* terms in each of the extreme large and small mass limits. Would it then be possible to find a simple two-parameter interpolating formula, analogous to (8), that connected the extreme limits in a smooth manner? And if so, how accurate would such an interpolating formula be in the intermediate region?

The leading terms are determined as follows. In the large mass limit, this is the first term, $\frac{m^4}{360\pi^2}\left(\frac{eB}{m^2}\right)^4$, in (3), corresponding to the first nonlinear correction to classical electrodynamics, whose coefficient comes from the one-fermion loop with four external photon lines, a straightforward perturbative calculation. In the small mass limit, the leading term in (4) is the logarithmic term, $-\frac{m^4}{24\pi^2}\left(\frac{eB}{m^2}\right)^2 \log\frac{m^2}{eB}$, whose coefficient is fixed by the one-loop QED

beta function [19]. Motivated by the interpolation formula, Eq. (8), which was used in the QCD case, we propose the following interpolating function for the effective action

$$S_{\text{interpolating}} = -\frac{e^2B^2}{8\pi^2}\left(\frac{d_1 + \frac{1}{3}\log\left(\frac{m^2}{m^2+eB}\right) - d_2\,\frac{m^2}{eB}}{1 + 45d_2\left(\frac{m^2}{eB}\right)^3}\right). \tag{9}$$

This interpolating formula has the correct leading behaviour in both the large and small m limits. Figure 3 shows a comparison of the fit obtained with this form by adjusting the two parameters d_1 and d_2 (dash–dot curve) with the exact result (solid curve). Our best fit was obtained with parameter values: $d_1 = 0.7059$, and $d_2 = 1.5541$. Figure 3 also shows the percentage difference between the exact result and approximate expressions (dashed line). (Note that m^2 is expressed in units of eB.) Over the entire range of $\frac{m^2}{eB}$, the interpolating function is within 10% of the exact answer. Such precision is very surprising when we recall that the Euler-Heisenberg effective action has the problems (shared by the analogous QCD calculations) that the large mass expansion is asymptotic and the small mass expansion has a log divergence and a small radius of convergence.

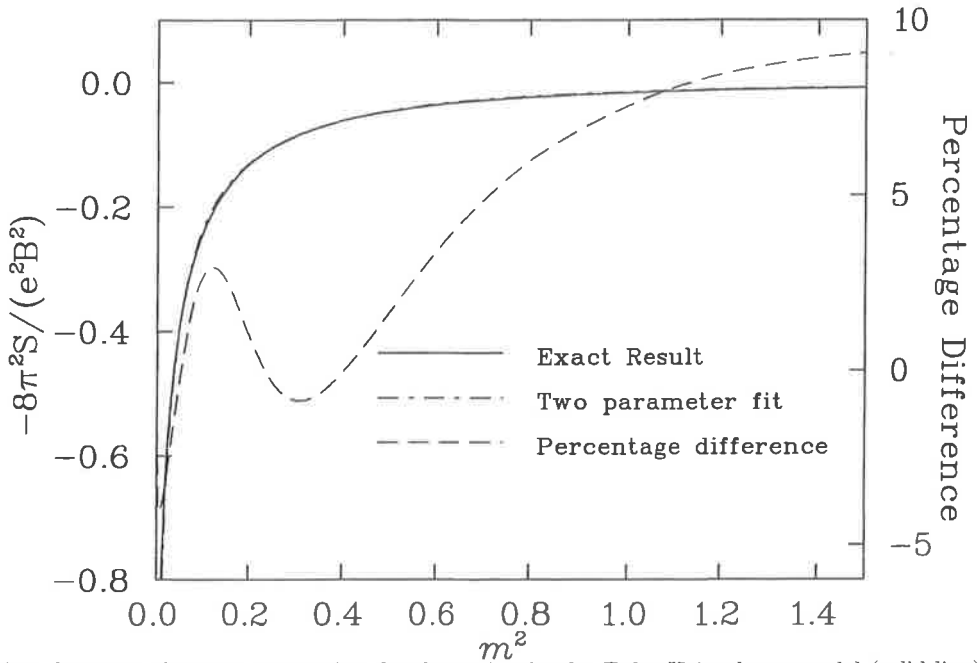

FIG. 3. Comparison between the exact expression for the action in the Euler-Heisenberg model (solid line) and the interpolating approximation given in Eq. (9) which builds in the correct chiral and heavy quark limits (dot–dashed line). Note that the agreement is so good that it is difficult to distinguish between the two curves on this scale. The percentage difference between the two is indicated by the dashed line.

In summary, the Euler-Heisenberg system presents a problem which exhibits many of the mathematical complications of the chiral extrapolation problem in QCD, yet it is exactly soluble. By carefully respecting both the high and low mass limits of the exact solution, we showed how to construct a simple extrapolation formula which reproduced the exact solution over the entire parameter range with surprisingly good accuracy. Since the mathematical structure of the problem of chiral extrapolation of the proton charge radius in QCD is essentially identical, this gives one confidence that a similar level of accuracy may be obtainable there. It is therefore extremely encouraging that the chiral extrapolation of even the present crude lattice data at very large quark masses yields a physical proton charge radius within one standard deviation of the experimental value. Even more important, this result lends enormous impetus to the quest for new lattice data at lower quark mass which will better constrain the chiral extrapolation. It suggests that the next generation of supercomputers (available within 2–3 years) may well provide sufficient information that, in combination with these chiral extrapolation techniques, one should be able to calculate accurate hadron properties at the physical quark mass.

II. ACKNOWLEDGEMENTS:

GD is supported by the U.S. Department of Energy grant DE-FG02-92ER40716.00, and thanks the CSSM at Adelaide for hospitality and support while this work was begun. This work was also supported by the Australian Research Council and the University of Adelaide.

---

[1] W. Detmold, W. Melnitchouk, J. W. Negele, D. B. Renner and A. W. Thomas, Phys. Rev. Lett. **87**, 172001 (2001), [hep-lat/0103006]; D. B. Leinweber, A. W. Thomas, K. Tsushima and S. V. Wright, Phys. Rev. D **61**, 074502 (2000) [hep-lat/9906027].
[2] D. B. Leinweber, D. H. Lu and A. W. Thomas, Phys. Rev. D **60**, 034014 (1999) [hep-lat/9810005].
[3] E. J. Hackett-Jones, D. B. Leinweber and A. W. Thomas, Phys. Lett. B **494**, 89 (2000) [hep-lat/0008018].
[4] V. Bernard, N. Kaiser and U. Meissner, Int. J. Mod. Phys. **E4**, 193 (1995) [hep-ph/9501384].
[5] M. Shifman, "Recent Progress in Heavy Quark Theory", [hep-ph/9505289] lectures at TASI 95, published in *QCD and Beyond*, D. E. Soper (Ed.), World Scientific, 1996.
[6] W. Heisenberg and H. Euler, "Folgerungen aus der Diracschen Theorie des Positrons", Z. Phys. **98**, 714 (1936).
[7] V. Weisskopf, "Uber die Elektrodynamik des Vakuums auf Grund der Quantentheorie des Elektrons", Kong. Dans. Vid. Selsk. Math-fys. Medd. XIV No. 6 (1936), reprinted in *Quantum Electrodynamics*, J. Schwinger (Ed.) (Dover, New York, 1958).
[8] J.Schwinger, "On Gauge Invariance and Vacuum Polarization", Phys. Rev. **82**, 664 (1951).
[9] S. Weinberg, *The Quantum Theory of Fields*, Vol. II, (Cambridge University Press, Cambridge, 1996).
[10] J. Donoghue, E. Golowich and B. Holstein, *Dynamics of the Standard Model* (Cambridge Univ. Press, 1992).
[11] A. Manohar, "Effective Field Theories", Lectures at the Schladming Winter School, March 1996 [hep-ph/9606222].
[12] W. Dittrich and M. Reuter, *Effective Lagrangians in Quantum Electrodynamics*, Lecture Notes in Physics, Vol. 220, (Springer, Berlin, 1985).
[13] I. S. Gradshteyn and I. M. Ryzhik, *Table of Integrals, Series, and Products*, Academic Press, New York, 1979.
[14] F. J. Dyson, "Divergence of Perturbation Theory in Quantum Electrodynamics", Phys. Rev. **85**, 631 (1952).
[15] J. C. Le Guillou and J. Zinn-Justin (Eds.), *Large-Order Behaviour of Perturbation Theory*, (North Holland, Amsterdam, 1990).
[16] C. M. Bender and S. A. Orszag, *Advanced Mathematical Methods for Scientists and Engineers* (McGraw-Hill, New York, 1978).
[17] G. V. Dunne and T. M. Hall, "Borel summation of the derivative expansion and effective actions", Phys. Rev. **D 60**, 065002 (1999) [hep-th/9902064].
[18] S. Blau, M. Visser and A. Wipf, "Analytic Results for the Effective Action", Int. J. Mod. Phys. **A6**, 5409 (1991).
[19] V. I. Ritus, "Lagrangian of an intense electromagnetic field and quantum electrodynamics at short distances", Sov. Phys. JETP **42**, 774 (1976).
[20] D. B. Leinweber and T. D. Cohen, Phys. Rev. D **47**, 2147 (1993) [hep-lat/9211058].

PHYSICAL REVIEW D, VOLUME 64, 094502

Chiral behavior of the rho meson in lattice QCD

D. B. Leinweber, A. W. Thomas, K. Tsushima, and S. V. Wright
Department of Physics and Mathematical Physics and Special Research Centre for the Subatomic Structure of Matter, University of Adelaide, Adelaide 5005, Australia
(Received 30 April 2001; published 8 October 2001)

In order to guide the extrapolation of the mass of the rho meson calculated in lattice QCD with dynamical fermions, we study the contributions to its self-energy, which vary most rapidly as the quark mass approaches zero, from the processes $\rho \to \omega\pi$ and $\rho \to \pi\pi$. It turns out that in analyzing the most recent data from the CP-PACS Collaboration, it is crucial to estimate the self-energy from $\rho \to \pi\pi$ using the same grid of discrete momenta as included implicitly in the lattice simulation. The correction associated with the continuum infinite volume limit can then be found by calculating the corresponding integrals exactly. Our error analysis suggests that a factor of 10 improvement in statistics at the lowest quark mass for which data currently exists would allow one to determine the physical rho mass to within 5%. Finally, our analysis throws light on a long-standing problem with the J parameter.

DOI: 10.1103/PhysRevD.64.094502 PACS number(s): 12.38.Gc, 11.15.Ha

I. INTRODUCTION

As the lightest vector meson, the ρ is of fundamental importance in the task of deriving hadron properties from QCD. Within lattice QCD, the ratio of π to ρ masses is often used as a measure of the approach to the chiral limit. For a long time lattice calculations were restricted to values of m_π/m_ρ above 0.8. However, with the remarkable improvements in actions, algorithms, and computing power, there are now lattice QCD results with dynamical fermions available for hadron masses with current quark masses such that m_π/m_ρ is entering the chiral regime. Nevertheless, in order to compare with the properties of physical hadrons it is still necessary to extrapolate the results to realistic quark masses [1].

In the past few years there have been some very promising developments in our understanding of how to extrapolate lattice data for hadron properties, such as mass [1], magnetic moments [2], charge radii [3], and the moments of structure functions [4], to the physical region. In doing so it is vital to include the rapid variation at small pion masses associated with those pion loops, which yield the leading and next-to-leading nonanalytic behavior. (This was crucial in arriving at a reasonable value for the sigma commutator [5], for example.) However, a formal expansion of hadron properties in terms of m_π fails to converge up to the region where lattice data exist. The crucial physics insight, which renders an accurate chiral extrapolation possible, is that the source of the pion field is a complex system of quarks and gluons, with a finite size characterized by a scale Λ. When the pion mass is greater than Λ, so that the Compton wavelength of the pion is smaller than the extended source, pion loops are suppressed as powers of m_π/Λ and hadron properties are smooth slowly varying functions of the quark mass. However, for pion Compton wavelengths bigger than the source ($m_\pi < \Lambda$) one sees rapid, nonlinear variations. Phenomenologically this transition occurs at $m_\pi \sim 500$ MeV or m_π/m_ρ around 0.5—the region now being addressed by lattice simulations with dynamical fermions.

Another difficulty associated with the extrapolation of lattice results that needs further investigation is the discretization of momenta inherent in all lattice calculations. In this regard we mention not only the finite lattice spacing but the fact that there is a minimum possible nonzero momentum available because of the finite volume of the lattice. This issue is absolutely critical to the interpretation of the recent CP-PACS data for dynamical fermions [6], in which a first result[1] is reported at $m_\pi/m_\rho \sim 0.4$. As we explain in detail, the only reason that it is possible to measure the ρ mass there is that the calculation is done in a finite volume. We show that taking the finite lattice size and finite lattice spacing into account is a necessary requirement when extrapolating to the physical region. These effects become especially significant for the case of the ρ meson, which has a p-wave, two-pion decay mode.

In Sec. II we summarize the key physical ideas and the necessary formulas for extrapolating the mass of the ρ meson to the physical pion mass. This includes a discussion of the limiting behavior at small and large quark mass. We then show the result of our fitting procedure and analyze the uncertainty in extracting the ρ mass at the physical point. We show that a factor of 10 increase in the number of gauge field configurations at the lowest quark mass presently accessible would be sufficient to determine the physical ρ mass to within 5%. In Sec. III, we discuss the consequences of this analysis for the J parameter and conclude with a brief summary and outlook for the future.

II. CHIRAL EXTRAPOLATION FORMULA

The success of our earlier work concerning the extrapolation of the N and Δ masses [1] leads us to consider a similar approach to the latest two-flavor, dynamical QCD data on the ρ meson [6,7]. Once again our guiding principle is to retain those self-energy contributions which yield the most rapid

[1]Although CP-PACS finds no evidence of residual errors for the lowest mass point, they caution that it is premature to draw firm conclusions based on the present low statistics.

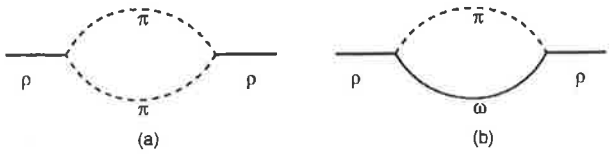

FIG. 1. The most significant self-energy contributions to the ρ meson mass.

variation with m_π near the chiral limit – i.e., those terms which yield the leading nonanalytic (LNA) behavior and the dominant next-to-leading nonanalytic (NLNA) behavior. These processes are illustrated in Fig. 1. The $\rho\to\omega\pi$ term, shown in Fig. 1(b), yields the LNA contribution to the ρ mass. The $\rho\to\pi\pi$ term [Fig. 1(a)] not only yields the NLNA behavior but, of course, the width of the ρ once m_π goes below $m_\rho/2$.

In order to evaluate these self-energy terms, we take the usual interactions [8,9]:

$$\mathcal{L}_{\rho\pi\pi}=\tfrac{1}{2}f_{\rho\pi\pi}\vec{\rho}^{\mu}\cdot[\vec{\pi}\times(\partial_\mu\vec{\pi})-(\partial_\mu\vec{\pi})\times\vec{\pi}] \tag{1}$$

and

$$\mathcal{L}_{\omega\rho\pi}=g_{\omega\rho\pi}\varepsilon_{\mu\nu\alpha\beta}(\partial^\mu\omega^\nu)(\partial^\alpha\vec{\rho}^{\beta})\cdot\vec{\pi}. \tag{2}$$

These lead to the following expressions in the limit, where the mass of the vector mesons (ρ and ω, taken to be degenerate) is much bigger than the mass of the pion:

$$\Sigma^{\rho}_{\pi\pi}=-\frac{f^2_{\rho\pi\pi}}{6\pi^2}\int_0^\infty\frac{dkk^4u^2_{\pi\pi}(k)}{w_\pi(k)(w^2_\pi(k)-\mu^2_\rho/4)}, \tag{3}$$

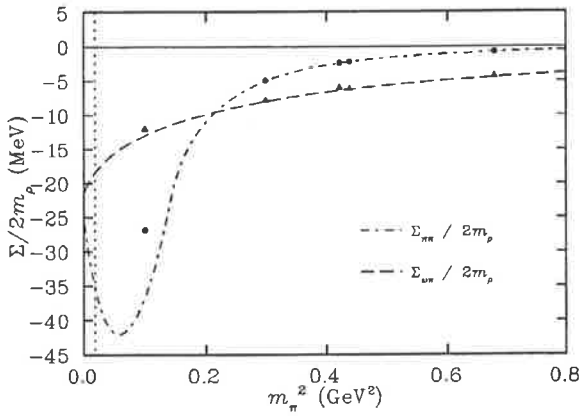

FIG. 2. Variation with pion mass of the self-energy contributions to the ρ meson, Eqs. (3) and (4), for a dipole form factor with $\Lambda_{\pi\omega}=630$ MeV. The solid points indicate the value of the self-energy when calculated at the discrete momenta allowed on the lattices considered in this investigation. The difference between the curves and points is an indication of the physics missing because of finite lattice size and spacing.

$$\Sigma^{\rho}_{\pi\omega}=-\frac{g^2_{\omega\rho\pi}\mu_\rho}{12\pi^2}\int_0^\infty\frac{dkk^4u^2_{\pi\omega}(k)}{w^2_\pi(k)}. \tag{4}$$

In analogy with the heavy baryon limit, we have neglected the kinetic energy of the heavy vector mesons. Here $\Sigma^{\rho}_{\pi\omega}$ and $\Sigma^{\rho}_{\pi\pi}$ correspond to the processes shown in Figs. 1(a) and 1(b), respectively. The pion energy is given by $w_\pi(k)=\sqrt{k^2+m^2_\pi}$, and $u_{\pi\pi}$ and $u_{\pi\omega}$ are dipole form factors governed by a mass parameter reflecting the finite size of the pion source. In the chiral limit these have the standard LNA and NLNA behavior (independent of the forms chosen for $u_{\pi\pi}$ and $u_{\pi\omega}$):

$$\Sigma^{\rho}_{\pi\pi}|_{\rm NLNA}=-\frac{f^2_{\rho\pi\pi}}{4\pi^2\mu^2_\rho}m^4_\pi\ln(m_\pi),$$

$$\Sigma^{\rho}_{\pi\omega}|_{\rm LNA}=-\frac{\mu_\rho g^2_{\omega\rho\pi}}{24\pi}m^3_\pi, \tag{5}$$

while they are suppressed as inverse powers of m_π once m_π is comparable with the dipole mass parameter.[2] Finally, the $\rho\to\pi\pi$ term contains the unitarity cut for $m_\pi<\mu_\rho/2$ (as well as an imaginary piece determined by the width).

The formal solution to the Dyson-Schwinger equation for the ρ propagator places the self-energy contributions in the denominator of the propagator and thereby modifies the ρ mass as [10]

$$m_\rho=\sqrt{m^2_0+\Sigma}$$

$$\approx m_0+\frac{\Sigma}{2m_0}, \tag{6}$$

where $\Sigma=\Sigma^{\rho}_{\pi\pi}+\Sigma^{\rho}_{\pi\omega}$ and the bare mass m_0, is taken to be analytic in the quark mass. Guided by the lattice data at large m_π, we will take m_0 to be $c_0+c_2m^2_\pi$.

The dipole form factors are defined as

$$u_{\pi\pi}(k)=\left(\frac{\Lambda^2_{\pi\pi}+\mu^2_\rho}{\Lambda^2_{\pi\pi}+4w^2_\pi}\right)^2, \tag{7}$$

$$u_{\pi\omega}(k)=\left(\frac{\Lambda^2_{\pi\omega}-\mu^2_\pi}{\Lambda^2_{\pi\omega}+k^2}\right)^2, \tag{8}$$

where μ_π and μ_ρ are the physical masses of the π and ρ mesons. The normalization of $u_{\pi\pi}$ is chosen to be unity at the ρ pole and the coupling constant $f_{\rho\pi\pi}=6.028$, is chosen to reproduce the width of the ρ (i.e., the imaginary part of the self-energy). In the $\rho\to\omega\pi$ case we take $g_{\omega\rho\pi}=16$ GeV^{-1} [11]. The m^2_π dependence of the self-energies of Eqs. (3) and (4) is shown in Fig. 2 by the dot-dash and dashed curves,

[2]Note that all masses (e.g., the ρ mass, μ_ρ) and coupling constants should, in principle, be evaluated in the chiral limit. However, as the variations from the physical values are typically of the order 10%, we use the physical values.

respectively. The interesting behavior of the $\rho \to \pi\pi$ self-energy has been noted in many earlier works. In the context of lattice QCD, it was discussed by DeGrand [12] and by Leinweber and Cohen [10] and most recently by Szczepaniak and Swanson [13]. Other studies have looked at the self-energy as a function of p^2 (invariant mass of the vector meson) for mixed m_π [14–16].

Finally, the lattice data alone cannot separately determine $\Lambda_{\pi\pi}$ and $\Lambda_{\pi\omega}$. In order to constrain them we have therefore made the reasonable, physical assumption that the size of the source of the pion field should be the same regardless of whether the intermediate state involves an ω or a π. Thus we require that $\Lambda_{\pi\pi}$ is chosen so as to reproduce the same mean-square radius of the source as would be generated by the choice of $\Lambda_{\pi\omega}$. Equating the mean-square radii results in the following relationship:

$$\Lambda_{\pi\pi} = 2\sqrt{\Lambda_{\pi\omega}^2 - \mu_\pi^2}. \tag{9}$$

An alternative procedure, which could be imposed in future analyses, would be to constrain the difference in the meson self-energy terms to reproduce the observed $\rho - \omega$ mass difference [14–17].

Fitting procedure

As we hinted in the Introduction, the fact that CP-PACS is able to extract a measurement of the ρ mass at $m_\pi/m_\rho < 0.5$ is at first sight extremely surprising. Once the ρ is able to decay one would expect to measure not the ρ mass but the two-pion threshold. The origin of this result is the quantization of the pion momentum on the lattice and in particular the fact that the lowest (nonzero) pion momentum available is $2\pi/aL$, where is L is the spatial dimension of the lattice. For the relatively small lattice used by CP-PACS at the lowest pion mass this corresponds to more than 400 MeV/c momentum. This is why the ρ remains stable.

Motivated by Eq. (6), and wishing to preserve the correct leading nonanalytic behavior of the self-energies, we have chosen to fit the ρ mass with the simple phenomenological form:

$$m_\rho = c_0 + c_2 m_\pi^2 + \frac{\Sigma^\rho_{\pi\omega}(\Lambda_{\pi\omega}, m_\pi) + \Sigma^\rho_{\pi\pi}(\Lambda_{\pi\pi}, m_\pi)}{2(c_0 + c_2 m_\pi^2)}. \tag{10}$$

Given the constraint relating $\Lambda_{\pi\pi}$ and $\Lambda_{\omega\pi}$, this involves three adjustable parameters. At large m_π the self-energies are suppressed by inverse powers of m_π and the ρ mass becomes a simple linear function of m_π^2 (or the quark mass).

In the finite periodic volume, of the lattice, the available momenta k are discrete:

$$k_\mu = \frac{2\pi n_\mu}{aL_\mu}, \tag{11}$$

where L_μ is the number of lattice sites in the μ direction, and the integer n_μ obeys

$$-\frac{L_\mu}{2} < n_\mu \leq \frac{L_\mu}{2}. \tag{12}$$

Therefore to simulate the calculations that are done on the lattice, we should replace the continuous integrals over k in Eqs. (3) and (4) with a discrete sum over $|\vec{k}|$. However when $|\vec{k}|$ is zero, the case of a pion emitted with zero momentum, the integrands vanish, and hence do not contribute to the self-energy. In fact there is no contribution to the self-energies until $k_\mu = \pm 2\pi/aL_\mu$. There is therefore a momentum gap on the lattice for p-wave channels, produced by this discretization of momenta.

We have investigated this momentum dependence by evaluating the self-energy integrals, Eqs. (3) and (4), by summing the integrand at the allowed values of the lattice three-momenta

$$4\pi \int_0^\infty k^2\, dk = \int d^3k \approx \frac{1}{V}\left(\frac{2\pi}{a}\right)^3 \sum_{k_x, k_y, k_z},$$

where the k_μ are defined by Eqs. (11) and (12) and V is the spatial volume of the lattice. The results for the self-energy contributions are presented in Fig. 2. The self-energy calculated on the lattice (the solid circles and triangles) differs little from the full self-energy calculation in the high quark mass (m_π^2) region. Furthermore, the effect in the $\rho \to \omega\pi$ self-energy contribution is also small at low pion mass. The biggest change is in the $\rho \to \pi\pi$ self-energy calculation, at lower quark mass. This is the region in which one might expect the biggest corrections because one is approximating a principal value integral on a finite mesh. This change in behavior, particularly at the lowest data point ($m_\pi^2 \approx 0.1$ GeV^2), indicates that the $\pi\pi$ self-energy contribution is significantly understated in the lattice simulations. Upon calculating the full self-energy contribution via the continuous integrals, the magnitude of the self-energy is increased by about 10 MeV, which is 30% of the self-energy contribution at this point. These results for $\Sigma^\rho_{\pi\pi}$ and $\Sigma^\rho_{\pi\omega}$ are used in Eq. (10) to fit the lattice data.

Recent dynamical fermion lattice QCD results are presented in Fig. 3. The scale parameters relating the lattice QCD results to physical quantities have been adjusted [1] by 5% for the CP-PACS and UKQCD results. The effect is to increase the ρ mass from CP-PACS and decrease the mass from UKQCD, providing better agreement between the two independent simulations. As the χ^2 of the following fits is dominated by the CP-PACS data, we focus on this data set.

Our fits using Eq. (10) are based on the lowest five lattice masses given by CP-PACS. We selected the lowest lying masses because to move further away from the chiral limit would necessitate additional terms beyond the first two analytic terms of Eq. (10). The results of the fit are shown as the open squares in Figs. 3, 4, and 5. The parameters of the fit c_0, c_2, and $\Lambda_{\pi\omega}$, are then used in an exact evaluation of Eq. (10) using the full integrals in Eqs. (3) and (4). This result is illustrated by the solid lines in Figs. 4 and 5. We note that the value $\Lambda_{\pi\omega} = 630$ MeV for the best fit, results in a softer form factor than one might expect. We do not consider this to be

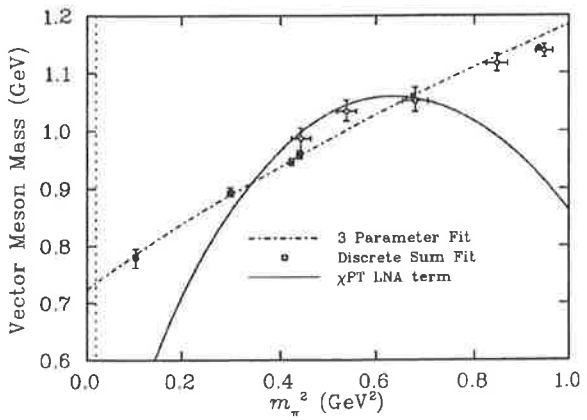

FIG. 3. Vector meson (ρ) mass from CP-PACS [6] (filled circles) and UKQCD [7] (open circles) as a function of m_π^2. The dash-dot curve is the naïve three parameter fit, Eq. (13). The open squares (which are barely distinguishable from the data) represent the fit of Eq. (10) to the data with the self-energy contributions calculated as a discrete sum of allowed lattice momenta. We have used a dipole form factor, with $\Lambda_{\pi\omega}=630$ MeV. The solid curve is Eq. (13) with the parameter c_3 fixed to the value given by chiral perturbation theory.

of significant concern in the present paper because, as we shall discuss below, the current lattice results at low m_π are not precise enough to constrain the chiral behavior.

It is interesting to note the similarity of the results to those of Ref. [10]. There it was found that fitting quenched lattice data with a linear extrapolation, and improving the extrapolation by adding on the $\rho\to\pi\pi$ effects, predicted essentially the same physical mass, but that the chiral behavior was significantly different.

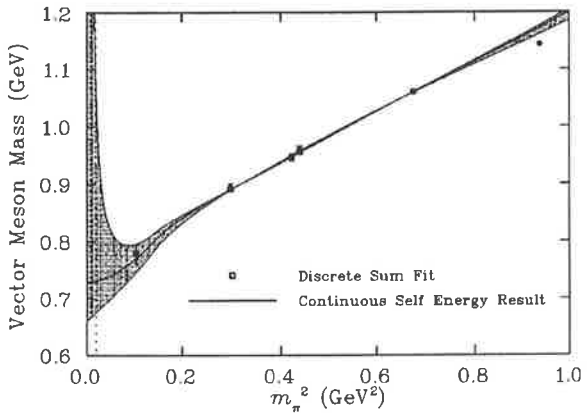

FIG. 4. Analysis of the lattice data for the vector meson (ρ) mass calculated by CP-PACS as a function of m_π^2. The squares represent the fit of Eq. (10) to the data with the self-energy contributions calculated as a discrete sum of allowed lattice momenta. The solid curve is for continuous (integral) self-energy contributions to Eq. (10). We have used a dipole form factor, with optimal $\Lambda_{\pi\omega}=630$ MeV. The shaded area is bounded below by a 1σ error bar. The upper bound is limited by the constraint $\Lambda_{\pi\omega}>\mu_\pi$, as discussed in the text.

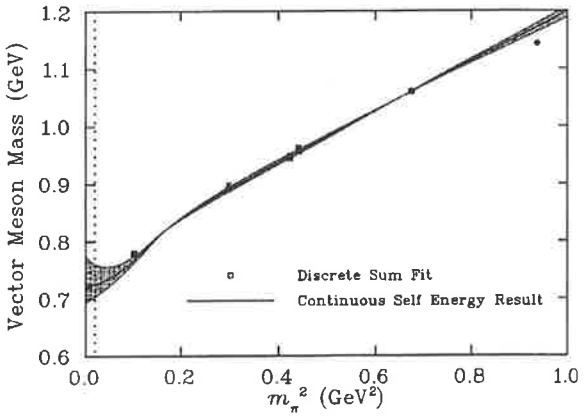

FIG. 5. The graph is as described in Fig. 3 except that the error bar on the lowest data point ($m_\pi^2\approx 0.1$ GeV^2) has been reduced by a factor of $\sqrt{10}$. This equates to an improvement of ten times in the statistics, which we do not consider an unreasonable goal for the future. The dipole mass of the best fit is then $\Lambda_{\pi\omega}=660$ MeV. The shaded area is bounded above and below by a 1σ error bar.

For comparison, we also show a popular three parameter fit, motivated by chiral perturbation theory:

$$m_\rho = c_0 + c_2 m_\pi^2 + c_3 m_\pi^3. \tag{13}$$

This naïve three parameter fit is illustrated by the dash-dot curve in Fig. 3. However, since the value of c_3 in Eq. (13) is commonly treated as a fitting parameter, we are not guaranteed that it has the correct value required by chiral perturbation theory (χPT). The value for the best fit is found to be -0.21 GeV^{-2}. As outlined above, our expressions for the ρ self-energies have the correct LNA and NLNA coefficients by construction. Indeed, if the coefficient c_3 is constrained to the correct value[3] ($-g_{\omega\rho\pi}^2/48\pi=-1.70$ GeV^{-2}), the best fit possible by varying c_1 and c_2 is shown as the solid line in Fig. 3. As was also found in the case of the nucleon [1], the lack of convergence of the formal expansion is such that it is not sufficient to fix the coefficient of the LNA term in a cubic fit to that predicted by χPT, as the resulting form will not fit the data.

The importance of the accuracy of the lowest mass point cannot be overstated. We stress that CP-PACS emphasized the preliminary nature of the lowest data point, because of the relatively low statistics. Nevertheless, in order to prepare for future more accurate data, we have carried out a standard error analysis including this point and the results are presented in Fig. 4. The lower bound on the shaded area was found by increasing the minimum χ^2 per degree of freedom of the fit by 1. We were unable to do this with the upper bound. The result is actually limited by the physics of the

[3]In Ref. [18] the m_π dependence of the LNA term to the ρ mass is given by $-(1/12\pi f^2)(\frac{2}{3}g_2^2+g_1^2)m_\pi^3$. This would result in a value of the m_π^3 coefficient of -1.71 GeV^{-2}, in excellent agreement with the value used here.

TABLE I. Table of fit parameters c_0, c_2, c_3, $\Lambda_{\pi\omega}$, the ρ-meson mass at μ_π, the value of the J parameter, and the pion mass at which the J parameter is calculated. All values are in appropriate powers of GeV. The cubic fit refers to Eq. (13) while the dipole refers to Eq. (10) with a dipole form factor. We find that the error in the J parameter is halved if the statistics on the lowest point are increased by a factor of 10.

Fit form	c_0	c_2	c_3	$\Lambda_{\pi\omega}$	M_ρ	J	m_π^2
Cubic	0.723	0.668	−0.207	···	0.735	0.44 (8)	0.223 (7)
Dipole	0.776	0.427 32	···	0.630	0.731	0.45 (7)	0.225 (4)

process. In the case of a dipole form factor this means $\Lambda_{\pi\omega} > \mu_\pi$, and that is the upper limit we have shown here.

It is not unreasonable to expect an improvement in the accuracy of the calculated lattice mass values, and as a Gedanken experiment we have explored the possibility of a tenfold increase in the number of gauge configurations at the lowest pion mass. For the purposes of the simulation, we did not change the value of the data point, but simply reduced the size of the error bar by $\sqrt{10}$. As can be seen in Fig. 5, the improvement in the predictive power is dramatic. The uncertainty in the physical mass has been reduced to the 2% level. Additional improvement in the accuracy of the extrapolation would result from the availability of additional data in the low pion mass region. However, it must be noted that the provision of data around 0.2 GeV^2 and higher would probably not assist greatly in the determination of the dipole mass (Λ); it is primarily determined by points nearer the physical region. We present the parameters of these fits in Table I.

We have examined the model dependence of our paper by repeating the above fits with a monopole form factor. As can be seen in Fig. 6, the model dependence is at the level of 15 MeV at the physical pion mass with current data, and would have been at the few MeV level had the error bar been reduced by a factor of $\sqrt{10}$. This reinforces the claim in Ref. [1] that this extrapolation method is not very sensitive to the form chosen for the ultraviolet cutoff.

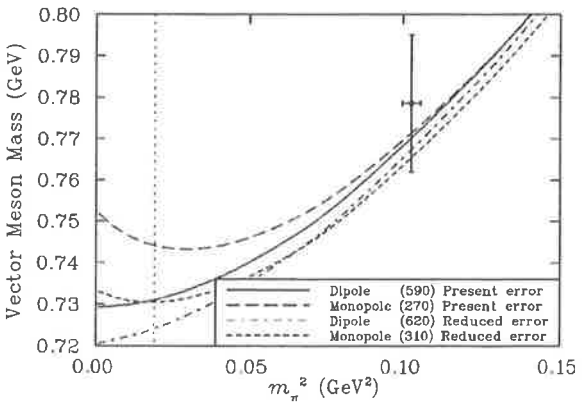

FIG. 6. A magnification of the physical pion mass region of our extrapolation results. The solid and long dashed lines represent the best fit dipole and monopole results for a fit with the present accuracy of the lattice QCD results. The dash-dot and short dashed lines are the dipole and monopole results for a reduction in the error bar of the lowest lattice data by a factor of $\sqrt{10}$. The model dependence of the choice of the form the factor is $\mathcal{O}(2\%)$.

III. J PARAMETER

A commonly perceived failure with quenched lattice QCD calculations of meson masses is the inability to correctly determine the J parameter. This dimensionless parameter was proposed as a quantitative measure, independent of chiral extrapolations, thus making it an ideal lattice observable [19]. The form of the J parameter is

$$J = m_\rho \left.\frac{dm_\rho}{dm_\pi^2}\right|_{m_\rho/m_\pi = 1.8} \tag{14}$$

$$\simeq m_{K^*} \frac{m_{K^*} - m_\rho}{m_K^2 - m_\pi^2}. \tag{15}$$

By using Eq. (15) and the experimentally measured masses of the K(495.7 MeV), K^*(892.1 MeV), π(138.0 MeV), and ρ(770.0 MeV), Lacock and Michael [19] determined

$$J = 0.48(2).$$

However, previous attempts by the lattice community to reproduce this value have been around 20% too small. In the case of quenched calculations, this has been cited as evidence of a quenching error (see, for example, the review in [20]). It was noted by Lee and Leinweber [21] that the inclusion of the self-energy of the ρ meson generated by two-pion intermediate states (excluded in the quenched calculations) acts to increase the J parameter.

In Fig. 7 we present the value of the J parameter obtained from Eq. (14) and our best fit to the lattice results using Eq. (10). The vertical dotted line indicates the value of m_π^2, where the J parameter is to be evaluated, i.e., $m_\rho/m_\pi = 1.8$. The horizontal dashed line, plotted between the values of the squares of the physical pion and kaon masses, shows the experimental estimate of the J parameter from Eq. (15). This equation suggests that the evaluation of J may be approximated by the slope of the vector meson mass extrapolation between these points. The cusp shown in Fig. 7, associated with the cut in $\Sigma^\rho_{\pi\pi}$, suggests otherwise. We stress that while the detailed slope of the curve is parameter dependent, the presence of the cusp is a model independent consequence of the two pion cut in the rho spectral function.

As a point of comparison, we have also calculated J using the naïve cubic chiral extrapolation, Eq. (13), described above. The results of our investigations are summarized in Table I. The value of the J parameter is similar for both fits as it is evaluated at $m_\pi^2 \sim 0.22$ GeV^2. The effects introduced

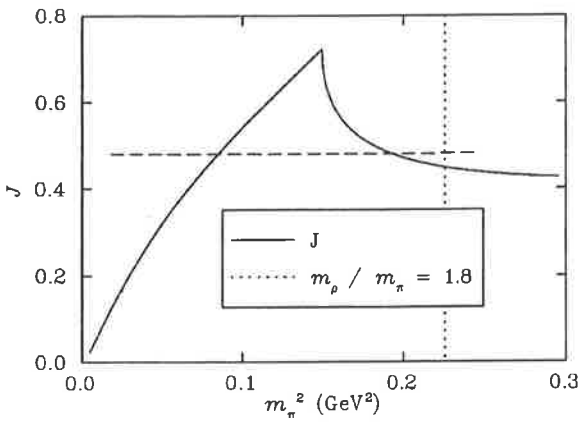

FIG. 7. The solid curve is a plot of the value of the J parameter as a function of m_π^2 obtained from Eq. (14) and the best fit to the lattice results given by Eq. (10). The vertical dotted line shows the point at which the J parameter is evaluated ($m_\rho/m_\pi=1.8$). The horizontal line displays the experimental value (0.48) plotted between the physical values of m_π^2 and m_K^2.

into the extrapolations by chiral physics do not begin playing a large role until m_π^2 falls below 0.2 GeV^2. Had the J parameter been evaluated at $m_\pi^2=0.19$ or 0.09 GeV^2, one would find perfect agreement with the linear ansatz of Eq. (15).

IV. CONCLUSION

We have explored the quark mass dependence of the ρ meson including the constraints imposed by chiral symmetry. The pionic self-energy diagrams are unique in that they give rise to the leading (and next-to-leading) nonanalytic behavior and yield a rapid variation of the meson mass near the chiral limit. These are the lowest energy states with given quantum numbers that have significant couplings to the ρ meson. Other meson intermediate states are suppressed by large mass terms in the denominators of the propagators, and also by smaller couplings.

We find that the predictions of two-flavor, dynamical-fermion lattice QCD results are succinctly described by Eq. (10) with terms defined in Eqs. (3) and (4) for $m_\pi \leq 800$ MeV. We have shown that our formula gives model independent results at the 2% level for the physical mass of the ρ meson. However, firm conclusions concerning agreement between the extrapolated lattice results and experiment cannot be made until the systematic errors in the extraction of the scale of masses can be reduced below the current level of 10% and accurate measurements are made at $m_\pi \sim 300$ MeV or lower.

We have also calculated the J parameter by directly evaluating the derivative of our mass extrapolation formula. We find that the empirical estimate based on differences of meson masses misses important nonanalytic effects in the derivative of m_ρ with respect to m_π^2, as illustrated in Fig. 7.

Finally we have investigated the effects of an improvement in the statistics of the lattice data. Present lattice data are not yet sufficiently precise to independently constrain the behavior near the chiral limit. With the best data available one finds a ρ-meson mass of 731 MeV with 1σ bounds at 675 and 1062 MeV. One could constrain the bounds by using phenomenological guidance for the form factors, but we would prefer to wait for better lattice data. Figure 5 suggests that the ρ-meson mass could be known to within 5% in the very near future.

Note added. Since the submission of this manuscript, the CP-PACS Collaboration has released a preprint [22], with work showing J as a function of mass. We note that their analysis does not address the chiral physics studied here. As a result, their curves will omit the general feature of a cusp in the J parameter as discussed in this manuscript. A similar comment applies to the MILC Collaboration [23]. We look forward to seeing a similar analysis to that presented here applied to these new simulation results.

ACKNOWLEDGMENTS

The authors would like to thank C. R. Allton, S. R. Sharpe, J. Speth, and A. G. Williams for helpful discussions. We would particularly like to thank A. P. Szczepaniak for drawing our attention to a correction in the $\omega\pi$ self-energy. This work was supported by the Australian Research Council.

APPENDIX

In this Appendix we present the evaluation of the leading nonanalytic terms of the $\Sigma^\rho_{\pi\omega}$ and $\Sigma^\rho_{\pi\pi}$ self-energy contributions to the ρ-meson mass. By the definition in Eq. (10) all the nonanalytic behavior is contained in these two terms.

We note that the form of the self-energy contribution from $\rho\to\pi\omega$ is the same as that for the process σ_{NN} discussed in Ref. [1]. Using the results found in that paper we can write (for the choice of a sharp cutoff $[\theta(\Lambda-k)]$ for the form factor $u_{\pi\omega}$)

$$\Sigma^\rho_{\pi\omega}=-\frac{g_{\omega\rho\pi}\mu_\rho}{12\pi^2}\left[m_\pi^3\arctan\left(\frac{\Lambda}{m_\pi}\right)+\frac{\Lambda^3}{3}-\Lambda m_\pi^2\right]. \tag{A1}$$

The chiral behavior of this expression is obtained by expanding it in m_π about $m_\pi=0$ (the chiral limit). We find that in this limit

$$\Sigma^\rho_{\pi\omega}=-\frac{g_{\omega\rho\pi}\mu_\rho}{12\pi^2}\left(\frac{\Lambda^3}{3}-\Lambda m_\pi^2+\frac{\pi}{2}m_\pi^3-\frac{1}{\Lambda}m_\pi^4+\mathcal{O}(m_\pi^6)\right), \tag{A2}$$

with the leading non-analytic term being of order m_π^3:

$$\Sigma^\rho_{\pi\omega}|_{\rm LNA}=-\frac{\mu_\rho g^2_{\omega\rho\pi}}{24\pi}m_\pi^3. \tag{A3}$$

The $\rho\to\pi\pi$ self-energy contribution is slightly more complicated. If we again choose a θ function for the form factor we can analytically integrate Eq. (3) giving

$$\Sigma^{\rho}_{\pi\pi}=-\frac{f^2_{\rho\pi\pi}}{6\pi^2}\frac{1}{2(\mu_\rho/2)}\left(2\sqrt{m_\pi^2-(\mu_\rho/2)^2}(m_\pi^2-(\mu_\rho/2)^2)\left\{\arctan\left(\frac{\Lambda-(\mu_\rho/2)+\sqrt{\Lambda^2+m_\pi^2}}{\sqrt{m_\pi^2-(\mu_\rho/2)^2}}\right)\right.\right.$$
$$-\arctan\left(\frac{\Lambda+(\mu_\rho/2)+\sqrt{\Lambda^2+m_\pi^2}}{\sqrt{m_\pi^2-(\mu_\rho/2)^2}}\right)-\arctan\left(\frac{m-(\mu_\rho/2)}{\sqrt{m_\pi^2-(\mu_\rho/2)^2}}\right)+\left.\arctan\left(\frac{m+(\mu_\rho/2)}{\sqrt{m_\pi^2-(\mu_\rho/2)^2}}\right)\right\}$$
$$-[3m_\pi^2-2(\mu_\rho/2)^2](\mu_\rho/2)\ln\left(\frac{\sqrt{\Lambda^2+m_\pi^2}+\Lambda}{m_\pi}\right)-\Lambda(\mu_\rho/2)\sqrt{\Lambda^2+m_\pi^2}\left.\right), \tag{A4}$$

where Λ regulates the cutoff of the integral. The region in which we are interested (the chiral limit) has $m_\pi<(\mu_\rho/2)$. Thus the arguments of the arctans are complex. We use the relationship

$$\arctan(z)=\frac{i}{2}\ln\left(\frac{1-iz}{1+iz}\right) \tag{A5}$$

to rewrite this expression in terms of logarithms with real arguments. Collecting the logarithms together results in the following expression for the $\rho\to\pi\pi$ self-energy, for $m_\pi<(\mu_\rho/2)$:

$$\Sigma^{\rho}_{\pi\pi}=-\frac{f^2_{\rho\pi\pi}}{6\pi^2}\frac{1}{2(\mu_\rho/2)}\left\{-[(\mu_\rho/2)^2-m_\pi^2]^{3/2}\right.$$
$$\times\ln\left(\frac{m_\pi^2[m_\pi^2-(\mu_\rho/2)^2]+\Lambda^2[m_\pi^2-2(\mu_\rho/2)^2]-2\Lambda(\mu_\rho/2)\sqrt{(\Lambda^2+m_\pi^2)[(\mu_\rho/2)^2-m_\pi^2]}}{m_\pi^2[\Lambda^2+m_\pi^2-(\mu_\rho/2)^2]}\right)$$
$$\left.-[3m_\pi^2-2(\mu_\rho/2)^2](\mu_\rho/2)\ln\left(\frac{\sqrt{\Lambda^2+m_\pi^2}+\Lambda}{m_\pi}\right)-\Lambda(\mu_\rho/2)\sqrt{\Lambda^2+m_\pi^2}\right\}. \tag{A6}$$

Looking at just the lowest order, nonanalytic, terms in the expansion about $m_\pi=0$, we have

$$\Sigma^{\rho}_{\pi\pi}|_{\mathrm{LNA}}=-\frac{f^2_{\rho\pi\pi}}{6\pi^2}\frac{1}{2(\mu_\rho/2)}\left[\left(2(\mu_\rho/2)^3-3(\mu_\rho/2)m_\pi^2+\frac{3}{4}\frac{m_\pi^4}{(\mu_\rho/2)}\right)+[3m_\pi^2-2(\mu_\rho/2)^2](\mu_\rho/2)\right]\ln(m_\pi)$$
$$=-\frac{f^2_{\rho\pi\pi}}{4\pi^2\mu_\rho^2}m_\pi^4\ln(m_\pi), \tag{A7}$$

which is the result given in Eq. (5).

[1] D.B. Leinweber, A.W. Thomas, K. Tsushima, and S.V. Wright, Phys. Rev. D **61**, 074502 (2000).

[2] D.B. Leinweber, D.H. Lu, and A.W. Thomas, Phys. Rev. D **60**, 034014 (1999); E.J. Hackett-Jones, D.B. Leinweber, and A.W. Thomas, Phys. Lett. B **489**, 143 (2000); D.B. Leinweber and A.W. Thomas, Phys. Rev. D **62**, 074505 (2000).

[3] E.J. Hackett-Jones, D.B. Leinweber, and A.W. Thomas, Phys. Lett. B **494**, 89 (2000).

[4] W. Detmold, W. Melnitchouk, J.W. Negele, D.B. Renner, and A.W. Thomas, hep-lat/0103006.

[5] D.B. Leinweber, A.W. Thomas, and S.V. Wright, Phys. Lett. B **482**, 109 (2000).

[6] CP-PACS-Collaboration, S. Aoki *et al.*, Phys. Rev. D **60**, 114508 (1999).

[7] UKQCD Collaboration, C.R. Allton *et al.*, Phys. Rev. D **60**, 034507 (1999).

[8] P.A. Carruthers, *Introduction to Unitary Symmetry* (Interscience, New York,1966).

[9] R.K. Bhaduri, *Models of the Nucleon: From Quarks to Soliton*, Vol. 22 of Lecture Notes and Supplements in Physics (Addison-Wesley, Redwood City, CA, 1988).

[10] D.B. Leinweber and T.D. Cohen, Phys. Rev. D **49**, 3512 (1994).

[11] M. Lublinsky, Phys. Rev. D **55**, 249 (1997).

[12] T.A. DeGrand, Phys. Rev. D **43**, 2296 (1991).

[13] A.P. Szczepaniak and E.S. Swanson, Phys. Rev. Lett. (to be published) hep-ph/0006306.

[14] M.A. Pichowsky, S. Walawalkar, and S. Capstick, Phys. Rev. D **60**, 054030 (1999).

[15] K.L. Mitchell and P.C. Tandy, Phys. Rev. C **55**, 1477 (1997).

[16] L.C.L. Hollenberg, C.D. Roberts, and B.H.J. McKellar, Phys. Rev. C **46**, 2057 (1992).

[17] P. Geiger and N. Isgur, Phys. Rev. Lett. **67**, 1066 (1991); P. Geiger and N. Isgur, Phys. Rev. D **41**, 1595 (1990); **44**, 799 (1991).
[18] E. Jenkins, A.V. Manohar, and M.B. Wise, Phys. Rev. Lett. **75**, 2272 (1995).
[19] UKQCD Collaboration, P. Lacock and C. Michael, Phys. Rev. D **52**, 5213 (1995).
[20] T. Yoshie, Nucl. Phys. (Proc. Suppl.) **63**, 3 (1998).
[21] F.X. Lee and D.B. Leinweber, Phys. Rev. D **59**, 074504 (1999).
[22] CP-PACS Collaboration, A.A. Khan *et al.*, hep-lat/0105015.
[23] C. Bernard *et al.*, Phys. Rev. D **64**, 054506 (2001).

Presented by A. W. Thomas at the
Int. Symposium on Nuclear Physics
(Mumbai, Dec. 2000)
ADP-01-05/T440

A New Slant on Hadron Structure

W. Detmold[1], D. B. Leinweber[1], W. Melnitchouk[1,2], A. W. Thomas[1] and S. V. Wright[1]
[1] *Special Research Centre for the Subatomic Structure of Matter, and Department of Physics and Mathematical Physics, Adelaide University, 5005, Australia*
[2] *Jefferson Lab, 12000 Jefferson Avenue, Newport News, VA 23606, USA*

Abstract

Rather than regarding the restriction of current lattice QCD simulations to quark masses that are 5–10 times larger than those observed, we note that this presents a wonderful opportunity to deepen our understanding of QCD. Just as it has been possible to learn a great deal about QCD by treating N_c as a variable, so the study of hadron properties as a function of quark mass is leading us to a much deeper appreciation of hadron structure. As examples we cite recent progress in using the chiral properties of QCD to connect hadron masses, magnetic moments, charge radii and structure functions calculated at large quark masses within lattice QCD with the values observed physically.

I. INTRODUCTION

In striving to understand the properties of QCD the generalization to an arbitrary number of colours, N_c, particularly the limit $N_c \to \infty$ (or "large N_c") has been extremely valuable. It has even proven possible to distinguish between models of hadron structure and to guide the further developments of such models on the basis of their large N_c behaviour [1]. Until recently it has generally been regarded as an unfortunate liability that current limitations on computer power restrict lattice QCD simulations with dynamical fermions to large quark masses. We would like to present a rather different view concerning the lattice data at large quark masses. In particular, we argue that like the behaviour as a function of N_c, lattice results as a function of quark mass offer extremely valuable new insights into the nature of QCD and especially into hadron structure.

To be a little more quantitative, the restriction to large quark masses in lattice simulations means typically 50 MeV or higher. Thus, in order to compare hadron properties calculated on the lattice one has to extrapolate as a function of quark mass (on top of all the other extrapolations, lattice spacing, lattice size, etc.) all the way to the physical light quark masses, around 5 or 6 MeV. Such extrapolations are complicated enormously by the fact that chiral symmetry is spontaneously broken in QCD. The mass of the pion, which is the Goldstone boson corresponding to this broken symmetry [2], behaves as:

$$m_\pi^2 \propto \bar{m}, \qquad \text{(with} \quad \bar{m} = m_u = m_d \neq 0), \tag{1}$$

as the quark mass, $\bar{m}$, moves away from zero – this is the Gell Mann-Oakes-Renner (GOR) relation. While Eq.(1) is, in principle, only guaranteed for quark masses, near zero, explicit lattice calculations show that it holds over an enormous range, as high as $m_\pi \sim 1$GeV. For convenience, rather than measuring the deviation from exact chiral symmetry using $\bar{m}$, which is scale dependent, we shall use m_π^2.

In terms of m_π, current lattice calculations are typically restricted to pion masses larger than 500 MeV, with some pioneering work reporting preliminary results as low as 310 MeV. In order to compare these results with experimental data on hadron properties it is necessary to extrapolate the calculations at large pion masses to the physical value. In doing so it is crucial to respect the constraints imposed by chiral symmetry in QCD. In particular, as we discuss below, the existence of Goldstone bosons necessarily leads to behaviour which is **non-analytic** in the quark mass.

The structure of this article is that we first explain the origin of the non-analyticity associated with Goldstone boson loops. We then explain, using the specific case of the nucleon mass, how this non-analytic structure has been incorporated into a new method for extrapolating hadron masses from the large values characteristic of lattice calculations to the physical region. The consequences of this for the sigma commutator are then explained. Next we turn to recent results for baryon electromagnetic properties. Finally we discuss the most recent investigations of the proton structure function, especially the importance of chiral symmetry in connecting existing calculations of lattice moments with data. We conclude with a summary of the promised insights into the nature of hadron structure within QCD that follow from all these investigations.

II. GOLDSTONE BOSON LOOPS AND NON-ANALYTICITY

For our purposes the primary significance of spontaneous chiral symmetry breaking in QCD is that there are contributions to hadron properties from loops involving the resulting Goldstone bosons. These loops have the unique property that they give rise to terms in an expansion of most hadronic properties as a function of quark mass which are not analytic. As a simple example we consider the nucleon mass. The most important chiral corrections to M_N come from the processes $N \to N\pi \to N$ (σ_{NN}) and $N \to \Delta\pi \to N$ ($\sigma_{N\Delta}$). (We will come to what it means to say these are the most important shortly.) We write $M_N = M_N^{\rm bare} + \sigma_{NN} + \sigma_{N\Delta}$. In the heavy baryon limit one has

$$\sigma_{NN} = -\frac{3g_A^2}{16\pi^2 f_\pi^2}\int_0^\infty dk \frac{k^4 u^2(k)}{k^2 + m_\pi^2}, \tag{2}$$

where g_A, f_π are strictly evaluated in the chiral limit. Here $u(k)$ is a natural high momentum cut-off which is the Fourier transform of the source of the pion field (e.g. in the cloudy bag model (CBM) it is $3j_1(kR)/kR$, with R the bag radius [3]). From the point of view of PCAC it is natural to identify $u(k)$ with the axial form factor of the nucleon, a dipole with mass parameter 1.02 ± 0.08GeV.

Regardless of the form chosen for the ultra-violet cut-off, one finds that σ_{NN} is a non-analytic function of the quark mass. The leading non-analytic (LNA) piece of σ_{NN} is independent of the form factor and gives

$$\sigma_{NN}^{LNA} = -\frac{3g_A^2}{32\pi f_\pi^2} m_\pi^3 \sim \bar{m}^{\frac{3}{2}}. \tag{3}$$

This has a branch point, as a function of $\bar{m}$, at $\bar{m} = 0$. Such terms can only arise from Goldstone boson loops.

A. Case Study: the Nucleon Mass

It is natural to ask how significant this non-analytic behaviour is in practice. If the pion mass is given in GeV, $\sigma_{NN}^{LNA} = -5.6 m_\pi^3$ and at the physical pion mass it is just –17 MeV. However, at only three times the physical pion mass, $m_\pi = 420$MeV, it is –460MeV – half the mass of the nucleon. If one's aim is to extract physical nucleon properties from lattice QCD calculations this is extremely important. The most sophisticated lattice calculations with dynamical fermions are only just becoming feasible at such low masses and to connect to the physical world one must extrapolate from $m_\pi \sim 500$MeV to $m_\pi = 140$MeV. Clearly one must have control of the chiral behaviour.

Figure 1 shows recent lattice calculations of M_N as a function of m_π^2 from CP-PACS and UKQCD [4]. The dashed line indicates a fit which naively respects the presence of a LNA term,

$$M_N = \alpha + \beta m_\pi^2 + \gamma m_\pi^3, \tag{4}$$

with α, β and γ fitted to the data. While this gives a very good fit to the data, the chiral coefficient γ is only -0.761, compared with the value -5.60 required by chiral symmetry. If one insists that γ be consistent with QCD the best fit one can obtain with this form is the dash-dot curve. This is clearly unacceptable.

An alternative suggested recently by Leinweber et al. [5], which also involves just three parameters, is to evaluate σ_{NN} and $\sigma_{N\Delta}$ with the same ultra-violet form factor, with mass parameter Λ, and to fit M_N as

$$M_N = \alpha + \beta m_\pi^2 + \sigma_{NN}(m_\pi, \Lambda) + \sigma_{N\Delta}(m_\pi, \Lambda). \tag{5}$$

Using a sharp cut-off ($u(k) = \theta(\Lambda - k)$) these authors were able to obtain analytic expressions for σ_{NN} and $\sigma_{N\Delta}$ which reveal the correct LNA behaviour – and next to leading (NLNA) in the $\Delta\pi$ case, $\sigma_{N\Delta}^{NLNA} \sim m_\pi^4 \ln m_\pi$.

FIGURES

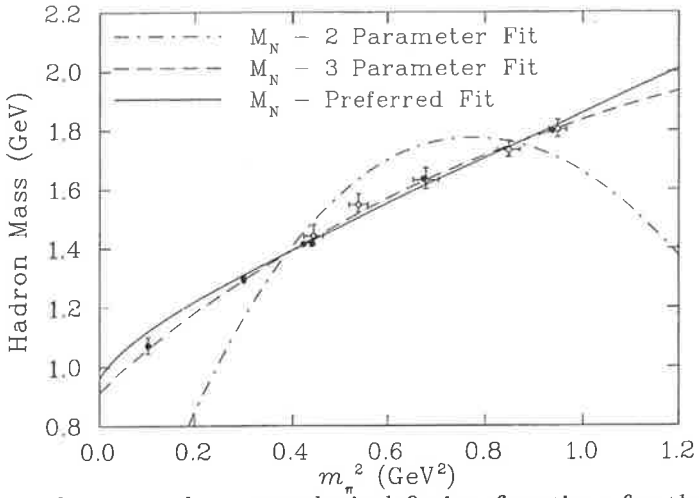

FIG. 1. A comparison between phenomenological fitting functions for the mass of the nucleon – from Ref. [5]. The two parameter fit corresponds to using Eq.(4) with γ set equal to the value known from χPT. The three parameter fit corresponds to letting γ vary as an unconstrained fit parameter. The solid line is the two parameter fit based on the functional form of Eq.(5).

These expressions also reveal a branch point at $m_\pi = M_\Delta - M_N$, which is important if one is extrapolating from large values of m_π to the physical value. The solid curve in Fig. 1 is a two parameter fit to the lattice data using Eq.(5), but fixing Λ at a value suggested by CBM simulations to be equivalent to the preferred 1 GeV dipole. A small increase in Λ is necessary to fit the lowest mass data point, at $m_\pi^2 \sim 0.1$ GeV^2, but clearly one can describe the data very well while preserving the exact LNA and NLNA behaviour of QCD.

B. Consequences for the Sigma Commutator

The analysis of the lattice data for M_N, incorporating the correct non-analytic behaviour, can yield interesting new information concerning the sigma commutator of the nucleon:

$$\sigma_N = \frac{1}{3}\langle N|[Q_{i5},[Q_{i5},H_{QCD}]]|N\rangle = \langle N|\bar{m}(\bar{u}u+\bar{d}d)|N\rangle. \tag{6}$$

This is a direct measure of chiral SU(2) symmetry breaking in QCD, and the widely accepted experimental value is 45 ± 8MeV [6]. (Although there are recent suggestions that it might be as much as 20 MeV larger [7].) Using the Feynman-Hellmann theorem one can also write

$$\sigma_N = \bar{m}\frac{\partial M_N}{\partial \bar{m}} = m_\pi^2 \frac{\partial M_N}{\partial m_\pi^2}. \tag{7}$$

Historically, lattice calculations have evaluated $< N|(\bar{u}u+\bar{d}d)|N >$ at large quark mass and extrapolated this scale dependent quantity to the "physical" quark mass, which had to be determined in a separate calculation. The latest result with dynamical fermions, $\sigma_N = 18 \pm 5$ MeV [8], illustrates how difficult this procedure is. On the other hand, if one has a fit to M_N as a function of m_π which is consistent with chiral symmetry, one can evaluate σ_N

directly using Eq.(7). Using Eq.(5) with a sharp cut-off yields $\sigma_N \sim 55$ MeV, while a dipole form gives $\sigma_N \sim 45$ MeV [9]. The residual model dependence can only be removed by more accurate lattice data at low m_π^2. Nevertheless, the result $\sigma_N \in (45, 55)$ MeV is in very good agreement with the data. In contrast, the simple cubic fit, with γ inconsistent with chiral constraints, gives $\sim$ 30 MeV. Until the experimental situation regarding σ_N improves, it is not possible to draw definite conclusions regarding the strangeness content of the nucleon. However, the fact that two-flavour QCD reproduces the current prefered value should certainly stimulate some thought and a lot of work.

III. ELECTROMAGNETIC FORM FACTORS

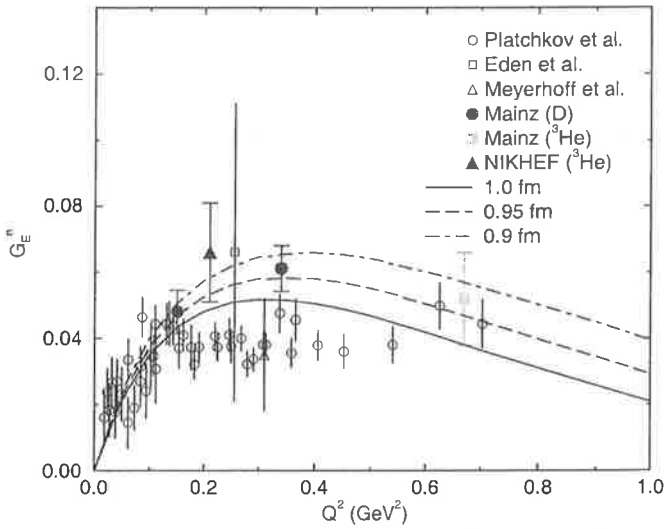

FIG. 2. Recent data for the neutron electric form factor in comparison with CBM calculations for a confining radius around 0.95fm – from Ref. [10].

It is a general consequence of quantum mechanics that the long-range charge structure of the proton comes from its π^+ cloud ($p \to n\pi^+$), while for the neutron it comes from its π^- cloud ($n \to p\pi^-$). However, it is not often realized that the LNA contribution to the nucleon charge radius goes like $\ln m_\pi$ and diverges as $\bar{m} \to 0$ [11]. This cannot be reproduced by a constituent quark model. Figure 2 shows the latest data from Mainz and NIKHEF for the neutron electric form factor, in comparison with CBM calculations for a confinement radius between 0.9 and 1.0 fm. The long-range π^- tail of the neutron plays a crucial role.

While there are only limited (and indeed quite old) lattice data for hadron charge radii, recent experimental progress in the determination of hyperon charge radii has led us to examine the extrapolation procedure for obtaining charge data from the lattice simulations [12]. Figure 3 shows the extrapolation of the lattice data [13] for the charge radius of the proton. Clearly the agreement with experiment is much better once the chiral log required by chiral symmetry is correctly included, than if, for example, one simply made a linear extrapolation in the quark mass (or m_π^2). Full details of the results for all the octet baryons may be found in Ref. [12].

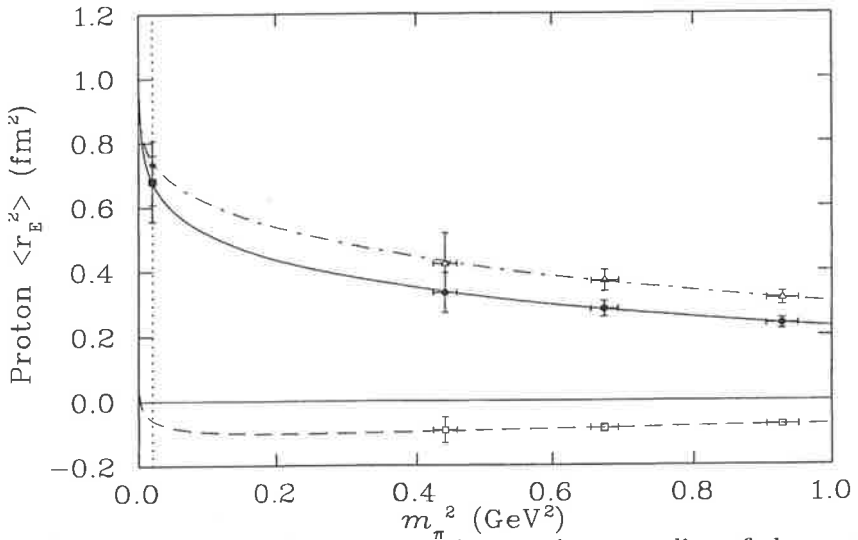

FIG. 3. Fits to lattice results for the squared electric charge radius of the proton – from Ref. [12]. Fits to the contributions from individual quark flavours are also shown: the u-quark sector results are indicated by open triangles and the d-quark sector results by open squares. Physical values predicted by the fits are indicated at the physical pion mass, where the full circle denotes the result predicted from the first extrapolation procedure and the full square denotes the baryon radius reconstructed from the individual quark flavor extrapolations. (N.B. The latter values are actually so close as to be indistinguishable on the graph.) The experimental value is denoted by an asterisk.

The situation for baryon magnetic moments is also very interesting. The LNA contribution in this case arises from the diagram where the photon couples to the pion loop. As this involves two pion propagators the expansion of the proton and neutron moments is:

$$\mu^{p(n)} = \mu_0^{p(n)} \mp \alpha m_\pi + \mathcal{O}(m_\pi^2). \tag{8}$$

Here $\mu_0^{p(n)}$ is the value in the chiral limit and the linear term in m_π is proportional to $\bar{m}^{\frac{1}{2}}$, a branch point at $\bar{m} = 0$. The coefficient of the LNA term is $\alpha = 4.4\mu_N \mathrm{GeV}^{-1}$. At the physical pion mass this LNA contribution is $0.6\mu_N$, which is almost a third of the neutron magnetic moment. *No constituent quark model can or should get better agreement with data than this.*

Just as for M_N, the chiral behaviour of $\mu^{p(n)}$ is vital to a correct extrapolation of lattice data. One can obtain a very satisfactory fit to some rather old data, which happens to be the best available, using the simple Padé [14]:

$$\mu^{p(n)} = \frac{\mu_0^{p(n)}}{1 \pm \frac{\alpha}{\mu_0^{p(n)}} m_\pi + \beta m_\pi^2} \tag{9}$$

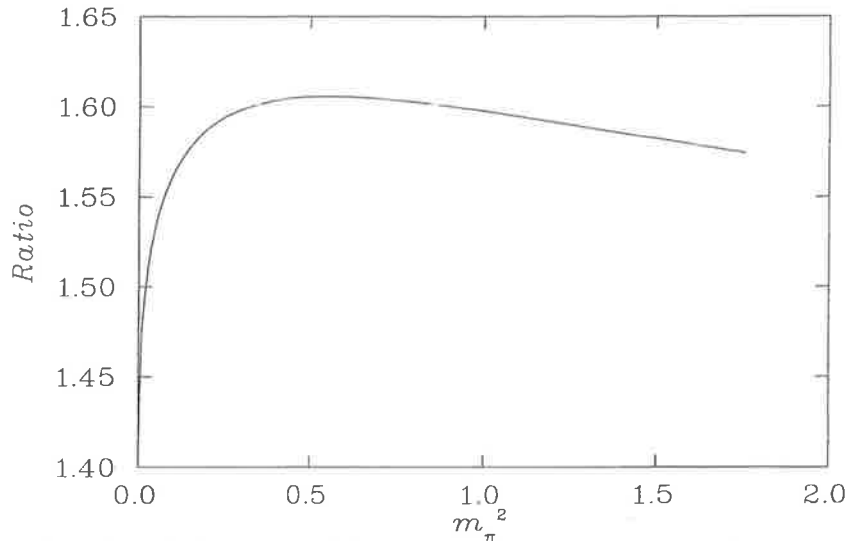

FIG. 4. Absolute value of the ratio of the proton to neutron magnetic moments as a function of m_π^2 obtained from the Padé approximants in Eq. (9). We stress that the behaviour as $m_\pi^2 \to 0$ is *model independent.*

The data can only determine two parameters and Eq.(9) has just two free parameters while guaranteeing the correct LNA behaviour as $m_\pi \to 0$ **and** the correct behaviour of heavy quark effective theory (HQET) at large m_π^2. The extrapolated values of μ^p and μ^n at the physical pion mass, $2.85 \pm 0.22\mu_N$ and $-1.90 \pm 0.15\mu_N$, respectively, are currently the best estimates from non-perturbative QCD [14]. For more details of this fit we refer to Ref. [14], while for the application of similar ideas to other members of the nucleon octet we refer to Ref. [15], and for the strangeness magnetic moment of the nucleon we refer to Ref. [16].

Incidentally, from the point of view of the naive quark model it is interesting to plot the ratio of the absolute values of the proton and neutron magnetic moments as a function of m_π^2. The agreement of the constituent quark result, namely 3/2, with the experimental value to within a few percent is usually taken as a major success. However, we see from Fig. 4 that it is in fact fortunate to obtain such close agreement [17]. We stress that the large slope of the ratio near $m_\pi^2 = 0$ is *model independent.*

IV. STRUCTURE FUNCTIONS

The parton distribution functions (PDFs) of the nucleon are light-cone correlation functions which, in the infinite momentum frame, are interpreted as probability distributions for finding specific partons (quarks, antiquarks, gluons) in the nucleon. They have been measured in a variety of high energy processes, ranging from deep-inelastic lepton scattering to Drell-Yan and massive vector boson production in hadron–hadron collisions. A wealth of experimental information now exists on spin-averaged PDFs, and an increasing amount of data is being accumulated on spin-dependent PDFs [18].

At high momentum transfer (Q^2) the dominant component of the PDFs are determined by non-perturbative matrix elements of certain "leading twist" operators. In principle these matrix elements, which correspond to moments of the measured structure functions, contain vital information about the non-perturbative structure of the target. An extensive phe-

nomenology has been developed over the years within model QCD studies, and in some cases remarkable predictions have been made from the insight gained into the non-perturbative structure of the nucleon. An example is the $\bar{d} - \bar{u}$ asymmetry, predicted [19] on the basis of the nucleon's pion cloud [20], which has been spectacularly confirmed in recent experiments at CERN and Fermilab [21]. Other predictions, such as asymmetries between strange and antistrange [22] and spin-dependent sea quark distributions, $\Delta\bar{u} - \Delta\bar{d}$, still await experimental confirmation. Note that none of these could be anticipated without insight into the non-perturbative structure of QCD.

Despite the phenomenological successes in correlating deep-inelastic and other high energy data with low energy hadron structure, the *ad hoc* nature of some of the assumptions made in deriving the low energy models from QCD leaves open a number of questions about the ability to reliably assign systematic errors to the model predictions. One approach in which structure functions can be calculated systematically from first principles, and which at the same time allows one to search for and identify the relevant low energy QCD degrees of freedom, is lattice QCD.

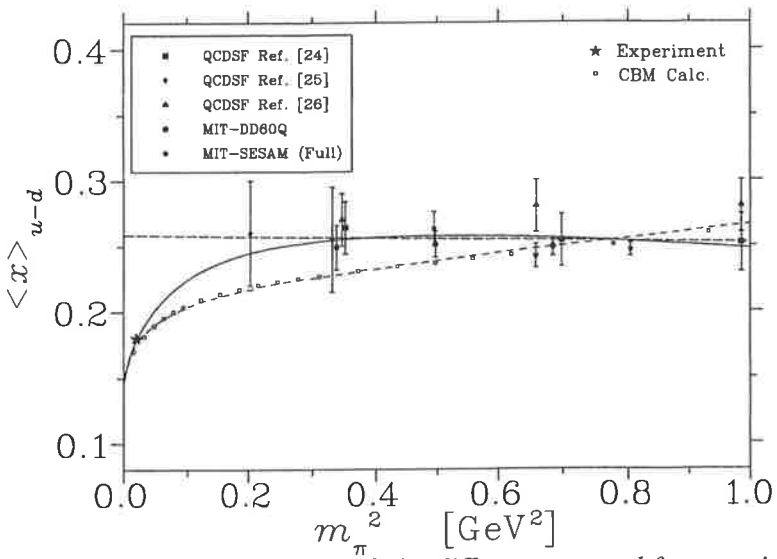

FIG. 5. First moment of the difference $u - d$ from various lattice QCD simulations (QCDSF [24–26] and MIT [27]), at a scale $Q^2 = 4$ GeV^2. Calculations from the CBM are shown as small squares. The dashed curve is a simple fit which is linear in m_π^2, while the solid curve incorporates the constraints of chiral symmetry, as in Eq.(10).

Early calculations of structure function moments within lattice QCD were performed by Martinelli and Sachrajda [23]. However, the most comprehensive analysis has been performed by the QCDSF Collaboration [24–26] – albeit within quenched QCD. Recently the MIT group has performed the first full (unquenched) QCD calculations of non-singlet moments [27]. The moments from the full QCD simulations are very similar to those from the quenched calculations. This is consistent with the suggestions of chiral quark models, like the CBM, that in the mass region currently accessible quark loops are suppressed.

As for the other nucleon properties discussed above, we propose to extraplate the lattice data to the physical pion mass using a formula which is compatible with the LNA structure

of the PDFs. This behaviour was derived recently, with the result that the LNA behaviour involved a term in $m_\pi^2 \ln m_\pi$ [28]. For an initial investigation we concentrate on the non-singlet combination of PDFs, $u-d$, in which "disconnected" quark loops cancel. Calculations based on the CBM (which incorporate the LNA chiral structure just discussed) actually produce quite a reasonable description of the behaviour of the moments of the PDFs as a function of quark mass, as shown in Fig. 5 (open squares). More important from the phenomenological point of view, the CBM calculations (for the n'th moment of the PDFs) can be fit with the simple expansion in m_π:

$$\langle x_u^n - x_d^n \rangle = a_n + b_n m_\pi^2 + a_n c_{\rm LNA} m_\pi^2 \ln\left(\frac{m_\pi^2}{m_\pi^2 + \mu^2}\right) \ , \tag{10}$$

where $c_{\rm LNA}$ is model independent.

The scale μ in Eq.(10) is effectively the scale at which the rapid, chiral variation at low m_π turns off. The best fit to the lattice data is obtained with a value $\mu \sim 0.4 - 0.5$ GeV – a very similar scale to that found, for example, for the magnetic moments. Clearly Eq.(10) gives a very good description of the lattice data for the first moment of the non-singlet distribution $d - u$. Taking into account the rapid chiral variation as $m_\pi^2 \to 0$ there is also quite good agreement between the extrapolated value of the first moment and the experimentally determined moment. A similar result holds for the second and third moments too [29].

V. CONCLUSION

In the light of the numerous examples presented in this brief review, it should be evident that the study of hadron properties as a function of quark mass shows a clear pattern:

- In the region of quark masses $\bar{m} > 60$ MeV or so (m_π greater than typically 400-500 MeV) hadron properties are smooth, slowly varying functions of something like a constituent quark mass, $M \sim M_0 + c\bar{m}$ (with $c \sim 1$).
- Indeed, $M_N \sim 3M, M_{\rho,\omega} \sim 2M$ and magnetic moments behave like $1/M$.
- As $\bar{m}$ decreases below 60 MeV or so, chiral symmetry leads to rapid, non-analytic variation, with $\delta M_N \sim \bar{m}^{3/2}, \delta\mu_H \sim \bar{m}^{1/2}$ and $\delta < r^2 >_{\rm ch} \sim \ln \bar{m}$.
- Chiral quark models like the cloudy bag provide a natural explanation of this transition. The scale is basically set by the inverse size of the pion source – the inverse of the bag radius in the bag model.

These are remarkable results that will have profound consequences for our further exploration of hadron structure within QCD as well as the analysis of the vast amount of data now being taken concerning unstable resonances. In terms of immediate results for the structure of the nucleon, we note that the careful incorporation of the correct chiral behaviour of QCD into the extrapolation of its properties calculated on the lattice has produced:

- The best values of the proton and neutron magnetic moments from QCD.

- The best value of the sigma commutator.
- Improved values for the charge radii of the baryon octet.
- Improved values for the magnetic moments of the hyperons.
- Good agreement between the extrapolated moments of the non-singlet distribution $u - d$ and the experimentally measured moments.

In addition, although we did not have time to discuss it, this approach has led to the best current value for the strangeness magnetic moment of the proton from lattice QCD [16].

Clearly, while much has been achieved, even more remains to be done. It is vital that lattice calculations with dynamical fermions are pushed to the lowest possible quark masses, taking advantage of developments of improved actions and so on. It is also vital to further develop our understanding of the physics of chiral extrapolation by comparison with these new calculations, by looking at new applications and by further comparison with chiral models.

Acknowledgements

We would like to thank E. Hackett-Jones, J. Negele, K. Tsushima, A. Williams and R. Young for helpful discussions of the matters discussed here. This work was supported by the Australian Research Council and the University of Adelaide.

REFERENCES

[1] T. D. Cohen, hep-ph/9512275.

[2] H. Pagels, Phys. Rept. **16**, 219 (1975).

[3] S. Theberge, A. W. Thomas and G. A. Miller, Phys. Rev. **D22** (1980) 2838; A. W. Thomas, Adv. Nucl. Phys. **13** (1984) 1.

[4] S. Aoki *et al.* [CP-PACS], Phys. Rev. **D60** (1999) 114508 ; C. R. Allton *et al.* [UKQCD], Phys. Rev. **D60** (1999) 034507 .

[5] D. B. Leinweber *et al.*, Phys. Rev. **D61** (2000) 074502 [hep-lat/9906027].

[6] J. Gasser, H. Leutwyler and M. E. Sainio, Phys. Lett. **B253**, 252 (1991).

[7] M. Knecht, `hep-ph/9912443`.

[8] **SESAM** Collaboration, S. Gusken *et al.*, *Phys. Rev.* **D59**, 054504 (1999).

[9] D. B. Leinweber *et al.*, Phys. Lett. **B482** (2000) 109 [hep-lat/0001007].

[10] D. H. Lu *et al.*, in Proc. Int. Conf. Few Body Problems (Taipei, 2000), to appear in Nucl. Phys. **A**; D. H. Lu *et al.*, Phys. Rev. **C60** (1999) 068201 [nucl-th/9807074].

[11] D. B. Leinweber and T. D. Cohen, Phys. Rev. **D47** (1993) 2147 [hep-lat/9211058].

[12] E. J. Hackett-Jones, D. B. Leinweber and A. W. Thomas, Phys. Lett. B **494**, 89 (2000) [hep-lat/0008018].

[13] D.B. Leinweber, R.M. Woloshyn and T. Draper, Phys. Rev. **D43** (1991) 1659.

[14] D. B. Leinweber *et al.*, Phys. Rev. **D60** (1999) 034014 [hep-lat/9810005].

[15] E. J. Hackett-Jones, D. B. Leinweber and A. W. Thomas, Phys. Lett. B **489**, 143 (2000) [hep-lat/0004006].

[16] D. B. Leinweber and A. W. Thomas, Phys. Rev. D **62**, 074505 (2000) [hep-lat/9912052].

[17] D. B. Leinweber, A. W. Thomas and R. D. Young, hep-ph/0101211.

[18] M. Erdmann, Talk given at 8th International Workshop on Deep Inelastic Scattering and QCD (DIS 2000), Liverpool, England, 25-30 Apr. 2000, hep-ex/0009009; E.W. Hughes and R. Voss, Ann. Rev. Nucl. Part. Sci. 49, 303 (1999).

[19] A. W. Thomas, Phys. Lett. B **126**, 97 (1983).

[20] E.M. Henley and G.A. Miller, Phys. Lett. B 251, 453 (1990); A.I. Signal, A.W. Schreiber and A.W. Thomas, Mod. Phys. Lett. A 6, 271 (1991); W. Melnitchouk, A.W. Thomas and A.I. Signal, Z. Phys. A 340, 85 (1991); S. Kumano, Phys. Rev. D43, 3067 (1991); S. Kumano and J.T. Londergan, Phys. Rev. D 44, 717 (1991); W.-Y.P. Hwang, J. Speth and G.E. Brown, Z. Phys. A339, 383 (1991).

[21] P. Amaudraz et al., Phys. Rev. Lett. 66, 2712 (1991). A. Baldit et al., Phys. Lett. B 332, 244 (1994). E.A. Hawker et al., Phys. Rev. Lett. 80, 3715 (1998).

[22] A.I. Signal and A.W. Thomas, Phys. Lett. B 191, 206 (1987); X. Ji and J. Tang, Phys. Lett. B362, 182 (1995); S.J. Brodsky and B.-Q. Ma, Phys. Lett. B 381,317 (1996); W. Melnitchouk and M. Malheiro, Phys. Rev. C 55, 431 (1997).

[23] G. Martinelli and C.T. Sachrajda, Phys. Lett. B 196, 184 (1987); Nucl. Phys. B306, 865 (1988).

[24] M. Göckeler, R. Horsley, E. M. Ilgenfritz, H. Perlt, P. Rakow, G. Schierholz and A. Schiller, Phys. Rev. **D 53**, 2317 (1996).

[25] M. Göckeler, R. Horsley, E. M. Ilgenfritz, H. Perlt, P. Rakow, G. Schierholz and A. Schiller, Nucl. Phys. Proc. Suppl. 53, 81 (1997).

[26] C. Best *et al.*, hep-ph/9706502.

[27] D. Dolgov *et al.*, hep-lat/0011010.

[28] A.W. Thomas, W. Melnitchouk and F.M. Steffens, Phys. Rev. Lett. 85, 2892 (2000).
[29] W. Detmold, W. Melnitchouk, J. W. Negele, D. B. Renner and A. W. Thomas, hep-lat/0103006.

ADP-00-24/T407

The Sigma Commutator from Lattice QCD

Stewart V. Wright, Derek B. Leinweber and Anthony W. Thomas[a]

[a]Department of Physics and Mathematical Physics
and Special Research Centre for the Subatomic Structure of Matter,
University of Adelaide, Adelaide 5005, Australia

As a direct source of information on chiral symmetry breaking within QCD, the sigma commutator is of considerable importance. Since hadron structure is a non-perturbative problem, numerical calculations on a space-time lattice are currently the only rigorous approach. With recent advances in the calculation of hadron masses within full QCD, it is of interest to see whether the sigma commutator can be calculated directly from the dependence of the nucleon mass on the input quark mass. We show that, provided the correct chiral behaviour of QCD is respected in the extrapolation to realistic quark masses, one can indeed obtain a fairly reliable determination of the sigma commutator using present lattice data. For two-flavour dynamical fermion QCD the sigma commutator lies between 45 and 55 MeV based on recent data from CP-PACS and UKQCD.

1. WHAT IS THE SIGMA COMMUTATOR ?

In the quest to understand hadron structure within QCD, small violations of fundamental symmetries play a vital role. The sigma commutator, σ_N:

$$\sigma_N = \frac{1}{3}\langle N|\,[Q_{i5},[Q_{i5},\mathcal{H}]]\,|N\rangle = \bar{m}\,\langle N|\,\bar{u}u+\bar{d}d\,|N\rangle = \bar{m}\frac{\partial M_N}{\partial \bar{m}} \tag{1}$$

(with Q_{i5} the two-flavour (i=1, 2, 3) axial charge) is an extremely important example of such a symmetry.

2. PREVIOUS ATTEMPTS

σ_N cannot be accessed directly by experimental measurements. However, one can infer from world data a value of 45 ± 8 MeV [1]. This result has been under some scrutiny recently due to the progress in new determinations of the pion-nucleon scattering lengths [2,3] and new phase shift analyses [4,5]. The full lattice QCD calculations upon which our work is based involve only two active flavours, the heavier third flavour is approximated by a renormalisation of the strong coupling constant. As a guide, recent work suggests that the best value of σ_N may be 8 to 26 MeV larger than the value quoted above [6].

One can notionally use QCD to directly calculate the value of σ_N, but in practice the calculation has proven to be difficult. Early attempts [7] to extract σ_N from the quark mass dependence of the nucleon mass (using Eq.(1)) in quenched QCD with naive

extrapolations produced values in the range 15 to 25 MeV. Attention subsequently turned to determining σ_N by calculating the scalar matrix element of the nucleon $\langle N|\bar{u}u+\bar{d}d|N\rangle$. There it was discovered that the sea-quark loops make a dominant contribution to σ_N [8,9]. These works, based on quenched QCD simulations found values in the 40 to 60 MeV range, which are more compatible with the experimental values quoted earlier.

On the other hand, the most recent estimate of σ_N, and the only one based on a two-flavour, dynamical-fermion lattice QCD calculation, comes from the SESAM collaboration. They obtain a value of 18 ± 5 MeV [10], through a direct calculation of the scalar matrix element $\langle N|\bar{u}u + \bar{d}d|N\rangle$ and the quark mass $\bar{m}$.

The fact that neither $\langle N|\bar{u}u + \bar{d}d|N\rangle$, nor $\bar{m}$ is renormalisation group invariant introduces a major difficulty in calculating the sigma commutator in this approach. One must reconstruct the scale invariant result from the product of the scale dependent matrix element and the scale dependent quark masses. The latter are extremely difficult to determine precisely and are the chief sources of uncertainty. Furthermore, since lattice calculations are made at quite large pion masses, typically above 500 or 600 MeV, one needs to extrapolate, in the pion mass down to the physical value at 140 MeV. An important innovation adopted by Dong *et al.* was to extrapolate $\langle N|\bar{u}u + \bar{d}d|N\rangle$ using a form motivated by chiral symmetry, namely $a + b\bar{m}^{\frac{1}{2}}$. Regrettably, the value of b used was *not* constrained by chiral symmetry and higher order terms of the chiral expansion were not considered. Furthermore, since the work was based on a quenched calculation, the chiral behaviour implicit in the lattice results involves incorrect chiral physics [11].

3. THE CURRENT CALCULATION

Our recent work [12] was motivated by the improvements in computing power, together with the development of improved actions [13], which have led to accurate calculations of the mass of the nucleon within *full QCD* (for two flavours) as a function of $\bar{m}$ down to $m_\pi \sim 500$ MeV. (Since m_π^2 is proportional to $\bar{m}$ over the range studied we choose to display all results as a function of m_π^2.) We showed that provided that one has control over the extrapolation of this lattice data to the physical pion mass, one can calculate σ_N from $\sigma_N = m_\pi^2 \partial M_N / \partial m_\pi^2$ (which is equivalent to Eq. (1) where $\bar{m}$ was used) at $m_\pi = 140$ MeV. This approach has the important advantage that one *only* needs to work with renormalization group invariant quantities.

Chiral perturbation theory (χPT) predicts that the leading non-analytic (LNA) correction to the self energy contribution to the nucleon mass is proportional to m_π^3 (or $\bar{m}^{3/2}$). It can be seen in Fig. 2 that the preliminary point from CP-PACS [14] at $m_\pi^2 \sim 0.1$ GeV^2 does indeed suggest some curvature in this low mass region. These observations led the CP-PACS group to extrapolate their data with the simple, phenomenological form:

$$M_N = \tilde{\alpha} + \tilde{\beta} m_\pi^2 + \tilde{\gamma} m_\pi^3, \tag{2}$$

rather than a naive linear form ($\tilde{\gamma} \equiv 0$), as shown in Fig. 1. The corresponding fit to the combined data set, using Eq. (2), is shown as the short-dashed curve in Figs. 1 and 2. We found that this fit gives $\sigma_N = 29.7$ MeV. The difficulty with this purely phenomenological analysis was discussed in Ref. [16]. The problem is that a derivative is required when evaluating σ_N and the value of $\tilde{\gamma}$ found in the fit (-0.761 GeV^{-2}) is almost an order of

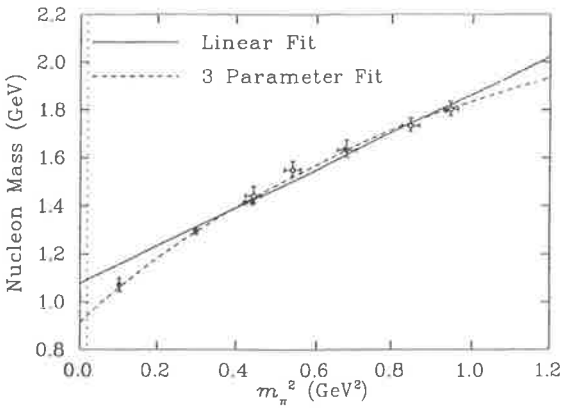

Figure 1. Nucleon mass versus m_π^2. The solid data points are CP-PACS results [14], whilst the open points are UKQCD data [15]. Both curves are fits using Eq. (2). The solid curve has $\tilde{\gamma} \equiv 0$, whilst the short-dashed curve has $\tilde{\gamma}$ unconstrained. The vertical line indicates the physical pion mass.

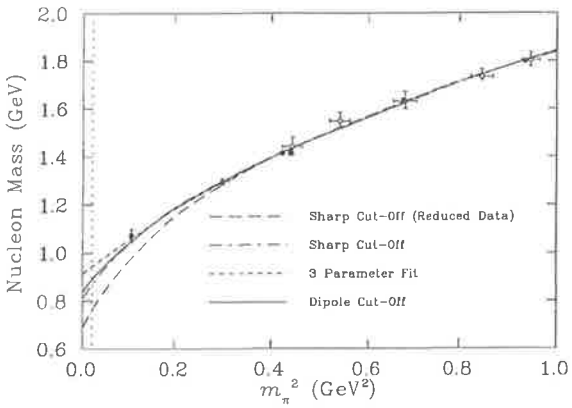

Figure 2. Data as labelled in Fig. 1. The solid curve is a fit to Eq. (3) with a dipole form factor, the dashed curve is the same fit using a sharp cut-off form factor. The long-dash curve is a fit to Eq. (3) *excluding* the lowest data point.

magnitude smaller than the model independent LNA coefficient, $\gamma^{\rm LNA} = -5.60$ GeV^{-2}, indicated by χPT.

Recently, an alternative approach was suggested in Ref. [16]. There it was realised that the pion loop diagrams shown in Fig. 3 yield not only the most important non-analytic structure, but also give rise to the most significant variation in the nucleon mass as $m_\pi \to 0$. This leads to the following extrapolation function for M_N:

$$M_N = \alpha + \beta m_\pi^2 + \sigma_{NN}(m_\pi, \Lambda) + \sigma_{N\Delta}(m_\pi, \Lambda)\,, \tag{3}$$

where σ_{NN} and $\sigma_{N\Delta}$ are the self-energy contributions of Figs. 3(a) and 3(b), respectively, using a cut-off in momentum controlled by Λ. The full analytic expressions for σ_{NN} and $\sigma_{N\Delta}$ are given in Ref. [16]. For our purposes it suffices that they have precisely the correct LNA and next-to-leading non-analytic behaviour required by chiral perturbation theory as $m_\pi \to 0$. In addition, $\sigma_{N\Delta}$ contains the correct, square root branch point

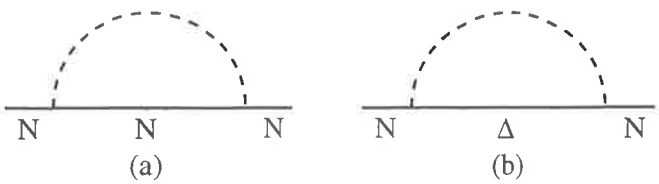

Figure 3. One-loop pion induced self energy of the nucleon.

($\sim [m_\pi^2 - (M_\Delta - M_N)^2]^{\frac{3}{2}}$) at the $\Delta - N$ mass difference, which is essential for extrapolations from above the $\Delta - N\pi$ threshold.

Fitting Eq. (3) to the data, including the point near 0.1 GeV^2, gives the dot-dash curve in Fig. 2. The corresponding value of σ_N is 54.6 MeV and the physical nucleon mass is 870 MeV. Omitting the lowest data point from the fit yields the long-dash curve in Fig. 2 with $\sigma_N = 65.8$ MeV, demonstrating the need for lattice simulations of QCD at light quark masses.

4. CONCLUSION

The importance of the inclusion of the correct chiral behaviour is clearly seen by the fact that it increases the value of the sigma commutator from the 30 MeV of the unconstrained cubic fit to around 50 MeV. Nevertheless, it is a remarkable result that the present lattice data for two-flavour dynamical-fermion QCD, yields a stable [12] and accurate answer for the sigma commutator, an answer which is already within the range of the experimental values.

This work was supported by the Australian Research Council.

REFERENCES

1. J. Gasser, H. Leutwyler and M. E. Sainio, *Phys. Lett.* **B253**, 252 (1991).
2. D. Sigg *et al.*, *Nucl. Phys.* **A609** (1996) 269;
   D. Chatellard *et al.*, *Nucl. Phys.* **A625**, 855 (1997).
3. T. E. Ericson, B. Loiseau and A. W. Thomas, Nucl. Phys. **A663-664**, 541 (2000), `hep-ph/9907433`.
4. M. M. Pavan, R. A. Arndt, I. I. Strakovsky and R. L. Workman, `nucl-th/9912034`.
5. D. V. Bugg, PiN Newsletter **15** (1999) 319.
6. M. Knecht, `hep-ph/9912443`.
7. See for example, S. Cabasino *et al.*, *Nucl. Phys. B* (Proc. Suppl.) **20**, 399 (1991).
8. S. J. Dong, J. F. Lagae and K. F. Liu, *Phys. Rev.* **D54**, 5496 (1996).
9. M. Fukugita, Y. Kuramashi, M. Okawa and A. Ukawa, *Phys. Rev.* **D51**, 5319 (1995).
10. **SESAM** Collaboration, S. Gusken *et al.*, *Phys. Rev.* **D59**, 054504 (1999).
11. S.R. Sharpe, *Phys. Rev.* **D56**, 7052 (1997).
    J.N. Labrenz and S.R. Sharpe, *Phys. Rev.* **D54**, 4595 (1996).
12. D. B. Leinweber, A. W. Thomas and S. V. Wright, hep-lat/0001007. To appear in *Phys. Lett.* **B**.
13. B. Sheikholeslami and R. Wohlert, *Nucl. Phys.* **B259** (1985) 609;
    M. Alford, W. Dimm, P. Lepage, *Phys. Lett.* **B361**, 87 (1995);
    P. Hasenfratz, *Nucl. Phys.* (Proc. Suppl.) **B63**, 53 (1998).
14. **CP-PACS** Collaboration, S. Aoki *et. al.*, *Phys. Rev.* **D60**, 114508 (1999).
15. **UKQCD** Collaboration, C. R. Allton *et. al.*, Phys. Rev. **D60**, 034507 (1999).
16. D. B. Leinweber, A. W. Thomas, K. Tsushima, and S. V. Wright, Phys. Rev. **D61**, 074502 (2000), `hep-lat/9906027`.

ADP-00-01/T390

Lattice QCD Calculations of the Sigma Commutator

D. B. Leinweber*, A. W. Thomas†, and S. V. Wright‡
Department of Physics and Mathematical Physics
and Special Research Centre for the Subatomic Structure of Matter,
University of Adelaide, Adelaide 5005, Australia

Abstract

As a direct source of information on chiral symmetry breaking within QCD, the sigma commutator is of considerable importance. With recent advances in the calculation of hadron masses within full QCD it is of interest to see whether the sigma commutator can be calculated directly from the dependence of the nucleon mass on the input quark mass. We show that provided the correct chiral behaviour of QCD is respected in the extrapolation to realistic quark masses one can indeed obtain a fairly reliable determination of the sigma commutator using present lattice data. Within two-flavour, dynamical-fermion QCD the value obtained lies in the range 45 to 55 MeV.

In the quest to understand hadron structure within QCD, small violations of fundamental symmetries play a vital role. The sigma commutator, σ_N:

$$\sigma_N = \frac{1}{3} \langle N | [Q_{i5}, [Q_{i5}, \mathcal{H}]] | N \rangle \tag{1}$$

(with Q_{i5} the two-flavour (i=1, 2, 3) axial charge) is an extremely important example. Because Q_{i5} commutes with the QCD Hamiltonian in the chiral SU(2) limit, the effect of the double commutator is to pick out the light quark mass term from $\mathcal{H}$:

$$\sigma_N = \langle N | \left(m_u \bar{u}u + m_d \bar{d}d \right) | N \rangle \tag{2}$$

Neglecting the very small effect of the $u-d$ mass difference we can write Eq. (2) in the form

$$\sigma_N = \langle N | \bar{m} \left(\bar{u}u + \bar{d}d \right) | N \rangle \tag{3}$$

$$= \bar{m} \frac{\partial M_N}{\partial \bar{m}} \tag{4}$$

*dleinweb@physics.adelaide.edu.au
†athomas@physics.adelaide.edu.au
‡swright@physics.adelaide.edu.au

with $\bar{m} = (m_u + m_d)/2$. Equation (4) follows from the Feynman-Hellman theorem [3].

While there is no direct experimental measurement of σ_N, the value inferred from world data has been 45 ± 8 MeV [4] for some time. Recently there has been considerable interest in this value because of progress in the determination of the pion-nucleon scattering lengths [5, 6] and new phase shift analyses [7, 8]. For an excellent summary of the sources of the proposed variations and the disagreements between various investigators we refer to the excellent review of Kneckt [9]. For our purposes the experimental value is of limited interest as the full lattice QCD calculations upon which our work is based involve only two active flavours. Nevertheless, as a guide, the current work suggests that the best value of σ_N may be between 8 and 26 MeV larger than the value quoted above [9].

Numerous calculations of σ_N have been made within QCD motivated models [10] and there has been considerable work within the framework of chiral perturbation theory [11]. However, direct calculations of σ_N within QCD itself have proven to be difficult. Early attempts [12] to extract σ_N from the quark mass dependence of the nucleon mass in quenched QCD (using Eq.(4)) produced values in the range 15 to 25 MeV. Attention subsequently turned to determining σ_N by calculating the scalar matrix element of the nucleon $\langle N|\bar{u}u + \bar{d}d|N\rangle$. There it was discovered that the sea quark loops make a dominant contribution to σ_N [14, 15]. These works, based on quenched QCD simulation, found values in the 40 to 60 MeV range, which are more compatible with the experimental values quoted earlier.

On the other hand, the most recent estimate of σ_N, and the only one based on a two-flavour, dynamical-fermion lattice QCD calculation, comes from the SESAM collaboration. They obtain a value of 18 ± 5 MeV [13], through a direct calculation of the scalar matrix element $\langle N|\bar{u}u + \bar{d}d|N\rangle$. The discrepancy from the quenched results of Refs. [14, 15] is not so much an unquenching effect in the scalar matrix element but rather a significant suppression of the quark mass in going from quenched to full QCD. The difficulty in all approaches which evaluate $\langle N|\bar{u}u + \bar{d}d|N\rangle$ is that neither it nor $\bar{m}$ is renormalization group invariant. One must reconstruct the scale invariant result from the product of the scale dependent matrix element and the scale dependent quark masses. The latter are extremely difficult to determine precisely and are the chief source of uncertainty in this approach.

An additional difficulty in extracting σ_N from lattice studies is the need to extrapolate from quite large pion masses, typically above 500 or 600 MeV. An important innovation adopted by Dong *et al.*, but not by the SESAM collaboration, was to extrapolate the computed values of $\langle N|\bar{u}u + \bar{d}d|N\rangle$ using a form motivated by chiral symmetry, namely $a + b\bar{m}^{\frac{1}{2}}$. On the other hand, the value of b used was *not* constrained by chiral symmetry and higher order terms of the chiral expansion were not considered. Furthermore, since the work was based on a quenched calculation, the chiral behaviour implicit in the lattice results involves incorrect chiral coefficients [16].

Our work is motivated by recent, dramatic improvements in computing power which, together with the development of improved actions [17], mean that we now have accurate calculations of the mass of the nucleon within *full QCD* (for two flavours) as a function of $\bar{m}$ down to $m_\pi \sim 500$ MeV. (Since m_π^2 is proportional to $\bar{m}$ over the range studied we choose to display all results as a function of m_π^2.) In addition, CP-PACS has recently published a result at $m_\pi \sim 300$ MeV , albeit with somewhat large errors. Provided that one has control over the extrapolation of this lattice data to the physical pion mass, $m_\pi \equiv \mu = 140$ MeV, one can calculate σ_N by evaluating Eq. (4) at the physical pion mass. Note that this approach has the important advantage over the calculation of the scalar density that one *only* needs to work with renormalization group invariant quantities. We therefore turn to a consideration of the method of extrapolation.

The lattice data for the nucleon mass calculated by UKQCD [1] and CP-PACS [2] is shown in Fig. 1. Both groups cite a 10% uncertainty in setting the lattice scale, so we have scaled the former down and the latter up by 5% so that the data sets are consistent. Over almost the entire range of m_π^2, the data shows a dependence on quark mass that is essentially linear. However, the preliminary point at $m_\pi^2 \sim 0.1$ GeV^2 suggests some curvature in the low mass region. This is indeed expected on the basis of chiral symmetry with the leading non-analytic (LNA) correction (in terms of $\bar{m}$) being proportional to m_π^3 ($\bar{m}^{3/2}$):

$$\delta M_N^{\rm LNA} = \gamma^{\rm LNA} m_\pi^3 \,, \;\; \gamma^{\rm LNA} = \frac{-3g_A^2}{32\pi f_\pi^2} \,. \tag{5}$$

These observations led the CP-PACS group to extrapolate their data with the simple, phenomenological form:

$$M_N = \tilde{\alpha} + \tilde{\beta} m_\pi^2 + \tilde{\gamma} m_\pi^3 \,. \tag{6}$$

The corresponding fit to the combined data set, using Eq. (6), is shown as the short-dashed curve in Fig. 1 and the parameters $(\tilde{\alpha}, \tilde{\beta}, \tilde{\gamma}) = (0.912, 1.69, -0.761)$ (the units are appropriate powers of GeV). This yields a value for the sigma commutator, $\sigma_N^{(p)} = 29.7$ MeV, where the superscript stands for "phenomenological".

The difficulty with this purely phenomenological analysis was discussed in Ref. [18]. That is, the value of $\tilde{\gamma} = -0.761$ is almost an order of magnitude smaller than the model independent LNA term, $\gamma^{\rm LNA} = -5.60$ GeV^{-2}. Clearly this presents some concern when evaluating σ_N, because of the derivative required. An alternative approach to this problem was recently suggested by Leinweber et al. [18]. They realised that the pion loop diagrams, Fig. 2(a) and 2(b) not only yield the most important non-analytic structure in the expression for the nucleon mass, but amongst all the possible meson baryon states which contribute to the nucleon mass within QCD, they alone give rise to a significant variation of the nucleon mass as $m_\pi \to 0$. In Ref. [18] it was suggested that one should extrapolate M_N as a function of quark mass using:

$$M_N = \alpha + \beta m_\pi^2 + \sigma_{NN}(m_\pi, \Lambda) + \sigma_{N\Delta}(m_\pi, \Lambda) \,, \tag{7}$$

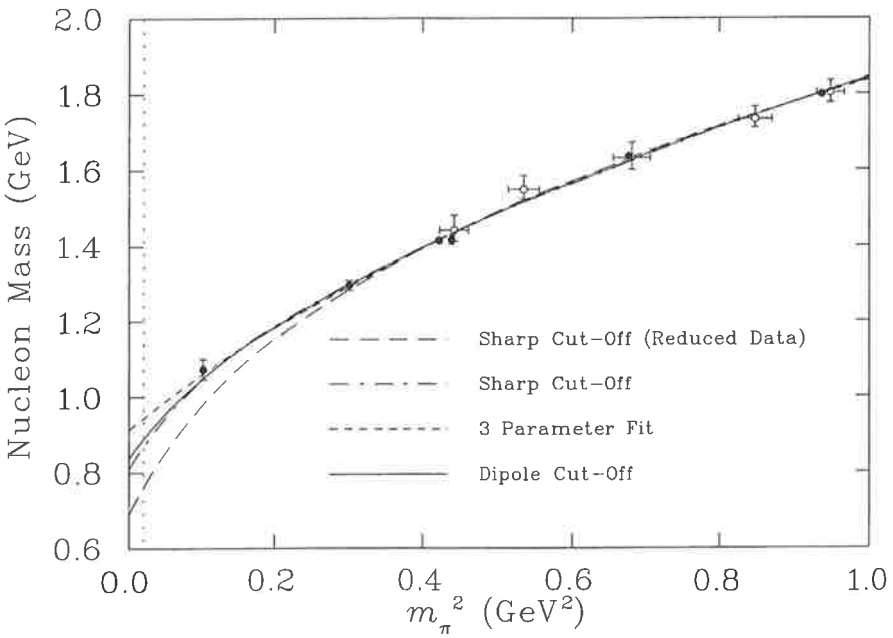

Figure 1: Nucleon mass calculated by CP-PACS (solid points) and UKQCD (open points), as a function of m_π^2, both are scaled by 5% to improve consistency. The solid curve is a fit to Eq. (7) with a 1.225 GeV dipole form factor, while the dashed curve is the same fit using a sharp cut-off form factor (θ-function). The short-dash curve is a fit to Eq. (6), and the long-dash curve is a fit to Eq. (7) *excluding* the lowest data point. The vertical line indicates the physical pion mass.

where σ_{NN} and $\sigma_{N\Delta}$ are the self-energy contributions of Figs. 2(a) and 2(b), respectively, using a sharp cut-off in momentum, $\theta(\Lambda - k)$. The full analytical expressions for σ_{NN} and $\sigma_{N\Delta}$ are given in Ref. [18]. For our purposes it suffices that they have precisely the correct LNA and next-to-leading non-analytic behaviour required by chiral perturbation theory as $m_\pi \to 0$. In addition, $\sigma_{N\Delta}$ contains the correct, square root branch point ($\sim [m_\pi^2 - (M_\Delta - M_N)^2]^{\frac{3}{2}}$) at the $\Delta - N$ threshold, which is essential for extrapolations from above the $\Delta - N$ threshold.

Fitting Eq. (7) to the data, including the point near 0.1 GeV^2, gives the dot-dash curve in Fig. 1 ($(\alpha, \beta, \Lambda) = (1.42, 0.564, 0.661)$). The corresponding value of σ_N is 54.6 MeV and the physical nucleon mass is 870 MeV. Omitting the lowest data point from the fit yields the long-dash curve in Fig. 1 ($(\alpha, \beta, \Lambda) = (1.76, 0.386, 0.789)$) with $\sigma_N = 65.8$ MeV. Clearly the curvature associated with the chiral corrections at low quark mass is extremely important in the evaluation of σ_N.

In order to estimate the error in the extracted value of σ_N we would need to have the full data set on a configuration by configuration basis. As this is not

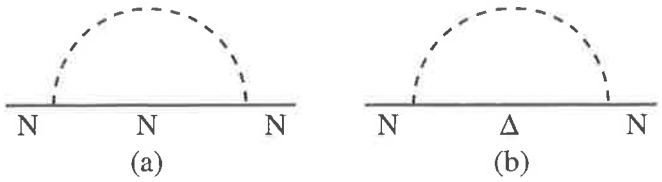

Figure 2: One-loop pion induced self energy of the nucleon.

Scaling		σ_N		
CP-PACS	UKQCD	Dipole	Sharp	Cubic
5	-5	47.2 ± 1.8	54.6 ± 2.0	29.7
10	0	48.1 ± 1.9	54.9 ± 2.0	28.6
0	-10	45.4 ± 1.9	54.3 ± 1.9	31.0

Table 1: Sigma Commutator Values. The **Dipole** and **Sharp** results were calculated with our preferred form of $\alpha + \beta m_\pi^2 + \sigma_{NN}(\Lambda, m_\pi) + \sigma_{N\Delta}(\Lambda, m_\pi)$ with either a dipole form factor for the $N\pi$ vertex or a θ-function. The values of dipole parameter (Λ_D) were (1.225, 1.250, 1.175) GeV. The **Cubic** results are for the $\alpha + \beta m_\pi^2 + \gamma m_\pi^3$ extrapolation function, with γ *unconstrained* by chiral symmetry – as explained in the text this produces an unreliable value for σ_N.

available, the errors that we quote are naive estimates only. The extracted value of σ_N is very well determined by the present data, the result being 54.6 ± 2.0 MeV. Since the process of setting the physical mass scale via the string tension is thought to have a systematic error of 10%, one might naively expect this to apply to σ_N. However, *all* masses in the problem including the pion (or quark) mass, as well as that of the nucleon, scale with the lattice parameter a. It turns out that when one uses Eq. (4) at the physical pion mass (which means a slightly different value of $\bar{m}a$ if a changes), the value of σ_N is extremely stable. If, for example, one raises the CP-PACS data by 15% and the UKQCD data by 5% (instead of 5% and -5%, respectively) the value of σ_N shifts from 54.6 ± 2.0 to 55.2 ± 2.1 MeV. We present calculations in Table 1 that show, for a variety of scalings of the lattice data, how stable our results are.

The remaining issue, for the present data, is the model dependence associated with the choice of a sharp cut-off in the pionic self-energies. Our investigations in Ref. [18] showed that Eq. (7) could reproduce the dependence of M_N on m_π^2 within the cloudy bag model, and that it could also describe the dependence of pion self-energy terms calculated with dipole form factors. Thus we believe that any model satisfying the essential chiral constraints and fitting the lattice data should give essentially the same answer. We checked this by numerically fitting the lattice data (solid curve) with the form of Eq. (7) but with σ_{NN} and $\sigma_{N\Delta}$ calculated with dipole form factors of mass Λ_D at all pion-baryon vertices. Since the preferred phenomenological form of the $N\pi$ form factor is a dipole, we regard the dipole result shown in the first line of Table 1 as our best estimate, namely $\sigma_N = 47.2 \pm 1.8$ MeV with fit parameters $(\alpha, \beta, \Lambda_D) = (2.02, 0.398, 1.225)$. A

remaining source of error is that, although the lattice results were calculated with an improved action, there still is an error associated with the extrapolation to the infinite volume, continuum limit. The importance of the inclusion of the correct chiral behaviour is clearly seen by the fact that it increases the value of the sigma commutator from the 30 MeV of the unconstrained cubic fit to around 50 MeV.

Clearly an enormous amount of work remains to be done before we will fully understand the structure of the nucleon within QCD. It is vital that the rapid progress on improved actions and faster computers continue and that we have three flavour calculations within full QCD at masses as close as possible to the physical quark masses. Nevertheless, it is a remarkable result that the present lattice data for dynamical-fermion, two-flavour QCD, yields such a stable and accurate answer for the sigma commutator, an answer which is already within the range of the experimental values. The implications of this result for models of hadron structure need to be explored urgently.

One of us (SVW) would like to acknowledge helpful discussions with Tom Cohen at an early stage of this work. We would also like acknowledge helpful comments from Chris Allton, Craig Roberts and Robert Perry. This work was supported in part by the Australian Research Council.

References

[1] **UKQCD** Collaboration, C. R. Allton *et. al.*, `hep-lat/9808016`.

[2] **CP-PACS** Collaboration, S. Aoki *et. al.*, *Phys. Rev.* **D60**, 114508 (1999), `hep-lat/9902018`.

[3] R. P. Feynman, *Acta Phys. Polon.* **24** (1963) 697–722;
R. P. Feynman, *Phys. Rev.* **56** (1939) 340;
H. Hellman, *Einführung in die Quantenchemie.* Deutick Verlag, Leipzig, 1937;
S. T. Epstein, *Amer. J. Phys.* **22** (1954) 614.

[4] J. Gasser, H. Leutwyler and M. E. Sainio, *Phys. Lett.* **B253**, 252 (1991).

[5] D. Sigg *et al.*, *Nucl. Phys.* **A609** (1996) 269;
D. Chatellard *et al.*, *Nucl. Phys.* **A625**, 855 (1997).

[6] T. E. Ericson, B. Loiseau and A. W. Thomas, "Precision determination of the πN scattering lengths and the charged πNN coupling constant", `hep-ph/9907433`.

[7] M. M. Pavan, R. A. Arndt, I. I. Strakovsky and R. L. Workman, "New result for the pion nucleon sigma term from an updated VPI/GW πN partial-wave and dispersion relation analysis", `nucl-th/9912034`.

[8] D. V. Bugg, "Summary of the Conference", to be published in the proceedings of 8th International Symposium on Meson-Nucleon Physics

and the Structure of the Nucleon (MENU 99), Zuoz, Switzerland, 16-20 Aug 1999.

[9] M. Knecht, `hep-ph/9912443`.

[10] I. Jameson, A. A. Rawlinson and A. W. Thomas, *Austral. J. Phys.* **47**, 45 (1994);
R. E. Stuckey and M. C. Birse, *J. Phys.* G **G23**, 29 (1997), `hep-ph/9602312`.

[11] U. Meissner, "Chiral dynamics: Status and perspectives", `hep-ph/9810276`;
V. Bernard, N. Kaiser and U. G. Meissner, *Z. Phys.* **C60**, 111 (1993), `hep-ph/9303311`.

[12] See for example, S. Cabasino *et al.*, *Nucl. Phys. B* (Proc. Suppl.) **20**, 399 (1991).

[13] **SESAM** Collaboration, S. Gusken *et al.*, *Phys. Rev.* **D59**, 054504 (1999), `hep-lat/9809066`.

[14] S. J. Dong, J. F. Lagae and K. F. Liu, *Phys. Rev.* **D54**, 5496 (1996), `hep-ph/9602259`.

[15] M. Fukugita, Y. Kuramashi, M. Okawa and A. Ukawa, *Phys. Rev.* **D51**, 5319 (1995), `hep-lat/9408002`.

[16] S.R. Sharpe, *Phys. Rev.* **D56**, 7052 (1997), `hep-lat/9707018`;
J.N. Labrenz and S.R. Sharpe, *Phys. Rev.* **D54**, 4595 (1996), `hep-lat/9605034`.

[17] B. Sheikholeslami and R. Wohlert, *Nucl. Phys.* **B259** (1985) 609;
M. Alford, W. Dimm, P. Lepage, *Phys. Lett.* **B361**, 87 (1995);
P. Hasenfratz, *Nucl. Phys.* (Proc. Suppl.) **B63**, 53 (1998).

[18] D. B. Leinweber, A. W. Thomas, K. Tsushima, and S. V. Wright, "Baryon masses from lattice QCD: Beyond the perturbative chiral regime", `hep-lat/9906027`. To appear in *Phys. Rev.* **D**.

ADP-99-38/T375

Chiral Corrections to Baryon Masses Calculated within Lattice QCD

Anthony W. Thomas*, Derek B. Leinweber†, Kazuo Tsushima‡, and Stewart V. Wright§

Department of Physics and Mathematical Physics
and Special Research Centre for the Subatomic Structure of Matter,
University of Adelaide, Australia 5005

Consideration of the analytic properties of pion-induced baryon self energies leads to new functional forms for the extrapolation of light baryon masses. These functional forms reproduce the leading non-analytic behavior of chiral perturbation theory, the correct non-analytic behavior at the $N\pi$ threshold and the appropriate heavy-quark limit. They involve only three unknown parameters, which may be obtained by fitting lattice QCD data. Recent dynamical fermion results from CP-PACS and UKQCD are extrapolated using these new functional forms. We also use these functions to probe the limit of applicability of chiral perturbation theory.

1. Introduction

Chiral symmetry requires that the nucleon mass has the form

$$m_N(m_\pi) = m_N(0) + \alpha m_\pi^2 + \beta m_\pi^3 + \gamma m_\pi^4 \ln m_\pi + \dots \ ,$$

for small m_π, where $m_N(0)$, α, β, and γ are functions of the strong coupling constant $\alpha_s(\mu)$. Recent work [1] has shown that using physical insights from chiral perturbation theory and heavy quark effective theory one can derive new functional forms which describe the extrapolation of light baryon masses as functions of the pion mass (m_π). These forms are applicable beyond the chiral perturbative regime and have been compared successfully with predictions from the Cloudy Bag Model [2] and recent dynamical fermion lattice QCD calculations.

2. Analyticity

By now it is well established that chiral symmetry is dynamically broken in QCD and that the pion is almost a Goldstone boson. It is strongly coupled to baryons and therefore plays a significant role in the N and Δ self energies. In the limit where the baryons are heavy, the pion-induced self energies of the N and Δ, to one loop, are given by the

*athomas@physics.adelaide.edu.au
†dleinweb@physics.adelaide.edu.au
‡ktsushim@physics.adelaide.edu.au
§swright@physics.adelaide.edu.au

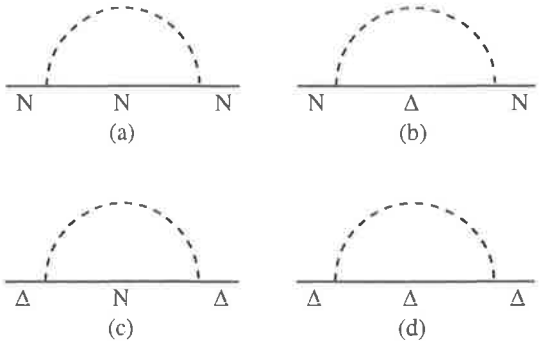

Figure 1. One-loop pion induced self energy of the nucleon and the delta.

processes shown in Fig. 1(a–d). We label these by σ_{NN}, $\sigma_{N\Delta}$, $\sigma_{\Delta N}$, and $\sigma_{\Delta\Delta}$. Note that we have restricted the intermediate baryon states to those most strongly coupled, namely the N and Δ states. Other intermediate states are suppressed by the baryon form factor describing the extended nature of baryons.

The leading non-analytic contribution (LNAC) of these self energy diagrams is associated with the infrared behavior of the corresponding integrals – i.e., the behavior as the loop momentum $k \to 0$. As a consequence, it should not depend on the details of a high momentum cut-off, or form factor. In particular, it is sufficient for studying the LNAC to evaluate the self energy integrals using a simple sharp cut-off, $u(k) = \theta(\Lambda - k)$ as the choice of form factor. The explicit forms of the self energy contributions for σ_{NN}, $\sigma_{N\Delta}$ and so on are given in [1]. Moreover, there is little phenomenological difference between this step function and the more natural dipole, provided one can tune the cut-off parameter Λ. The self energies involving transitions of $N \to \Delta$ or $\Delta \to N$ are characterized by a branch point at $m_\pi = \Delta M$.

2.1. Chiral Limit

The leading non-analytic (LNA) terms are those which correspond to the lowest order non-analytic functions of m_q – i.e., odd powers or logarithms of m_π. By expanding the expressions given in [1], we find that the LNA contributions to the nucleon/delta masses are in agreement with the well known results of χPT [4,5].

Of course, our concern with respect to lattice QCD is not so much the behavior as $m_\pi \to 0$, but the extrapolation from high pion masses to the physical pion mass. In this context the branch point at $m_\pi^2 = \Delta M^2$ is at least as important as the LNA behaviour near $m_\pi = 0$.

2.2. Heavy Quark Limit

Heavy quark effective theory suggests that as $m_\pi \to \infty$ the quarks become static and hadron masses become proportional to the quark mass. In this spirit, corrections are expected to be of order $1/m_q$ where m_q is the heavy quark mass. Thus we would expect the pion induced self energy to vanish as $1/m_q$ as the pion mass increases. The presence of a fixed cut-off Λ acts to suppress the pion induced self energy for increasing pion masses. While some m_π^2 dependence in Λ is expected, this is a second-order effect and does not

alter this qualitative feature. Indeed, in the large m_π limit of the equations, we find that they tend to zero at least as fast as $1/m_\pi^2$.

The agreement with both the chiral limit and expected behaviour in the heavy quark limit suggests the following functional form for the extrapolation of the nucleon mass [1]:

$$M_N = \alpha_N + \beta_N m_\pi^2 + \sigma_{NN}(m_\pi, \Lambda) + \sigma_{N\Delta}(m_\pi, \Lambda)\,. \tag{1}$$

3. Lattice Data Analysis

We consider two independent lattice simulations of the N and Δ masses from CP-PACS [6] and UKQCD [7]. Both of these use improved actions to study baryon masses in full QCD with two light flavours. We find that the two data sets are consistent, provided one allows the parameters introducing the physical scale to float within systematic errors of 10%.

We begin by considering the functional form suggested in Section 2 with the cut-off Λ fixed to the value determined by fitting CBM calculations. This is shown as the solid curve in Fig. 2. In order to perform model independent fits (i.e. with Λ unconstrained), it is essential to have lattice simulations at light quark masses approaching $m_\pi^2 \sim 0.1$ GeV^2. This fit is illustrated by the dash-dot curve.

Common practice in the lattice community to use a polynomial expansion for the mass dependence of hadron masses. Motivated by χPT the lowest odd power of m_π allowed is m_π^3:

$$M_N = \alpha + \beta m_\pi^2 + \gamma m_\pi^3 \tag{2}$$

The result of such a fit for the N is shown in the dashed curve of Fig. 2. The coefficient of the m_π^3 term, which is the leading non-analytic term in the quark mass, in the three parameter fit is -0.761. This disagrees with the coefficient of -5.60 known from χPT (which is correctly incorporated in Eq. (1), the solid and dash-dot curves) by almost an order of magnitude. This clearly indicates the failings of such a simple fitting procedure.

4. Summary

In the quest to connect lattice measurements with the physical regime, we have explored the quark mass dependence of the N and Δ baryon masses using arguments based on analyticity and heavy quark limits. We have determined a method to access quark masses beyond the regime of chiral perturbation theory. This method reproduces the leading non-analytic behavior of χPT and accounts for the internal structure for the baryon under investigation. We find that the leading non-analytic term of the chiral expansion dominates from the chiral limit up to the branch point at $m_\pi = \Delta M \simeq 300$ MeV, beyond which χPT breaks down. The predictions of the CBM, and two-flavour dynamical-fermion lattice QCD results, are succinctly described by the formulae derived in [1]. The curvature around $m_\pi = \Delta M$, neglected in previous extrapolations of the lattice data, leads to shifts in the extrapolated masses of the same order as the departure of lattice estimates from experimental measurements.

Acknowledgments

This work was supported in part by the Australian Research Council.

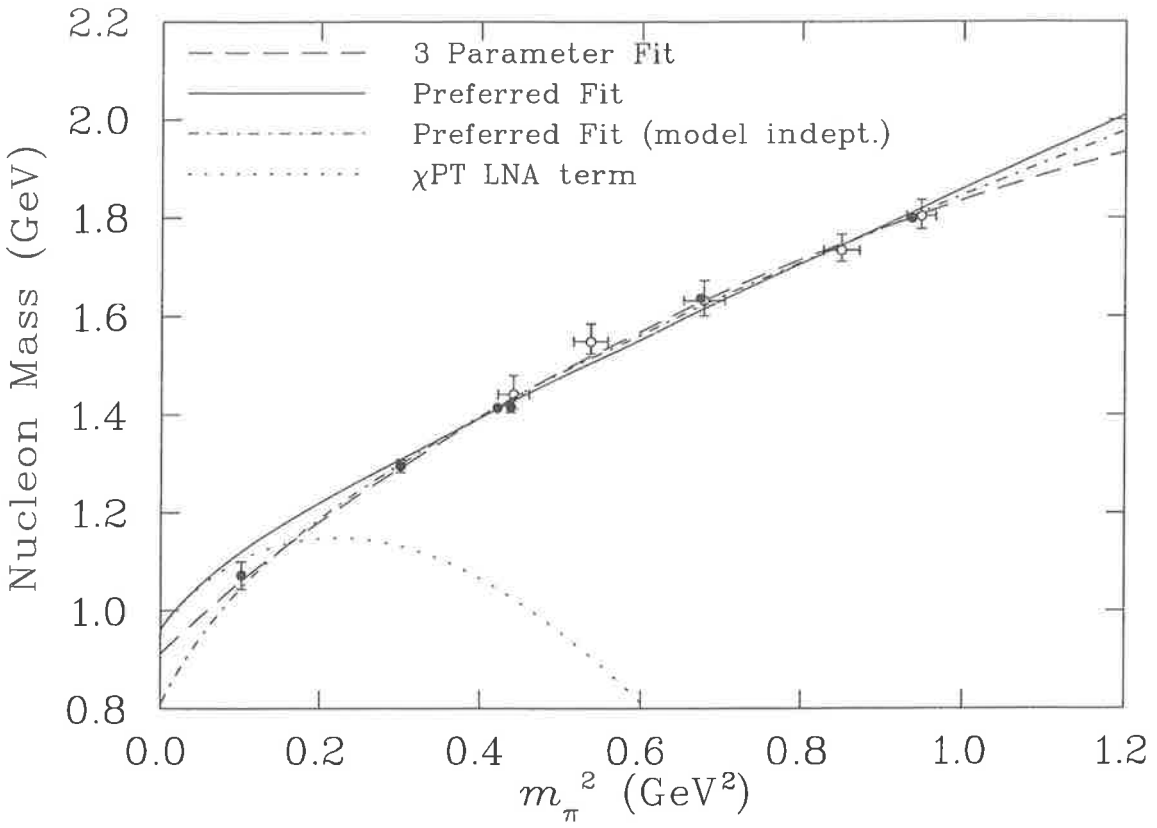

Figure 2. A comparison between phenomenological fitting functions for the mass of the nucleon. The dotted curve corresponds to using Eq. (2) with γ set equal to the value known from χPT. The three parameter fit (dashed) corresponds to letting γ vary as an unconstrained fit parameter. The solid and dash-dot curves correspond to our preferred fit of the functional form of Eq. (1) with Λ from the CBM and as a fit parameter respectively. The lattice data from are CP-PACS (solid) and UKQCD (open), each with a 5% scale change.

REFERENCES

1. D.B. Leinweber, A.W. Thomas, K. Tsushima and S.V. Wright, hep-lat/9906027.
2. A. W. Thomas, Adv. Nucl. Phys. **13** (1984) 1; G.A. Miller, Int. Rev. Nucl. Phys., **2** (1984) 190.
3. A.W. Thomas and G. Krein, Phys. Lett. **B456** (1999) 5.
4. E. Jenkins, Nucl. Phys. **B368** (1992) 190.
5. R.F. Lebed, Nucl. Phys. **B430** (1994) 295.
6. S. Aoki *et al.* [CP-PACS-Collaboration Collaboration], hep-lat/9902018.
7. C.R. Allton *et al.* [UKQCD Collaboration], hep-lat/9808016.

Baryon mass extrapolation

Derek B. Leinweber, Anthony W. Thomas, Kazuo Tsushima and Stewart V. Wright[a] *

[a]Department of Physics and Mathematical Physics and Special Research Centre for the Subatomic Structure of Matter, University of Adelaide, Australia 5005

Consideration of the analytical properties of pion-induced baryon self-energies leads to new functional forms for the extrapolation of light baryon masses. These functional forms reproduce the leading non-analytic behavior of chiral perturbation theory, the correct heavy-quark limit and have the advantage of containing information on the extended structure of hadrons. The forms involve only three unknown parameters which may be optimized by fitting to present lattice data. Recent dynamical fermion results from CP-PACS and UK-QCD are extrapolated using these new functional forms. We also use these functions to probe the limit of the chiral perturbative regime and shed light on the applicability of chiral perturbation theory to the extrapolation of present lattice QCD results.

1. FORMALISM

In recent years there has been tremendous progress in the computation of baryon masses within lattice QCD. Still, it remains necessary to extrapolate the calculated results to the physical pion mass ($\mu = 140$ MeV) in order to make a comparison with experimental data. In doing so one necessarily encounters some non-linearity in the quark mass (or m_π^2), including the non-analytic behavior associated with dynamical chiral symmetry breaking. We recently investigated this problem for the case of the nucleon magnetic moments [1]. It is vital to develop a sound understanding of how to extrapolate to the physical pion mass.

1.1. Self-Energy Contributions

Chiral symmetry is dynamically broken in QCD and the pion alone is a near Goldstone boson. It is strongly coupled to baryons and plays a significant role in N and Δ self-energies. The one-loop pion induced self-energies of the N and Δ are given by the processes shown in Fig. 1.

In the standard heavy baryon limit, the analytic expression for the pion cloud correction to the masses of the N and Δ are of the form [2]

$$\delta M_N = \sigma_{NN} + \sigma_{N\Delta}\,; \quad \delta M_\Delta = \sigma_{\Delta\Delta} + \sigma_{\Delta N}\,, \quad (1)$$

*Supported by the Australian Research Council.

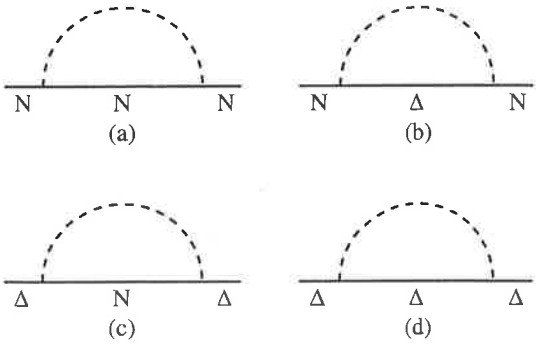

Figure 1. One-loop pion induced self-energy of the nucleon and the delta.

where

$$\sigma_{NN} = \sigma_{\Delta\Delta} = -\frac{3\,g_A^2}{16\,\pi^2 f_\pi^2}\int_0^\infty dk \frac{k^4 u_{NN}^2(k)}{w^2(k)}\,, \quad (2)$$

$$\sigma_{N\Delta} = -\frac{6\,g_A^2}{25\,\pi^2 f_\pi^2}\int_0^\infty dk \frac{k^4 u_{N\Delta}^2(k)}{w(k)(\Delta M + w(k))}\,, \quad (3)$$

$$\sigma_{\Delta N} = \frac{3\,g_A^2}{50\,\pi^2 f_\pi^2}\int_0^\infty dk \frac{k^4 u_{N\Delta}^2(k)}{w(k)(\Delta M - w(k))}\,. \quad (4)$$

Here $\Delta M = M_\Delta - M_N$, $g_A = 1.26$ is the axial charge of the nucleon, $w(k) = \sqrt{k^2 + m_\pi^2}$ is the pion energy and $u_{NN}(k)$, $u_{N\Delta}(k)$, ... are the $NN\pi$, $N\Delta\pi$, ... form factors associated with the emission of a pion of three-momentum k. The

form factors reflect the finite size of the baryonic source of the pion field and suppress the emission probability at high virtual pion momentum. As a result, the self-energy integrals are not divergent.

The leading non-analytic (LNA) contribution of these self-energy diagrams is associated with the infrared behavior of the corresponding integrals; i.e. the behavior as $k \to 0$. As a consequence, the leading non-analytic behavior does not depend on the details of the form factors. Indeed, the well known results of chiral perturbation theory [3,4] are reproduced even when the form factors are approximated by $u(k) = \theta(\Lambda - k)$.

Of course, our concern with respect to lattice QCD is not so much the behavior as $m_\pi \to 0$, but the extrapolation from high pion masses to the physical pion mass. In this context the branch point at $m_\pi^2 = \Delta M^2$, associated with transitions of $N \to \Delta$ or $\Delta \to N$, is at least as important as the LNA behavior near $m_\pi = 0$.

Heavy quark effective theory suggests that as $m_\pi \to \infty$ the quarks become static and hadron masses become proportional to the quark mass. In this spirit, corrections are expected to be of order $1/m_q$ where m_q is the heavy quark mass. The presence of a cut-off associated with the form factor acts to suppress the pion induced self energy for increasing pion masses, as evidenced by the m_π^2 in the denominators of Eqs. (2), (3) and (4). While some m_π^2 dependence in the form factor is expected, this is a second-order effect and does not alter the qualitative feature of the self-energy corrections tending to zero as $1/m_\pi^2$ in the heavy quark limit.

Rather than simplifying our expressions to just the LNA terms, we retain the complete expressions [2], as they contain important physics that would be lost by making a simplification. We note that keeping the entire form is not in contradiction with χPT. However, as one proceeds to larger quark masses, differences between the full forms and the expressions in the chiral limit will become apparent, highlighting the importance of the branch point and the form factor reflecting the finite size of baryons.

As a result of these considerations, we propose to use the analytic expressions for the self-energy integrals corresponding to a sharp cut-off in order to incorporate the correct LNA structure in a simple three-parameter description of the m_π dependence of the N and Δ masses. In the heavy quark limit hadron masses become proportional to the quark mass. Hence we can simulate a linear dependence of the baryon masses on the quark mass, m_q, in this region, by adding a term involving m_π^2. The functional form for the mass of the nucleon suggested by this analysis is then:

$$M_N = \alpha_N + \beta_N m_\pi^2 + \sigma_{NN}(\Lambda_N) + \sigma_{N\Delta}(\Lambda_N)\,, \quad (5)$$

while that for the Δ is:

$$M_\Delta = \alpha_\Delta + \beta_\Delta m_\pi^2 + \sigma_{\Delta\Delta}(\Lambda_\Delta) + \sigma_{\Delta N}(\Lambda_\Delta)\,. \quad (6)$$

1.2. Model Dependence

The use of a sharp cut-off, $u(k) = \theta(\Lambda - k)$, as a form factor may seem somewhat unfortunate given that phenomenology suggests a dipole form factor better approximates the axial-vector form factor. However, the sensitivity to such model-dependent issues is shown to be negligible in Fig. 2. There, the self-energy contribution $\sigma_{NN}(= \sigma_{\Delta\Delta})$ for a 1 GeV dipole form factor (solid curve) is compared with a sharp cut-off form factor combined with the standard $\alpha + \beta\, m_\pi^2$ terms of (5) or (6). Optimizing Λ, α and β provides the fine-dash curve of Fig. 2. Differences are at the few MeV level indicating negligible sensitivity to the actual analytic structure of the form factor.

Here we have focused on the pion self-energy contribution to the N and Δ form factors. Only the pion displays a rapid mass dependence as the chiral limit is approached. Other mesons participating in similar diagrams do not give rise to such rapidly changing behavior and can be accommodated in the $\alpha + \beta\, m_\pi^2$ terms of (5) or (6). Moreover, the form factor suppresses the contributions from more massive intermediate states including multiple pion dressings. Other multi-loop pion contributions renormalize the vertex and hence we use the renormalized coupling g_A as a measure of the pion-nucleon coupling.

2. ANALYSIS

We consider two independent dynamical-fermion lattice simulations of the N and Δ

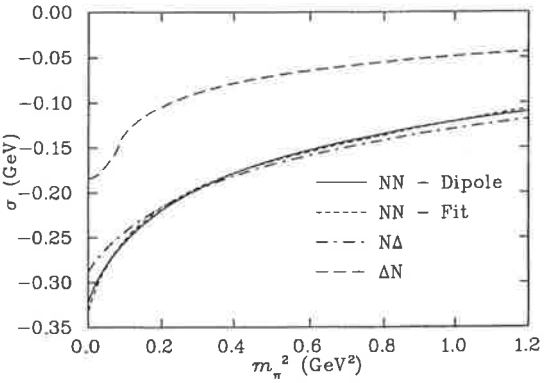

Figure 2. The self-energy contribution σ_{NN} for a 1 GeV dipole form factor (solid curve) is compared with a sharp cut-off form factor $\theta(\Lambda_N - k)$ (fine-dash curve). Self-energy contributions $\sigma_{N\Delta}$ (dot-dash) and $\sigma_{\Delta N}$ (long-dash) for a 1 GeV dipole are also illustrated.

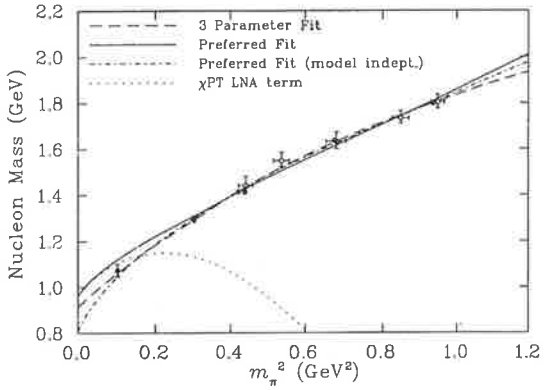

Figure 3. A comparison of phenomenological fitting functions for the mass of the nucleon. The solid curve corresponds to our preferred fit of the functional form of (5) with Λ constrained to reproduce a 1 GeV dipole form factor. The dash-dot curve illustrates the unconstrained fit. The three parameter fit (dashed) corresponds to letting γ of (7) vary as an unconstrained fit parameter. The dotted curve corresponds to (7) with γ set equal to the value known from χPT. The lattice data from are CP-PACS (solid) and UKQCD (open), each with a 5% scale change to provide consistency.

masses. We select results from CP-PACS's [5] $12^3 \times 32$ and $16^3 \times 32$ simulations at $\beta = 1.9$, and UKQCD's [6] $12^3 \times 24$ simulations at $\beta = 5.2$.

Figure 3 displays fits of (5) to the lattice data. In order to perform fits in which Λ is unconstrained, it is essential to have lattice simulations at light quark masses approaching $m_\pi^2 \sim 0.1$ GeV^2.

It is common to see the use of the following χPT-motivated expression for the mass dependence of hadron masses,

$$M_N = \alpha + \beta m_\pi^2 + \gamma m_\pi^3 \,. \qquad (7)$$

The result of such a fit for the N is shown as the dashed curve in Fig. 3. The coefficient of the m_π^3 term in a three parameter fit is -0.761. This disagrees with the coefficient of -5.60 known from χPT (which is correctly incorporated in (5) and illustrated as the solid and dash-dot curves of Fig. 3) by almost an order of magnitude. This clearly indicates the failings of (7).

The dotted curve of Fig. 3 indicates the leading non-analytic term of the chiral expansion dominates from the chiral limit up to the branch point at $m_\pi = \Delta M \simeq 300$ MeV, beyond which χPT breaks down. The curvature around $m_\pi = \Delta M$, neglected in previous extrapolations of the lattice data, leads to shifts in the extrapolated masses of the same order as the departure of lattice estimates from experimental measurements.

REFERENCES

1. D. B. Leinweber, D. H. Lu, and A. W. Thomas, Phys. Rev. **D60** (1999) 034014, hep-lat/9810005.
2. D.B. Leinweber, A.W. Thomas, K. Tsushima and S.V. Wright, "Baryon masses from lattice QCD: Beyond the perturbative chiral regime," hep-lat/9906027.
3. E. Jenkins, Nucl. Phys. **B368**, 190 (1992).
4. R.F. Lebed, Nucl. Phys. **B430**, 295 (1994).
5. CP-PACS-Collaboration (S. Aoki *et al.*), UTCCP-P-61, hep-lat/9902018.
6. UKQCD Collaboration (C. R. Allton *et al.*), Phys. Rev. **D60** (1999) 034507, hep-lat/9808016.

PHYSICAL REVIEW D, VOLUME 61, 074502

Baryon masses from lattice QCD: Beyond the perturbative chiral regime

Derek B. Leinweber,* Anthony W. Thomas,† Kazuo Tsushima,‡ and Stewart V. Wright§
Department of Physics and Mathematical Physics and Special Research Centre for the Subatomic Structure of Matter, University of Adelaide, Australia 5005

(Received 29 June 1999; revised manuscript received 21 September 1999; published 22 February 2000)

Consideration of the analytic properties of pion-induced baryon self-energies leads to new functional forms for the extrapolation of light baryon masses. These functional forms reproduce the leading non-analytic behavior of chiral perturbation theory, the correct non-analytic behavior at the $N\pi$ threshold and the appropriate heavy-quark limit. They involve only three unknown parameters, which may be obtained by fitting to lattice data. Recent dynamical fermion results from CP-PACS and UKQCD are extrapolated using these new functional forms. We also use these functions to probe the limit of applicability of chiral perturbation theory to the extrapolation of lattice QCD results.

PACS number(s): 12.38.Gc, 11.15.Ha

I. INTRODUCTION

In the last year there has been tremendous progress in the computation of baryon masses within lattice QCD. Improved quark [1] and gluon [2] actions, together with increasing computer speed, means that one already has results for N, Δ and vector meson masses for full QCD with two flavors of dynamical quarks. Although the results are mainly in the regime where the pion mass (m_π) is above 500 MeV, there has been some exploration as low as 300–400 MeV on a 3.0 fm lattice by CP-PACS [3].

In spite of these impressive developments it is still necessary to extrapolate the calculated results to the physical pion mass ($\mu = 140$ MeV) in order to make a comparison with experimental data. In doing so one necessarily encounters some non-linearity in the quark mass (or m_π^2), including the non-analytic behavior associated with dynamical chiral symmetry breaking. Indeed, the recent CP-PACS study [4] did report the first behavior of this kind in baryon systems.

As the computational resources necessary to include three light flavors with realistic masses will not be available for many years, it is vital to develop a sound understanding of how to extrapolate to the physical pion mass. We recently investigated this problem for the case of the nucleon magnetic moments [5].

The cloudy bag model (CBM) [6] is an extension of the MIT bag model incorporating chiral symmetry. It therefore generates the same leading non-analytic (LNA) behavior as chiral perturbation theory (χPT). This model was recently generalized to allow for variable quark and pion masses in order to explore the likely mass dependence of the magnetic moment [5]. This work led to several important results:

(i) A series expansion of $\mu_{p(n)}$ in powers of m_π is not a useful approximation for m_π larger than the physical mass.

(ii) On the other hand, the behavior of the model, after adjustments to fit the lattice data at large m_π, was well determined by the simple Padé approximant

$$\mu_{p(n)} = \frac{\mu_0}{1 + \frac{\alpha}{\mu_0} m_\pi + \beta m_\pi^2}. \tag{1}$$

(iii) Equation (1) not only builds in the Dirac moment at moderately large m_π^2 but has the correct LNA behavior of chiral perturbation theory:

$$\mu = \mu_0 - \alpha m_\pi,$$

with α a model independent constant, as $m_\pi^2 \to 0$.

(iv) Fixing α at the value given by chiral perturbation theory and adjusting μ_0 and β to fit the lattice data yielded values of μ_p and μ_n of $(2.85 \pm 0.22)\mu_N$ and $(-1.96 \pm 0.16)\mu_N$, respectively, at the physical pion mass. These are significantly closer to the experimental values than the usual linear extrapolations in m_q.

Clearly it is vital to extend the lattice calculations of baryon magnetic moments to lower values of m_π than the 600 MeV used in the study just outlined. It is also important to include dynamical quarks. Nevertheless, the apparent success of the extrapolation procedure suggested by the CBM study gives us strong encouragement to investigate the same approach for baryon masses.

Accordingly, in this paper we study the variation of the N and Δ masses with m_π (or equivalently m_q). Section II is devoted to considerations of the low-lying singularities and pion-induced cuts in the complex plane of the nucleon and Δ spectral representation. The analytic properties of the derived phenomenological form are consistent with both chiral perturbation theory and the expected behavior at large m_q. This phenomenological form is eventually fitted to recent two-flavor, full QCD measurements made by CP-PACS [3] and UKQCD [7]. However, to gain some insight into the parameters and behavior of the functional form we examine the N and Δ masses as described in the CBM in Sec. III. In section IV we apply the analytic form to the lattice data. Section V is reserved for a summary of our findings.

*Email address: dleinweb@physics.adelaide.edu.au
†Email address: athomas@physics.adelaide.edu.au
‡Email address: ktsushim@physics.adelaide.edu.au
§Email address: swright@physics.adelaide.edu.au

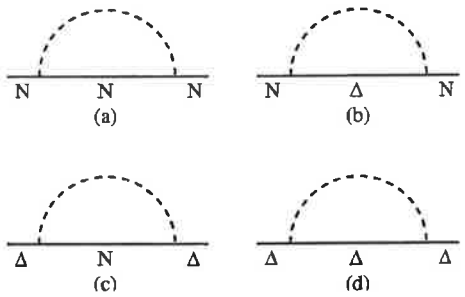

FIG. 1. One-loop pion induced self-energy of the nucleon and the delta.

II. ANALYTICITY

By now it is well established that chiral symmetry is dynamically broken in QCD and that the pion is almost a Goldstone boson. As a result it is strongly coupled to baryons and therefore plays a significant role in the N and Δ self-energies. In the limit where the baryons are heavy, the pion induced self-energies of the N and Δ, to one loop, are given by the processes shown in Fig. 1. Note that we have restricted the intermediate baryon states to those most strongly coupled, namely the N and Δ states.

The analytic expression for the pion cloud correction to the masses of the N and Δ is of the form [8]

$$\delta M_N = \sigma_{NN} + \sigma_{N\Delta}, \tag{2}$$

where

$$\sigma_{NN} = -\frac{3}{16\pi^2 f_\pi^2} g_A^2 \int_0^\infty dk \frac{k^4 u_{NN}^2(k)}{w^2(k)}, \tag{3}$$

$$\sigma_{N\Delta} = -\frac{3}{16\pi^2 f_\pi^2} \frac{32}{25} g_A^2 \int_0^\infty dk \frac{k^4 u_{N\Delta}^2(k)}{w(k)[\Delta M + w(k)]}, \tag{4}$$

and

$$\delta M_\Delta = \sigma_{\Delta\Delta} + \sigma_{\Delta N}, \tag{5}$$

where

$$\sigma_{\Delta\Delta} = \sigma_{NN}, \tag{6}$$

$$\sigma_{\Delta N} = \frac{3}{16\pi^2 f_\pi^2} \frac{8}{25} g_A^2 \int_0^\infty dk \frac{k^4 u_{N\Delta}^2(k)}{w(k)[\Delta M - w(k)]}. \tag{7}$$

We note that $\Delta M = M_\Delta - M_N$, $g_A = 1.26$ is the axial charge of the nucleon, $w(k) = \sqrt{k^2 + m_\pi^2}$ is the pion energy and $u_{NN}(k)$, $u_{N\Delta}(k)$, ... are the $NN\pi$, $N\Delta\pi$, ... form factors associated with the emission of a pion of three-momentum k. We have used SU(6) symmetry to relate the four coupling constants to the $NN\pi$ coupling, which, in turn, has been related to $g_A/2f_\pi$ by chiral symmetry. The form factors arise naturally in any chiral quark model because of the finite size of the baryonic source of the pion field—which suppresses the emission probability at high virtual pion momentum. As a result, the self-energy integrals are not divergent.

The leading non-analytic contribution (LNAC) of these self-energy diagrams is associated with the infrared behavior of the corresponding integrals—i.e., the behavior as $k \to 0$. As a consequence, the leading non-analytic behavior should not depend on the details of the high momentum cutoff or the form factors. In particular, it should be sufficient for studying the LNAC to evaluate the self-energy integrals using a simple sharp cutoff, $u(k) = \theta(\Lambda - k)$. In Sec. III we shall compare the results with those calculated using a phenomenological, dipole form factor and show that this is in fact an effective simplification.

Using a θ function for the form factors, the $NN\pi$ and $\Delta\Delta\pi$ integrals [cf. Figs. 1(a) and 1(d), respectively], which are equal, are easily evaluated in the heavy baryon approximation used here:

$$\sigma_{NN} = \sigma_{\Delta\Delta} = -\frac{3}{16\pi^2 f_\pi^2} g_A^2 \int_0^\Lambda dk \frac{k^4}{w^2(k)} = -\frac{3g_A^2}{16\pi^2 f_\pi^2}\left[m_\pi^3 \arctan\left(\frac{\Lambda}{m_\pi}\right) + \frac{\Lambda^3}{3} - \Lambda m_\pi^2 \right]. \tag{8}$$

The integral corresponding to the process shown in Fig. 1(b), with a θ function form factor, may be analytically evaluated. For $m_\pi > \Delta M$,

$$\sigma_{N\Delta} = -\frac{g_A^2}{25\pi^2 f_\pi^2}\left\{ 12(m_\pi^2 - \Delta M^2)^{3/2}\left[\arctan\left(\frac{\sqrt{m_\pi^2 + \Lambda^2} + \Delta M + \Lambda}{\sqrt{m_\pi^2 - \Delta M^2}}\right) - \arctan\left(\frac{\Delta M + m_\pi}{\sqrt{m_\pi^2 - \Delta M^2}}\right)\right] + 3\Delta M(3m_\pi^2 - 2\Delta M^2)\ln\left(\frac{\sqrt{m_\pi^2 + \Lambda^2} + \Lambda}{m_\pi}\right) - 3\sqrt{m_\pi^2 + \Lambda^2}\,\Delta M\Lambda + 6\Delta M^2\Lambda - 6m_\pi^2\Lambda + 2\Lambda^3 \right\}, \tag{9}$$

while for $m_\pi < \Delta M$ we find

$$\sigma_{N\Delta}=-\frac{g_A^2}{25\pi^2 f_\pi^2}\left\{-6(\Delta M^2-m_\pi^2)^{3/2}\left[\ln\left(\frac{\sqrt{\Delta M^2-m_\pi^2}+\sqrt{m_\pi^2+\Lambda^2}+\Delta M+\Lambda}{\sqrt{\Delta M^2-m_\pi^2}-\sqrt{m_\pi^2+\Lambda^2}-\Delta M-\Lambda}\right)-\ln\left(\frac{\sqrt{\Delta M^2-m_\pi^2}+\Delta M+m_\pi}{\sqrt{\Delta M^2-m_\pi^2}-\Delta M-m_\pi}\right)\right]\right.$$
$$\left.+3\Delta M(3m_\pi^2-2\Delta M^2)\ln\left(\frac{\sqrt{m_\pi^2+\Lambda^2}+\Lambda}{m_\pi}\right)-3\sqrt{m_\pi^2+\Lambda^2}\Delta M\Lambda+6\Delta M^2\Lambda-6m_\pi^2\Lambda+2\Lambda^3\right\}. \quad (10)$$

Similar results are easily obtained for the process shown in Fig. 1(c). For $m_\pi>\Delta M$, the analytic form is

$$\sigma_{\Delta N}=\frac{g_A^2}{100\pi^2 f_\pi^2}\left\{-12(m_\pi^2-\Delta M^2)^{3/2}\left[\arctan\left(\frac{\sqrt{m_\pi^2+\Lambda^2}-\Delta M+\Lambda}{\sqrt{m_\pi^2-\Delta M^2}}\right)+\arctan\left(\frac{\Delta M-m_\pi}{\sqrt{m_\pi^2-\Delta M^2}}\right)\right]\right.$$
$$\left.+3\Delta M(3m_\pi^2-2\Delta M^2)\ln\left(\frac{\sqrt{m_\pi^2+\Lambda^2}+\Lambda}{m_\pi}\right)-3\sqrt{m_\pi^2+\Lambda^2}\Delta M\Lambda-6\Delta M^2\Lambda+6m_\pi^2\Lambda-2\Lambda^3\right\}, \quad (11)$$

while for $m_\pi<\Delta M$

$$\sigma_{\Delta N}=\frac{g_A^2}{100\pi^2 f_\pi^2}\left\{6(\Delta M^2-m_\pi^2)^{3/2}\left[\ln\left(\frac{\sqrt{\Delta M^2-m_\pi^2}+\sqrt{m_\pi^2+\Lambda^2}-\Delta M+\Lambda}{\sqrt{\Delta M^2-m_\pi^2}-\sqrt{m_\pi^2+\Lambda^2}+\Delta M-\Lambda}\right)+\ln\left(\frac{\sqrt{\Delta M^2-m_\pi^2}+\Delta M-m_\pi}{\sqrt{\Delta M^2-m_\pi^2}-\Delta M+m_\pi}\right)\right]\right.$$
$$\left.+3\Delta M(3m_\pi^2-2\Delta M^2)\ln\left(\frac{\sqrt{m_\pi^2+\Lambda^2}+\Lambda}{m_\pi}\right)-3\sqrt{m_\pi^2+\Lambda^2}\Delta M\Lambda-6\Delta M^2\Lambda+6m_\pi^2\Lambda-2\Lambda^3\right\}. \quad (12)$$

The self-energies involving transitions of $N\to\Delta$ or $\Delta\to N$ are characterized by the branch point at $m_\pi=\Delta M$.

A. Chiral limit

Chiral perturbation theory is concerned with the behavior of quantities such as the baryon self-energies as $m_q\to 0$. For the expressions derived above, this corresponds to taking the limit $m_\pi\to 0$. The leading non-analytic terms are those which correspond to the lowest order non-analytic functions of m_q—i.e., odd powers or logarithms of m_π. By expanding the expressions given above, we find that the LNA contribution to the nucleon/Δ mass [Eq. (8)] is given by

$$M_{N(\Delta)}^{LNA}=-\frac{3}{32\pi f_\pi^2}g_A^2 m_\pi^3, \quad (13)$$

in agreement with a well-known result of χPT [9]. A careful expansion of the $\Delta\pi$ contribution to the nucleon self-energy, Eq. (9), yields the LNA term

$$\sigma_{N\Delta}(m_\pi,\Lambda)\sim\frac{3g_A^2}{16\pi^2 f_\pi^2}\frac{32}{25}\frac{3}{8\Delta M}m_\pi^4\ln(m_\pi) \quad (14)$$

as $m_\pi\to 0$ which is again as expected from χPT [10]. For the $N\pi$ contribution to the self-energy of the Δ, the LNA term in the chiral limit of Eq. (11) yields

$$\sigma_{\Delta N}(m_\pi,\Lambda)\sim-\frac{3g_A^2}{16\pi^2 f_\pi^2}\frac{8}{25}\frac{3}{8\Delta M}m_\pi^4\ln(m_\pi). \quad (15)$$

Of course, our concern with respect to lattice QCD is not so much the behavior as $m_\pi\to 0$, but the extrapolation from high pion masses to the physical pion mass. In this context the branch point at $m_\pi^2=\Delta M^2$ is at least as important as the LNA near $m_\pi=0$. We shall return to this point later. We note that Banerjee and Milana [11] found the same non-analytic behavior as $m_\pi\to\Delta M$ that we find. However, they were not concerned with finding a form that could be used at large pion masses—i.e. one that is consistent with heavy quark effective theory.

B. Heavy quark limit

Heavy quark effective theory suggests that as $m_\pi\to\infty$ the quarks become static and hadron masses become proportional to the quark mass. This has been rather well explored in the context of successful nonrelativistic quark models of charmonium and bottomium [12]. In this spirit, corrections are expected to be of order $1/m_q$ where m_q is the heavy quark mass. Thus we would expect the pion induced self-energy to vanish as $1/m_q$ as the pion mass increases. The presence of a fixed cutoff Λ acts to suppress the pion induced self-energy for increasing pion masses, as evidenced by the m_π^2 in the denominators of Eqs. (3), (4) and (7). While some m_π^2 dependence in Λ is expected, this is a second-order effect and does not alter the qualitative features. By expanding the $\arctan(\Lambda/m_\pi)$ term in Eq. (8) for small Λ/m_π, we find

$$\sigma_{NN}=-\frac{3g_A^2}{16\pi^2 f_\pi^2}\frac{\Lambda^5}{5m_\pi^2}+\mathcal{O}\left(\frac{\Lambda^7}{m_\pi^4}\right), \quad (16)$$

which vanishes for $m_\pi \to \infty$. Indeed, in the large m_π (heavy quark) limit, both Eqs. (9) and (11) tend to zero as $1/m_\pi^2$.

C. Analytic form

We now have the chiral and heavy quark limits for each of the four integrals in Fig. 1. These expressions, which contain a single parameter, Λ, are correct in the chiral limit—i.e., they reproduce the first two non-analytic terms of χPT. They also have the correct behavior in the limit of large pion mass; namely they vanish like $1/m_\pi^2$. The latter feature would be destroyed if we were to retain only the LNA pieces of the self-energies as they would diverge at large m_π faster than m_q. Rather than simplifying our expressions to just the LNA terms, we therefore retain the complete expressions, as they contain important physics that would be lost by making a simplification.

We note that keeping the entire form is not in contradiction with χPT, as we have already shown that the leading non-analytic structure of χPT is contained in this form. However, as one proceeds to larger quark (pion) masses, differences between the full forms and the expressions in the chiral limit will become apparent. For example, the branch point at $m_\pi^2 = \Delta M^2$, which is an essential non-analytic component of the m_π dependence of the self-energy and which should dominate in the region $m_\pi \sim \Delta M$, is also satisfactorily incorporated in Eqs. (9) and (11). Yet the LNA chiral terms given in Sec. II A know nothing of this branch point and are clearly inappropriate in the region near and beyond $m_\pi^2 = \Delta M^2$.

As a result of these considerations, we propose to use the analytic expressions for the self-energy integrals corresponding to a sharp cutoff in order to incorporate the correct LNA structure in a simple three-parameter description of the m_π dependence of the N and Δ masses. In the heavy quark limit hadron masses become proportional to the quark mass. Moreover, as we shall see in the next section, the MIT bag model leads to a linear dependence of the mass of a baryon on the current quark mass far below the scale at which one would expect the heavy quark limit to apply. This is a simple consequence of relativistic quantum mechanics for a scalar confining field. On the other hand, lattice calculations indicate that the scale at which the pion mass exhibits a linear dependence on m_q is much larger than that for baryons.[1] In fact, over the range of masses of interest to us, explicit lattice calculations show that m_π^2 is proportional to m_q. Hence we can simulate a linear dependence of the baryon masses on the quark mass, m_q, in this region, by adding a term involving m_π^2. The functional form for the mass of the nucleon suggested by this analysis is then

$$M_N = \alpha_N + \beta_N m_\pi^2 + \sigma_{NN}(m_\pi, \Lambda) + \sigma_{N\Delta}(m_\pi, \Lambda), \quad (17)$$

while that for the Δ is

$$M_\Delta = \alpha_\Delta + \beta_\Delta m_\pi^2 + \sigma_{\Delta\Delta}(m_\pi, \Lambda) + \sigma_{\Delta N}(m_\pi, \Lambda). \quad (18)$$

The mass in the chiral limit is given by

$$M_N^{(0)} = \alpha_N + \sigma_{NN}(0, \Lambda) + \sigma_{N\Delta}(0, \Lambda), \quad (19)$$

where the meson cloud effects are explicitly contained in $\sigma_{NN}(0,\Lambda) + \sigma_{N\Delta}(0,\Lambda)$. The mass of the Δ in the chiral limit is calculated in an analogous way. We know that Eqs. (17) and (18) have the correct behavior in the chiral limit. Individually, they also have the correct heavy quark behavior.[2] Between the chiral and heavy-quark limits there are no general guidelines, so in the next section we shall compare our functional form to the cloudy bag model, a successful phenomenological approach incorporating chiral symmetry and the correct heavy quark limit.

III. BARYON MASSES WITHIN THE CBM

As a guide to the quark mass dependence of the N and Δ masses we consider the cloudy bag model [6,13]. This is a minimal extension of the MIT bag model such that chiral symmetry is restored, which has proved quite successful in a number of phenomenological studies of baryon properties and meson-baryon scattering [6,15–17]. Within the CBM, a baryon is viewed as a superposition of a bare quark core and bag plus meson states. The linearized CBM Lagrangian with pseudovector pion-quark coupling (to order $1/f_\pi$) is [18]

$$\begin{aligned}\mathcal{L} = {} & [\bar{q}(i\gamma^\mu \partial_\mu - m_q)q - B]\theta_V \\ & - \frac{1}{2}\bar{q}q\,\delta_S + \frac{1}{2}(\partial_\mu \boldsymbol{\pi})^2 - \frac{1}{2}m_\pi^2 \boldsymbol{\pi}^2 \\ & + \frac{\theta_V}{2f_\pi}\bar{q}\gamma^\mu \gamma_5 \boldsymbol{\tau} q \cdot \partial_\mu \boldsymbol{\pi}, \end{aligned} \quad (20)$$

where B is the bag constant, f_π is the π decay constant, θ_V is a step function (unity inside the bag volume and vanishing outside) and δ_S is a surface delta function. In a lowest order perturbative treatment of the pion field, the quark wave function is not effected by the pion field and is simply given by the MIT bag solution [19–21].

In principle the πNN form factor can be directly calculated within the model. It dies off at large momentum transfer because of the finite size of the baryon source. Rather

[1] One does not expect such linear behavior to appear for quark masses lighter than the charm quark mass where the pseudoscalar mass is 3.0 GeV. Even at this scale the quarks are still somewhat relativistic.

[2] With regard to the difference, $M_\Delta - M_N$, heavy quark effective theory (HQET) suggests that this difference should vanish as $m_\pi \to \infty$. This is only guaranteed by Eqs. (17) and (18) [through Eq. (16)] if the entire mass difference arises from the pion self-energy. While one could enforce this condition through the introduction of additional parameters and a more complicated analytic structure for the higher-order terms of Eqs. (17) and (18), we prefer to focus on the regime of m_π^2 from 1 GeV^2 to the chiral limit. As we shall see, Eqs. (17) and (18) are quite adequate for this purpose.

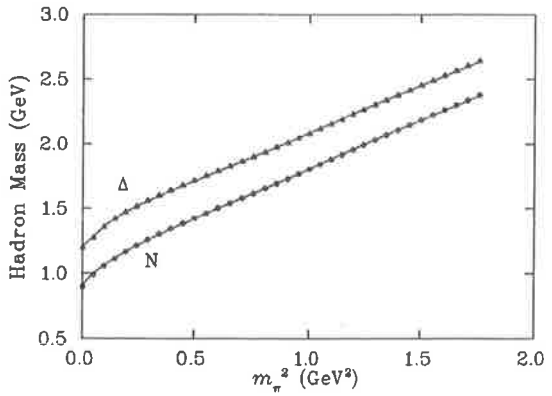

FIG. 2. The pion mass dependence of the N and Δ baryons generated in the CBM using a dipole form factor with $\Lambda_D = 1$ GeV. Fits of Eqs. (17) and (18) to the CBM results are illustrated by the curves.

than using this calculated form factor, which is model dependent, we have chosen to use a common phenomenological form, namely a simple dipole

$$u(k)=\frac{(\Lambda_D^2-\mu^2)^2}{(\Lambda_D^2+k^2)^2}, \tag{21}$$

where k is the magnitude of the loop (3-)momentum, μ is the physical pion mass (139.6 MeV), and Λ_D is a regulation parameter.

In the standard CBM treatment, where the pion is treated as an elementary field, the current quark mass, m_q, is not directly linked to m_π. Most observables are not sensitive to this parameter, as long as it is in the range of typical current quark masses. For our present purpose it is vital to relate the m_q inside the bag with m_π. Current lattice simulations indicate that m_π^2 is approximately proportional to m_q over a wide range of quark masses [3]. Hence, in order to model the lattice results, we scale the mass of the quark confined in the bag as $m_q=(m_\pi/\mu)^2 m_q^{(0)}$, with $m_q^{(0)}$ being the current quark mass corresponding to the physical pion mass μ. $m_q^{(0)}$ is treated as an input parameter to be tuned to the lattice results, but in our magnetic moment study it turned out to lie in the range 6–7 MeV, which is very reasonable.

The parameters of the CBM are obtained as follows. The bag constant B and the phenomenological parameter z_0 are fixed by the physical nucleon mass and the stability condition,[3] $dM_N/dR=0$, for a given choice of R_0 and $m_q^{(0)}$. For each subsequent value of the pion mass or the quark mass considered, ω_0 and R are determined simultaneously from the linear boundary condition [19–21] and the stability condition. In this work we have calculated the mass of the N and Δ baryons as a function of squared pion mass (as illustrated in Fig. 2). The Δ calculation is similar to that for the N; however, the value of B is fixed to be the same as that used for the nucleon, while z_0 is adjusted to fit the observed mass difference, taking into account the pionic contribution to this quantity, at the physical value $m_\pi=\mu$ ($m_q=m_q^{(0)}$).

TABLE I. Parameters for fitting Eqs. (17) and (18) to the CBM data. Here we have taken $R_0=1.0$ fm and $m_q^{(0)}=6.0$ MeV. The Error column denotes the relative difference from the experimental values which were used as a constraint in generating the CBM data.

Baryon	α (GeV)	β (GeV^{-1})	Λ (GeV)	M_B (GeV)	Error
N	1.09	0.739	0.455	0.948	0.8%
Δ	1.37	0.725	0.419	1.236	0.3%

As expected on quite general grounds (and discussed in Sec. II), as the pion mass increases the mass of the baryon does indeed become linear in m_π^2. In addition, from the curvature at low pion mass, we see that the non-analytic structure is important in the region m_π below 400 MeV.

We now fit our functional forms for the baryon masses, Eqs. (17) and (18), to the CBM data. We note that the CBM data are generated using a phenomenologically motivated, dipole form factor, whereas the functional form used in the fit involves a θ cutoff. In order to simulate the fitting procedure for lattice data, our fit to the CBM results involves only pion masses above the physical branch point at $M_\Delta=M_N$, followed by an extrapolation to lower pion mass.

It can be seen from Fig. 2 that our extrapolation to the physical pion mass is in good agreement with the CBM calculations: at the physical pion mass the extrapolated N mass is within 0.8% of the experimental value to which the CBM was fitted, while the Δ is within 0.3% of the experimental value. We present the parameters of our fit in Table I. The value for the sharp cutoff (Λ) is 0.44(2) GeV, compared to $\Lambda_D=1$ GeV for the dipole form factor.

It was noted in Sec. II that the constant α in our functional form is not the mass of the baryon in the chiral limit, but rather this is given by $M_N^{(0)}=\alpha_N+\sigma_{NN}(0,\Lambda)$

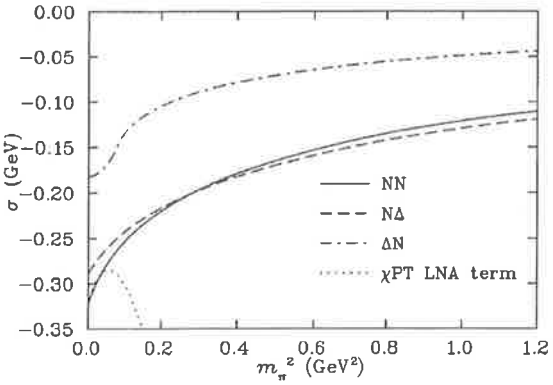

FIG. 3. Pion induced self-energy corrections for a 1 GeV dipole form factor. The LNA term of χPT tracks the $NN\pi$ contribution up to $m_\pi \sim 0.2$ GeV, beyond which the internal structure of the nucleon becomes important.

[3]Note that while z_0, B and the πNN form factor may all depend on m_q, this dependence is expected to be a smaller effect and we ignore such variations in order to avoid an excess of parameters.

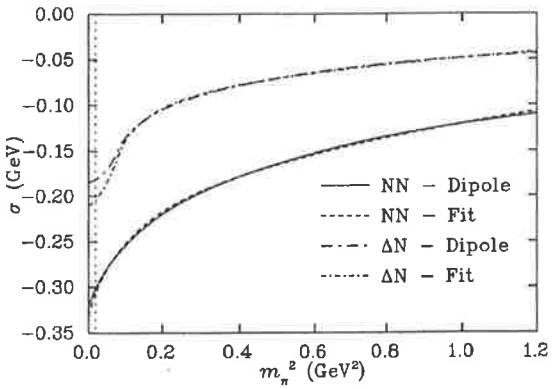

FIG. 4. Comparison between the nucleon and Δ self-energies, σ_{NN} and $\sigma_{\Delta N}$, calculated using a dipole form factor (solid and long-dash-dotted curves, respectively) and fits using the form $\alpha+\beta m_\pi^2+\sigma_{ij}(m_\pi,\Lambda)$, based on a sharp cut-off in the momentum of the virtual pion (dashed and short-dash-dotted curves respectively).

$+\sigma_{N\Delta}(0,\Lambda)$—with an analogous expression for the Δ. We find that the extrapolated N and Δ masses in the chiral [SU(2)-flavor] limit are $(M_N^{(0)},M_\Delta^{(0)})=(905,1210)$ MeV, compared with the CBM values (898,1197) MeV.

The mass dependence of the pion induced self-energies, σ_{ij}, for the 1 GeV dipole form factor, is displayed in Fig. 3. The choice of a 1 GeV dipole corresponds to the observed axial form factor of the nucleon [22], which is probably our best phenomenological guide to the pion-nucleon form factor [23]. We note that σ_{NN} tends to zero smoothly as m_π grows and it is only below $m_\pi^2\sim 0.3$ GeV^2 that there is any rapid variation. That this behavior cannot be well described by a polynomial expansion is illustrated by the dotted curve in Fig. 3. There we expanded σ_{NN} about $m_\pi=0$ as a simple polynomial, $\alpha+\beta m_\pi^2+\gamma m_\pi^3$, with γ fixed at the value required by chiral symmetry. Clearly the expansion fails badly for m_π beyond 300–400 MeV.

The behavior of the $N\pi$ contribution to the self-energy of the Δ is especially interesting. In particular, the effect of the

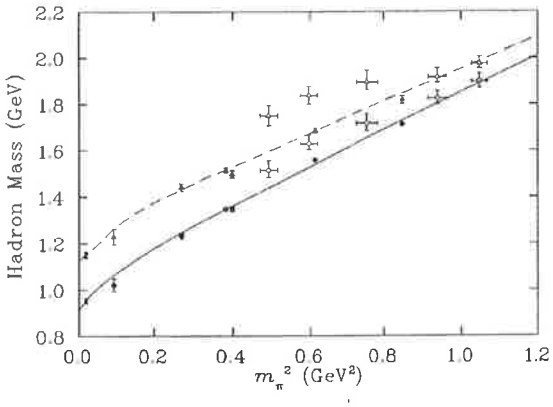

FIG. 5. Baryon masses calculated by UKQCD (open points) and CP-PACS (solid points), as a function of m_π^2. The solid (dashed) curve illustrates a fit to the combined data sets for N (Δ). The leftmost data points are our extrapolated values of the baryon masses at the physical pion mass.

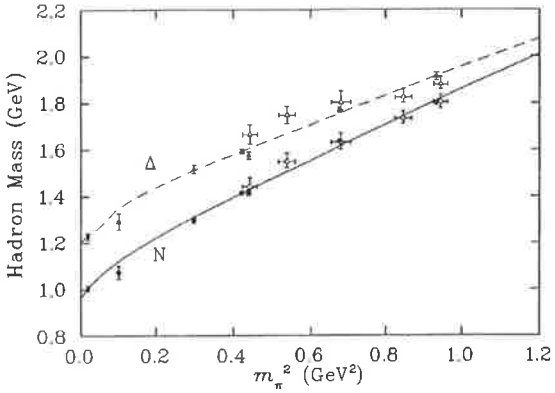

FIG. 6. UKQCD and CP-PACS baryon masses with 5% adjustments in the scale parameters to improve the agreement between the two data sets. (The key is as described in Fig. 5.)

branch point at $m_\pi=\Delta M$ is seen in the curvature at $m_\pi^2\sim 0.1$ GeV^2. For comparison, we note that while there is also a branch point in the nucleon self-energy at the same point—see Eq. (9)—the coefficient of $(m_\pi^2-\Delta M^2)^{3/2}$ vanishes at this point. As a consequence there is little or no curvature visible in the latter quantity at the same point. The correct description of this curvature is clearly very important if one wishes to obtain the ΔN mass difference at the physical pion mass. The fact that, as shown in Fig. 2, our simple three parameter phenomenological fitting function can reproduce N and Δ masses within the CBM, including this curvature, suggests that this should also provide a reliable form for extrapolating lattice data into the region of small pion mass.

Figure 4 illustrates the degree of residual model dependence in our use of Eqs. (17) and (18). There the variation of the nucleon self-energy, σ_{NN}, calculated with a 1 GeV dipole form factor (solid curve) is fit using the form $\alpha+\beta m_\pi^2+\sigma_{NN}(m_\pi,\Lambda)$ (dashed curve, with $\alpha=-0.12$ GeV, $\beta=0.39$ GeV^{-1} and $\Lambda=0.57$ GeV). Note that the devia-

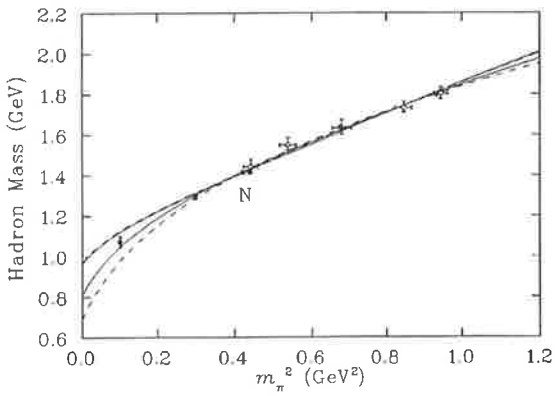

FIG. 7. UKQCD and CP-PACS nucleon masses with scale parameters adjusted by 5%. The data are as described in Fig. 5. The dashed lines represent fits without the point at 0.1 GeV^2. The solid lines include this point. The top pair of lines are fits with Λ fixed at 0.455 GeV, a value preferred on the basis of our CBM analysis. The bottom pair have Λ as a fit parameter.

TABLE II. Parameters for fits of Eqs. (17) and (18) to lattice data. Here we fix Λ ($\Lambda_N=0.455$ and $\Lambda_\Delta=0.419$) and vary α and β. The mass of the baryon at the physical pion mass is M_N (M_Δ) and the mass in the chiral limit is $M_N^{(0)}$ ($M_\Delta^{(0)}$). The scaling columns represent adjustments to the scale parameters providing physical dimensions to the lattice data.

Scaling		N				Δ			
CP-PACS	UKQCD	α (GeV)	β (GeV^{-1})	M_N (GeV)	$M_N^{(0)}$ (GeV)	α (GeV)	β (GeV^{-1})	M_Δ (GeV)	$M_\Delta^{(0)}$ (GeV)
0%	0%	1.10	0.778	0.954	0.910	1.29	0.680	1.150	1.125
+5%	−5%	1.15	0.736	1.003	0.961	1.36	0.602	1.227	1.203
0%	−10%	1.10	0.767	0.957	0.914	1.31	0.624	1.169	1.145
+10%	0%	1.20	0.707	1.050	1.008	1.42	0.581	1.285	1.262

tions are at the level of a few MeV. For the Δ the self-energy, $\sigma_{\Delta N}$, is again calculated using a 1 GeV dipole form factor and fit with our standard fitting function, $\alpha+\beta m_\pi^2 + \sigma_{\Delta N}(m_\pi,\Lambda)$. The quality of the fit (with $\alpha=-0.062$ GeV, $\beta=0.024$ GeV^{-1} and $\Lambda=0.53$ GeV) is not as good as for the nucleon case. Nevertheless, the difference between the two curves at the physical pion mass (vertical dotted line) is only about 20 MeV. At the present stage of lattice calculations this seems to be an acceptable level of form factor dependence for such a subtle extrapolation.

IV. LATTICE DATA ANALYSIS

We consider two independent lattice simulations of the N and Δ masses, both of which use improved actions to study baryon masses in full QCD with two light flavors. The CP-PACS [3] lattice data are generated on a plaquette plus rectangle gauge action with improvement coefficients based on an approximate block-spin renormalization group analysis. The $\mathcal{O}(a)$-improved Sheikholeslami-Wohlert clover action is used with a mean-field improved estimate of the clover coefficient $c_{SW}=1.64$–1.69. This estimate is likely to lie low relative to a nonperturbative determination [14] and may leave residual $\mathcal{O}(a)$ errors.

Ideally one would like to work with lattice data in which the infinite-volume continuum limit is taken prior to the chiral limit. Until such data are available, we select results from their $12^3\times32$ and $16^3\times32$ simulations at $\beta=1.9$. Lattice spacings range from 0.25 fm to 0.19 fm and provide physical volumes of 2.7 fm to 3.5 fm on a side. While the volumes are large enough to avoid significant finite volume errors, the coarse lattice spacings necessitate the use of improved actions. Systematic uncertainties the order of 10% are not unexpected.

The UKQCD [7] group uses a standard plaquette action with the $\mathcal{O}(a)$-improved Sheikholeslami-Wohlert action. At a β of 5.2, UKQCD uses $c_{SW}=1.76$, which is lower than the current non-perturbative value [14] of 2.017, again leaving some residual $\mathcal{O}(a)$ errors. Lattice spacings are necessarily smaller, ranging from 0.13 to 0.21 fm. We select their $12^3\times24$ data set as providing better statistical errors than their largest volume simulation. Physical volumes are 1.6–2.6 fm on a side, suggesting that finite volume errors may be an issue on the smallest physical volume where the dynamical quark mass is lightest.

In full QCD, the renormalized lattice spacing is a function of both the bare coupling and the bare quark mass. In order to determine the lattice spacing, the UKQCD Collaboration

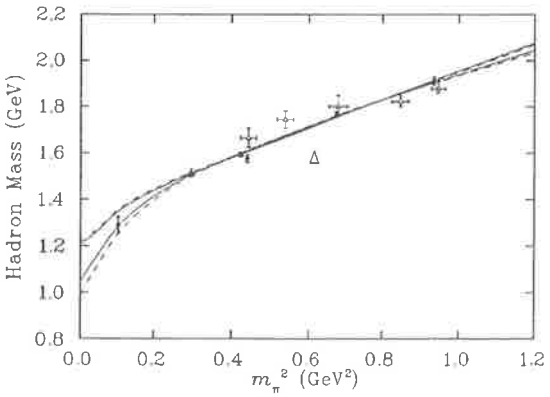

FIG. 8. UKQCD and CP-PACS Δ-baryon masses with scale parameters adjusted by 5%. The data are as described in Fig. 5. The dashed lines represent fits without the point at 0.1 GeV^2. The solid lines include this point. The top pair of lines are fits with Λ fixed at 0.419 GeV, a value preferred on the basis of our CBM analysis. The bottom pair have Λ as a fit parameter.

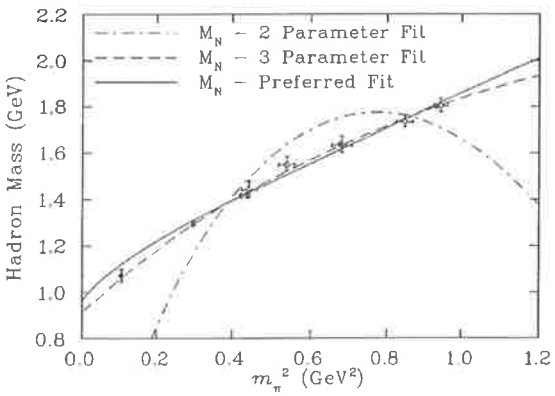

FIG. 9. A comparison between phenomenological fitting functions for the mass of the nucleon. The two parameter fit corresponds to using Eq. (22) with γ set equal to the value known from χPT. The three parameter fit corresponds to letting γ vary as an unconstrained fit parameter. The solid line is the fit for the functional form of Eq. (17), fit (d) of Table III.

TABLE III. Parameters for the fits shown in Fig. 7. Parameter sets (a) and (b) are obtained by excluding the lowest data point from the fit, while (c) and (d) include it. Parameter sets (a) and (c) are fits with 3 parameters, and sets (b) and (d) are fits with Λ fixed to the phenomenologically preferred value.

Fit	α (GeV)	β (GeV^{-1})	Λ (GeV)	M_N (GeV)
(a)	1.76	0.386	0.789	0.763
(b)	1.15	0.727	0.455	1.010
(c)	1.42	0.564	0.661	0.870
(d)	1.15	0.736	0.455	1.003

TABLE IV. Parameters for the fits shown in Fig. 8. Parameter sets (a) and (b) are obtained by excluding the lowest data point from the fit, while (c) and (d) include it. Parameter sets (a) and (c) are fits with 3 parameters, and sets (b) and (d) are fits with Λ fixed to the phenomenologically preferred value.

Fit	α (GeV)	β (GeV^{-1})	Λ (GeV)	M_Δ (GeV)
(a)	1.64	0.414	0.683	1.042
(b)	1.37	0.587	0.419	1.240
(c)	1.54	0.475	0.616	1.095
(d)	1.36	0.602	0.419	1.230

calculates the force between two static quarks at a distance r_0 [24], while CP-PACS considers the string tension directly. While the two approaches yield similar results in the quenched approximation, string breaking in full QCD may introduce some systematic error in the extraction of the string tension at large distances. In fact we find that the two data sets are consistent, provided one allows the parameters introducing the physical scale to float within systematic errors of 10%. A thorough investigation of these systematic errors lies outside the scope of this investigation. Instead we simply rescale the UKQCD and CP-PACS data sets in combining them into a single, consistent data set.

We begin by considering the functional form suggested in Sec. II with the cutoff Λ fixed to the value determined by fitting the CBM calculations. The resulting fits to the baryon masses are shown in Fig. 5 for the unshifted lattice data and Fig. 6 where each data set is adjusted by 5% to provide consistency. The extrapolations are indicated by the solid (dashed) curve for N (Δ). The resulting fit parameters and masses[4] are listed in Table II.

In examining fits in which the cutoff is allowed to vary as a fit parameter, we found it instructive to also study the dependence of the fit on the number of points included. This dependence is shown for the N in Fig. 7 and for the Δ in Fig. 8. In particular, we compare fits including the lowest lattice point (at around 0.1 GeV^2) and then excluding it. When we fix the value of Λ the fits are stable and insensitive to the lowest point. They tend to lie slightly above the lowest data point. However, given the caution expressed by the CP-PACS Collaboration for the lowest point, we view these fits as reasonably successful. In contrast, when the value of Λ is treated as a fitting parameter, it is sensitive to the inclusion of the lowest point. Hence, to perform model independent fits, it is essential to have lattice simulations at light quark masses approaching $m_\pi^2 \sim 0.1$ GeV^2. An analysis of the current data suggests $\Lambda = 0.661$ GeV and provides a nucleon mass 130 MeV lower than the CBM-constrained fit. Tables III and IV summarize parameters and physical baryon masses for N and Δ respectively.

[4]The errors bars for the extrapolated baryon masses at the physical pion mass displayed in the figures are naive estimates only. We are unable to perform a complete analysis without the lattice results on a configuration by configuration basis.

It is common practice in the lattice community to use a polynomial expansion for the mass dependence of hadron masses. Motivated by χPT the lowest odd power of m_π allowed is m_π^3:

$$M_N = \alpha + \beta m_\pi^2 + \gamma m_\pi^3. \tag{22}$$

The results of such fits are shown in Figs. 9 and 10 for N and Δ respectively. The corresponding parameters are reported in Table V. As can be seen in Table V, the coefficient of the m_π^3 term, which is the leading non-analytic term in the quark mass, disagrees with the coefficient known from χPT by almost an order of magnitude. This clearly indicates the failings of such a simple fitting procedure. We recommend that future fitting and extrapolation procedures should be based on Eqs. (17) and (18), which are consistent with χPT and the heavy quark limit.

V. SUMMARY

In the quest to connect lattice measurements with the physical regime, we have explored the quark mass dependence of the N and Δ baryon masses using arguments based on analyticity and heavy quark limits. In the region where

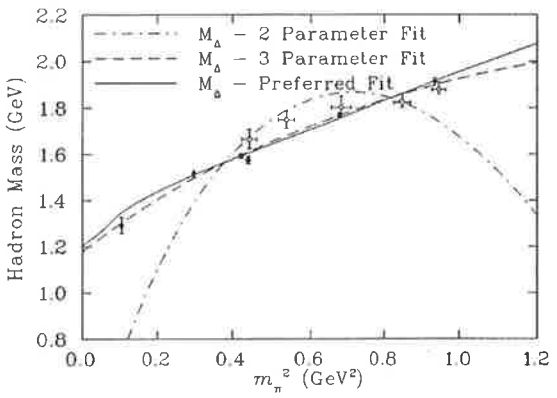

FIG. 10. A comparison between phenomenological fitting functions for the mass of the Δ. The two parameter fit corresponds to using Eq. (22) with γ set equal to the value known from χPT. The three parameter fit corresponds to letting γ vary as an unconstrained fit parameter. The solid line is the fit for the functional form of Eq. (18), fit (d) of Table IV.

TABLE V. Parameter sets for the fits shown in Figs. 9 and 10. Set (a) is for the 2 parameter fit of Eq. (22) with γ from χPT, (b) for the 3 parameter fit of Eq. (22), and (c) for the preferred functional form.

	N				Δ			
Fit	α (GeV)	β (GeV^{-1})	γ or Λ (GeV^{-2}) or (GeV)	M_N (GeV)	α (GeV)	β (GeV^{-1})	γ or Λ (GeV^{-2}) or (GeV)	M_Δ (GeV)
(a)	−0.128	7.38	−5.60	−0.001	0.182	7.09	−5.60	0.304
(b)	0.912	1.69	−0.761	0.943	1.18	1.45	−0.703	1.202
(c)	1.15	0.736	0.455	1.003	1.37	0.602	0.419	1.227

m_π is larger than 500 MeV, the lattice data can be reasonably well described by the simple form $\alpha+\beta m_\pi^2$, which is linear in the quark mass. The additional curvature associated with chiral corrections only appears below this region. This can be understood quite naturally within chiral quark models, like the cloudy bag, which lead to a cutoff on high momentum virtual pions, thus suppressing the self-energy diagrams quite effectively as m_π^2 increases. The pionic self-energy diagrams which we consider are unique in that only these diagrams give rise to the leading non-analytic behavior which yields a rapid variation of baryon masses in the chiral limit. Loops involving heavier mesons or baryons cannot give rise to such a rapid variation.

Based on these considerations, we have determined a method to access quark masses beyond the regime of chiral perturbation theory. This method reproduces the leading non-analytic behavior of χPT and accounts for the internal structure of the baryon under investigation. We find that the predictions of the CBM, and two flavor, dynamical fermion lattice QCD results, are succinctly described by the formulas of Eqs. (17) and (18) with terms defined in Eqs. (8)–(12). We believe that Eqs. (8)–(12) are the simplest one can write down which involve a single parameter, yet incorporate the essential constraints of chiral symmetry and the heavy quark limit.

Firm conclusions concerning agreement between the extrapolated lattice results and experiment cannot be made until the systematic errors can be reduced below the current level of 10% and accurate measurements are made at $m_\pi \sim 300$ MeV or lower. The significance of non-linear behavior in extrapolating nucleon and Δ masses as a function of m_π^2 to the chiral regime has been evaluated. We find that the leading non-analytic term of the chiral expansion dominates from the chiral limit up to the branch point at $m_\pi=\Delta M$. The curvature around $m_\pi=\Delta M$, neglected in previous extrapolations of the lattice data, leads to shifts in the extrapolated masses of the same order as the departure of lattice estimates from experimental measurements.

ACKNOWLEDGMENTS

We would like to thank Pierre Guichon and Tom Cohen for helpful discussions. This work was supported in part by the Australian Research Council.

[1] B. Sheikholeslami and R. Wohlert, Nucl. Phys. **B259**, 609 (1985).
[2] M. Alford, W. Dimm, and P. Lepage, Phys. Lett. B **361**, 87 (1995); P. Hasenfratz, Nucl. Phys. B (Proc. Suppl.) **63**, 53 (1998).
[3] CP-PACS Collaboration, S. Aoki *et al.* Phys. Rev. D **60**, 114508 (1999).
[4] CP-PACS Collaboration, Yoshinobu Kuramashi for the collaboration, hep-lat/9904003.
[5] D. B. Leinweber, D. H. Lu, and A. W. Thomas, Phys. Rev. D **60**, 034014 (1999); Report No. ADP-99-18-T360, hep-ph/9905414.
[6] A. W. Thomas, Adv. Nucl. Phys. **13**, 1 (1984); G. A. Miller, Int. Rev. Nucl. Phys. **2**, 190 (1984).
[7] UKQCD Collaboration, C. R. Allton *et al.*, Phys. Rev. D **60**, 034507 (1999).
[8] A. W. Thomas and G. Krein, Phys. Lett. B **456**, 5 (1999).
[9] E. Jenkins, Nucl. Phys. **B368**, 190 (1992).
[10] R. F. Lebed, Nucl. Phys. **B430**, 295 (1994).
[11] M. K. Banerjee and J. Milana, Phys. Rev. D **54**, 5804 (1996).
[12] D. B. Leinweber, Nucl. Phys. **A470**, 477 (1987); R. K. Bhaduri, L. E. Cohler, and Y. Nogami, Nuovo Cimento A **65**, 376 (1981); E. Eichten, K. Gottfried, T. Kinoshita, K. D. Lane, and T. M. Yan, Phys. Rev. D **21**, 203 (1980).
[13] S. Theberge, A. W. Thomas, and G. A. Miller, Phys. Rev. D **22**, 2838 (1980); **23**, 2106(E) (1981).
[14] K. Jansen and R. Sommer, Nucl. Phys. **B530**, 185 (1998).
[15] D. H. Lu, A. W. Thomas, and A. G. Williams, Phys. Rev. C **57**, 2628 (1998).
[16] D. H. Lu, K. Tsushima, A. W. Thomas, A. G. Williams, and K. Saito, Phys. Lett. B **441**, 27 (1998); E. A. Veit *et al.*, Phys. Rev. D **31**, 1033 (1985).
[17] E. A. Veit, A. W. Thomas, and B. K. Jennings, Phys. Rev. D **31**, 2242 (1985).
[18] A. W. Thomas, J. Phys. G **7**, L283 (1981).
[19] A. Chodos, R. L. Jaffe, K. Johnson, C. B. Thorn, and V. F. Weisskopf, Phys. Rev. D **9**, 3471 (1974).
[20] A. Chodos, R. L. Jaffe, K. Johnson, and C. B. Thorn, Phys.

Rev. D **10**, 2599 (1974).
[21] T. DeGrand, R. L. Jaffe, K. Johnson, and J. Kiskis, Phys. Rev. D **12**, 2060 (1975).
[22] T. Kitagaki *et al.*, Phys. Rev. D **28**, 436 (1983).
[23] R. Bockmann, C. Hanhart, O. Krehl, S. Krewald, and J. Speth, Phys. Rev. C **60**, 055212 (1999); A.W. Thomas and K. Holinde, Phys. Rev. Lett. **63**, 2025 (1989); P.A. Guichon, G. A. Miller, and A. W. Thomas, Phys. Lett. **124B**, 109 (1983).
[24] R. Sommer, Nucl. Phys. **B411**, 839 (1994).